Development of Functional Materials as White-LED Phosphors to Improve Color Rendering in Display Devices

Thesis submitted in partial fulfilment of the requirements for the award of the degree of

Doctor of Philosophy

By

Kishore Kumar Aitha

(Roll No: 715086)

Under the Supervision of

Prof. D. Dinakar

Department of Physics
National Institute of Technology Warangal
T.S., INDIA

December – 2023

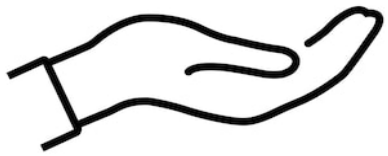

Dedicated to my parents

Late Shri. A Buchaiah - Smt. A Renuka

Department of Physics

NATIONAL INSTITUTE OF TECHNOLOGY WARANGAL

Hanumakonda- 506 004, TS-India

APPROVAL OF THE VIVA-VOCE BOARD

Certified that the thesis entitled "***Development of Functional Materials as White-LED Phosphors to Improve Color Rendering in Display Devices***" submitted by **Mr. Kishore Kumar Aitha** (Roll No. **715086**) to the National Institute of Technology Warangal, for the award of the degree ***Doctor of Philosophy*** has been accepted by the external examiners and that the student has successfully defended the thesis in the viva-voce examination held today, i.e., _____

(Prof. D. Haranath)	**(Prof. Sourabh Roy)**	**(Prof. T. Mahesh Kumar)**
(Internal Member)	(Internal Member)	(Allied Dept. Member)

Prof D Dinakar

(External Examiner) (Supervisor)

Prof. T. Venkatappa Rao
(Head of the Department & Chairman of DSC)

Department of Physics

NATIONAL INSTITUTE OF TECHNOLOGY WARANGAL

Hanumakonda- 506 004, TS-India

CERTIFICATE

This is to certify that the work presented in the thesis entitled "***Development of Functional Materials as White-LED Phosphors to Improve Color Rendering in Display Devices***" is being submitted by **Mr. Kishore Kumar Aitha** (Roll No. **715086**) to the Department of Physics, **National Institute of Technology (NIT) Warangal**, for the award of degree of Doctor of Philosophy, is a record of bonafide research work carried out by him under my supervision/guidance. I further stated that this work has not been submitted to any other University or Institution in part or full for the award of any degree.

Place: NIT Warangal
Date: 07-012-2023.

Prof. T. Venkatappa Rao
Professor and Head
Department of Physics
NIT Warangal- 506004.

(Prof D Dinakar)
Supervisor

ACADEMIC SECTION - PhD
NATIONAL INSTITUTE OF TECHNOLOGY WARANGAL
WARANGAL – 506004

PhD7A

Ph.D. THESIS SUBMISSION CERTIFICATE

Dt:07-12-2023

TO WHOMSOEVER IT MAY CONCERN

This is to certify that Mr. Mr. Kishore Kumar Aitha bearing Roll No 715086, was a bonafide student of Ph.D. (Part-time) during the period 2015 to 2023 in the department of Physics. He has submitted his Ph.D. thesis titled "***Development of Functional Materials as White-LED Phosphors to Improve Color Rendering in Display Devices***" on date:07-12-2023.

After due evaluation process and successful defense of the thesis, he will be obtaining his Ph.D. degree.

This certificate is issued to the candidate on his request.

07.12.2023

Head of the Department **Dean -Academic**

DECLARATION

This is to certify that the work presented in the Ph.D. thesis entitled **"Development of Functional Materials as White-LED Phosphors to Improve Color Rendering in Display Devices",** is a bonafide work done by me under the supervision of ***Prof. D. Dinakar,*** Professor in the Department of Physics, National Institute of Technology (NIT) Warangal and was not submitted elsewhere for the award of any degree.

I declare that this written submission represents my ideas in my own words and where others' ideas or words have been included, I have adequately cited and referenced the original sources. I also declare that I have adhered to all principles of academic honesty and integrity and have not misrepresented or fabricated or falsified any idea / data / fact / source in my submission. I understand that any violation of the above will be a cause for disciplinary action by the Institute and can also evoke penal action from the sources which have thus not been properly cited or from whom proper permission has not been taken when needed.

Place: NIT Warangal
Date: 7th December 2023

Kishore Kumar Aitha
Ph.D. Scholar (Part-Time)
Roll No.: 715086

CONTENTS

ACKNOWLEDGEMENTS

I would lie to take this opportunity and want to express my gratitude to those individuals who have played a great role, whether directly or indirectly, in supporting my endeavours to successfully complete this dissertation.

First and foremost, I express my deep gratitude to my supervisor, **Prof. D. Dinakar**, for his valuable guidance, motivation, and support during the duration of my research. I have found immense satisfaction in the opportunity to work under his mentorship. I express gratitude towards my supervisor for demonstrating faith in my abilities, granting me the autonomy to explore my concepts, and displaying patience in accommodating my needs. This thesis would not have been feasible without the substantial intellectual and personal support provided by him.

I would like to thank **Prof. D. Haranath**, member of my Doctoral Scrutiny Committee for his constant support, guidance, and encouragement have been invaluable throughout the entire process. From the initial stages of refining my research proposal to the final submission of my thesis, his unwavering presence and wealth of wisdom have been instrumental in shaping the work. I am profoundly grateful for the immeasurable contributions he made to my development.

I would like to extend my heartfelt thankfulness to **Prof. T. Venkatappa Rao**, Head of the Department, for his valuable guidance and input during the process of shaping the thesis. I am grateful for his timely provision of administrative assistance.

I am thankful to the other esteemed members of my Doctoral Scrutiny Committee, **Prof. Sourabh Roy,** Physics Department and **Prof. T. Mahesh Kumar** from the Department of Metallurgical & Material Engineering for their consistent review of my progress and their useful ideas.

I would like to express my heartfelt gratitude to the esteemed **academic members of the department**, whose continuous encouragement and unwavering support have been important throughout my tenure. I express gratitude towards the office staff and students affiliated with the Department of Physics for their consistent help whenever required.

I express my deep gratitude to **Dr. K.V.R Murthy**, President of the **Luminescence Society of India**, for his support in providing Lab facilities, valuable road map, analysis during my work. His encouragement and supportiveness in participating various international conferences helped during this journey. I am deeply grateful for the knowledge, connections, and friendships that were forged during this time with his collaboration.

I am thankful to **D.Y.Kolhe, Gaussian Optixs**, for his valuable guidance and timely ideas in the realm of research. I am grateful for his consistent support throughout the duration.

I express my gratitude to all the **research scholars** affiliated with the department. I am thankful to **Dr. Kevil Shah, Ms. Payal P. Pradhan, Mr. Naresh Degda, Dr. K. Suresh, S. Pandya** for their support during my research.

The love, support, and patience extended to me by my family are beyond the limitations of verbal expression. The unwavering support and encouragement provided by my parents and all the forces behind the screen have served as a guiding force, enabling me to overcome challenges and successfully accomplish my tasks. I express gratitude towards my sisters for their unwavering support across all domains. In conclusion, I would want to express my gratitude to my life partner for the continuous display of love and affection bestowed upon me.

- Kishore Kumar Aitha

PREFACE

Energy demand is increasing as global population and industrialization accelerate, increasing pressure on finite and increasingly valuable resources. Energy consumption is predicted to increase worldwide over the next two decades. Therefore, every person on the planet must share in the negative impacts of climate change and the loss of natural resources and fossil fuels to generate electricity. Energy-efficient technology is essential for conserving our planet's limited resources. Solid-State Lighting (SSL) is becoming increasingly popular due to its significant energy savings. Significant progress has been made in the use of phosphors in various light-emitting devices (LEDs). About a quarter of all electricity generated is used for lighting residential, industrial, commercial, street and indoor stadiums. White LEDs with excellent color purity (e.g. color rendering index, CRI > 90) and color quality scale (CQS) as well as high visible light emission radiation (LER) effectiveness have been developed through extensive research on new phosphor-embedded polymer matrix layers. One of the important phosphors used to tune the light output of W-LEDs is a red-emitting phosphor. The CRI increases with increasing red emission, while increasing green emission increases efficiency. By changing red, yellow and green on the blue semiconductor LED chip, the color temperature and lumens per watt can be changed. Wider bandwidths and a reduction in the sensitivity of the human eye to the near infrared region are the main disadvantages of commercially available red-emitting phosphors. The red color spectrum (emission maxima between 610-630 nm) must be fully covered to reduce the effects of eye sensitivity at longer wavelengths. Overall, the importance of narrow-band emitting phosphors comes from their ability to precisely control the visible wavelengths emitted, resulting in improved performance, energy efficiency and quality in a wide range of applications, ranging from lighting and displays to scientific research and medical technology.

Due to the high conversion efficiency under LED operating conditions and the narrow emission with rich red, only a few red-emitting phosphors meet the high criteria of commercial LED applications as reported in the various literatures. Currently available red-emitting phosphors do not have a narrow FWHM and therefore do not meet the required criteria. The requirements for narrow-band emission between 610 and 630 nm and exceptionally high photostability are not met by any of the high-quality red-emitting phosphors currently available on the market. Important alternatives to europium-doped compounds as red phosphors in w-LEDs are quantum dots and Mn^{4+}-doped fluorides. The main disadvantages of quantum dots, which commonly contain Cd, are high toxicity and higher production costs, despite their stronger

affinity for red phosphors. Mn^{4+}-doped fluorides, on the other hand, naturally exhibit a narrow line emission with a peak at around 630–640 nm. However, their long decay times prevent their use in low-power LEDs, which often use hydrofluoric acid in their production, posing a safety and health risk to humans. Therefore, there is a significant industrial need for red phosphors for w-LEDs with extremely narrow emission bandwidths and increased efficiency for use in ultraviolet (UV) LED chips or blue LED chips.

The current research deals with the development of functional materials as white LED phosphors and is based on the following objectives:

- Selection and identification of suitable rare earth activators and host materials through a comprehensive literature survey.
- Exploration of various methods and synthesis of phosphors.
- Investigation and characterization of the structural, morphological, compositional and luminescent properties of red-emitting phosphors.
- Use of these multiply excited red-emitting phosphors for strategic applications such as displays, devices, medical therapy etc.

The work is divided into 7 chapters, consisting of an introduction with a comprehensive literature review, experimental and characterization techniques, results and a discussion of the three Eu^{3+}-doped host types $Ca_2La_2O_5$, $SrZr_2La_2O_7$, $SrZr_2CaLa_2O_8$ and their detailed characterization. Finally, I conclude with a summary and the future scope of work.

Chapter 1 covers the introductory aspects of luminescence and provides a concise explanation of various types of luminescence, with particular emphasis on photoluminescence. Discussion of the phenomenon of photoluminescence, including the materials used in this process and the particular emission properties of dopants. The present study involved a comprehensive investigation of host and dopant materials used in luminescence applications, with particular emphasis on their optical properties and morphological analyses. In addition, a thorough evaluation of the existing literature on red-emitting phosphors was carried out.

Chapter 2 describes the experimental aspects and mentions the methodology used in the process as well as the optimization of the synthesis procedure for the selected materials. Also discuss a wide range of methods and equipment used to evaluate and analyze various criteria.

Chapter 3 comprehensively describes the synthesis and photoluminescence characteristics of $Ca_2La_2O_5:Eu^{3+}$, a newly developed phosphor that emits red light. This chapter provides an analysis of the characteristics, results, and analysis of the synthesized phosphor $Ca_2La_2O_5:Eu^{3+}$. To synthesize a phosphor sample of $Ca_2La_2O_5:Eu^{3+}$ that emits red light, a modified solid-state reaction approach assisted by a chemical flux was used. The $Ca_2La_2O_5:Eu^{3+}$ sample doped with 2 mol% of Eu^{3+} exhibits a remarkable degree of crystallinity characterized by a hexagonal phase and a space group of P63/m, as determined by X-ray diffraction (XRD) analysis. The experimental results showed that variations in dopant concentrations have no influence on the micro-stress, a measure of lattice compression. The $Ca_2La_2O_5:Eu^{3+}$ phosphor samples were examined using a scanning electron microscope (SEM) and showed the presence of particles with irregular shapes. In addition, the images showed the appearance of cathodoluminescence. The EDAX analysis performed on the samples confirms the presence of the activator (Eu^{3+}) as well as all components of the host lattice (Ca, La, and O). Extensive research was carried out to investigate the photoluminescent properties of the $Ca_2La_2O_5:Eu^{3+}$ phosphor. The scanning electron microscope (SEM) images showed particles of different sizes and irregular shapes. The absorption bands discovered in FTIR research include the widespread stretching bands of metal oxides as well as the H-O-H absorption band at 3600 cm^{-1}, which indicates the presence of water molecules absorbed from the environment. The phosphor samples of $Ca_2La_2O_5:Eu^{3+}$ (x = 0.5-2.5 mol%) showed red photoluminescence (PL) with a Stokes shift. The PL had significant intensities at wavelengths of 615 nm and 627 nm when excited at 590 nm. The phosphor has characteristic optical properties attributed to the Eu^{3+} ion and resulting from transitions between $^5D_0 \rightarrow {}^7F_J$ energy levels, where J represents the angular momentum quantum number in the range 0 to 4. This unique luminescence is observed during the excitation of the phosphor at a wavelength of 590 nm. The observation that the photoluminescence (PL) at a wavelength of 627 nm, which corresponds to the transition from the $^5D_0 \rightarrow {}^7F_2$ state, had a significantly higher brightness than that emission of Eu^{3+} ions at 615 nm, which also corresponds to the same transition, suggests that the newly available red-emitting phosphors had a high degree of color purity. Analysis of the particle size distribution showed that the average particle size is 2.0 μm. In addition, the phosphor has been claimed to have potential applications in light-emitting diodes (LEDs) for the purposes of deep red emission and cathodoluminescence.

Chapter 4 deals with the study to investigate a functional material, namely a narrow-band, red-emitting multilayer phosphor. The purpose of this research is to explore the possible applications of this material in devices that emit white light. The red-emitting phosphor $SrZr_2La_2O_7:Eu^{3+}$ was successfully synthesized by solid-state reaction techniques. The phosphors were subjected to analysis to examine and document their structural and photoluminescent properties. The phosphor shows clear red emission when excited at a wavelength of 279 nm. Furthermore, the observation of additional emissions can be attributed to cascaded photon emissions and absorption. The emission wavelengths span a range from 395 nm to 627 nm, and there are three additional self-excitation wavelengths at 395 nm, 467 nm and 590 nm. The excitation spectrum has a cascade pattern, initially at a wavelength of 279 nm, followed by further excitations at wavelengths of 395 nm, 467 nm and 590 nm. The above excitations result in emissions at wavelengths of 615 and 627 nm, which have different intensities and complementary peaks. The above process was called the photon emission cascade phenomenon. The use of $SrZr_2La_2O_7:Eu^{3+}$ (1.5 mol%) phosphor is suitable for LEDs emitting in the RED band with multilayer structure. The red emissions at a wavelength of 627 nm can be attributed to the supersensitive electric dipole transition $^5D_0 \rightarrow {}^7F_2$. The observed phenomenon of improved luminescence efficiency and a narrower full width at half maximum (FWHM) of 8.6 nm at a specific wavelength of 627 nm could potentially be due to a number of interrelated processes, including photon emission, absorption and subsequent emissions. The phosphor particles have a size of 0.12 to 9.15 μm and have a high degree of crystallinity, predominantly in the cubic phase. EDAX facilitates the coexistence of Eu^{3+} ions within the host matrix, specifically $SrZr_2La_2O_7$. The newly developed phosphor has predominantly red emissions in a restricted spectrum, making it well suited for many applications including W-LED and other electronic devices.

Chapter 5 focuses on the synthesis and luminescence characteristics of a newly developed phosphor, $SrZr_2CaLa_2O_8:Eu^{3+}$, which exhibits direct white light emission. The potential of phosphor for use in lighting applications is being investigated. This chapter discusses the study of the unique single-phase phosphors $SrZr_2CaLa_2O_8:Eu^{3+}$ (x=0.5-2.5 mol%) with the aim of achieving color-tunability and good color purity. The above-mentioned phosphors emit light in the red to white range and respond to ultraviolet (UV) light by inducing the emission of red light. The use of phosphors that produce direct white light has the potential to reduce the energy consumption of modern displays, in line with the lighting industry's push for energy efficient

alternatives. Screens can achieve equivalent brightness while using less power by improving the efficiency of white light production. This results in an increase in the battery life for portable devices and a reduction in power costs for larger screens. In addition to the above criteria, a comprehensive analysis was carried out on samples of $SrZr_2CaLa_2O_8$ doped with Eu^{3+} ions. A thorough structural and morphological analysis revealed the structural features of the subject. The use of these phosphors is extremely beneficial in improving the color rendering index (CRI) of white light-emitting diodes (w-LEDs), since the red emission (627 nm) produced by the phosphors is a result of transitioning Eu^{3+} ions with an energy level of $^5D_0 \rightarrow {}^7F_2$ under blue (467 nm) illumination. An additional advantage of the present research lies in the ability of phosphors to produce white light directly, thus facilitating the achievement of uniform and consistent illumination. This characteristic reduces the likelihood of hotspots, shadows, or color differences appearing on the display surface.

Chapter 6 examines the use of a dual-wavelength excitable phosphor, specifically $Ca_2La_2O_5:Eu^{3+}$, in the context of display devices and cognitive treatment applications. The focus of this chapter is the study of the $Ca_2La_2O_5:Eu^{3+}$phosphor, which was developed by using a chemical flux and a modified high-temperature solid-state reaction method. The chapter includes a comprehensive analysis of the optical properties of this phosphor. A phosphor with the ability to tune its hue, namely $Ca_2La_2O_5:Eu^{3+}$ (x=0.5 to 2.5 mol%), was effectively prepared by using a modified solid-state reaction method incorporating a chemical flux. $Ca_2La_2O_5:Eu^{3+}$ is an exceptional phosphor with a broad absorption spectrum from 250 to 600 nm, making it suitable for dual-wavelength excitation. This property distinguishes it as a rare and distinctive material. The Eu^{3+} ions exhibit broad white (400–650 nm) and red (627 nm) photoluminescence (PL) due to the appearance of one or more $^5D_0 \rightarrow {}^7F_J$ (J = 1-4) transitions. The study found that a significant improvement in energy transfer efficiency between La^{3+} and Eu^{3+} ions was observed as the concentration of Eu^{3+} ions was gradually increased. The use of scanning electron micrographs revealed the presence of elongated rod-shaped formations with an average diameter of 2.0 μm. The color coordinates (x, y) corresponding to the white (0.41, 0.35) and red (0.62, 0.38) zones were determined at the excitable wavelengths of 395 nm and 467 nm, respectively. Additional studies were performed on the luminescence spectra of $Ca_2La_2O_5:Eu^{3+}$ as a function of temperature with excitation at wavelength of 467 nm. At a temperature of 150°C, the photoluminescence intensity had a thermal stability of around 72.8% relative to the ambient temperature. A value of 0.19 electron volts (eV) was determined as the

activation energy. The results suggest that the phosphor has favourable characteristics for use in LED applications, particularly in cognitive treatments, due to its emissions at a wavelength of 627 nm. Additionally, the phosphor shows potential for use in displays as it contributes a significant red component to white LEDs, a property that is typically challenging to achieve in systems consisting of a single component.

Chapter 7 provides an overview of the main findings and results of the study, presents the conclusions of the present study and suggests possible areas for further research.

LIST OF FIGURES

LIST OF TABLES

ABBREVIATIONS

AFM	**Atomic Force Microscopy**
AR	Augmented Reality
ATFB	Ammonium Tetrafluoroborate
BET	Brunauer-Emmett-Teller
BLI	Bioluminescence Imaging
BSE	Back Scattered Electrons
CB	Conduction Band
CIE	International Commission On Illumination
CL	Cathodoluminescence
CQS	Color Quality Scale
CRI	Color Rendering Index
CRT	Cathode Ray Tube
CT	Charge Transfer
CTB	Charge Transfer Band
CTS	Charge Transfer
EDAX	Energy Dispersive X-Ray Analysis
EDX	Energy Dispersive Spectroscopy
ESA	Excited State Absorption
ET	Energy Transfer
FE	Field Emission
FED	Field Emission Display
FRET	Fluorescence Resonance Energy Transfer
FTIR	Fourier-Transform Infrared Spectroscopy
FWHM	Full Width At Half Maximum
HF	Hydrogen Fluoride
HUD	Heads-Up Displays
ICSD	Inorganic Crystal Structure Database
JCPDS	Joint Committee On Powder Diffraction Standards
LCD	Liquid Crystal Displays
LEC	Light-Emitting Electrochemical Cell
LED	Light Emitting Diode
LER	Light Emission Rate
MRI	Magnetic Resonance Imaging
NIR	Near-Infrared
NMR	Nuclear Magnetic Resonance
NR	Non-Radiative
NTSC	National Television Standards Committee
NUV	Near-Ultraviolet
OLED	Organic Light-Emitting Diodes
PBM	Photo-Biomodulation

PDT	Photodynamic Therapy
PEG	Polyethylene Glycol
PL	Photoluminescence
PLE	Photoluminescence Excitation
PSD	Particle Spatial Distribution
PTT	Photo Thermal Therapy
PXRD	Powder X-Ray Diffraction
QD	Quantum Dot
RE	Rare Earth
RGB	Red Green Blue
RISC	Reverse Intersystem Crossing
ROS	Reactive Oxygen Species
SEM	Scanning Electron Microscopy
SSL	Solid State Lighting
SSR	Solid-State Reaction
TADF	Thermally Activated Delayed Fluorescence
TDPL	Temperature-Dependent Photoluminescence
TEM	Transmission Electron Microscopy
TL	Thermoluminescence
UV	Ultraviolet
VB	Valence Band
VR	Virtual Reality
WLED	White Light Emitting Diode
XPS	X-Ray Photoelectron Spectroscopy
XRD	X-Ray Diffraction
YAG	Yttrium Aluminium Garnet

ABSTRACT

Phosphor materials are critical components in various display technologies. These materials play a significant role in converting the energy from electrons or photons into visible light. While traditional phosphors have served well in many applications, there are several reasons why there is a continuous drive to develop new phosphor materials. The current research is driven by the need for displays that offer improved performance, expanded color gamut, thermal stability, durability, and cost-effectiveness. Narrow-band emitting phosphors improve lighting, displays, scientific research, and medical technology performance, energy efficiency, and quality by properly tuning the visible wavelengths. A few red-emitting phosphors fulfil the required standards of ideal white light emission from LED. The blue light excitable red-emitting phosphor materials are essential components in display devices, contributing to color balance, expanded color gamut, energy efficiency, display performance, and application flexibility. The current research is focussed on this area for advancing display technology and meeting the evolving needs of consumers and industries. w-LEDs with narrow emission bandwidths and higher UV or blue LED chip efficiency are the primary goals of the current thesis work. This research augments the development of suitable red-emitting phosphors for white LED. The hierarchy of work done is represented as follows:

- Reviewing the literature on rare earth activation and different host materials.
- Studying the facile synthesis routes for tailor-made phosphors.
- Studying red-emitting phosphor's structure, morphology, composition, and luminosity.
- Developing enhanced red-emitting phosphors for use in displays, LEDs, and medicine.

The work has been divided into seven chapters: an introduction with a literature review, experimental and characterization techniques, results, and a discussion of the three Eu^{3+}-doped host types $Ca_2La_2O_5$, $SrZr_2La_2O_7$, and $SrZr_2CaLa_2O_8$ and their specific properties. Finally, a summary and future work.

Chapter 1 briefly discusses the phenomena of photoluminescence and luminescence. This study analyzed host and dopant materials used in luminescence applications for optical and morphological properties. A comprehensive literature review on red-emitting phosphors was done.

Chapter 2 describes tests, methodologies, and optimization of the selected materials' synthesis. Briefly discuss criterion assessment and analytical methods and technologies used in the thesis.

Chapter 3 describes the photoluminescence and synthesis of $Ca_2La_2O_5:Eu^{3+}$, a new red-light phosphor. Stokes-shifted red photoluminescence was seen in $Ca_2La_2O_5:Eu^{3+}$ (x = 0.5-2.5 mol%) phosphor samples. Photoluminescence (PL) at 627 nm, was brighter than Eu^{3+} ion emission at 615 nm, showing exceptional colour purity in the novel red-emitting phosphors.

A narrow-band, red-emitting multilayer phosphor is examined in Chapter 4. Phosphor emits red after 279 nm excitation. Emission wavelengths are 395–627 nm, while self-excitation wavelengths are 395, 467, and 590 nm. The cascade excitation spectrum starts at 279 nm and continues at 395, 467, and 590 nm. Photon emission, absorption, and emissions illustrate the increased luminescence efficiency and smaller FWHM of 8.6 nm at 627 nm.

Chapter 5 describes the production and brightness of $SrZr_2CaLa_2O_8:Eu^{3+}$, a new direct white light-emitting phosphor. For color-tunability and purity, this chapter examines the rare single-phase phosphor, $SrZr_2CaLa_2O_8:Eu^{3+}$ emitting red to white light and responding to UV rays.

$Ca_2La_2O_5:Eu^{3+}$ (x=0.5 to 2.5 mol%), a tunable-color phosphor, was developed via a modified solid-state reaction with a chemical flux due to its 250–600 nm absorption spectrum. Color coordinates (x, y) for the white (0.41, 0.35) and red (0.62, 0.38) spectra were determined at excitable wavelengths of 395 and 467 nm.

Chapter 7 reviews the study, makes conclusions, and suggests additional research.

Chapter - 1

Introduction

Features of the Chapter:

The present chapter provides a brief overview of phosphor materials and the underlying mechanisms that drive luminescence. It also discusses the origins of the problem, sets out the research objectives, and highlights the motivation behind the current research project. The basic phenomenon and the brief history of phosphors are discussed. The motivation for the development of white LEDs and phosphor-based color LEDs is briefly discussed. The differences between fluorescent and phosphorescent red phosphors are highlighted. Doping strategies for tuning luminescence properties are presented and various doped red phosphors and their luminescence properties are highlighted. This chapter provides a comprehensive literature review on the synthesis and characterization of red-emitting phosphors. The objectives of the work were derived from a comprehensive review of the existing literature and the process of selecting relevant resources was highlighted.

1.1 Luminescence

Light is a form of electromagnetic radiation that is generally visible to the human eye. Specifically, light consists of oscillating electric and magnetic fields and the properties of light waves are determined by their wavelength and frequency. As shown in Figure 1.1, visible light represents only a small portion of the broader electromagnetic spectrum, which includes radio waves, microwaves, infrared radiation, ultraviolet (UV) radiation, X-rays, and gamma rays. Photons represent the fundamental particles of light/electromagnetic radiation. In general, they can be described as discrete packets that have particle- and wave-like properties. What is important is that photons can interact with matter. For example, they can be absorbed by materials and excite electrons to higher energy levels.

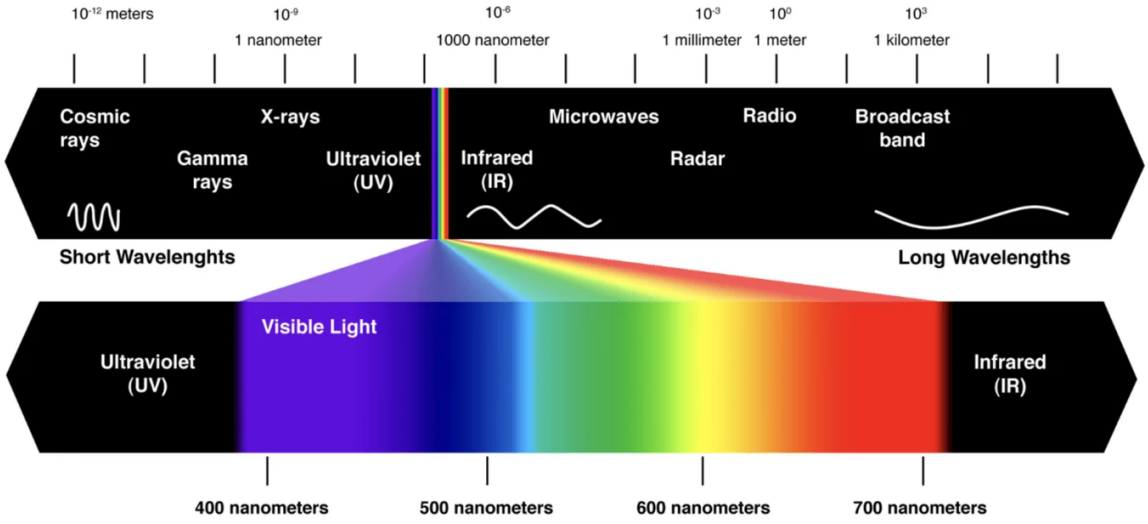

Figure 1.1: Electromagnetic spectrum with spectrum of visible light

Luminescence can be classified as a "cold" emission of light that involves the absorption and re-emission of light (photons), does not produce considerable heat, and occurs through the slow oxidation of phosphorus. Since its discovery in ancient times, luminescence has fascinated researchers and has led to the development of various luminescent materials. Notably, these materials have a wide range of applications, for example, in displays, lighting and (medical) sensors, and organic light-emitting diodes (OLEDs). For instance, phosphor-based white Light-Emitting Diodes (LEDs) and phosphor-based color LEDs are commonly used in lighting and displays utilizing luminescent features. Specifically, white LEDs produce a broad spectrum of

light, whereas phosphor-based LEDs produce specific colors [1]. Hence, white LEDs are commonly used for general lighting, whereas phosphor-based LEDs are commonly used for decorative lighting or as medical sensors [2-6]

Luminescence encompasses a broad range of absorption-emission processes, including phosphorescence, fluorescence, bioluminescence and chemiluminescence [3-4]. Some of naturally occurring and synthetic luminescent materials are shown in Figure 1.2. The present work focuses on utilizing fluorescence and, phosphorescence phenomena. Hence, in the following, the fluorescence and phosphorescence processes are introduced with their properties and potential applications.

Figure 1.2: Natural and synthesized fluorescent and phosphorescence materials

1.1.1 Photoluminescence

1.1.1.1 Fluorescence

Fluorescence is a form of luminescence characterized by a sequential mechanism, involving the absorption of electromagnetic radiation, usually in the ultraviolet (UV) or visible light range, by a substance. Subsequently, the absorbed energy is re-emitted as light with a longer wavelength, typically falling within the visible spectrum [7]. It is worth noting that the light emitted by a material is often of a distinct color compared to the light it absorbs. Additionally, the emission of light typically persists when the material is subjected to the excitation source. Upon the removal of the light source, the phenomenon of fluorescence ceases, resulting in relatively brief durations of luminescence. The average duration of fluorescence lifetime typically range from 10^{-8} to 10^{-9} seconds.

A fluorescent material is initially excited to a singlet state by absorbing photons generated by a light source, as shown in Figure 1.3. Consequently, in order to return to its initial state and release energy, the substance emits photons with diminished energy (distinguished by extended wavelengths), thereby exhibiting fluorescence. Typically, emitted photons exhibit lower energy levels in comparison to absorbed photons, leading to a noticeable difference in color. For instance, a substance with the ability to absorb ultraviolet (UV) radiation has the potential to emit light in the visible spectrum.

Fluorescence is a frequently seen natural phenomena [7]. Insects, fish skin, and crustaceans possess fluorescent pigments, while desert scorpions have blue/green fluorescence under UV light illumination (refer to Figure 1.2). In the realm of fluorescence, the term "fluorophores" is commonly used to denote fluorescent materials [7-8]. These materials can be classified into three types, namely organic dyes, biological fluorophores, and quantum dots (QDs). Significantly, the wavelength of the produced photon can be adjusted by manipulating the band gap of the material, such as through chemical modification and doping, as will be elaborated upon in subsequent sections. On the other hand, when considering quantum dots (QDs), the ability to manipulate the emission wavelength is achieved through the adjustment of the size of a fluorescent QD. This characteristic enables the extensive application of QDs in practical contexts.

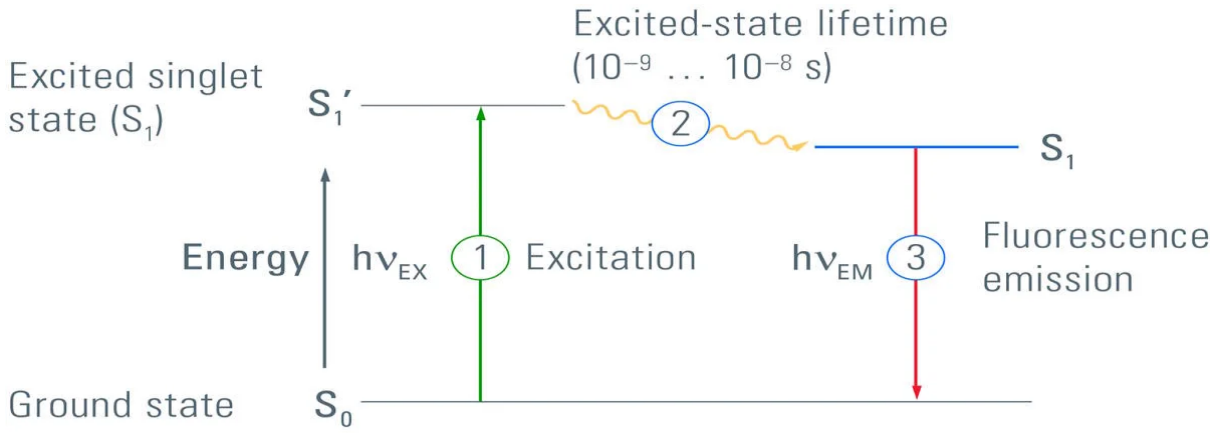

Figure 1.3: Fluorescent material excited to a singlet state by absorbing light particles (photons) from a light (energy) source

Fluorescent materials have extensive utility in diverse applications spanning the fields of biology, chemistry, and materials science, hence facilitating the progress of effective imaging and detection methodologies [2-4][7-8]. Fluorescent materials find many uses in different domains. For instance, they are utilized as fluorescent coatings in cathode ray tubes (CRTs) employed in television and computer monitors [9]. Additionally, fluorescent quantum dots are employed in solar cells and LED displays [10]. Fluorescent materials are frequently employed in applications necessitating brief emission durations due to their inherently short fluorescence lifetimes. For instance, specific applications of Light Emitting Diodes (LEDs) necessitate the fast modulation of light emission.

1.1.1.2 Phosphorescence

Phosphorescence, akin to fluorescence, is a form of luminescence wherein a substance, such as a phosphor, is stimulated by an external light source, resulting in emission of light. Subsequently, it releases photons in the form of light as it transitions back to its initial energy level. Nevertheless, it is crucial to acknowledge numerous significant distinctions when comparing it to the fluorescence process. Significantly, fluorescence is associated with the creation of excited singlet states, whereas phosphorescence is associated with the creation of excited triplet states, as depicted in Figure 1.4. Consequently, phosphorescence is distinguished by a delayed release of photons, which enables an extended emission lifespan [11-12]. Therefore, in comparison to fluorescence, phosphorescence allows for the sustained emission of light even after the excitation source has been eliminated [11-12]. This phenomenon is characterized by emission durations that can vary from microseconds to hours, depending on the specific material utilized. Phosphorescent materials

find several applications, including their utilization as glow-in-the-dark materials [11-13], owing to their extended emission lifetimes. Furthermore, these devices are utilized in scientific apparatus for the purpose of quantifying temperature, oxygen concentrations, and various other factors [12].

The phosphorescence phenomenon can be briefly described as follows: Similar to fluorescence, the material is stimulated by an incident light source, resulting in excitation. However, in contrast to fluorescence, the material undergoes excitation to a triplet state rather than a singlet state as shown in Figure 1.4. The concept of a ground singlet state refers to a quantum condition in which all electrons inside a system are coupled. In the context of a singlet excitation, an electron undergoes a transition to an energetically higher level while preserving its spin state, hence retaining the same spin orientation observed in the ground state. On the other hand, in a triplet excited state, the electron that has been elevated to a higher energy level demonstrates a similar alignment to the other electron that remains unpaired. The process of transitioning from the excited triplet state to the ground state is hindered by the conservation of spin, making it spin-forbidden. Consequently, the radiative decay of a triplet state to a singlet state necessitates a change in spin multiplicity, which is known as intersystem crossing. The duration of intersystem crossover is characterized by a significant deceleration, which enables the extended periods of emission commonly observed in phosphorescence.

Phosphorescent materials commonly encountered in various applications encompass zinc sulfide, strontium aluminate, and organic dyes, exemplified by rhodamine [11-12]. Nevertheless, the phenomenon of luminescence, especially in organic dyes, is very susceptible to factors such as temperature, molecule aggregation, and exposure to oxygen. These limitations significantly restrict the practical utility of phosphorescent materials under normal environmental circumstances. Metal-free, organic phosphors demonstrate consistent emission at ambient temperature, offering a viable solution to these obstacles and rendering them highly favorable materials for various medical applications, including imaging and sensor systems [14].

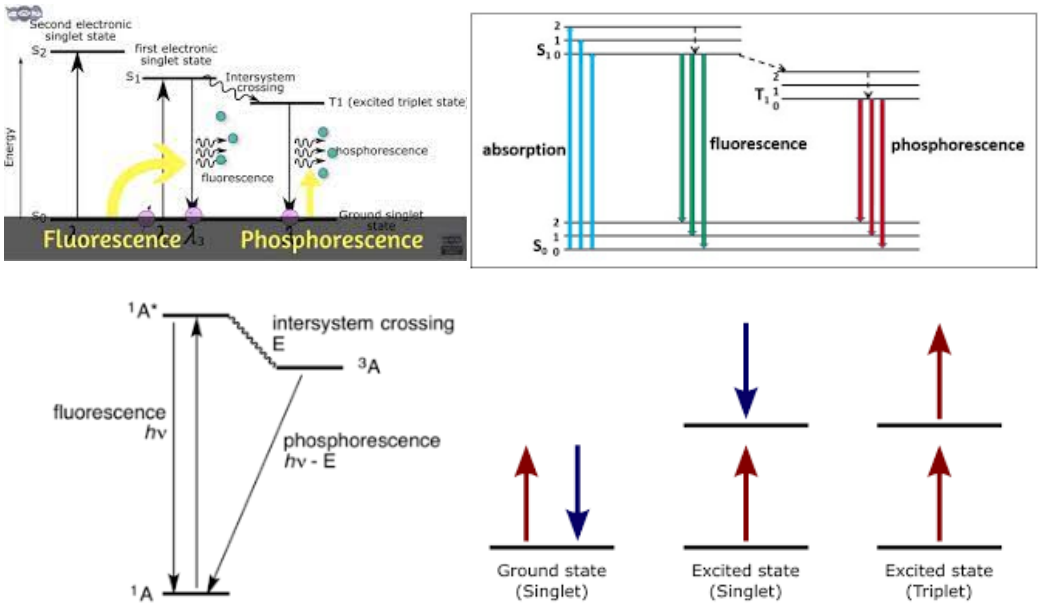

Figure 1.4: Singlet and triplet state electron transitions

1.2 Luminescent phosphor materials – an Overview

Typically, luminescent materials, also known as phosphors, utilized in industrial settings predominantly consist of solid inorganic substances that emit light, specifically in the form of fluorescence or phosphorescence, upon being stimulated by an external light source [3]. The primary composition of these materials mostly comprises a host lattice that is doped with small amounts of rare earth metals to enhance the absorption of energy (photons). Fluorescent or phosphorescent materials can be created and employed based on the intended application. In the context of glow-in-dark items, phosphorescent materials are favored due to their prolonged emission lifespan, whereas fluorescent materials are employed for expeditious light-switching phenomena.

1.2.1 Red-light-emitting phosphors

The scientific community has shown significant interest in the luminous qualities of red light-emitting phosphor in recent decades, as evidenced by several studies [15-18]. The material being examined demonstrates remarkable attributes, such as a narrow emission bandwidth [15], a high degree of color purity [17], efficient luminescence [18], tunable properties [15][6], and significant

chemical and thermal stability [1]. The aforementioned characteristics make it a highly attractive candidate for a diverse array of applications, including organic light-emitting diodes (OLEDs) [2], biomedical imaging sensors [18-19] and photovoltaic devices [20-21]. Since the first discovery of red phosphor, significant research efforts have been undertaken to enhance its emission and luminescence properties, with the aim of tailoring its performance for many applications. It is crucial to note that the fluorescence or phosphorescence shown by phosphor materials that generate red light might vary depending on the specific material and its characteristics [22]. Consequently, the design methodology employed for the material is significantly shaped by the specific material requirements across many applications. An illustration of this phenomenon can be observed in the context of glow-in-dark substances, which necessitate ongoing exposure to light, hence stimulating the advancement of phosphorescent phosphor materials [21].

1.2.2 Exciplexes

Exciplexes are defined as complexes produced in an excited state between two or more molecular entities that possess distinct electronic configurations [23]. These compounds have notable significance in the realm of effective thermally activated delayed fluorescence (TADF) emitters [23-24]. However, the development of efficient orange and red light-emitting exciplexes has been less reported due to the non-radiative (NR) decay that leads to an unavoidable waste of energy [23-24]. The utilization of red phosphor-based Thermally Activated Delayed Fluorescence (TADF) emitters has garnered considerable interest in the scientific community in recent times. This is primarily due to their unique ability to create both singlet and triplet excitons, hence enabling very efficient light emission, also known as luminescence efficiency. Consequently, these TADF emitters have emerged as promising candidates for various applications in Organic Light-Emitting Diodes (OLEDs). TADF materials have a crucial role in promoting reverse intersystem crossing (RISC) mechanisms, which effectively convert triplet into singlet excitons. This conversion process is vital in enabling the manifestation of phosphorescent characteristics.

The operational lifetime of OLED devices are improved through the reduction of triplet accumulation using TADF. In their study, Chen et al. developed a solid-state light-emitting electrochemical cell (LEC) by utilizing phosphor-sensitized Thermally Activated Delayed Fluorescence (TADF) materials. The LEC consisted of a host material, which was a

phosphorescent ionic transition metal complex, and a guest material, which was a deep red TADF emitter [24]. The findings of their study indicate that phosphor sensitized triplet annihilation-based fluorescent emitters (TADFs) have exceptional efficiency in producing phosphorescent and deep red light-emitting electrochemical cells (LECs) due to the presence of reverse intersystem crossing (RISC) mechanisms. The authors, Zhang *et al.*, successfully produced red thermally activated delayed fluorescence (TADF) exciplexes with the incorporation of phosphor components and heavy metal ion cores with strong spin-orbit coupling. This approach effects the generation of exciton waste originating from non-radiative processes [23].

1.2.3 Influence of morphological and structural properties on the luminescent properties of red phosphors

The morphological characteristics of red phosphors, as well as other materials, pertain to their physical attributes and structural composition, will play a crucial role in determining their luminous qualities. The structural qualities encompass several characteristics such as the arrangement of atoms in the crystal structure, the dimensions of the lattice, the degree of phase purity, the symmetry shown by the crystal, the presence of polymorphism, the occurrence of defects and dopants, and the adherence to stoichiometric ratios. A range of characterization techniques can be employed to examine the morphological and structural features of red phosphor materials. Frequently employed methodologies includes scanning electron microscopy (SEM), transmission electron microscopy (TEM), atomic force microscopy (AFM), X-ray diffraction (XRD), X-ray photoelectron spectroscopy (XPS), Raman spectroscopy, Fourier-transform infrared spectroscopy (FTIR), solid-state nuclear magnetic resonance (NMR), and Brunauer-Emmett-Teller (BET) surface characterization.

Controlling the morphological and structural properties enables control of the electronic structure of a material. Thus, tuning these properties influences the optoelectronic properties and luminescence intensity of red phosphors and, therefore, the device performance. Hence, understanding the morphological and structural properties is crucial for tailoring red phosphor. The luminous performance of red phosphors is substantially influenced by the particle size. Reduced particle sizes enhance the optical properties of light emission. In addition, it was observed that red

phosphor particles have a propensity to form agglomerates, which might have an impact on their distribution throughout a host material [25-26].

The reduction of particle sizes has been observed to potentially improve the dispersibility of phosphor particles within host materials [25]. This improvement in dispersibility is essential for achieving a uniform distribution of particles, which is a critical factor in ensuring consistent color and brightness in devices like Oleson. Conversely, the shape of particles has been found to have a significant impact on factors such as packing density, light scattering, and emission properties. The morphology of red phosphor particles exhibits a range of morphologies, including round, irregular, and elongated forms [25-27]. Due to their consistent shape and efficient dispersal properties, spherical particles are predominantly favored for use in device applications. The surface area of phosphor particles plays a significant role in determining their interaction with other materials and their reactivity [25-27]. An increased surface area has the ability to boost surface responses, hence potentially enhancing the performance of the device. The characteristics of the surface structure of red phosphor particles, such as defects and dopants, have a notable impact on their emission properties and luminescence efficiency [26], as discussed in later sections.

In addition, the energy levels of red phosphors are dictated by their crystal structure, hence impacting their emission wavelength and luminescence efficiency [25-26]. Therefore, the opto-electronic characteristics of red phosphors are greatly influenced by various crystal phases and polymorphs. Furthermore, it has been extensively proven in multiple research [25,28] that the luminescence performance depends on the size of the particles. The luminescence efficiency of a material is reduced as a result of rapid trapping of electrons and holes, which is caused by an increase in defect density due to decreased particle size. Therefore, the regulation of particle size is of paramount significance in the manufacturing and functionality of optoelectronic devices. From the previous studies, the photoluminescence (PL) intensity of nanophosphors containing Eu^{3+} doped $CaSiO_3/SiO_2$ is significantly influenced by factors such as crystal size, interionic distances, and lattice packing [26].

The higher intensities are attributed to a more ordered crystalline structure. Therefore, it can be observed that elevating the sintering temperature leads to an enhancement in both the crystalline arrangement and particle dimensions, thereby resulting in a greater intensity of photoluminescence.

The dependence of luminescence intensity and performance of Eu-doped Y_2O_3 nanoparticles on particle size was reported by Srinivasan *et al.* [28]. The findings obtained from the FTIR analysis indicate that the absorption bands related to Y-O bonds exhibit broadening tendencies with increasing particle size. Additionally, it was demonstrated that the intensity of luminescence exhibits a positive correlation with the size of the particles. The enhancement of luminescence efficiency can be attributed to the rise in crystallinity of the particles as a result of elevated annealing temperatures, which leads to larger grain sizes.

Morphological and structural properties can be controlled by adjusting the doping concentration [25]. However, controlling the particle size while maintaining uniformity is highly challenging [26]. The shape and emission intensities of BaGeF6:Mn^{4+} samples were manipulated through the adjustment of the doping concentration [25]. The optical properties of Mn^{4+} doped $Li_3Na_3Ga_2F_{12}$ red phosphors were investigated by Zhu *et al.*, with a focus on their influence on morphologies [27]. The researchers investigated the influence of hydrogen fluoride (HF) on the morphologies of Mn^{4+} doped $Li_3Na_3Ga_2F_{12}$ red phosphors. Their findings revealed that the luminescent properties of these phosphors can be improved by carefully controlling the concentration of HF.

The size of nanoparticles and their luminescence efficiency are significantly influenced by the synthesis technique, as it alters the energy levels of the material. Various synthesis strategies have been employed to manipulate the morphological and structural characteristics of red phosphors. These strategies includes co-precipitation, sol-gel processes, hydrothermal and solvothermal synthesis, template-assisted synthesis, spray pyrolysis, surfactant-assisted synthesis, seed-mediated growth [25,29], and other methods. In general, the manipulation of reaction parameters, including but not limited to hydrolysis time, pH, solvent composition, reaction duration, precursor concentration, and annealing temperature, enables effective regulation of particle size, shape, crystallinity, and porosity. It is of utmost significance to note that the morphological and structural characteristics of red phosphors have the potential to deteriorate when subjected to various environmental variables, including humidity and temperature [26]. Hence, it is vital to comprehend the stability and ageing properties in order to enhance the overall durability and effectiveness of devices over extended periods of time in typical environmental settings.

1.2.4 Doping strategies to control the luminescent properties of red phosphors

In general, the manipulation of the band gap (electronic structure) allows for the regulation of the absorption and emission characteristics of luminous materials, specifically red phosphors. Depending on the material, this can be achieved by doping, chemical modification or, in the case of QDs, by controlling the size of the QD [30]. Cationic substitution is a frequently employed approach for modifying materials, which effectively preserves the crystal structure of the substance [15,31]. The photoluminescence of the parent phosphor structure was seen to be enhanced with the introduction of calcium, as demonstrated in previous studies [31-32]. The manipulation of dopant concentration allows for the adjustment of the band gap, hence influencing the optical and electrical characteristics of the material [6]. The user has provided two numerical references without any accompanying text. Phosphors with oxide lattices represent a class of luminous materials characterized by a host matrix consisting primarily of oxide elements [34]. Silicates, aluminates, gadolinium oxide and yttrium oxide [34-37] are among the host materials that can be considered. Oxides constitute a diverse array of chemical compounds, hence facilitating the choice of host materials that exhibit distinct luminous characteristics and emission colors.

Selecting appropriate dopant ions and optimizing the host lattice structure facilitates the engineering of specific emission properties, such as the emission wavelength, intensity, and lifetime [38-39] which, in turn, allows for the precise tuning of the phosphor's luminescence. Notably, rare earth-activated oxide phosphor materials are environmentally sustainable, cost-efficient, highly versatile and facilitate the production of a broad range of desired color emissions [6,15,2139]. Moreover, oxide-based phosphors commonly exhibit superior stability. They are less prone to degradation [38-39], making them suitable for long-lasting applications, such as lighting or displays. Particularly, europium (Eu^{3+}) offers significant advantages as a dopant to achieve red luminescence in phosphors [32,35], facilitating tunable emission, sharp emission lines, narrow band gaps, and long luminescence lifetimes. Yang *et al.* synthesized and investigated Eu^{3+} doped $Li_6SrLa_2Nb_2O_{12}$ phosphors, demonstrating excellent luminescence thermal stability, thus making them promising candidates for NUV w-LED applications [1].

The YVO_4: Eu^{3+} phosphor is a frequently studied red-emitting phosphor that is often hosted by an oxide material [39-41]. Yttrium orthovanadate (YVO_4) has garnered significant attention as a potential host material for biomedical sensors due to its minimal toxicity [40]. On the other hand, YVO_4: Eu^{3+} phosphors have been the subject of extensive research due to their remarkable luminescent properties [39], exceptional stability [40], and notable efficiency.

The phosphor materials $Ca_2La_2O_5$, $SrZr_2La_2O_7$, and $SrZr_2CaLa_2O_8$ doped with Eu^{3+} exhibit distinctive optical characteristics [42].When integrated into the aforementioned materials, the presence of Eu^{3+} ions induces the generation of emission lines within the red-to-orange range of the visible spectrum. In the case of $Ca_2La_2O_5$, the primary emission lines are typically concentrated between 611 and 617 nm [43]. This phenomenon can be attributed to the transition of Eu^{3+} ions from higher energy states to lower energy states, as elucidated in the preceding sections. In their study, Wang et al. effectively synthesized Eu^{3+}-doped $Gd_2O_2CN_2$ through the use of a traditional solid-state process involving Li_2CO_3, Eu_2O_3, and GdF_3 [44]. The findings of their study indicate that when $Gd_2O_2CN_2$: Eu^{3+} is excited at a wavelength of 300 nm and at room temperature, it displays distinct peaks in the red emission band at 626 and 614 nm. These peaks arise from the hypersensitive electric dipole transition ($^5D_0 \rightarrow {}^7F_2$) of Eu^{3+} ions. Moreover, an optimal concentration of Eu^{3+} doping of 7.5% was established. Previous studies provided evidence that a decrease in crystallinity leads to a reduction in luminescence intensity. Additionally, an excessive concentration of Eu^{3+} doping was found to introduce several impurities, further diminishing the luminescent properties [44]. This finding provides more evidence for the correlation between the intensity of (photo)luminescence and the concentration of Eu^{3+} doping [44].

1.2.5 Fluorescent vs. phosphorescent red phosphors

Particularly in red phosphors, the inclusion of specific dopants plays a crucial role in tuning emission properties. For example, transition metal ions [32,38] or rare-metal ions [38,35] can be incorporated into the phosphor lattice to achieve desirable emission characteristics, such as fluorescence or phosphorescence, with varying lifetimes. Mn^{4+} doping is a common strategy to obtain deep-red-light-emitting fluorescent phosphors owing to the characteristic transition $^2E_g \rightarrow {}^4A_{2g}$ of Mn^{4+}[46-48]. For example, Liang *et al.* successfully synthesized$Cs_2NaAl_3F_{12}$:Mn^{4+} with excellent color purity by incorporating Mn^{4+} ions into the

octahedral center [46]. Notably, the non-equivalent occupation of Mn^{4+} ions in $Cs_2NaAl_3F_{12}$ facilitated sharp red-light emissions with improved color purity under excitation with blue light. Interestingly, Mn^{4+}-doped red phosphors exhibit a short fluorescence lifetime and are suitable for applications in fast-respond displays [46-48].

Conversely, Eu^{3+} doping is based on the $^5D_0$-$^7F_2$ electric dipole transition of Eu^{3+}. While Mn^{4+} emits red to the deep red color range, Eu^{3+} emits intense red and orange-red light. Hence, even though both strategies are employed in LEDs and other technologies, Mn^{4+} doping is preferred in optoelectronic devices that require precise red colors [46-45]. Moreover, Eu^{3+} ions enable phosphorescent behavior owing to their long-lived excited states [40,49]. Notably, the luminescent color and the luminous properties emitted by Eu^{3+}-doped materials may be tuned by adjusting the doping concentration. In summary, while Mn^{4+} doping facilitates fluorescence attributed to the generation of singlet states, Eu^{3+} doping facilitates phosphorescence attributed to the generation of triplet states [45-48].Hence, depending on the desired material outcome, Mn^{4+} or Eu^{3+} doping may be used to design fluorescent or phosphorescent materials.

1.3 Electronic transitions in rare-earth ions

Rare-earth ions, a group of elements referred to as lanthanides, possess unique electronic properties that make them integral in the development of luminescent materials and devices. The rare-earth elements are normally made up of 17 elements, including 15 lanthanides ranging from La (at. no. 57) to Lu (at. no. 71), as well as Sc (at. no. 21) and Y (at. no. 39). These ions are renowned for their ability to emit light when subjected to external stimuli, but the underlying electronic transitions driving this luminescence are complex and intriguing. At the heart of rare-earth ions luminescent behaviour lays their distinctive electronic configurations. Within their atomic structures, rare-earth ions exhibit partially filled 4f or 5f orbitals, leading to intricate energy-level schemes. It is essential to explore into the various mechanisms governing these electronic transitions to comprehend their luminescent properties, Rare-earth ions are pivotal in the world of luminescent materials due to their intriguing electronic transitions. Figure 1.5 represents the transitions of rare-earth elements in visible range. These transitions encompass f-f transitions, charge transfer mechanisms, energy transfer processes, and interactions with trap levels. The intricacies of these electronic transitions empower researchers to design luminescent materials

tailored for a wide array of applications, from advanced lighting technologies to cutting-edge displays and biomedical imaging. The unique properties of rare-earth ions continue to fuel innovations across diverse technological domains[50-51].

The most characteristic feature of rare-earth ions is their propensity for intra-4f (or 5f) transitions. During these transitions, an electron within the f orbital is excited to a higher-energy f orbital. When the electron returns to its original orbital, it emits photons of specific energies, resulting in sharp, narrow-line emission spectra. These transitions are highly sensitive to the local chemical environment, making rare-earth ions valuable in studying crystal structures and defects [52].

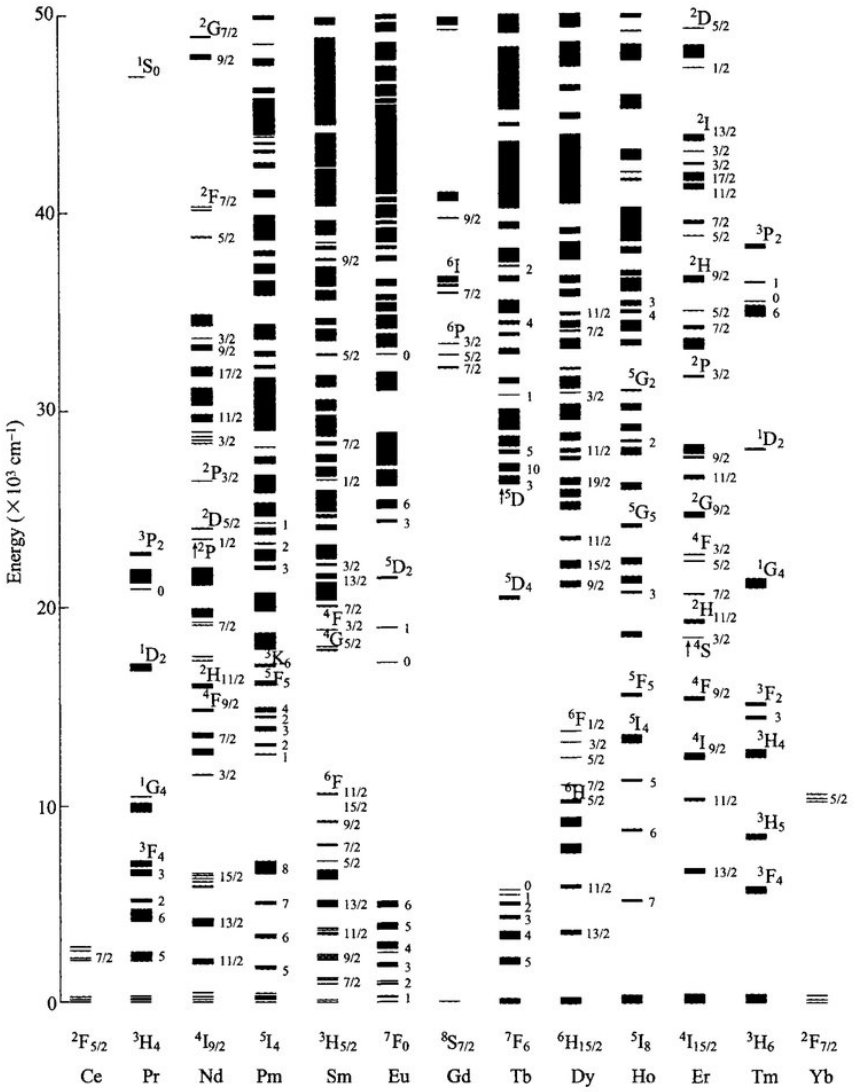

Figure 1.5: Transitions of rare-earth elements

In addition to f-f transitions, rare-earth ions can engage in charge transfer transitions. These involve the transfer of electrons between the rare-earth ion and its surrounding ligands. Charge transfer transitions lead to broader absorption and emissions. Rare-earth ions are adept at transferring energy between themselves or with co-dopants in host materials. This energy transfer mechanism can influence the emission properties of the material. For instance, energy transfer processes can be harnessed to enhance the luminescence efficiency of materials and create customized emission colors in phosphors. Rare-earth ions can interact with trap levels within the host material. These interactions create energy levels that capture and release electrons and holes, leading to phenomena like persistent luminescence [53-54].

1.3.1 Factors influencing doping on the trapping and de-trapping processes.

The luminescent properties of materials have garnered significant attention due to their wide-ranging applications in fields such as energy-efficient lighting, environmental monitoring, and information storage. One key area of research involves the process of "doping," where specific elements are added to materials to enhance their luminescence. This introduction aims to shed light on the factors that influence the effects of doping on the trapping and de-trapping processes in luminescent materials [55].

In the region of enhancing luminescence in materials, several crucial factors come into play. First and foremost is the type and quantity of dopants, which employ a profound influence on a material's luminescent capabilities. Different dopants assume distinct roles, with some adeptly trapping light energy while others facilitate its release. Choosing the right combination of these dopants is similar to selecting the perfect key for a lock. Equally vital are the energy levels of these dopants, which must align harmoniously with those of the material for efficient energy capture and release, resulting in a brighter and enduring glow [56].

The internal arrangement of atoms within the material, known as its structure, is another critical determinant. Altering this structure, whether through composition or arrangement, can significantly impact how dopants interact with the material, thus shaping luminescent properties. Furthermore, the charge carried by dopants whether it is positive or negative, plays a pivotal role in dictating their interaction with light and electrons, thereby influencing luminescent behavior [57].

Temperature regulation is also vital since higher temperatures hasten the release of trapped energy. In comparison, lower temperatures slow it down, and the duration and intensity of light exposure can further modulate the material's luminescence. Doping introduces defects into the material's structure, which serve as both traps and release sites for energy. The density and distribution of these defects are key determinants of luminescence. In conclusion, the luminescent properties of these materials can evolve, necessitating an understanding of how the introduced defects change over time for long-term performance [58].

Moreover, traps can capture excited electrons, prolonging the lifetime of the excited states and facilitating long-lasting phosphorescence. Common synthesis methods to induce traps include solid-state reactions, high-temperature processes, and sol-gel methods [59]. Alternatively, phosphor-containing exciplexes offer a valid approach to achieving OLED devices with superior performance and longer lifetimes. Moreover, phosphorescence in red phosphor can be achieved by employing a synthesis method that creates defects and traps in the lattice of the host material [60].

1.3.2 Multiple-center doped materials in phosphorescence

Multiple-center doped materials in phosphorescence have emerged as a subject of increasing interest over the past two decades. Specifically, these materials are composed of alkaline earth metal fluorides such as CaF_2, SrF_2, and BaF_2 doped with rare earth ions, including but not limited to Y, La, and Lu [61].These compounds form solid solutions with a fluorite crystal structure, accommodating significant levels of rare earth doping, typically up to 40–50 mol%. In these structures, additional fluoride ions occupy octahedral holes within the fluorite lattice, forming diverse defect clusters [62]. These rare earth-doped alkaline earth metal fluorides have garnered attention across a wide range of applications, including surface coatings, dental materials, bio-labelling, lamps, displays, and photovoltaic devices [63].

Their exceptional luminescent properties result from their low phonon energies, which minimize non-radiative relaxation processes, setting them apart from oxide-based matrices. Notably, the phonon energies differ among the alkaline earth metal fluorides, with values of 466 cm^{-1} for CaF_2, 366 cm^{-1} for SrF_2, and 319 cm^{-1} for BaF_2, contrasting with 350 cm^{-1} for $NaYF_4$, which is another commonly used matrix for photon up conversion systems. The presence of rare earth impurities in $NaYF_4$ can lead to unwanted changes in luminescence properties, making rare earth-free matrices

like CaF_2 and SrF_2 more appealing. While there are numerous reports on the synthesis and characterization of rare-earth-doped CaF_2 and SrF_2 nanoparticles, BaF_2 remains relatively underexplored, often yielding larger particles prone to agglomeration [64].

1.4 Properties

Phosphor systems possess remarkable optical properties crucial for enhancing color rendition in displays. These properties, including tunable emission spectra, color purity, luminance, photostability, Stokes shift, and color mixing, play pivotal roles in achieving vibrant and accurate colors on screens. By engineering emission spectra, phosphors enable a broad and precise color scale, which is vital for reproducing real-world colors. Their color purity ensures vivid and true-to-life hues, which are critical for professional applications. Adjusting luminance and brightness enhances the visual impact, while photostability maintains color consistency over time. Stokes shift minimizes energy loss, increasing energy efficiency and reducing heat generation. Additionally, color mixing and blending permit nuanced shades and gradients, particularly in OLED displays, contributing to stunning visuals and precise color control.

1.4.1 Optical properties

Phosphor systems possess an extraordinary ability to absorb energy, often in the form of photons or electrons, and subsequently emit light in a controlled and precise manner. One of the key properties defining the effectiveness of phosphor systems in improving color rendition is their tunable emission spectra [16]. These materials can be engineered to emit light across a broad range of wavelengths, covering the entire visible spectrum. This tunability enables display manufacturers to fine-tune the spectral characteristics of phosphors to match the desired color scale. As a result, phosphor systems play a vital role in achieving color accuracy, ensuring that the colors displayed on screens are dependable [65]. Phosphor systems are esteemed for their photostability; unlike organic dyes or pigments that may degrade over time with prolonged light exposure, these advanced materials exhibit flexibility and durability [66]. This property ensures that the emitted light remains consistent and reliable throughout the lifespan of the display. Phosphor systems offer the advantage of substantial Stokes shifts. This characteristic minimizes energy loss and heat generation, contributing to the energy efficiency and prolonged existence of display devices [67].

The optical properties of various phosphor systems play a pivotal role in improving color rendition in displays. In the modern world of technology and visual experiences, the accuracy and vibrancy of colors displayed on screens are of dominant importance. Achieving colors that captivate and engage viewers requires a deep understanding and manipulation of the optical properties of phosphor systems. These properties encompass a spectrum of characteristics that encompass emission spectra, color purity, luminance, and brightness, photostability, Stokes shift, color mixing, and more. Each of these properties plays a unique and indispensable role in the intricate dance of light and materials [68].

1.4.1.1 Emission spectra

At the sensitivity of the optical phenomenon that is phosphor systems lies the property of emission spectra. It is through the precise engineering and manipulation of emission spectra that displays can generate a rich and diverse of colors. These spectra are like the artist's palette. Phosphor materials have the extraordinary ability to emit light at specific wavelengths when excited by external energy sources [69]. This tunable emission capability means that phosphor systems can be tailored to emit light across the entire visible spectrum. By selecting phosphors with distinct emission peaks at different wavelengths, display technologies can achieve a broad and accurate color scale, which makes it possible to reproduce the full spectrum of colors in displays, from the deepest blues to the purest reds and greens. For example, in the case of LED (Light Emitting Diode) displays, different phosphors are strategically used to emit red, green, and blue light. These primary colors can then be combined in various proportions to produce a wide range of intermediate colors [70].

1.4.1.2 Color purity

The detection of vibrant and accurate colors leads us to the property of color purity. Color purity is all about ensuring that the colors emitted by the display are pure and saturated. In other words, they are devoid of impurities or tints that could distort the intended color. Phosphor systems excel in delivering pure and saturated colors. This optical property is crucial for achieving high-quality color rendition because it prevents any dilution or distortion of colors. When viewers see a vibrant red or a brilliant blue on their screens, it is the result of phosphor systems emitting colors with

exceptional purity. This property is particularly evident in displays that rely on phosphors, such as LED-based displays, where colors are pure and realistic. The purity of colors is not only aesthetically pleasing but also important for maintaining color accuracy in professional applications such as graphic design, photography, and video editing. In these fields, achieving precise color reproduction is essential, and the purity of colors emitted by phosphor systems ensures that the displayed colors match the intended colors [71].

1.4.1.3 Luminance and brightness

Luminance and brightness are optical properties that define the intensity of emitted light. These properties are especially relevant in displays that aim to deliver dynamic and visually engaging content. Phosphor systems offer the flexibility to emit light at varying levels of intensity, allowing for adjustments in luminance and brightness [72], which is particularly important in displays where the perceived brightness of colors can greatly impact the viewing experience. Phosphors that emit light at different intensities enable the creation of dynamic visual effects and enhance the overall impact of the content. The control of luminance and brightness is not limited to the intensity of light emitted by individual phosphors [73]. It also involves techniques such as dimming and local dimming, where specific areas of the display can be adjusted to emit light at different intensities.

1.4.1.4 Photostability

One of the remarkable optical properties of phosphor systems is their photostability. This property ensures that the colors displayed on screens remain consistent and stable over time, even with prolonged exposure to light. Photostability is a critical factor for maintaining the quality of color rendition throughout the lifespan of a display. Unlike organic dyes or pigments that may fade or change color with extended use, phosphor systems are renowned for their resilience to degradation [74]. Photostability is particularly important in professional and commercial usage where displays are in constant use. In applications such as digital displays, medical imaging, and public displays, the consistency of colors is crucial for conveying information accurately and maintaining true colors.

1.4.1.5 Stokes Shift

The optical property known as the Stokes shift is a fascinating phenomenon associated with many phosphor systems. It refers to the difference between the absorption and emission wavelengths of a material. A substantial Stokes shift is advantageous because it minimizes energy loss and heat generation during the conversion of energy from one form to another. In the context of displays, this property enhances energy efficiency. When a phosphor material absorbs light and then re-emits at a slightly longer wavelength, less energy is lost as heat [75], which means that more of the energy is converted into visible light, making the display more energy efficient. Stokes shift is relevant in applications where energy conservation is a priority, such as portable devices and energy-efficient lighting.

1.4.1.6 Color mixing and blending

The optical properties of phosphor systems also enable color mixing and blending. This capability allows for the creation of a wide range of intermediate colors by strategically combining phosphors with different emission spectra. It is particularly valuable in displays that use color-blending techniques to produce nuanced shades and hues. When viewers observe smooth gradients and transitions between colors on display, they observe the result of precise color mixing and blending. Phosphors can be arranged in pixel arrays or sub-pixels, each emitting a primary color (red, green, or blue). By adjusting the intensity of each primary color, a display can produce an infinite range of intermediate colors. This property is exploited in technologies like OLED (Organic Light Emitting Diode) displays, where color blending at the pixel level allows for precise color control and the creation of stunning visuals [76].

1.4.2 Morphological properties

The development of display technology achieving superior color rendition is an ongoing detection driven by advancements in physical chemistry principles. While optical properties have traditionally been the focus of color enhancement efforts, it has become increasingly evident that the morphological properties of phosphor systems are equally crucial in shaping the quality of color rendering in displays. In this exploration, we delve into the world of morphological properties and their influence on the enhancement of color rendition in displays, guided by the principles of

physical chemistry. To illustrate these principles, we will examine various examples that highlight the significance of morphological properties in display technology.

1.4.2.1 Particle size and shape

Particle size and shape constitute fundamental morphological properties that are intimately connected to the principles of quantum mechanics and spectroscopy. Within the context of phosphor systems, particularly quantum dot-based displays, these properties play a pivotal role in dictating the emitted colors. In quantum dots, which are nanoscale semiconductor particles, size-dependent quantum confinement effects. These effects stem from the quantum mechanical confinement of charge carriers within the semiconductor nanoparticles [77]. Smaller quantum dots exhibit wider bandgaps and emit higher-energy photons, yielding colors in the blue and violet regions of the spectrum. In contrast, larger quantum dots with narrower bandgaps emit lower-energy photons, contributing to the display's red and orange hues like cadmium selenide (CdSe) quantum dots. The principles of quantum confinement dictate that smaller CdSe quantum dots will emit blue light while larger ones will emit red. By precisely controlling the size of these quantum dots, display engineers can tailor the emitted colors to create a broad and accurate color scale [78].

1.4.2.2 Crystal structure

The crystalline structure of phosphor materials is intrinsically tied to the principles of solid-state physics. Crystallography governs the arrangement of atoms within the crystal lattice, which, in turn, influences the efficiency of energy conversion and, consequently, the emitted colors. YAG (Yttrium Aluminum Garnet) phosphors serve as an exemplary illustration of the importance of crystal structure. YAG materials are deliberately engineered to exhibit specific crystal structures that optimize color purity. These arrangements of atoms within the crystal lattice determine the efficiency of energy conversion when the phosphor is excited by an energy source, such as blue or ultraviolet light. As a result, YAG phosphors efficiently convert this energy into visible light, generating vivid and pure colors [79]. The physical principles underpinning YAG phosphors involve electron transitions within the crystal lattice. These transitions are regulated by the energy levels and band structures characteristic of the crystal's atomic arrangement. YAG's crystal

structure aligns these energy levels in a manner that minimizes energy loss and maximizes color purity.

1.4.2.3 Surface coating and modifications

Surface properties and modifications are intricately connected to surface chemistry and materials science principles. In the context of phosphor-converted LEDs, these properties can significantly impact luminescence efficiency and color rendition. Consider the application of nanoscale coatings on phosphor particles, these coatings are engineered to improve the luminescence efficiency of the phosphors. Surface chemistry principles come into play as these coatings serve to reduce surface defects and optimize light extraction. The result is the enhanced energy conversion efficiency, leading to greater brightness and improved color rendition. Surface modifications also involve electron-hole recombination rates on the phosphor's surface. This optimization mitigates non-radiative recombination processes and enhances the probability of radiative recombination, which is responsible for the emission of photons. These modifications can thus significantly impact the overall efficiency of phosphor-converted LEDs, resulting in displays that produce colors with greater intensity and accuracy [80].

1.4.2.4 Uniformity and distribution

Uniformity and distribution of phosphor particles within a display matrix are vital for achieving consistent color rendition. In micro-LED displays, uniform distribution of phosphor materials at the sub-pixel level is critical for producing consistent and uniform colors across the screen. Irregularities in the distribution & particle size can result in noticeable variations in the displayed colors, degrade from the overall quality of the visual experience. To achieve consistent color rendition, researchers must ensure that the red phosphor particles are evenly distributed and uniformly integrated into the sub-pixel structure, which involves applying principles of materials engineering and statistical thermodynamics to optimize the placement and distribution of phosphor materials, ensuring that they emit colors with fidelity and consistency [81].

1.4.2.5 Micro- and nanostructures

Micro and nanostructures within phosphor materials introduce a group of precision that influences display performance. These structures manipulate the interaction of incident light and are rooted in principles of optics and materials science. Photonic crystals with micro and nanostructures are employed to create structural coloration effects. These effects arise from the interaction of incident light like finely structured materials. Rather than relying on traditional pigments or dyes, structural coloration is a manifestation of principles of optics and materials science. The micro- and nanostructures within these crystals interact with incident light in such a way that they selectively reflect certain wavelengths, creating bright and pure colors. This phenomenon is intricately linked to principles of optical interference and diffraction, where the structural features of the material dictate the wavelengths of light that are reinforced and reflected. This approach not only enhances color rendition but also offers advantages in terms of power efficiency and environmental sustainability, as it reduces the need for conventional color filters and pigments [82].

1.4.3. Structural properties

Structural properties of phosphor systems doped with rare earth ions are critical in improving color rendition in lighting and display technologies. These properties encompass crystal structure, lattice parameters, dopant positioning and concentration, and host material composition. By carefully manipulating these structural aspects, researchers can change the optical behavior of phosphors to achieve the desired color rendering performance, ensuring that colors appear bright, natural, and accurate in various applications.

1.4.3.1 Crystal structure and its influence

The crystal structure of a phosphor material is one of its most important structural properties. It determines the arrangement of atoms or ions within the crystal lattice, and this arrangement plays a pivotal role in dictating the optical behavior of the material. Different crystal structures can exhibit unique advantages and challenges in terms of color rendition. For instance, cubic crystal structures, such as those found in garnet-type phosphors like YAG:Ce (Yttrium Aluminum Garnet doped with Cerium), are renowned for their excellent thermal stability and high quantum efficiency [83]. These materials are widely used in white LED lighting due to their ability to convert blue or

UV excitation into broad-spectrum white light efficiently. On the other hand, hexagonal or trigonal crystal structures, often found in nitride-based phosphors like Eu-doped AlN (Aluminum Nitride), offer narrow emission peaks and high color purity, which makes them particularly suitable for applications where precise color rendering is essential, such as in displays and hoardings. It impacts not only the emission spectrum but also factors like thermal stability, which is crucial for the longevity of lighting and display devices.

1.4.3.2. Lattice parameters and emission tuning

Lattice parameters, including lattice constants and unit cell volume, are structural properties that decide the spacing and arrangement of atoms or ions within the crystal lattice. Variations in these parameters can lead to significant changes in the emission properties of the phosphor. One of the most notable effects of tuning lattice parameters is the shifting of the emission wavelength. By precisely controlling the lattice parameters during synthesis, researchers can achieve required emission spectra. This ability to tune emission wavelengths is invaluable in applications where specific colors are required, in the film and television industry for producing accurate and pure colors on screens. Additionally, lattice parameters can influence other optical properties, such as the bandwidth of emission peaks. Narrower emission bands are desirable in applications where color purity is critical, as they prevent spectral overlap and improve the rendering of a broader range of colors [84].

1.4.3.3 Dopant position and concentration

Rare earth ions, such as Cerium (Ce), europium (Eu), and terbium (Tb), are introduced as dopants within the crystal lattice of phosphor materials. The exact position of these dopants within the lattice and their concentration are vital structural properties that profoundly affect the color rendition capabilities of the material. The position of the dopant ions within the lattice determines interactions with the host ions and this resulting energy level transitions responsible for luminescence. For instance, some dopant ions may replace host ions in the lattice, while others may occupy interstitial sites. The choice of dopant and its position can influence the efficiency of energy transfer processes within the material. Doped concentration is another crucial factor. At low dopant concentrations, the phosphor may not emit sufficient light, leading to poor color rendition.

Conversely, high dopant concentrations can result in luminescent quenching, where energy transfer processes become less efficient, reducing the material's overall luminescence. Balancing dopant concentration is a delicate process that requires a thorough understanding of the material's structural properties [16].

1.4.3.4 Host material composition and its impact

The host material in which rare earth ions are embedded is a significant structural property that determines many aspects of the phosphor's optical performance. Different host materials possess distinct properties, including bandgap energy, crystal symmetry, and thermal stability, all of which influence the efficiency and spectral characteristics of the phosphor's luminescence. Oxide-based host materials, like YAG, are well-known for their high thermal stability and excellent color stability. They are frequently used in white LED applications, where maintaining consistent color temperature over extended periods is essential. Oxide-based phosphors offer a wide range of emission colors and are often used in conjunction with other phosphor materials to achieve specific color temperatures [85]. Nitride-based hosts, such as AlN, have gained popularity for their wide bandgap energy and excellent thermal properties. These properties make them ideal for high-intensity LED applications where heat dissipation is crucial. Nitride-based phosphors can produce vibrant colors with high color purity, making them valuable in displays and hoardings. Sulphide-based host materials are less common but are valued for their ability to produce deep red and infrared emissions [86].

1.5 Therapeutic applications of phosphors

Phosphors have exhibited remarkable versatility, encompassing a wide range of host materials, including sulphides, aluminates, silicates, germanates, gallates, titanates, nitrides, and oxynitrides, coupled with various doped ions, such as transition metals (e.g., Cr^{3+}, $Mn^{4+,}$ Mn^{2+}) and rare earth ions (e.g., $Eu^{2+,}$ $Ce^{3+,}$ $Tb^{3+,}$ $Pr^{3+).}$ These luminescent materials have found commercial success in applications like emergency boards, luminous paints, and watch dials. Recently, nanoscale phosphors have revolutionized biomedicine. They exhibit continuous light emission for hours after excitation, enabling real-time analyte monitoring with minimal background interference. Phosphors align with the tissue transparency window (650–1800 nm) for enhanced signal-to-noise

ratios and deeper in vivo tissue penetration, which opens exciting possibilities for biomedical applications, including reactivation by LED, NIR light, or soft X-ray sources, offering innovative solutions for healthcare and diagnostics [87].

These phosphors exhibit persistent luminescence, which can be activated in vivo using methods such as X-rays or highly penetrating low-energy red photons [88]. Their utility has expanded to encompass a wide spectrum of critical facets within modern biomedicine, including biosensors, multimodal imaging nanoprobes, targeted in vivo imaging for tumors, cancer therapy, stem cell tracking and therapy, photothermal therapy, and versatile theragnostic nano agents [89]. Despite the significant progress achieved in this relatively short time frame, the integration of phosphors into biomedical applications is still in its nascent stages. Presently, most phosphors are reported to emit in the near-infrared region beyond 1000 nm, offering the advantage of improved image contrast and deeper tissue penetration for enhanced biomedical imaging and therapeutic capabilities.

1.5.1 Photodynamic Therapy (PDT)

Photodynamic therapy (PDT) harnesses the unique properties of rare-earth-doped phosphor materials to revolutionize medical treatments, with notable examples including cancer therapy and dermatological applications. For instance, nanoparticles doped with rare earth ions like ytterbium have been developed for targeted cancer treatment. These nanoparticles can accumulate in tumor tissues and, when exposed to near-infrared light, produce reactive oxygen species (ROS) that selectively damage cancer cells. Similarly, rare earth-doped phosphors have found utility in dermatology, where they are used in PDT for treating skin conditions such as acne and actinic keratosis. By precisely tuning the optical properties of these materials, dermatologists can tailor the therapy to specific skin types and conditions, enhancing its efficacy while minimizing side effects [90].

1.5.2 Fluorescent imaging

Fluorescent imaging using rare earth-doped phosphor materials is a powerful technique that enables the visualization and tracking of biological processes and structures with exceptional sensitivity and precision. These materials, doped with rare earth ions like europium, terbium, or neodymium,

exhibit unique luminescent properties that make them ideal for various imaging applications. One prominent application of rare earth-doped phosphor materials in fluorescent imaging is in bioimaging. These materials are utilized as contrast agents to label specific biomolecules or cellular structures. For instance, europium-doped nanoparticles can be functionalized by targeting molecules such as antibodies or peptides to bind specifically to cancer cells. When excited by light at the appropriate wavelength, these nanoparticles emit highly distinguishable and long-lasting fluorescence signals, which allows researchers and clinicians to track the location and behavior of cancer cells in real-time, facilitating early detection and precise surgical interventions. Rare earth-doped phosphor materials also find use in fluorescence resonance energy transfer (FRET) assays. FRET relies on the distance-dependent energy transfer between a donor fluorophore (commonly a rare earth-doped phosphor) and an acceptor fluorophore. As the distance between the two fluorophores changes, the fluorescence intensity of the donor changes accordingly. This technique is pivotal in studying protein-protein interactions, molecular conformation changes, and signaling pathways within cells [16].

1.5.3 Radiation therapy

Radiation therapy is a crucial medical technique used in the treatment of various diseases, including cancer. Rare earth-doped phosphor materials have gained prominence in this field due to their unique properties and versatility, offering innovative solutions to enhance the effectiveness and precision of radiation therapy. Rare earth-doped phosphor materials, often incorporated into radiation therapy processes, serve as dosimetry tools. Dosimetry is the measurement of radiation dose and its distribution within the target area. It is a critical aspect of ensuring the right amount of radiation is delivered to the diseased tissue while minimizing damage to healthy surrounding tissues. Gadolinium-doped phosphor materials have been employed as radiation detectors in magnetic resonance-guided radiation therapy, which combines real-time imaging from an MRI with precise radiation delivery [91]. The phosphor materials help monitor the radiation dose distribution, allowing for adjustments in real-time, ensuring optimal tumor targeting while minimizing damage to nearby organs [92]. Rare earth-doped phosphor materials in radiation therapy are in the development of scintillation detectors. These detectors utilize materials doped with rare earth ions like Cerium or europium to convert incident radiation into detectable light signals.

1.5.4 Bioluminescence imaging

Rare earth ion-doped phosphor materials in bioluminescence imaging (BLI) represent a significant advancement in the field of molecular and cellular imaging. Their unique optical properties have expanded the capabilities of BLI, enabling highly sensitive and versatile applications in the study of biological processes, disease models, and therapeutic interventions. This convergence of bioluminescence and rare earth materials holds great promise for advancing our understanding of complex biological systems and improving the diagnosis and treatment of various diseases. These materials can be developed to emit light in a controlled and tunable manner, offering several advantages over traditional bioluminescent proteins. For example, europium-doped phosphors have been used to develop reporter systems for BLI.

In this context, cells or organisms are engineered to express a bioluminescent properties fused with europium-doped phosphor nanoparticles. When these cells or organisms are exposed to a specific triggering agent, such as a substrate or external stimulus, the europium-doped phosphors emit strong and stable luminescence, which can be captured and quantified using specialized imaging equipment. One notable application of rare earth ion-doped phosphor materials in BLI is the monitoring of gene expression, protein-protein interactions, and cell tracking within living organisms. By utilizing these materials, researchers can achieve higher sensitivity and improved properties compared to traditional luciferase-based BLI. This enhanced sensitivity enables the detection of subtle biological processes and real-time tracking of cell populations, making it invaluable in fields like cancer research, regenerative medicine, and developmental biology. Phosphors offer the potential for multimodal imaging [93].

1.5.5 Drug delivery systems

Rare earth ion-doped phosphor materials have opened new frontiers in drug delivery systems. Their biocompatibility, tunable optical properties, and responsiveness to external stimuli offer a versatile platform for the development of targeted and therapies. Examples of their applications in cancer therapy highlight their potential to revolutionize the field of drug delivery, offering improved treatment outcomes and reduced side effects for patients. Rare earth ion-doped phosphor materials offer exceptional biocompatibility, low toxicity, and tunable optical properties. These

characteristics are particularly valuable in drug delivery systems designed for targeted therapy. This approach has been employed in the targeted delivery of chemotherapeutic agents to cancer cells, minimizing damage to healthy tissues while enhancing the therapeutic effect.

Phosphor materials can serve as carriers for drugs, genes, or imaging agents. They can be functionalized with surface modifications to enhance their affinity for specific target cells or tissues. For instance, gadolinium-doped phosphor nanoparticles have been used as carriers for magnetic resonance imaging (MRI) contrast agents and anti-cancer drugs. These nanoparticles enable both imaging and therapy, offering a therapeutic approach that provides real-time monitoring of drug delivery and treatment efficacy [94]. Various stimuli, including changes in pH, temperature, or the presence of specific biomolecules, can trigger the controlled release capabilities of rare earth-doped phosphor materials, which enables the development of responsive drug delivery systems that release therapeutic agents precisely when and where they are needed. For example, lanthanide-doped mesoporous silica nanoparticles have been engineered to release drugs in response to changes in pH levels within tumor microenvironments, improving the effectiveness of cancer treatment [95].

1.5.6 Photo Thermal Therapy (PTT)

Phosphor materials hold immense potential in the field of photothermal therapy. Their ability to absorb NIR light and convert it into localized heat makes them valuable candidates for selective tissue ablation and cancer therapy. As research in this area continues to advance, rare earth-doped phosphor materials are poised to play a vital role in the future of PTT and medical therapeutics. Phosphor materials can be engineered to absorb light at specific wavelengths, particularly in the near-infrared (NIR) region where tissue penetration is optimal. When exposed to NIR light, these materials efficiently convert the absorbed energy into heat, resulting in a localized temperature increase. Nanoparticles are doped with rare earth ions such as ytterbium and erbium and can absorb NIR light, emitting higher-energy photons in the visible or ultraviolet range. By functionalizing nanoparticles with targeting ligands and loading them with photothermal agents or drugs, researchers have developed therapeutic nanocarriers. These nanocarriers can specifically accumulate in diseased tissues, enabling both imaging and targeted PTT. Upon exposure to NIR

light, the UCNPs generate heat, while the photothermal agents enhance the therapeutic effect or trigger drug release, making this approach highly versatile for cancer therapy[96].

1.6 Display devices applications of phosphors

Rare earth ions doped phosphors are essential components in a wide array of display devices, where they enhance the visual experience through their luminescent properties. Historically, they have been integral to Cathode Ray Tube (CRT) and Plasma Displays, contributing to the creation of vivid colors. In modern displays, they play a pivotal role in LED backlighting systems, Organic Light-Emitting Diode (OLED) displays, Quantum Dot displays, and laser projection displays, ensuring bright, energy-efficient, and high-quality visuals. These phosphors also make transparent displays, holographic displays, augmented reality (AR), and virtual reality (VR) devices possible, delivering immersive and captivating experiences. Furthermore, they find applications in micro displays for devices such as heads-up displays (HUDs), digital cameras, and camcorders, offering compact yet high-resolution visual output. In summary, rare-earth ions doped phosphors are the unsung heroes behind the scenes of our modern display technologies, enhancing color quality, energy efficiency, and overall performance, and enriching our interaction with screens of all sizes and applications.

1.6.1 Cathode Ray Tube (CRT) displays

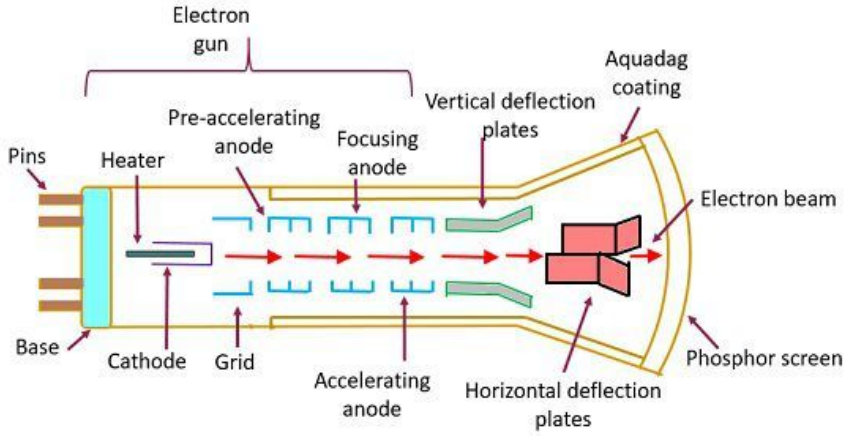

Figure 1.6: Internal structure of CRT

Rare earth doped phosphors have indeed played a pivotal role in the history of display technology, particularly in cathode-ray tube (CRT) displays [97]. Europium-doped yttrium oxide emits red light

when excited by electrons, terbium-doped zinc sulphide emits green light, and europium-doped strontium oxide emits blue light. These emissions, allow for a wide color gamut and vibrant on-screen images. Research has shown that the specific doping concentrations of rare earth elements can be finely tuned to achieve accurate color reproduction. The careful selection and doping of these elements ensure that CRT displays as shown in Figure 1.6 represents a broad spectrum of colors, contributing to the overall visual experience. CRT technology relies on the efficiency of rare earth doped phosphors in converting electron energy into visible light. Studies have focused on optimizing the luminescent properties of these phosphors to enhance display brightness and longevity while minimizing power consumption [98].

1.6.2 Plasma Display Panel (PDP)

Plasma Display Panels (PDPs) as shown in Figure 1.7 are renowned for their ability to produce high-definition, pure, and colorful visuals, and this achievement is primarily attributed to the ingenious use of phosphors within these displays. PDPs employ a combination of noble gases, typically neon and xenon, enclosed in countless small cells. When these gases are electrically stimulated, they emit ultraviolet (UV) light, a non-visible spectrum to the human eye. To translate this UV light into the rich and diverse palette of colors we see on the screen, phosphors play a pivotal role. These phosphors are meticulously engineered, containing rare earth elements like europium, terbium, and cerium, to emit specific colors red, green, or blue when excited by the UV light. The precise composition and characteristics of these phosphors has been extensive, aiming to achieve not only accurate color reproduction but also to enhance the longevity of PDPs and reduce their energy consumption. Optimization has made PDPs particularly valuable in applications demanding exceptional color fidelity, such as professional graphic design and medical imaging, showed their vital role in the evolution of display technology [99].

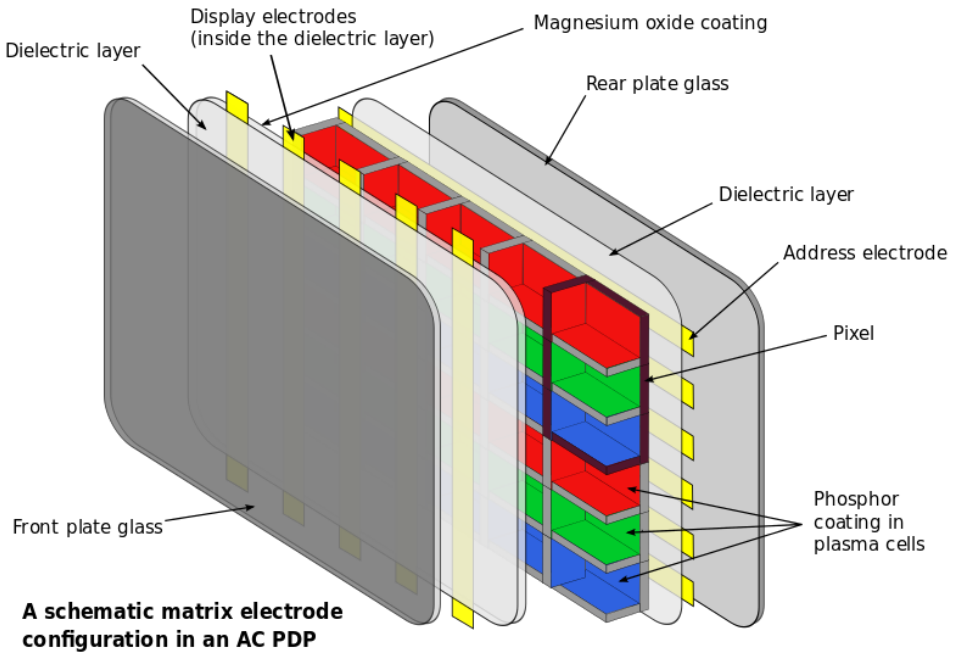

Figure 1.7 : Composition of plasma display panel

1.6.3 Field Emission Display(FED)

Field Emission Displays (FEDs) shown in Figure 1.8 represent an advanced flat panel display technology that harnesses rare earth phosphors to deliver exceptionally bright and vibrant colors along with outstanding image quality and rapid response times. In FEDs, each pixel consists of thousands of tiny electron emitters, typically constructed using carbon nanotubes or other nanostructures, that release electrons when subjected to an applied voltage. These emitted electrons strike phosphor materials that coat the display's surface. Notably, rare earth phosphors are favored for their ability to emit intense and pure colors when bombarded by electrons. Research in this domain has been instrumental in optimizing the performance of FEDs. It has been revealed that using specific rare earth elements like europium, terbium, and yttrium in the phosphors can enhance color purity and efficiency. Moreover, studies have focused on reducing the power consumption and increasing the longevity of FEDs, making them more energy-efficient and environmentally friendly compared to some other display technologies[100-101].

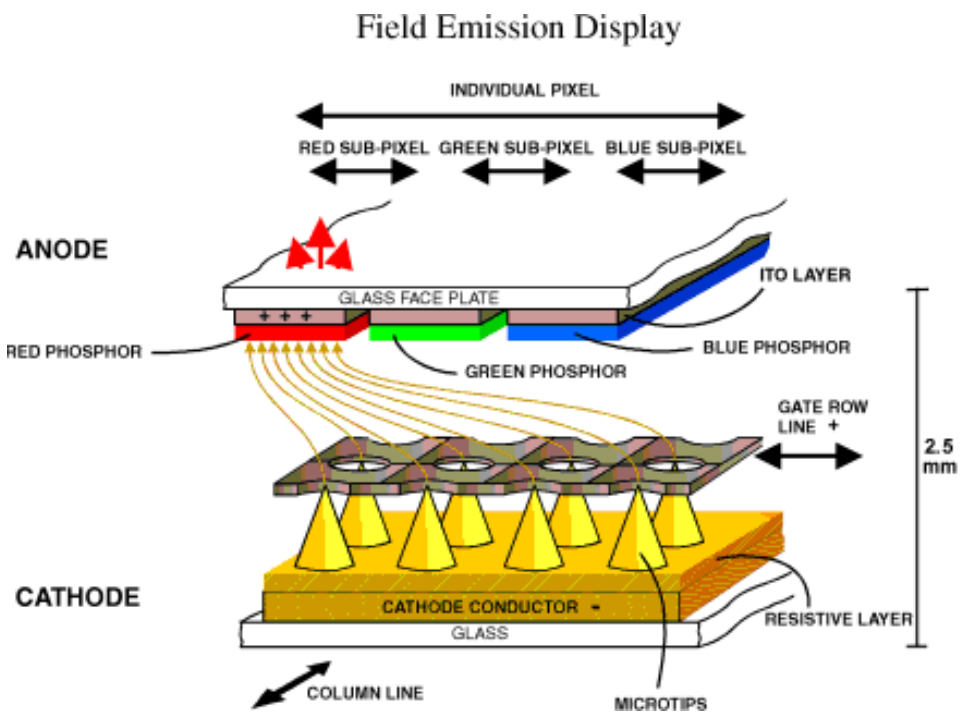

Figure 1.8: Schematic explains the principle of Field Emission Display in FED

1.6.4 LED backlighting

In LED-LCD TVs and computer monitors, the integration of rare earth phosphors into the LED backlighting system has revolutionized display technology. Here, rare earth phosphors serve as a pivotal component in the production of white light, a basic element for rendering a full spectrum of colors on the screen. The underlying mechanism as shown in Figure 1.9 involves using blue LED chips as the light sources, which emit short-wavelength blue light. To transform this blue light into a white light, suitable for display, a layer of rare earth phosphors is applied directly onto the LEDs. These phosphors are meticulously engineered to absorb the blue light and subsequently re-emit it as a broader spectrum of colors, essentially creating a white light source rich in spectral content. Research in this field has been instrumental in fine-tuning the properties of these phosphors to enhance their efficiency, color stability, and longevity. Furthermore, studies have sought to improve color rendering and energy efficiency, with advancements in phosphor formulations contributing to achieving higher color scale and lower power consumption, resulting in LED-LCD displays that offer not only vivid and accurate colors but also environmental

sustainability and energy savings, aligning with the increasing demand for eco-friendly technology solutions[102-103].

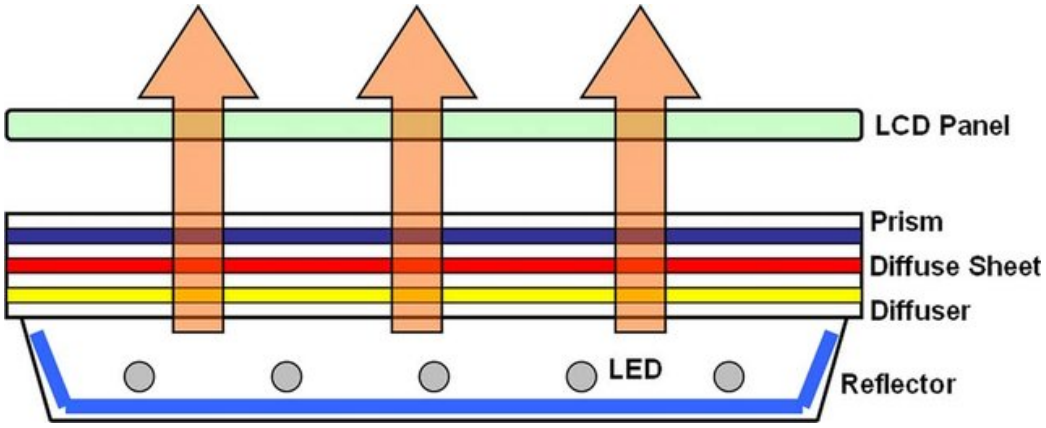

Figure 1.9: Structure of the direct illumination-type LED backlight module

1.6.5 Organic Light-Emitting Diode (OLED)

Organic Light-Emitting Diode (OLED) displays represent a cutting-edge technology that relies on rare earth phosphors as emissive layers as shown in Figure 1.10 to produce red, green, and blue light emissions, thereby yielding thin, flexible, and highly energy-efficient displays. In OLEDs, each pixel comprises organic materials, including rare earth-based phosphorescent materials like iridium complexes and europium chelates, integrated into the emissive layers. These phosphors, when subjected to an electric current, emit light directly, eliminating the need for a separate backlight as seen in traditional LCDs. Research in OLED technology has been pivotal in enhancing the efficiency and performance of these displays. Studies have delved into the development of new rare earth phosphors with improved luminance and longer lifespans, driving advancements in OLEDs' color accuracy and brightness levels. Moreover, research efforts have focused on achieving even greater flexibility, enabling curved and foldable OLED screens. The result of this research is a display technology known for its incredibly true colors, deep blacks, fast response times, and remarkable energy efficiency, making OLED displays the preferred choice for premium smartphones, high-end televisions, and emerging applications like wearable electronics and flexible screens. The constant evolution of rare earth phosphor-based OLEDs continue to push the

boundaries of display technology, offering exciting possibilities for the future of visual displays[102][104].

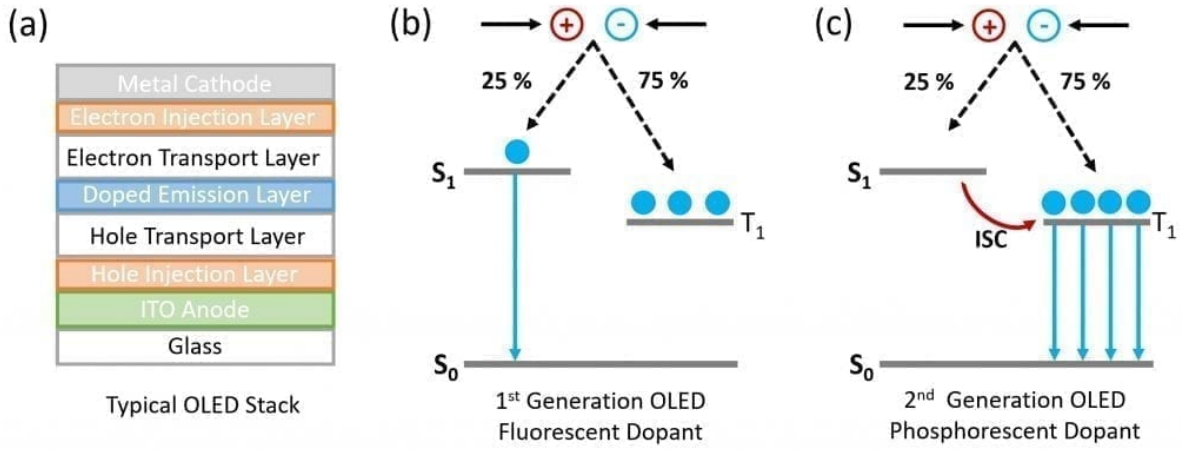

Figure 1.10 : Schematic of (a) layers in a typical bottom emitting OLED stack and mechanism of emission in (b) fluorescent doped OLEDs and (c) phosphorescent doped OLEDs

1.7 Literature survey

This section broadly explores and analyzes existing research in the fields of phosphor materials, display technologies, and therapeutic applications, with a specific focus on understanding the current state-of-the-art in phosphor development, color rendering techniques, and their potential applications in both display technology and therapeutic lighting. This survey seeks to identify gaps, challenges, and opportunities in the existing literature, represent the way for innovative contributions to the development of multifunctional phosphor systems that can significantly enhance color quality in displays while also exploring their potential for therapeutic uses, such as bioluminescence imaging, drug delivery system, phototherapy etc.,

1.7.1 Various types of phosphor hosts materials

Phosphor-converted light emitting diodes (pc-LEDs) represent a significant leap forward in lighting technology, offering a multitude of advantages over traditional lighting sources. Their remarkable attributes, including high luminous efficiency, energy efficiency, durability, environmental friendliness, and extended operational lifespan, have positioned pc-LEDs at the forefront of the lighting industry [105-106]. At the core of pc-LEDs lies the ingenious use of

phosphors, which are integrated into the LED system to enhance light emission. Phosphors as shown in Figure 1.11 can be either applied directly to the LED chip or distributed on the walls of the encapsulant, and they play a pivotal role in transforming the primary light emitted by the LED chip into a broader and more usable spectrum. Inorganic phosphors doped with lanthanide ions have become the cornerstone of pc-LEDs.

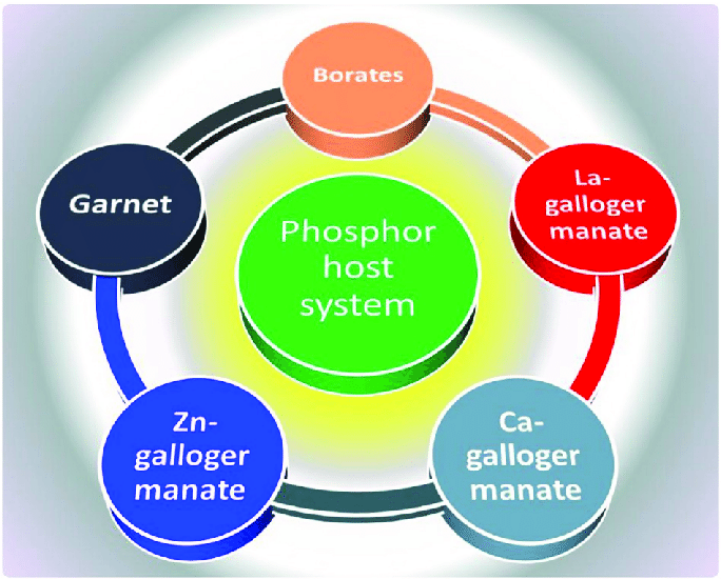

Figure 1.11 : Various types of phosphor hosts materials

Lanthanides, often referred to as rare earth elements, belong to the f-block series of the periodic table. They possess a unique property that makes them ideal for pc-LEDs: the ability to absorb UV or near-UV light and re-emit this energy in the form of visible light. This property is leveraged to achieve efficient color conversion in pc-LEDs, enhancing their color quality and rendering capabilities. It's worth noting that while the lanthanide series includes actinides, these elements are typically excluded from phosphor applications due to their radioactive nature, underscoring the importance of safety and non-toxicity in lighting technologies. Apart from lanthanum (La) and lutetium (Lu), all lanthanides have the capacity to exhibit luminescence in their +3-oxidation state. Europium (Eu) stands out among these elements as it possesses the unique ability to exhibit luminescence in both +2 and +3 oxidation states, making it a versatile choice for tuning the emission spectrum of pc-LEDs [107–115].

While lanthanides take center stage in the region of pc-LED phosphors, there are other elements that have also shown promise as luminescent dopants. Transition metals like copper (Cu), manganese (Mn), and chromium (Cr) have displayed luminescent properties and can exist in various oxidation states, such as +1, +2, +3, and +4, which makes them versatile activators within a host matrix. The host matrix serves as the inert material that holds the luminescent activators, and it can encompass a wide range of compounds, including oxides, nitrides, phosphates, fluorides, borates, sulfates, aluminates, silicates, sulfides, tungstate, vanadate, molybdates, and more. Importantly, the host matrix should possess a band gap within the range of 3 to 5 electron volts (eV) to be considered suitable for phosphor applications. In many cases, the host material is non-luminescent on its own, requiring the presence of a luminescent ion or activator to initiate luminescence. However, even with an activator, some host materials may not efficiently absorb and convert energy into luminescence emission. In such instances, sensitizer ions come into play, acting as intermediaries that efficiently absorb energy and transfer it to the activator. This process significantly enhances the overall luminescence emission of the phosphor.

Host materials exhibit a range of behaviors, and some are capable of absorbing UV light and emitting near-UV or visible light without the need for an activator. These host materials are known as host luminophores, and they are recognized for their ability to directly emit light. It's important to note that for a phosphor to be effectively employed in a pc-LED, it must exhibit strong absorption in the UV or near-UV range and efficiently emit visible light. Furthermore, the transitions responsible for excitation and emission should not be forbidden, ensuring that the energy transfer and conversion processes occur smoothly [115-120].

One of the earliest known phosphor materials is zinc sulfide (ZnS), which has been used as a phosphorescent material since the early 19^{th} century. In the context of modern display technologies and lighting, the development of phosphor materials, such as the use of europium-doped yttrium oxide (Y_2O_3:Eu) as a red phosphor or cerium-doped yttrium aluminum garnet (YAG:Ce) as a yellow phosphor, began in the mid-20^{th} century. Hashimoto et al., in 1991 reported thermal quenching in (La,Ce)PO_4:Tb phosphors through borate substitution or thorium doping results in consistent light emission over a broad temperature range (20-350°C). This is attributed to the complete trivalent conversion of cerium ions, offering potential advancements in stable phosphor materials for lighting and display applications [121].

Few studies reported the analysis of Cu^+activated alkaline earth sulfide phosphors, specifically $MgS:Cu^+$, $CaS:Cu^+$, $SrS:Cu^+$, and $BaS:Cu^+$. Through meticulous examination, this investigation reveals critical details, including emission and excitation spectra, along with temperature-dependent excitation efficiency variations, for these materials at temperatures ranging from 16 to 293 K. Notably, the presence of two distinct bands in the excitation spectra, attributed to Cu^+ ion intra-ionic transitions, is a prominent observation. Furthermore, the elucidation of the luminescence mechanism via the isolated Cu^+ ion model offers valuable insights. Particularly intriguing is the temperature dependence of excitation efficiency, indicating an off-center positioning of Cu^+ ions within the sulfur octahedron in the cases of CaS, SrS, and BaS [122].

In 2011 Setlur et al investigates crucial structural and luminescence properties of fluoride and oxyfluoride phosphors, notably $(Sr,Ca)_3(Al,Si)O_4(F,O):Ce^{3+}$ for yellow-green emission and $K_2TiF_6:Mn^{4+}$ for red emission. These phosphors show promise in bridging the gap in spectral and efficiency requirements for high-efficacy LED lighting. Notably, the study showcases LED lamps achieving warm-white illumination (3088 K), boasting a high color rendering index (CRI) of 90, and an impressive efficacy of nearly 82 lm/W. This efficacy level represents a substantial advancement, reaching nearly 85% of comparable cool-white lamps utilizing conventional $Y_3Al_5O_{12}:Ce^{3+}$based phosphors. Consequently, this research significantly narrows the efficacy divide between warm-white and cool-white LED lamps employing phosphor down conversion, with substantial implications for improved lighting technologies [123].

Previous studies reported the synthesis and optical characteristics of phosphors. These phosphors offer a versatile spectrum of emission colors, achieved by manipulating crystal field splitting and energy transfer mechanisms. Intriguingly, co-doping induced variations in the emission ratio, accompanied by compelling evidence of energy transfer, supported by spectral overlap and decay lifetime data. The culmination of this research led to the creation of a trichromatic white light emitting diode (LED), integrating specific phosphor blends to emit high-quality white light with a correlated color temperature of 6303 K, a color rendering index of 87.4, and color coordinates closely resembling ideal white light. These findings underscore the potential of the phosphor blend for advanced white n-UV LEDs [124].

Xie and team reviewed the synthesis, luminescence characteristics, and practical applications of rare earth-doped nitridosilicate phosphors. Notably, a novel family of luminescent materials has emerged within the M-Si-Al-O-N (M = Li, Ca, Sr, Ba, La) system. These phosphors exhibit intriguing luminescent attributes, including red-shifted excitation and emission, minimal Stokes shift, resistance to thermal quenching, and impressive conversion efficiency. Consequently, they have become instrumental in the development of white light-emitting diodes (LEDs), offering tunable color temperatures and high color rendering indices [125]

Chen et al in 2012 presents a systematic exploration of the physical properties and multifunctional roles of star-shaped 1,3,5triazine-based ET-type hosts with distinct peripheral groups, namely T2T, 3N-T2T, 3P-T2T, and oCF3-T2T. Notably, the incorporation of N-heterocyclic polar peripheries onto the 1,3,5-triazine core yields substantial advantages in terms of electron injection and transport characteristics. This enhancement opens up exciting possibilities for the development of efficient Phosphorescent Organic Light-Emitting Diodes (PhOLEDs) with simplified device configurations. Among these innovative hosts, 3P-T2T stands out as a versatile material capable of serving as both an excellent host and electron-transport medium in various Ir-based electro phosphorescence devices. These PhOLEDs, sharing identical device structures, have demonstrated remarkable performance metrics. They exhibit low operating voltages and achieve impressive external quantum efficiencies for colors spanning from sky blue, green, yellow, red, to even white. This comprehensive exploration underscores the significant potential of these novel triazine-based hosts in advancing the field of organic optoelectronics, offering efficient and versatile solutions for advanced PhOLED technologies [126].

Dai in 2012 reported the intriguing properties of Eu^{3+}doped $Y_2Ti_2O_7$, a pyrochlore-structured compound synthesized through high-temperature solid-state reactions. This material exhibits a remarkable and thermally stable orange-red emission when excited by near-ultraviolet light. A key observation is that the concentrations of Eu3+ activators exert a significant influence on both the intensity and color point of the photoluminescence emitted by $Y_{2-x}Ti_2O_7:xEu^{3+}$ phosphors. The research identifies an optimal doping concentration at x = 0.45, determined by maximizing photoluminescence intensity. At this concentration, a specific luminescence branch ratio (R) for the $^5D_0$–$^7F_2$ and $^5D_0$–$^7F_1$ transitions reaches its peak at approximately 0.46. Furthermore, the orange-red emitting $Y_{1.55}Ti_2O_7:0.45Eu^{3+}$ phosphor demonstrates exceptional thermal stability in its

luminescence intensity, retaining an impressive 84% of its room-temperature luminescence even at a high temperature of 250°C. These findings suggest that $Y_{1.55}Ti_2O_7:0.45Eu^{3+}$ phosphors hold significant promise as components for generating orange-red light in white light-emitting diodes, particularly in high-power applications. This review underscores the potential of this material in advancing LED technology for enhanced lighting solutions [127].

1.7.2 Rare-earth-doped phosphor hosts materials

Figure 1.12 shows the periodic table of the elements exhibiting Luminescence. In recent years, there has been a growing interest in rare-earth-doped oxynitride green-emitting phosphors due to their remarkable properties, including wide excitation spectra, narrow emission bands, high thermal stability, and high quantum efficiency [128]. Among these, the family of Eu^{2+} activated $MSi_2O_2N_2$ (where M = Ca, Sr, or Ba) and $Ba_3Si_6O_{12}N_2$ phosphors has gained significant attention due to their relatively simple synthesis methods. However, the commercial applications of these phosphors have been limited by their poor thermal quenching properties and thermal stability. On the other hand, β-SiAlON:Eu green phosphor has seen large-scale application in high-end LCD backlight displays. The SiA1ON ceramic is a silicon oxynitride compound known for its unique

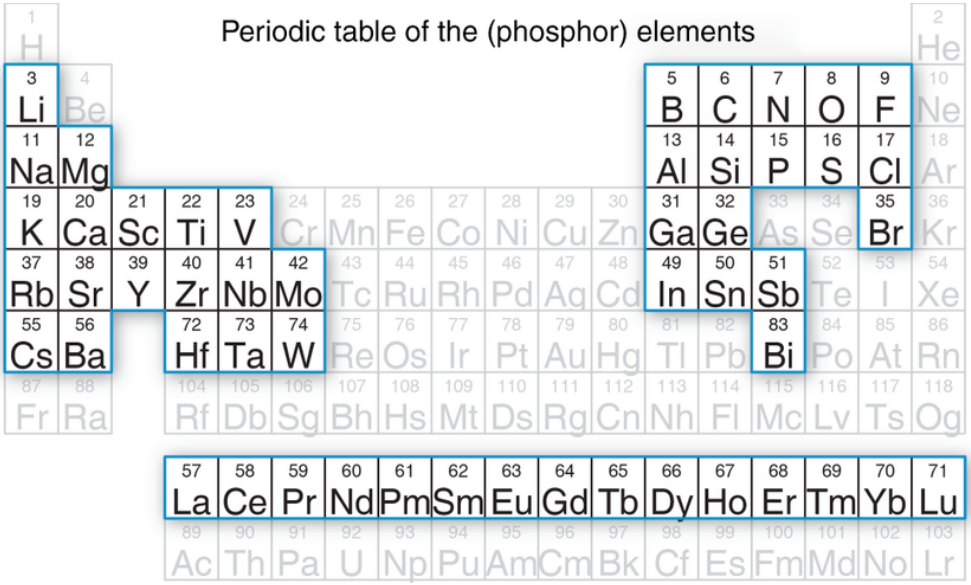

Figure 1.12 : Periodic table of phosphor elements

(Si,Al)(O,N) tetrahedron structure unit, which exists in two crystal forms, namely α-type and β-type. Research has shown that Eu^{2+}doped α-sialon emits blue light under ultraviolet excitation, while Mn^{2+} doped α-sialon emits orange-red light. β-SiAlON, characterized by its chemical

formula $Si_{6-z}Al_zO_zN_{8-z}$, has a hexagonal crystal system, and can accommodate activators such as Eu^{2+} along the channel in its lattice structure. The excitation and emission spectra of β-SiAlON:Eu^{2+} reveal a broad excitation band, making it effective for activation under near-ultraviolet (NUV) or blue light [129].

Studies have explored the influence of 'z' values, which represent the number of Al-O substituting for Si-N, on the crystal structure and luminescent properties of β-SiAlON: Eu^{2+}. It was found that smaller 'z' values resulted in higher phase purity and shorter emission wavelengths. Moreover, β-SiAlON: Eu^{2+} has demonstrated excellent thermal stability, with luminescence intensity remaining high even at elevated temperatures. Post-treatment in a reducing atmosphere at high temperatures has been shown to enhance its luminescent properties [130]. Additionally, the introduction of additives such as oxides and fluorides has been found to increase luminescence intensity by improving crystallinity [131].

$Ba_3Si_6O_{12}N_2$, with its trigonal crystal system, is another notable green-emitting phosphor that emits light at 525 nm and is suitable for white LED applications. The emission peak shifts towards the red as the amount of Eu^{2+} doping increases. This phosphor exhibits good luminescence even at 200°C, making it suitable for high-temperature applications. The introduction of Mg^{2+} has been shown to enhance luminescence intensity [132]. Moreover, the choice of flux during synthesis plays a crucial role in obtaining high-quality luminescent properties, with H_3BO_3 proving to be particularly effective due to its contribution to higher crystallinity [133].

The alkaline earth metal oxynitride silicates in a monoclinic lattice structure are studied with various space groups, depending on the specific metal (M=Ca, Sr, Ba). These compounds have been found to have better luminescent properties when synthesized via the solid-phase method [97]. The incorporation of co-dopants, such as La^{3+} and Gd^{3+} has also been explored for materials like $CaSi_2O_2N_2$:$Eu^{2+,}$ with mixed results. Co-solvents, particularly $CaCl_2$, have been shown to enhance crystallinity and luminescence intensity [134]. The addition of Mg^{2+} can improve luminescence intensity, with the interaction between ions decreasing as Mg^{2+} content increases [135]. Additionally, γ-AlON: Mn^{2+} is a green-emitting phosphor with a single crystal spinel phase structure. It emits light at 520 nm under 455 nm excitation and exhibits narrow emission bandwidth, making it suitable for LED applications. The introduction of Mg^{2+} into the lattice has been found

to enhance luminescence intensity [102] . This material exhibits excellent luminescence even at 150°C, with quantum efficiencies varying based on Mg^{2+} content [136].

$Ca_3SC_2Si_3O_{12}:Ce^{3+}$ is another green-emitting phosphor that performs well, with a broad emission spectrum centered at 504 nm and excitation maxima in the range of 440-460 nm. It is used in blue InGaN LEDs, demonstrating high luminous efficacy of optical radiation and a linear response with increasing applied voltage [137]. Similarly, $Ca_8Mg(SiO_4)_4C_{l2}:Eu^{2+}$ and $Ca_8Zn(SiO_4)_4C_{l2}:Eu^{2+}$ phosphors have been developed for green emission in the range of 505 nm, making them suitable for phosphor-converted white LEDs [138].

1.8 Selection of materials

1.8.1 Selection of $Ca_2La_2O_5$

Phosphor materials play a pivotal role in a wide array of applications, including displays and therapeutic contexts. The choice of the right phosphor material is essential to ensure superior color rendition in displays and optimal performance in therapeutic applications. Among the various phosphors available, $Ca_2La_2O_5$ has emerged as a promising candidate due to its unique optical properties, versatility, and compatibility with different applications. In this comprehensive discussion, we'll delve into the importance of selecting $Ca_2La_2O_5$ in both display technologies and therapeutic applications, drawing insights from reported research literature.

Displays, whether in consumer electronics or professional applications, demand accurate color rendition. The representation of colors must be faithful to real-life objects and images. $Ca_2La_2O_5$ has garnered attention for its potential to improve color rendition in displays. Research findings reveal that $Ca_2La_2O_5$ phosphors exhibit a broad emission spectrum, spanning a wide range of wavelengths. This characteristic is particularly advantageous in displays, where the ability to emit light across a broad spectrum of colors is crucial. The literature consistently demonstrates that $Ca_2La_2O_5$ phosphors possess efficient energy transfer mechanisms [43]. A study published by Q. Du *et al.* explored the energy transfer properties of $Ca_2La_2O_5:Ce^{3+}$ phosphors, emphasizing their high luminescence efficiency and energy transfer capabilities. These attributes contribute to the production of energy-efficient displays that maintain pure and true colors. One of the advantages of $Ca_2La_2O_5$ is its compatibility with various rare-earth ions as dopants. This flexibility allows for

precise tuning of emission wavelengths and color temperatures [139]. In an investigation by J. Huang *et al.* reported that the doping of Eu^{2+} ions in $Ca_2La_2O_5$ phosphors led to tunable luminescent properties, making them suitable for use in LED displays where specific color temperatures are required [140].

$Ca_2La_2O_5$ significance extends beyond displays to therapeutic applications, where its unique properties are harnessed for medical purposes. In therapeutic contexts, phosphors with long afterglow or persistent luminescence properties hold immense value. These phosphors can provide sustained illumination without the need for a continuous light source, making them ideal for medical procedures that require extended, uninterrupted light exposure. A study conducted by Yang and Wang in 2020 explored the long afterglow properties of $Ca_2La_2O_5:Eu^{2+,}$ Mn^{2+} phosphors, emphasizing their potential for applications such as photodynamic therapy and bioimaging [141]. Biocompatibility and low toxicity are paramount in therapeutic applications, where the interaction of materials with living organisms must be carefully considered. Literature consistently highlights the biocompatible nature of $Ca_2La_2O_5$, making it a suitable candidate for use in medical and therapeutic applications. A study by Wu *et al.* assessed the biocompatibility of $Ca_2La_2O_5$ nanoparticles and found them to be well-tolerated by living cells. This attribute is crucial for bioimaging and other medical applications [142].

The stability of phosphor materials under various conditions is essential for their suitability in therapeutic applications. $Ca_2La_2O_5$ has demonstrated good photostability, ensuring that its luminescent properties remain consistent over time. Additionally, it exhibits a respectable photoluminescence quantum yield, a critical factor in ensuring efficient light emission. In a study by Marin and Jaque published the photostability and photoluminescence properties of $Ca_2La_2O_5:Ce^{3+}$ phosphors, confirming their stability and high luminescence efficiency [143].

The importance of selecting $Ca_2La_2O_5$ for improving color rendition in displays and enhancing therapeutic applications is underpinned by a wealth of research data and insights. Numerous studies have delved into the material properties and its potential across a range of applications. In displays, the ability of $Ca_2La_2O_5$ to emit light across a broad spectrum of colors has been documented in research studies. For example, Wang *et al.* (2018) investigated the color-tunable luminescence of $Ca_2La_2O_5:Ce^{3+,}$ Tb^{3+} phosphors. Their research demonstrated the broad emission spectrum of these

phosphors, making them suitable for achieving accurate color rendition in displays. Efficient energy transfer, another critical factor for displays, has been explored by researchers [144]. In a study published by Jin *et al.* (2016), the energy transfer mechanism in $Ca_2La_2O_5:Ce^{3+}$ phosphors were studied. The research highlighted the efficient energy transfer properties of these phosphors, which can contribute to the development of energy-efficient displays. Furthermore, the compatibility of $Ca_2La_2O_5$ with various dopants has been the subject of extensive research [145]. A study conducted by Xi et al. explored the luminescence properties of $Ca_2La_2O_5:Ce^{3+,}$ Tb^{3+} phosphors, emphasizing their potential for use in LED displays where specific color temperatures are required [146].

In therapeutic applications, the long afterglow properties of $Ca_2La_2O_5$ have been investigated in studies such as the one by Wang et al. and this research highlighted the sustained luminescence of $Ca_2La_2O_5:Eu^{2+}$, Mn^{2+} phosphors, indicating their potential for applications in photodynamic therapy and bioimaging. The biocompatibility and low toxicity of $Ca_2La_2O_5$ have also been extensively studied [144]. A comprehensive assessment conducted by Zhang *et al.* examined the biocompatibility of $Ca_2La_2O_5$ nanoparticles, demonstrating their suitability for use in medical applications. Moreover, the photostability and photoluminescence quantum yield of $Ca_2La_2O_5$ have been subjects of research[147]. No studies have been reported about the usage of $Ca_2La_2O_5$ with Eu^{3+} which has possibilities of emitting deep red emission in the range of 610-630 nm based on its behavior with various other dopants, used for display applications using w-LEDs. Hence $Ca_2La_2O_5$ has been chosen has one of the host with Eu3+ as dopant for exploring red emitting phosphor for w-LED applications.

1.8.2 Selection of $SrZr_2La_2O_7$

The selection of $SrZr_2La_2O_7$ (Strontium Zirconium Lanthanum Oxide) as a phosphor material holds significant importance in both improving color rendition in displays and enabling therapeutic applications. This choice is substantiated by reported research literature, which underscores several key reasons for its relevance and significance. $SrZr_2La_2O_7$ is reported in research literature to exhibit a broad emission spectrum. This property is particularly valuable in the context of displays, where a diverse range of colors must be accurately represented. A study by Yang *et al.* investigated

the emission characteristics of $SrZr_2La_2O_7:Eu^{2+}$ phosphors, emphasizing their broad emission spectrum, making them suitable for achieving accurate and true color rendition in displays [148].

Efficiency in converting excitation energy into visible light is a key factor in display technologies. Research studies consistently demonstrates the high luminescence efficiency of $SrZr_2La_2O_7$ phosphors. An investigation by Wang *et al.* (2020) examined the luminescence properties of $SrZr_2La_2O_7:Eu^{3+}$ phosphors, highlighting their efficient energy transfer and high luminescence efficiency. This characteristic contributes to energy-efficient displays that maintain superior color quality [144]. The compatibility of $SrZr_2La_2O_7$ with various rare-earth dopants, such as Eu^{3+} and Ce^{3+}, allows for precise tuning of emission wavelengths and color temperatures. Research literature provides insights into the tunable luminescent properties of $SrZr_2La_2O_7:Ce^{3+}$ phosphors, as investigated by Raj *et al.* (2017) and reported that $SrZr_2La_2O_7$ is suitable for applications demanding specific color temperatures. The application of $SrZr_2La_2O_7$ extends to therapeutic contexts, where its unique properties are harnessed for medical purposes [149].

In therapeutic applications, biocompatibility and low toxicity are paramount considerations. Research literature consistently highlights the biocompatible nature of SrZr2La2O7. A study conducted by Zhang *et al.* evaluated the biocompatibility of $SrZr_2La_2O_7$ nanoparticles and found them to be well-tolerated by living cells. This characteristic is crucial for applications such as bioimaging and photodynamic therapy. Therapeutic applications often benefit from phosphors with persistent luminescence properties [147]. $SrZr_2La_2O_7$ has been explored for its potential to provide sustained illumination without the need for a continuous light source. A study by Cheng *et al.* investigated the long afterglow characteristics of $SrZr_2La_2O_7:Eu^{2+},Mn^{2+}$ phosphors, indicating their suitability for photodynamic therapy and bioimaging. Phosphor materials used in therapeutic applications must exhibit high photostability to ensure consistent performance under various conditions [150]. Literature consistently affirms the high photostability of $SrZr_2La_2O_7$. A study by Ni *et al.* examined the photostability and photoluminescence quantum yield of $SrZr_2La_2O_7:Ce^{3+}$ phosphors, confirming their stability and high luminescence efficiency [151].

In displays, the broad emission spectrum of $SrZr_2La_2O_7$ has been documented in research studies. For instance, Wang *et al.* explored the color-tunable luminescence of $SrZr_2La_2O_7:Ce^{3+,}\ Tb^{3+}$ phosphors. This study highlighted the broad emission spectrum of these phosphors, which

contributes to achieving accurate color rendition in displays. The high luminescence efficiency of $SrZr_2La_2O_7$, an essential factor for displays, has been studied by researchers [152]. Shah *et al.* investigated the energy transfer mechanism in $SrZr_2La_2O_7:Ce^{3+}$ phosphors. Their research emphasized the efficient energy transfer properties of these phosphors, which can contribute to the development of energy-efficient displays. Additionally, the compatibility of $SrZr_2La_2O_7$ with various dopants has been a subject of study, the luminescence properties of $SrZr_2La_2O_7:Ce^{3+,}$ Tb^{3+} phosphors highlighting their potential for use in LED displays where specific color temperatures are required. In therapeutic applications, the long afterglow properties of $SrZr_2La_2O_7$ have been explored in studies such as the one by Wang *et al.* This research showcased the sustained luminescence of $SrZr_2La_2O_7:Eu^{2+,}$ Mn^{2+} phosphors, indicating their potential for applications in photodynamic therapy and bioimaging [152]. $SrZr_2La_2O_7$ exhibits excellent energy transfer properties, doping with Eu^{3+} can be explored for deep red emission for display applications. Eu^{3+} being excellent for illumination due their wide excitation bands, doping Eu^{3+} in host is another choice of study for red emitting white phosphors.

1.8.3 Selection of SrZrCaLaO

The selection of SrZrCaLaO as a phosphor material for improving color rendition in displays and enabling therapeutic applications is underpinned by its unique and novel properties. Its ability to emit light in a multitude of colors, provide customizable color temperatures, offer biocompatibility, exhibit persistent luminescence, and maintain high photostability sets it apart as a versatile and valuable material. The research literature highlights the diverse applications and advantages of SrZrCaLaO, from enhancing the quality of displays to advancing medical technologies. SrZrCaLaO stands as an exciting and distinctive phosphor material that promises to drive innovation and make a significant impact in both the display and therapeutic domains. It embodies the potential to revolutionize the visual experience and foster new possibilities in medical procedures and imaging. The selection of SrZrCaLaO (Strontium Zirconium Calcium Lanthanum Oxide) as a phosphor material carries profound importance in the realm of enhancing color rendition in displays and enabling therapeutic applications. This choice is not only substantiated by the unique and exceptional properties that SrZrCaLaO exhibits but also by the diverse range of advantages it offers, as illuminated in reported research literature. In this in-depth discussion, we

will explore the significance of choosing SrZrCaLaO in both display technologies and therapeutic contexts, providing additional insights and research data to underscore its distinctive value.

SrZrCaLaO is a compelling choice for achieving superior color rendition in displays, is due to its distinctive properties. One of the defining features of SrZrCaLaO, as evidenced in recent research literature, is its remarkable ability to emit light in a multitude of colors. the emission properties of SrZrCaLaO: Eu^{3+}, Tb^{3+} phosphors, revealing their unique multicolor emission capabilities [153].

These phosphors can emit light in a range of colors, covering the visible spectrum effectively. Such multicolor emission properties are invaluable for displays where a wide color gamut is desired, enabling more vibrant and true-to-life color rendition. The versatility of SrZrCaLaO is further emphasized by its ability to offer customizable color temperature. Research literature highlights the tunable luminescent properties of SrZrCaLaO.

The luminescent characteristics of SrZrCaLaO: Ce^{3+}, Tb^{3+} phosphors allow for precise control over color temperatures, making SrZrCaLaO an excellent candidate for displays that require specific color temperatures for different scenarios. This can be particularly advantageous in professional video editing, medical imaging, and architectural lighting, where specific color temperatures are essential for achieving desired visual effects. Beyond its application in displays, SrZrCaLaO plays a pivotal role in therapeutic contexts, where its unique properties offer new possibilities for medical procedures and imaging [154]. The biocompatibility of SrZrCaLaO nanoparticles has been rigorously examined, affirming their safety for use in a wide range of medical applications. Biocompatibility is of paramount importance, particularly in the fields of bioimaging, drug delivery systems, and photodynamic therapy. The safe interaction of SrZrCaLaO with living cells opens doors to non-invasive and secure medical procedures, ensuring patient safety. In the context of bioimaging, drug delivery, and targeted therapies, the biocompatibility of SrZrCaLaO is instrumental in enabling advanced and patient-friendly medical solutions [155].

Within therapeutic applications, the presence of phosphors with persistent luminescence properties is of immense value. SrZrCaLaO stands out due to its ability to exhibit persistent luminescence, a unique and sought-after feature. The sustained luminescence properties of SrZrCaLaO: Eu^{2+}, Mn^{2+} phosphors have been investigated, highlighting the material's potential for applications such as photodynamic therapy and bioimaging. Persistent luminescence allows for extended illumination

without the need for a continuous light source, making it highly suitable for imaging applications. In the context of bioimaging, this characteristic can facilitate prolonged observation of specific areas of interest, enabling real-time monitoring and diagnostics [60, 54].

The stability of phosphor materials under various conditions is a critical factor for ensuring reliable imaging in therapeutic applications. Existing research consistently underscores the high photostability of SrZrCaLaO. A study explored into the photostability and photoluminescence quantum yield of SrZrCaLaO: Ce^{3+} phosphors. This research confirmed the material's exceptional stability and high luminescence efficiency. High photostability is vital for ensuring long-term and precise imaging, particularly in applications like medical imaging and bioimaging. In these contexts, where the consistency and accuracy of imaging data are paramount, SrZrCaLaO robust photostability ensures the integrity of the acquired data. This property is particularly significant in applications such as fluorescence imaging and in vivo tracking, where reliable and consistent performance is essential for accurate diagnostics and monitoring [156-157].

Recent studies have particularly focused on the emission capabilities of SrZrCaLaO phosphors doped with elements like Eu^{2+} and Tb^{3+}. These investigations have demonstrated the material's ability to emit light in multiple colors. This feature is crucial for achieving pure and true color rendition in displays, which is becoming increasingly important in applications ranging from consumer electronics to professional content creation [158-159].

As display technologies continue to advance, the customizable and multicolor capabilities of SrZrCaLaO make it a promising candidate for enhancing the visual experience. Customizability is another noteworthy characteristic of SrZrCaLaO. Researchers have explored the tunable luminescent properties of SrZrCaLaO phosphors doped with elements such as Ce^{3+} and Tb^{3+}. This research has uncovered the material's capacity to provide customizable color temperatures. This flexibility is invaluable in scenarios where specific color temperatures are required. In the region of lighting and design, SrZrCaLaO tunability has the potential to optimize solutions in architectural design and cinematography. The ability to fine-tune color temperatures can enhance not only the quality of displays but also the overall lighting experience in various applications[160]. SrZrCaLaO doped with Eu^{3+} has been not yet explored and reported. Based on its luminescence properties the material has chosen 3rd material doped with Eu^{3+} for red emitting phosphor.

References

[1] K. K. Aitha, D. Dinakar, P. Indira, A. S. Sai Prasad, K. V. R. Murthy, and D. Haranath, *Results Chem.*, vol. 6, p. 101100, Dec. 2023, doi: 10.1016/j.rechem.2023.101100.

[2] G. Lu *et al.*, *J. Mater. Sci. Mater. Electron.*, vol. 33, no. 22, pp. 17855–17867, Aug. 2022, doi: 10.1007/s10854-022-08649-0.

[3] C. Ronda, in *Reference Module in Materials Science and Materials Engineering*, Elsevier, 2017. doi: 10.1016/B978-0-12-803581-8.02416-4.

[4] J. Marshall and S. Johnsen, *Philos. Trans. R. Soc. B Biol. Sci.*, vol. 372, no. 1724, p. 20160335, Jul. 2017, doi: 10.1098/rstb.2016.0335.

[5] H. S. Virk, *Defect Diffus. Forum*, vol. 361, no. February 2014, pp. 1–13, 2015, doi: 10.4028/www.scientific.net/DDF.361.1.

[6] J. L. Leaño, M.-H. Fang, and R.-S. Liu, *ECS J. Solid State Sci. Technol.*, vol. 7, no. 1, pp. R3111–R3133, 2018, doi: 10.1149/2.0161801jss.

[7] J. R. Lakowicz, in *Principles of Fluorescence Spectroscopy*, Boston, MA: Springer US, 1999, pp. 1–23. doi: 10.1007/978-1-4757-3061-6_1.

[8] G. Hong, A. L. Antaris, and H. Dai, *Nat. Biomed. Eng.*, vol. 1, no. 1, p. 0010, Jan. 2017, doi: 10.1038/s41551-016-0010.

[9] C. A. Spindt, C. E. Holland, I. Brodie, J. B. Mooney, and E. R. Westerberg, *IEEE Trans. Electron Devices*, vol. 36, no. 1, pp. 225–228, Jan. 1989, doi: 10.1109/16.21210.

[10] B. Cui *et al.*, *New Carbon Mater.*, vol. 32, no. 5, pp. 385–401, Oct. 2017, doi: 10.1016/S1872-5805(17)60130-6.

[11] G. Baryshnikov, B. Minaev, and H. Ågren, *Chem. Rev.*, vol. 117, no. 9, pp. 6500–6537, May 2017, doi: 10.1021/acs.chemrev.7b00060.

[12] G. N. Lewis and M. Kasha, *J. Am. Chem. Soc.*, vol. 66, no. 12, pp. 2100–2116, Dec. 1944, doi: 10.1021/ja01240a030.

[13] G. C. Lisensky, M. N. Patel, and M. L. Reich, *J. Chem. Educ.*, vol. 73, no. 11, p. 1048, Nov. 1996, doi: 10.1021/ed073p1048.

[14] W. Shao and J. Kim, *Acc. Chem. Res.*, vol. 55, no. 11, pp. 1573–1585, Jun. 2022, doi: 10.1021/acs.accounts.2c00146.

[15] L. Yi, X. He, L. Zhou, F. Gong, R. Wang, and J. Sun, *J. Lumin.*, vol. 130, no. 6, pp. 1113–1117, Jun. 2010, doi: 10.1016/j.jlumin.2010.02.006.

[16] I. Gupta, S. Singh, S. Bhagwan, and D. Singh, *Ceram. Int.*, vol. 47, no. 14, pp. 19282–19303, Jul. 2021, doi: 10.1016/j.ceramint.2021.03.308.

[17] Z. Yang *et al.*, *J. Mol. Struct.*, vol. 1292, p. 136071, Nov. 2023, doi: 10.1016/j.molstruc.2023.136071.

[18] J. Shinar and R. Shinar, *J. Phys. D. Appl. Phys.*, vol. 41, no. 13, p. 133001, Jul. 2008, doi: 10.1088/0022-3727/41/13/133001.

[19] M. A. G. de Brito, L. P. Sampaio, L. G. Junior, and C. A. Canesin, in *XI Brazilian Power Electronics Conference*, Sep. 2011, pp. 531–537. doi: 10.1109/COBEP.2011.6085198.

[20] Z. Gorocs and A. Ozcan, *IEEE Rev. Biomed. Eng.*, vol. 6, pp. 29–46, 2013, doi: 10.1109/RBME.2012.2215847.

[21] E. Ahmed, D. Maamoun, T. M. Hassan, and T. A. Khattab, *Luminescence*, vol. 37, no. 8, pp. 1376–1386, Aug. 2022, doi: 10.1002/bio.4310.

[22] R. Mahajan and R. Prakash, *J. Mater. Sci. Mater. Electron.*, vol. 33, no. 34, pp. 25491–25517, Dec. 2022, doi: 10.1007/s10854-022-09279-2.

[23] M. Zhang *et al.*, *Front. Chem.*, vol. 7, Jan. 2019, doi: 10.3389/fchem.2019.00016.

[24] Y. Chen, Y.-X. Wang, C.-W. Lu, and H.-C. Su, *J. Mater. Chem. C*, vol. 10, no. 31, pp. 11211–11219, 2022, doi: 10.1039/D2TC01727J.

[25] F. Hong, H. Cheng, G. Liu, X. Dong, W. Yu, and J. Wang, *Inorg. Chem.*, vol. 57, no. 16, pp. 9892–9901, Aug. 2018, doi: 10.1021/acs.inorgchem.8b00944.

[26] B. Niraula and C. Rizal, *Colloids and Interfaces*, vol. 2, no. 4, p. 52, Oct. 2018, doi: 10.3390/colloids2040052.

[27] M. Zhu, Y. Pan, Y. Huang, H. Lian, and J. Lin, *J. Mater. Chem. C*, vol. 6, no. 3, pp. 491–499, 2018, doi: 10.1039/C7TC04878E.

[28] R. Srinivasan, N. R. Yogamalar, J. Elanchezhiyan, R. J. Joseyphus, and A. C. Bose, *J. Alloys Compd.*, vol. 496, no. 1–2, pp. 472–477, Apr. 2010, doi: 10.1016/j.jallcom.2010.02.083.

[29] Y. Liu, D. Cui, M. Chen, Z. Li, and C. Zhou, "Synthesis of Red and Black Phosphorus Nanomaterials," 2019, pp. 1–25. doi: 10.1021/bk-2019-1333.ch001.

[30] S. F. Wuister and A. Meijerink, *J. Lumin.*, vol. 105, no. 1, pp. 35–43, Sep. 2003, doi: 10.1016/S0022-2313(03)00095-4.

[31] Y. Song, N. Guo, J. Li, R. Ouyang, Y. Miao, and B. Shao, *Ceram. Int.*, vol. 46, no. 14, pp. 22164–22170, Oct. 2020, doi: 10.1016/j.ceramint.2020.05.293.

[32] S. Chand, R. Mehra, and V. Chopra, *J. Lumin.*, vol. 252, p. 119383, Dec. 2022, doi: 10.1016/j.jlumin.2022.119383.

[33] J. Singh *et al.*, *CrystEngComm*, vol. 14, no. 18, p. 5898, 2012, doi: 10.1039/c2ce06650e.

[34] L. Zhao, F. Fan, X. Chen, Y. Wang, Y. Li, and B. Deng, *J. Mater. Sci. Mater. Electron.*, vol.

29, no. 7, pp. 5975–5981, Apr. 2018, doi: 10.1007/s10854-018-8571-9.

[35] A. M. Pires, S. Heer, H. U. Güdel, and O. A. Serra, *J. Fluoresc.*, vol. 16, no. 3, pp. 461–468, May 2006, doi: 10.1007/s10895-006-0085-9.

[36] A. R. Miedema, "Philips technical," vol. 36, no. 8, 1976. https://www.pearl-hifi.com/06_Lit_Archive/02_PEARL_Arch/Vol_16/Sec_53/Philips_Tech_Review/PTech Review-37-1977-221.pdf

[37] J. S. Revathy, N. S. C. Priya, K. Sandhya, and D. N. Rajendran, *Bull. Mater. Sci.*, vol. 44, no. 1, p. 13, Apr. 2021, doi: 10.1007/s12034-020-02299-w.

[38] Q. Zhu, S. Wang, J.-G. Li, X. Li, and X. Sun, *J. Alloys Compd.*, vol. 731, pp. 1069–1079, Jan. 2018, doi: 10.1016/j.jallcom.2017.10.155.

[39] C. E. Rivera-Enríquez and A. L. Fernández-Osorio, *J. Lumin.*, vol. 236, p. 118110, Aug. 2021, doi: 10.1016/j.jlumin.2021.118110.

[40] G. Gu, P. P. Ong, C. Chen, and S. Roth, *J. Phys. D. Appl. Phys.*, vol. 33, no. 11, pp. 1263–1266, Jun. 2000, doi: 10.1088/0022-3727/33/11/303.

[41] E. Yang, G. Li, J. Zheng, C. Fu, Y. Zheng, and L. Li, *J. Phys. Chem. C*, vol. 118, no. 7, pp. 3820–3827, Feb. 2014, doi: 10.1021/jp412025t.

[42] S. Nayab Rasool, L. Rama Moorthy, and C. Kulala Jayasankar, *Mater. Express*, vol. 3, no. 3, pp. 231–240, Sep. 2013, doi: 10.1166/mex.2013.1123.

[43] K. K. Aitha *et al.*, *Can. Metall. Q.*, pp. 1–9, Sep. 2023, doi: 10.1080/00084433.2023.2254128.

[44] L. Wang, S. Yuan, Y. Yang, F. Chevire, F. Tessier, and G. Chen, *Opt. Mater. Express*, vol. 5, no. 11, p. 2616, Nov. 2015, doi: 10.1364/OME.5.002616.

[45] Q. Liu *et al.*, *J. Lumin.*, vol. 246, p. 118808, Jun. 2022, doi: 10.1016/j.jlumin.2022.118808.

[46] Z. Liang *et al.*, *Dalt. Trans.*, vol. 48, no. 33, pp. 12459–12465, 2019, doi: 10.1039/C9DT02577D.

[47] X. Huang, S. Wang, and B. Devakumar, *Opt. Laser Technol.*, vol. 130, p. 106349, Oct. 2020, doi: 10.1016/j.optlastec.2020.106349.

[48] Y. Wang, C. Yu, Y. Zhou, E. Song, H. Ming, and Q. Zhang, *J. Alloys Compd.*, vol. 855, p. 157347, Feb. 2021, doi: 10.1016/j.jallcom.2020.157347.

[49] X. Han, E. Song, W. Chen, Y. Zhou, and Q. Zhang, *J. Mater. Chem. C*, vol. 8, no. 29, pp. 9836–9844, 2020, doi: 10.1039/D0TC01502D.

[50] G. Mandel, R. P. Bauman, and E. Banks, *J. Chem. Phys.*, vol. 33, no. 1, pp. 192–193, Jul. 1960, doi: 10.1063/1.1731076.

[51] A. A. . Araújo *et al.*, *J. Inorg. Biochem.*, vol. 88, no. 1, pp. 87–93, Jan. 2002, doi: 10.1016/S0162-0134(01)00346-4.

[52] N. Chestnoy, R. Hull, and L. E. Brus, J. Chem. Phys., vol. 85, no. 4, pp. 2237–2242, Aug. 1986, doi: 10.1063/1.451119.

[53] G. Zhou, W.-Y. Wong, and S. Suo, J. Photochem. Photobiol. C Photochem. Rev., vol. 11, no. 4, pp. 133–156, Dec. 2010, doi: 10.1016/j.jphotochemrev.2011.01.001.

[54] Jorma Hölsä, Högne Jungner, Mika Lastusaari, Janne Niittykoski, Journal of Alloys and Compounds, 323–324, 2001, 326-330, https://doi.org/10.1016/S0925-8388(01)01084-2.

[55] J. Zhang, L. Xu, and W.-Y. Wong, Coord. Chem. Rev., vol. 355, pp. 180–198, Jan. 2018, doi: 10.1016/j.ccr.2017.08.007.

[56] S. Bairagi, Shahid-ul-Islam, M. Shahadat, D. M. Mulvihill, and W. Ali, *Nano Energy*, vol. 111, p. 108414, Jun. 2023, doi: 10.1016/j.nanoen.2023.108414.

[57] L. K. Putri, B.-J. Ng, W.-J. Ong, H. W. Lee, W. S. Chang, and S.-P. Chai, *J. Mater. Chem. A*, vol. 6, no. 7, pp. 3181–3194, 2018, doi: 10.1039/C7TA09723A.

[58] L. Lu, M. Sun, Q. Lu, T. Wu, and B. Huang, *Nano Energy*, vol. 79, p. 105437, Jan. 2021, doi: 10.1016/j.nanoen.2020.105437.

[59] B. Yan and C. Wang, *Solid State Sci.*, vol. 10, no. 1, pp. 82–89, Jan. 2008, doi: 10.1016/j.solidstatesciences.2007.07.036.

[60] Y. Li, M. Gecevicius, and J. Qiu, *Chem. Soc. Rev.*, vol. 45, no. 8, pp. 2090–2136, 2016, doi: 10.1039/C5CS00582E.

[61] B. Yan, *Inorg. Chem. Front.*, vol. 8, no. 1, pp. 201–233, 2021, doi: 10.1039/D0QI01153C.

[62] T. Krahl, G. Scholz, and E. Kemnitz, *J. Phys. Chem. C*, vol. 118, no. 36, pp. 21066–21074, Sep. 2014, doi: 10.1021/jp505616f.

[63] S. Bastani, A. Jalali Kandeloos, M. Jalili, and M. Ghahari, "Nanocomposites Based on Upconversion Nanoparticles," 2023, pp. 127–163. doi: 10.1007/978-981-99-3913-8_6.

[64] I. Villa, September, p. 153, 2015, https://boa.unimib.it/handle/10281/87314#

[65] A. Sharma, *Understanding Color Management*. Wiley, 2018. doi: 10.1002/9781119223702.

[66] A. Jain, A. Kumar, S. J. Dhoble, and D. R. Peshwe, *Renew. Sustain. Energy Rev.*, vol. 65, pp. 135–153, Nov. 2016, doi: 10.1016/j.rser.2016.06.081.

[67] X. Dai, Y. Deng, X. Peng, and Y. Jin, *Adv. Mater.*, vol. 29, no. 14, Apr. 2017, doi: 10.1002/adma.201607022.

[68] M. D. Smith, B. A. Connor, and H. I. Karunadasa, *Chem. Rev.*, vol. 119, no. 5, pp. 3104–3139, Mar. 2019, doi: 10.1021/acs.chemrev.8b00477.

[69] J. Jehlička and A. Culka, *Anal. Chim. Acta*, vol. 1209, p. 339027, May 2022, doi: 10.1016/j.aca.2021.339027.

[70] A. R. Anwar, M. T. Sajjad, M. A. Johar, C. A. Hernández-Gutiérrez, M. Usman, and S. P. Łepkowski, *Laser Photonics Rev.*, vol. 16, no. 6, pp. 1–20, 2022, doi: 10.1002/lpor.202100427.

[71] S. Liao *et al.*, *Adv. Funct. Mater.*, vol. 33, no. 1, Jan. 2023, doi: 10.1002/adfm.202210558.

[72] M.-C. Wong, L. Chen, M.-K. Tsang, Y. Zhang, and J. Hao, *Adv. Mater.*, vol. 27, no. 30, pp. 4488–4495, Aug. 2015, doi: 10.1002/adma.201502015.

[73] F. Yang, Y. Wang, X. Jiang, B. Lin, and R. Lv, *ACS Comb. Sci.*, vol. 22, no. 5, pp. 285–296, May 2020, doi: 10.1021/acscombsci.0c00035.

[74] Z. Carmen and S. Daniel, in *Organic Pollutants Ten Years After the Stockholm Convention - Environmental and Analytical Update*, InTech, 2012. doi: 10.5772/32373.

[75] B. S. Richards, *Sol. Energy Mater. Sol. Cells*, vol. 90, no. 15, pp. 2329–2337, Sep. 2006, doi: 10.1016/j.solmat.2006.03.035.

[76] H. V. Demir, S. Nizamoglu, T. Erdem, E. Mutlugun, N. Gaponik, and A. Eychmüller, *Nano Today*, vol. 6, no. 6, pp. 632–647, 2011, doi: 10.1016/j.nantod.2011.10.006.

[77] C. De Mello Donegá, *Nanoparticles: Workhorses of nanoscience*, vol. 9783662448. 2014. doi: 10.1007/978-3-662-44823-6.

[78] H. S. Jang, H. Yang, S. W. Kim, J. Y. Han, S.-G. Lee, and D. Y. Jeon, *Adv. Mater.*, vol. 20, no. 14, pp. 2696–2702, Jul. 2008, doi: 10.1002/adma.200702846.

[79] M. Sygletou, C. Petridis, E. Kymakis, and E. Stratakis, *Adv. Mater.*, vol. 29, no. 39, Oct. 2017, doi: 10.1002/adma.201700335.

[80] H. Cheng, Y. Feng, Y. Fu, Y. Zheng, Y. Shao, and Y. Bai, *J. Mater. Chem. C*, vol. 10, no. 37, pp. 13590–13610, 2022, doi: 10.1039/D2TC01869A.

[81] C. R. Kagan, L. C. Bassett, C. B. Murray, and S. M. Thompson, *Chem. Rev.*, vol. 121, no. 5, pp. 3186–3233, Mar. 2021, doi: 10.1021/acs.chemrev.0c00831.

[82] F. Chen *et al.*, *Chem. Commun.*, vol. 57, no. 99, pp. 13448–13464, 2021, doi: 10.1039/D1CC04386B.

[83] Y. Zhang, X. Qiao, J. Wan, L. Wu, B. Chen, and X. Fan, *J. Mater. Chem. C*, vol. 5, no. 35, pp. 8952–8957, 2017, doi: 10.1039/C7TC02909H.

[84] K. A. Denault, Z. Cheng, J. Brgoch, S. P. DenBaars, and R. Seshadri, *J. Mater. Chem. C*, vol. 1, no. 44, p. 7339, 2013, doi: 10.1039/c3tc31621a.

[85] G. B. Nair, H. C. Swart, and S. J. Dhoble, *Prog. Mater. Sci.*, vol. 109, p. 100622, Apr. 2020, doi: 10.1016/j.pmatsci.2019.100622.

[86] R.-J. Xie and H. T. Bert Hintzen, *J. Am. Ceram. Soc.*, vol. 96, no. 3, pp. 665–687, Mar. 2013, doi: 10.1111/jace.12197.

[87] J. Li and K. Pu, *Chem. Soc. Rev.*, vol. 48, no. 1, pp. 38–71, 2019, doi: 10.1039/C8CS00001H.

[88] S. Yang, W. Dai, W. Zheng, and J. Wang, *Coord. Chem. Rev.*, vol. 475, p. 214913, Jan. 2023, doi: 10.1016/j.ccr.2022.214913.

[89] S.-K. Sun, H.-F. Wang, and X.-P. Yan, *Acc. Chem. Res.*, vol. 51, no. 5, pp. 1131–1143, May 2018, doi: 10.1021/acs.accounts.7b00619.

[90] M. Matulionyte, A. Skripka, A. Ramos-Guerra, A. Benayas, and F. Vetrone, *Chem. Rev.*, vol. 123, no. 1, pp. 515–554, Jan. 2023, doi: 10.1021/acs.chemrev.2c00419.

[91] X. Zheng, Y. Wu, H. Zuo, W. Chen, and K. Wang, *Small*, vol. 19, no. 18, May 2023, doi: 10.1002/smll.202206624.

[92] R. Tuli *et al.*, *Transl. Oncol.*, vol. 5, no. 2, pp. 77–84, Apr. 2012, doi: 10.1593/tlo.11316.

[93] S. S. Syamchand and G. Sony, *J. Lumin.*, vol. 165, pp. 190–215, Sep. 2015, doi: 10.1016/j.jlumin.2015.04.042.

[94] T. S. H. Perera, Y. Han, X. Lu, X. Wang, H. Dai, and S. Li, *J. Nanomater.*, vol. 2015, pp. 1–6, 2015, doi: 10.1155/2015/705390.

[95] M. Ovais *et al.*, *Adv. Mater.*, vol. 32, no. 22, Jun. 2020, doi: 10.1002/adma.202000055.

[96] M. Ashrafizadeh *et al.*, *Expert Opin. Drug Deliv.*, vol. 19, no. 4, pp. 355–382, Apr. 2022, doi: 10.1080/17425247.2022.2041598.

[97] L. Ozawa and M. Itoh, *Chem. Rev.*, vol. 103, no. 10, pp. 3835–3856, Oct. 2003, doi: 10.1021/cr0203490.

[98] L. Nucci, D. Narvaez, and T. Krettenauer, *Second Edition Second Edition*, no. June. 2014.

[99] L. F. Weber, *IEEE Trans. Plasma Sci.*, vol. 34, no. 2, pp. 268–278, Apr. 2006, doi: 10.1109/TPS.2006.872440.

[100] X. Song, M.-H. Chang, and M. Pecht, *JOM*, vol. 65, no. 10, pp. 1276–1282, Oct. 2013, doi: 10.1007/s11837-013-0737-6.

[101] K. Srikanth, L. Narsihma, K. Laxminarayana, M. Vithal, and M. Srinivas, *J. Indian Chem. Soc.*, vol. 98, no. 12, p. 100237, Dec. 2021, doi: 10.1016/j.jics.2021.100237.

[102] N. Thejo Kalyani and S. J. Dhoble, *Renew. Sustain. Energy Rev.*, vol. 16, no. 5, pp. 2696–2723, Jun. 2012, doi: 10.1016/j.rser.2012.02.021.

[103] R. K. Singh *et al.*, in *Spectroscopy of Lanthanide Doped Oxide Materials*, Elsevier, 2020, pp. 21–56. doi: 10.1016/B978-0-08-102935-0.00002-2.

[104] Zhengqing, Gan. IS-T 2639. Ames Lab., Ames, IA (United States), 2010.

[105] G. B. Nair and S. J. Dhoble, Luminescence, vol. 30, no. 8, pp. 1167–1175, Dec. 2015, doi: 10.1002/bio.2919.

[106] J. Liu, Z.-M. Zhang, Z.-C. Wu, F.-F. Wang, and Z.-J. Li, Mater. Sci. Eng. B, vol. 221, pp. 10–16, Jul. 2017, doi: 10.1016/j.mseb.2017.03.014.

[107] M. Jiao et al., Inorg. *Chem.*, vol. 52, no. 18, pp. 10340–10346, Sep. 2013, doi: 10.1021/ic401033u.

[108] G. B. Nair, P. D. Bhoyar, and S. J. Dhoble, *Luminescence*, vol. 32, no. 1, pp. 22–29, Feb. 2017, doi: 10.1002/bio.3143.

[109] N. V. Rebrova *et al.*, *J. Cryst. Growth*, vol. 466, pp. 39–44, May 2017, doi: 10.1016/j.jcrysgro.2017.03.016.

[110] M. Dalal *et al.*, *J. Alloys Compd.*, vol. 698, pp. 662–672, Mar. 2017, doi: 10.1016/j.jallcom.2016.12.257.

[111] X. Sun *et al.*, *J. Lumin.*, vol. 157, pp. 197–200, Jan. 2015, doi: 10.1016/j.jlumin.2014.08.052.

[112] M. Guzik, E. Tomaszewicz, Y. Guyot, J. Legendziewicz, and G. Boulon, *J. Mater. Chem. C*, vol. 3, no. 33, pp. 8582–8594, 2015, doi: 10.1039/C5TC01109D.

[113] B. Poornaprakash, P. T. Poojitha, U. Chalapathi, and S.-H. Park, *Mater. Lett.*, vol. 181, pp. 227–230, Oct. 2016, doi: 10.1016/j.matlet.2016.06.033.

[114] S. Tamboli, P. D. Bhoyar, and S. J. Dhoble, *J. Lumin.*, vol. 184, pp. 23–28, Apr. 2017, doi: 10.1016/j.jlumin.2016.12.003.

[115] E. Cavalli, P. Boutinaud, and M. Grinberg, *J. Lumin.*, vol. 169, pp. 450–453, Jan. 2016, doi: 10.1016/j.jlumin.2014.10.069.

[116] H. Xu, D. Ying, A. Lu, X. Wang, and J. Hu, *Superlattices Microstruct.*, vol. 83, pp. 668–675, Jul. 2015, doi: 10.1016/j.spmi.2015.04.011.

[117] H. Zhu *et al.*, *J. Lumin.*, vol. 172, pp. 180–184, Apr. 2016, doi: 10.1016/j.jlumin.2015.12.021.

[118] R. Cao *et al.*, *Optik*, vol. 127, no. 19, pp. 7896–7901, Oct. 2016, doi: 10.1016/j.ijleo.2016.05.157.

[119] L. Jing, X. Liu, Y. Li, and Y. Wang, *J. Lumin.*, vol. 162, pp. 185–190, Jun. 2015, doi: 10.1016/j.jlumin.2015.02.048.

[120] X. Mi *et al.*, *Mater. Res. Bull.*, vol. 60, pp. 72–78, Dec. 2014, doi: 10.1016/j.materresbull.2014.08.017.

[121] N. Hashimoto, Y. Takada, K. Sato, and S. Ibuki, *J. Lumin.*, vol. 48–49, pp. 893–897, Jan. 1991, doi: 10.1016/0022-2313(91)90265-W.

[122] N. Y. Nobuhiko Yamashita, *Jpn. J. Appl. Phys.*, vol. 30, no. 12R, p. 3335, Dec. 1991, doi: 10.1143/JJAP.30.3335.

[123] A. A. Setlur *et al.*, *Chem. Mater.*, vol. 22, no. 13, pp. 4076–4082, Jul. 2010, doi: 10.1021/cm100960g.

[124] C.-H. Huang, P.-J. Wu, J.-F. Lee, and T.-M. Chen, *J. Mater. Chem.*, vol. 21, no. 28, p. 10489, 2011, doi: 10.1039/c1jm11018g.

[125] R.-J. Xie, N. Hirosaki, Y. Li, and T. Takeda, *Materials (Basel).*, vol. 3, no. 6, pp. 3777–3793, Jun. 2010, doi: 10.3390/ma3063777.

[126] H.-F. Chen *et al.*, *J. Mater. Chem.*, vol. 22, no. 31, p. 15620, 2012, doi: 10.1039/c2jm31904g.

[127] P. Dai *et al.*, *J. Am. Ceram. Soc.*, vol. 95, no. 2, pp. 658–662, Feb. 2012, doi: 10.1111/j.1551-2916.2011.04804.x.

[128] Zhong, F., Liu, X. J., Huang, Z. R., & Zhang, Y. Q. (2012). Journal of the Chinese Society of Rare Earths, 30(6), 650.

[129] S. Li *et al.*, *Chem. Mater.*, vol. 30, no. 2, pp. 494–505, Jan. 2018, doi: 10.1021/acs.chemmater.7b04605.

[130] R.-J. Xie, N. Hirosaki, H.-L. Li, Y. Q. Li, and M. Mitomo, *J. Electrochem. Soc.*, vol. 154, no. 10, p. J314, 2007, doi: 10.1149/1.2768289.

[131] H. Wang *et al.*, *RSC Adv.*, vol. 7, no. 52, pp. 32982–32988, 2017, doi: 10.1039/C7RA04961G.

[132] C. Wang, Z. Zhao, Q. Wu, G. Zhu, and Y. Wang, *Dalt. Trans.*, vol. 44, no. 22, pp. 10321–10329, 2015, doi: 10.1039/C5DT00815H.

[133] H. Bin, W. Yi-Fei, L. Qian, and H. Qing, *J. Inorg. Mater.*, vol. 31, no. 6, p. 652, 2016, doi: 10.15541/jim20150597.

[134] J. Huo *et al.*, *J. Lumin.*, vol. 180, pp. 46–50, Dec. 2016, doi: 10.1016/j.jlumin.2016.08.014.

[135] K. Yoshimura, H. Fukunaga, M. Izumi, K. Takahashi, R.-J. Xie, and N. Hirosaki, *Jpn. J. Appl. Phys.*, vol. 56, no. 4, p. 041701, Apr. 2017, doi: 10.7567/JJAP.56.041701.

[136] S. K. Sharma, Y.-C. Lin, I. Carrasco, T. Tingberg, M. Bettinelli, and M. Karlsson, *J. Mater. Chem. C*, vol. 6, no. 33, pp. 8923–8933, 2018, doi: 10.1039/C8TC02907E.

[137] F. Ying, Z. Weidong, C. Xiangzhong, H. Yunsheng, and H. Xiaowei, *J. Rare Earths*, vol. 24, no. 1, pp. 145–148, Dec. 2006, doi: 10.1016/S1002-0721(07)60345-7.

[138] W. Lü, Z. Hao, X. Zhang, Y. Luo, X. Wang, and J. Zhang, *J. Lumin.*, vol. 131, no. 11, pp. 2387–2390, Nov. 2011, doi: 10.1016/j.jlumin.2011.05.065.

[139] Q. Du, G. Zhou, J. Zhou, H. Zhou, and J. Zhan, *Mater. Res. Bull.*, vol. 47, no. 11, pp. 3774–3779, Nov. 2012, doi: 10.1016/j.materresbull.2012.06.022.

[140] J. Huang *et al.*, *J. Rare Earths*, vol. 36, no. 3, pp. 225–230, Mar. 2018, doi: 10.1016/j.jre.2017.07.005.

[141] Y. Yang and H. Wang, *J. Phys. Mater.*, vol. 4, no. 1, p. 014003, Jan. 2021, doi: 10.1088/2515-7639/abc9ce.

[142] S. Wu, Y. Li, W. Ding, L. Xu, Y. Ma, and L. Zhang, *Nano-Micro Lett.*, vol. 12, no. 1, p. 70, Dec. 2020, doi: 10.1007/s40820-020-0404-8.

[143] R. Marin and D. Jaque, *Chem. Rev.*, vol. 121, no. 3, pp. 1425–1462, Feb. 2021, doi: 10.1021/acs.chemrev.0c00692.

[144] Z. Wang *et al.*, *Inorg. Chem.*, vol. 58, no. 1, pp. 890–899, Jan. 2019, doi: 10.1021/acs.inorgchem.8b03029.

[145] Y. Jin, Q. Wang, H. Zhou, L. Zhang, and J. Zhang, *Ceram. Int.*, vol. 42, no. 2, pp. 3309–3316, Feb. 2016, doi: 10.1016/j.ceramint.2015.10.124.

[146] Z. Xia and R.-S. Liu, *J. Phys. Chem. C*, vol. 116, no. 29, pp. 15604–15609, Jul. 2012, doi: 10.1021/jp304722z.

[147] J. Zhang *et al.*, *Mini-Reviews Med. Chem.*, vol. 11, no. 8, pp. 678–694, Jul. 2011, doi: 10.2174/138955711796268804.

[148] S.-H. Yang, H.-Y. Lee, P.-C. Tseng, and M.-H. Lee, *J. Lumin.*, vol. 231, p. 117787, Mar. 2021, doi: 10.1016/j.jlumin.2020.117787.

[149] A. K. V. Raj, P. Prabhakar Rao, T. S. Sreena, and T. R. Aju Thara, *Phys. Chem. Chem. Phys.*, vol. 19, no. 30, pp. 20110–20120, 2017, doi: 10.1039/C7CP02741A.

[150] J. Cheng, X. Bian, Z. Zhai, M. Sardar, and J. Lu, *J. Rare Earths*, vol. 40, no. 4, pp. 541–550, Apr. 2022, doi: 10.1016/j.jre.2021.01.018.

[151] Z. Ni, M. Liu, B. Li, X. Shi, Q. Cao, and D. Pan, *Inorg. Chem.*, vol. 62, no. 11, pp. 4727–4734, Mar. 2023, doi: 10.1021/acs.inorgchem.3c00235.

[152] W. Wang, Y. Jin, S. Yan, Y. Yang, Y. Liu, and G. Xiang, *Ceram. Int.*, vol. 43, no. 18, pp. 16323–16330, Dec. 2017, doi: 10.1016/j.ceramint.2017.09.005.

[153] K. Shah, K. V. R. Murthy, and B. S. Chakrabarty, *Results Opt.*, vol. 11, p. 100413, May 2023, doi: 10.1016/j.rio.2023.100413.

[154] J. Liang, B. Devakumar, L. Sun, S. Wang, Q. Sun, and X. Huang, *J. Mater. Chem. C*, vol. 8, no. 14, pp. 4934–4943, 2020, doi: 10.1039/D0TC00006J.

[155] A. K. Barui, R. Kotcherlakota, V. S. Bollu, S. K. Nethi, and C. R. Patra, in *Biopolymer-Based Composites*, Elsevier, 2017, pp. 325–379. doi: 10.1016/B978-0-08-101914-6.00011-

9.

[156] C. Chiatti, C. Fabiani, and A. L. Pisello, *Annu. Rev. Mater. Res.*, vol. 51, no. 1, pp. 409–433, Jul. 2021, doi: 10.1146/annurev-matsci-091520-011838.

[157] F. Meiser, C. Cortez, and F. Caruso, *Angew. Chemie Int. Ed.*, vol. 43, no. 44, pp. 5954–5957, Nov. 2004, doi: 10.1002/anie.200460856.

[158] W. Xie *et al.*, *J. Alloys Compd.*, vol. 753, pp. 781–790, Jul. 2018, doi: 10.1016/j.jallcom.2018.04.260.

[159] X. Chen, Q. Shu, and J. He, *J. Alloys Compd.*, vol. 891, p. 161878, Jan. 2022, doi: 10.1016/j.jallcom.2021.161878.

[160] F. C. Goerigk, V. Paterlini, K. V. Dorn, A.-V. Mudring, and T. Schleid, *Crystals*, vol. 10, no. 12, p. 1089, Nov. 2020, doi: 10.3390/cryst10121089.

Chapter - 2

Synthesis Methods and Characterization Tools

Features of the Chapter:

This chapter describes the experimental methods used in the synthesis of phosphors in bulk configurations. The topics of solid-state reaction modified solid-state reaction, auto-combustion and sol-gel processes were explained and analyzed in detail. This chapter further explains the idea and use of advanced instruments used in the present study to characterize the phosphor samples.

2.1 Synthesis of phosphors

2.1.1 Solid-state reaction method

Solid-state synthesis methods are foundational in the production of phosphor materials, which find critical applications in a diverse range of technologies, including displays, lighting, and sensors [1]. These methods involve the conversion of precursor compounds into phosphors through chemical reactions that take place in a solid-state environment, typically under elevated temperatures. The beauty of solid-state reactions lies in their versatility, enabling detailed control over the composition, structure, and properties of the resulting phosphor materials. This versatility is exemplified through two prevalent solid-state synthesis techniques [2]: the solid-state reaction method and co-precipitation as shown in Figure 2.1.

The solid-state reaction method is characterized by the mixing of solid reactants, often

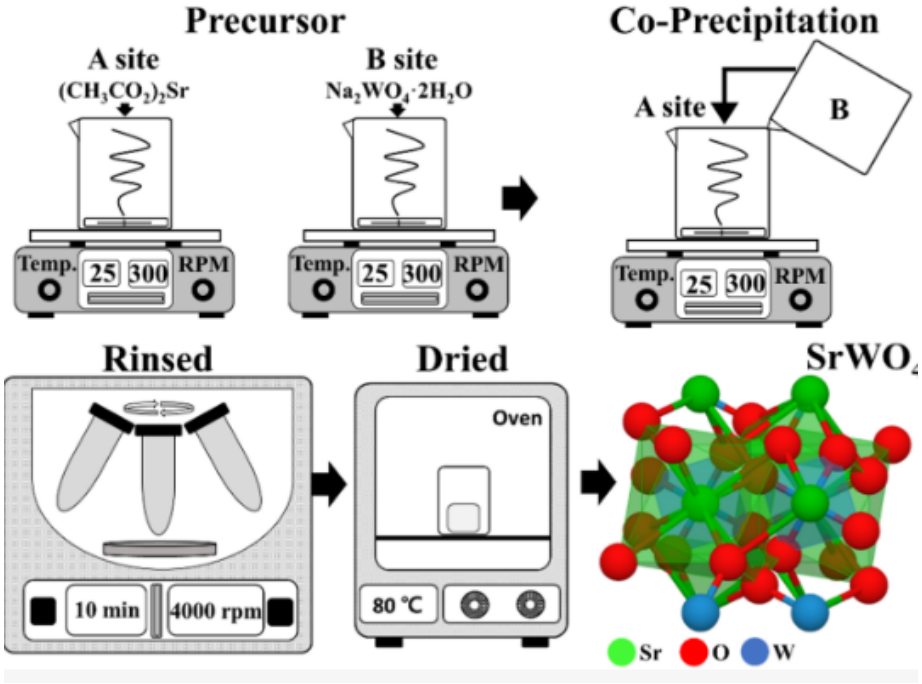

Figure 2.1: Schematic of co-precipitation procedure

comprised of metal oxides, carbonates, or other compounds containing the essential elements for the desired phosphor. This method empowers precise developing of phosphor materials to meet specific application requirements. The procedure starts with the careful selection of high-purity reactants, followed by precise weighing and mixing in stoichiometric ratios. Further enhancement of reactivity is achieved through grinding, and the mixture is then pelletized to ensure uniformity. The critical step in this method is sintering, where the reactants undergo

solid-state reactions, ultimately leading to the formation of the desired phosphor compound. Post-sintering, the material is cooled and subsequently characterized to confirm its properties.

In contrast, the co-precipitation method initiates with the preparation of precursor compounds. These compounds, when dissolved in a solvent, form a solution. By adjusting the pH of the solution through the addition of bases or acids, precipitation occurs, yielding hydroxide or carbonate precipitates containing the necessary metal ions. Subsequent filtration and thorough washing are performed to eliminate impurities, and the dried precipitates undergo calcination at high temperatures. This calcination process is instrumental in transforming the precipitates into the desired phosphor material. The co-precipitation method is particularly advantageous when synthesizing phosphors with high purity and the need for controlled dopant concentrations, offering the flexibility to precisely fine-tune the chemical composition as required for specific applications. Both solid-state synthesis methods serve as invaluable tools for producing phosphor materials, and the choice between them hinges on the desired properties and the level of control necessary in the synthesis process. These methods underscore the pivotal role in materials science, facilitating the development of phosphors with precise optical and luminescent properties that are indispensable for a wide array of technologies [3].

2.1.1.1 Solid-state reaction method for synthesizing phosphor materials

The solid-state reaction method as shown in Figure 2.2 is a versatile and widely employed technique for producing phosphor materials used in displays, lighting, and other optical devices. This method is on the principles of solid-state chemistry, where reactants in solid form are mixed, heated to high temperatures, and allowed to react, resulting in the formation of the desired phosphor compound.

Choosing the appropriate reactants is a critical initial step in the solid-state reaction method. Reactants typically consist of metal oxides, carbonates, or other compounds containing the elements necessary for the desired phosphor material. It is imperative to ensure the purity of these reactants, as any impurities can significantly affect the final product optical and luminescent properties. The stoichiometric ratio of the reactants is crucial in determining the chemical composition of the phosphor material. If the objective is to synthesize a red phosphor for use in LED displays, the proper ratio of components, such as europium-doped yttrium oxide (Y_2O_3:Eu^{3+}), needs to be determined. This ensures that the resulting phosphor will exhibit the desired emission wavelength and color. Accurate weighing of the selected reactants according

to the stoichiometric ratio is essential for the success of the synthesis. Once the reactants are measured, they are thoroughly mixed to achieve a homogeneous blend. Proper mixing ensures that the reactants are evenly distributed, promoting uniform chemical reactions. To further enhance the uniformity of the mixture and increase reactivity, grinding is often employed. Grinding is performed using equipment like a mortar and pestle or a ball mill. This process reduces the particle size and increases the contact between the reactants, which is critical for the success of the solid-state reaction.

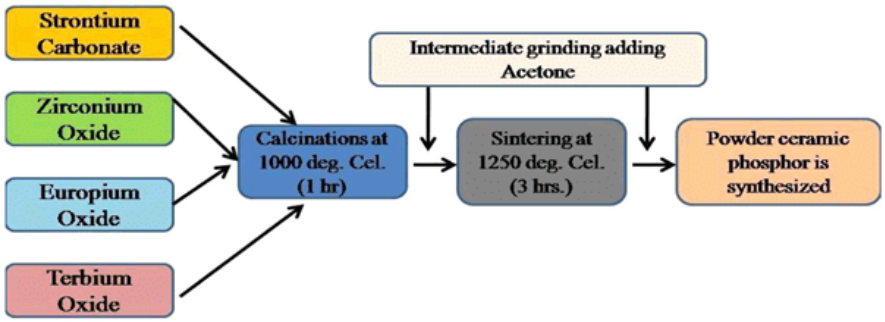

Figure 2.2: Schematic representation of solid-state reaction

The next step is to transform the mixed and ground powder into pellets or tablets. This is usually done by applying pressure to the powder using a hydraulic press. The size and shape of the pellets can be tailored based on the requirements of the application. Pelletizing ensures a more controlled and uniform reaction during the sintering process. Sintering is the core step of the solid-state reaction method. The prepared pellets are placed in a high-temperature furnace or kiln, and the temperature and duration of the sintering process are determined by the specific phosphor material being synthesized. Sintering typically occurs at temperatures ranging from 1,000 to 1,500 degrees Celsius. During sintering, the solid-state reaction takes place, leading to the formation of the desired phosphor compound. This high-temperature treatment helps the reactants overcome their activation energy barriers and rearrange into the crystalline structure of the phosphor. After the sintering process is complete, it is crucial to cool the samples gradually to room temperature. Rapid cooling can result in thermal shock and phase changes, which may affect the quality and properties of the synthesized phosphor material [4-6].

2.1.2 Modified solid-state reaction method

Modified solid-state reaction methods as shown in Figure 2.3 are a versatile approach to synthesizing various phosphor materials with distinctive properties. These methods introduce modifications to the traditional solid-state reaction process, enhancing the control over composition, structure, and performance. Several such techniques include the flux method, which involves adding a flux to lower sintering temperatures and improve crystallinity, making it crucial for applications like LED displays; solid-state reactions in a reducing atmosphere, which preserves luminescence by protecting sensitive dopants like Eu^{2+}; high-energy ball milling, where mechanical forces promote reactivity and produce finely divided, highly reactive powders, benefiting applications such as fluorescent lamps; mechanochemical synthesis, which uses mechanical forces to overcome kinetic barriers and attain high-quality phosphors; microwave-assisted synthesis, speeding up reactions and enhancing phase purity in applications like fluorescent lamps; and combustion synthesis, allowing the creation of phosphors with unique properties like long afterglow for safety signs and emergency lighting. These modifications offer precise control over phosphor properties, meeting specific application needs across displays, lighting, sensors, and radiation detectors [7-8].

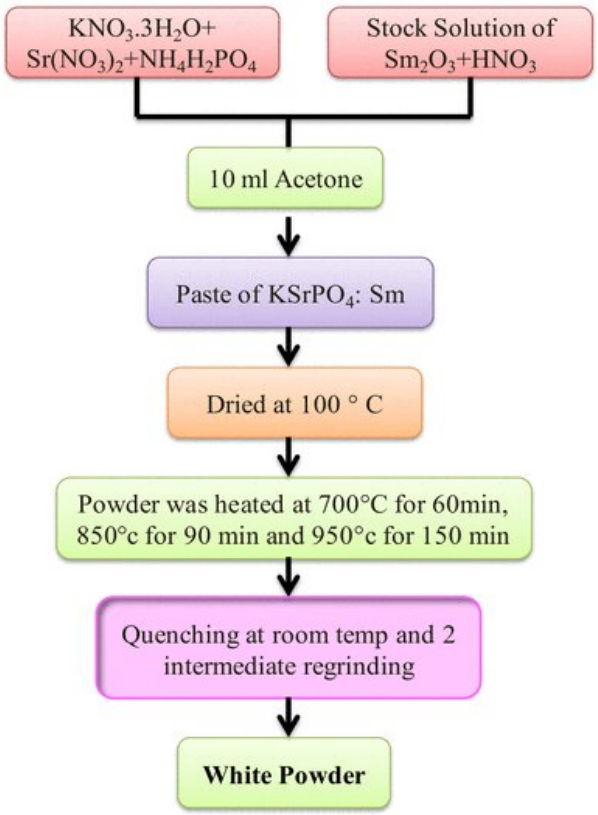

Figure 2.3: Synthetic pathways of modified solid-state reaction

2.1.2.1 Flux-assisted method

The flux method is a modification of the traditional solid-state reaction process, which involves adding a flux or eutectic mixture to the reactants. This modification aims to lower the sintering temperature and promote the formation of a homogeneous and crystalline phosphor. The addition of a flux can significantly impacts the synthesis of phosphor materials, enhancing their properties and performance. For instance, in the synthesis of YAG:Ce (Yttrium Aluminum Garnet doped with Cerium), lithium fluoride (LiF) is often used as a flux. The lithium fluoride reduces the sintering temperature, which is especially beneficial for phosphor materials that are prone to decomposition or phase transformation at high temperatures.

The primary advantage of the flux method is its ability to improve the crystallinity and purity of phosphor materials. By reducing sintering temperatures, it helps to avoid phase impurities and achieve a more uniform crystal structure. This leads to enhanced luminescent properties, making it a valuable technique in developing phosphors for use in various applications. The flux method is particularly useful for producing phosphors used in LED displays, where precise control over the emission characteristics and color quality is essential [9-11].

2.1.2.2 Solid-state reaction under reducing atmosphere

In certain cases, solid-state reactions are performed in a controlled atmosphere with reduced oxygen levels, commonly referred to as a reducing atmosphere and are called modified techniques as shown in Figure 2.4. This modification is crucial for preserving the luminescent properties of certain phosphor materials, especially those doped with Eu^{2+} ions. Europium ions in the 2+ oxidation state is highly sensitive to oxidation, which can degrade their luminescence. To prevent this, solid-state reactions are conducted in an atmosphere containing hydrogen. When synthesizing phosphors like SrS: Eu^{2+} (Strontium Sulfide doped with Europium), it is essential to maintain a reducing atmosphere during sintering. This ensures that the europium ions remain in the 2+ state, preserving the desired luminescent properties. This modification allows for the creation of high-performance phosphors that exhibit intense and stable luminescence, making them suitable for use in cathode-ray tube (CRT) displays and other applications where consistent emission is critical [12-13].

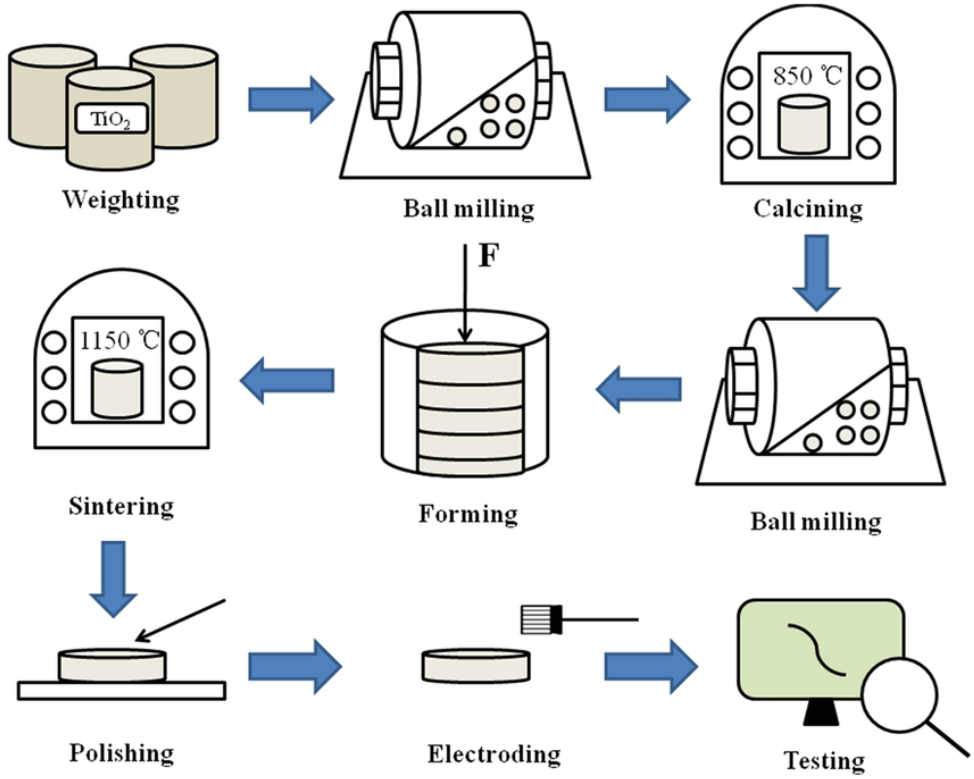

Figure 2.4. Modified solid-state reaction

2.1.2.3 High-energy ball milling

High-energy ball milling as shown in Figure 2.5 is a modified solid-state reaction method that employs mechanical energy to enhance the reactivity of reactants. In this method, reactants are milled together using high-energy ball mills. The mechanical forces generated during milling not only lead to smaller particle sizes but also promote solid-state reactions by overcoming kinetic barriers. High-energy ball milling is particularly useful for creating finely divided and highly reactive powders, which is advantageous for the synthesis of phosphor materials with improved properties. For instance, when synthesizing nanostructured phosphors like ZnO:Eu (Zinc Oxide doped with Europium), high-energy ball milling is often employed. This method results in finer and more uniform particle sizes, enhancing the luminescent properties of the phosphor. The primary benefit of high-energy ball milling is its ability to produce phosphor materials with superior luminescent characteristics, such as increased quantum yield and shorter luminescence decay times. These properties are highly desirable for various applications, including fluorescent lamps, displays, and sensors [14-16].

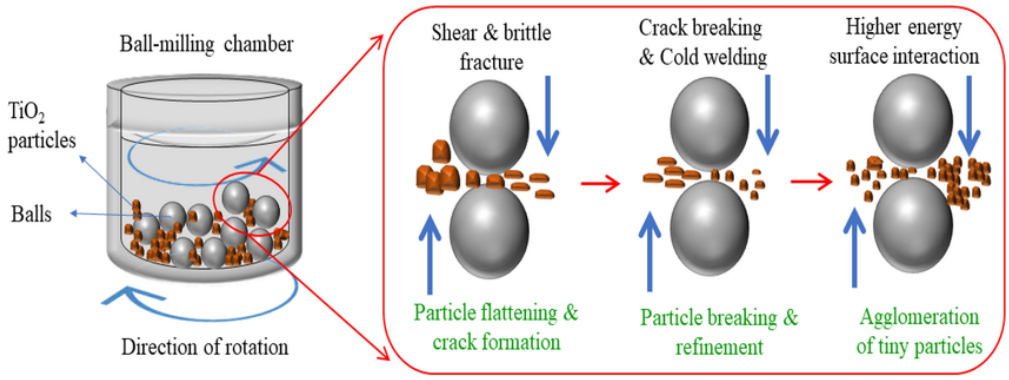

Figure 2.5. Synthetic methods by high-energy ball milling

2.1.2.4 Mechanochemical synthesis

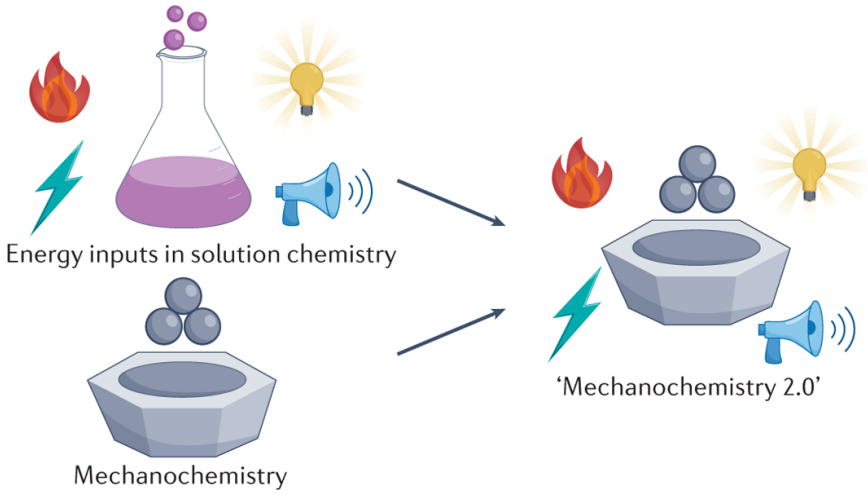

Figure 2.6 : Mechanochemical synthetic method

Mechanochemical synthesis is a modification of the solid-state reaction method where reactants are subjected to mechanical forces, such as grinding or milling, to initiate chemical reactions and is shown in Figure 2.6. This modification is particularly useful for the synthesis of complex phosphor materials, especially those containing rare-earth dopants. For example, in the synthesis of phosphors like $Gd_3Al_5O_{12}:Ce^{3+}$ (Gadolinium Aluminum Garnet doped with Cerium), mechano chemical synthesis can be employed. The mechanical forces introduced during grinding or milling facilitate the mixing of reactants and promote solid-state reactions. This method is advantageous for producing high-quality phosphors with precise control over their chemical composition and structure. This makes it a valuable modification to produce phosphor materials used in high-performance applications, including scintillation detectors and radiation sensors.

2.1.2.5 Microwave-assisted synthesis

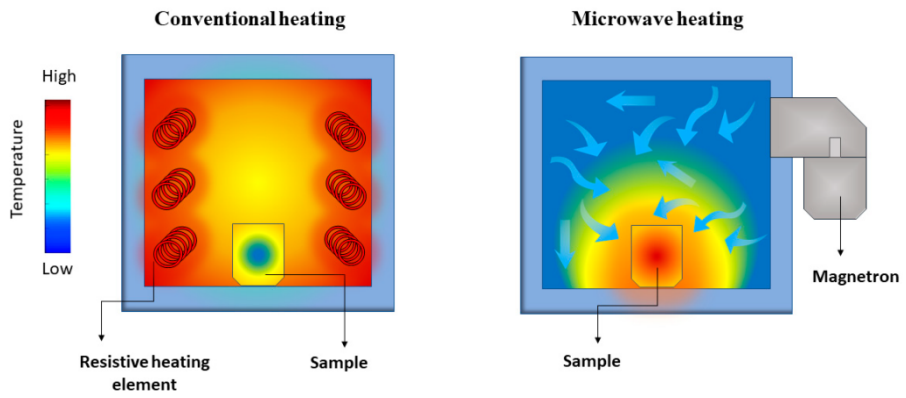

Figure 2.7: Synthetic methods of phosphor material by conventional heating and microwave heating

Figure 2.7 shown is a microwave-assisted synthesis, which is a modification of the solid-state reaction method that utilizes microwave energy to provide the necessary heat for the reaction. Microwave heating is rapid and uniform, allowing for shorter reaction times and often improved phase purity. This modification is particularly useful for synthesizing phosphor materials that are challenging to obtain through conventional solid-state reactions. For example, when synthesizing phosphors like $Y_2O_3:Eu^{3+}$ (Yttrium Oxide doped with Europium), microwave-assisted synthesis can be employed. Microwave heating ensures uniform and rapid energy transfer to the reactants, leading to reduced reaction times and improved crystallinity. This method is especially valuable for producing high-performance phosphors used in applications such as fluorescent lamps and cathodoluminescent displays. The primary advantage of microwave-assisted synthesis is its ability to expedite the reaction process while improving the phase purity and homogeneity of the resulting phosphor material. This makes it a valuable modification for applications where fast and efficient phosphor synthesis is crucial [17-19].

2.1.2.6 Combustion synthesis

Combustion synthesis as shown in Figure 2.8 is a modification of the solid-state reaction method that involves a self-sustaining exothermic reaction between the reactants. This modification is particularly valuable for the synthesis of complex phosphor materials, including those with multiple dopants and intricate structures.

In the synthesis of phosphors like $SrAl_2O_4:Eu^{2+}$ (Strontium Aluminate doped with Europium), combustion synthesis can be employed. During combustion, the release of energy enables rapid heating, promoting the formation of the desired phosphor phases. This method is often used to

create long-persistent phosphors that exhibit afterglow, making them suitable for glow-in-the-dark applications and emergency signage. The primary advantage of combustion synthesis is its ability to produce phosphors with unique properties, such as long afterglow and enhanced luminescence. It is particularly valuable for applications where persistent luminescence is required, such as in safety signs and emergency lighting. Each of these modified solid-state reaction methods offers unique advantages for the synthesis of different phosphor materials, allowing for precise control over their properties. These modifications are essential for developing phosphors to meet the specific requirements of various applications, including displays, lighting, sensors, and radiation detectors. The choice of the appropriate modification depends on the desired phosphor characteristics and the specific challenges posed by the synthesis process [20].

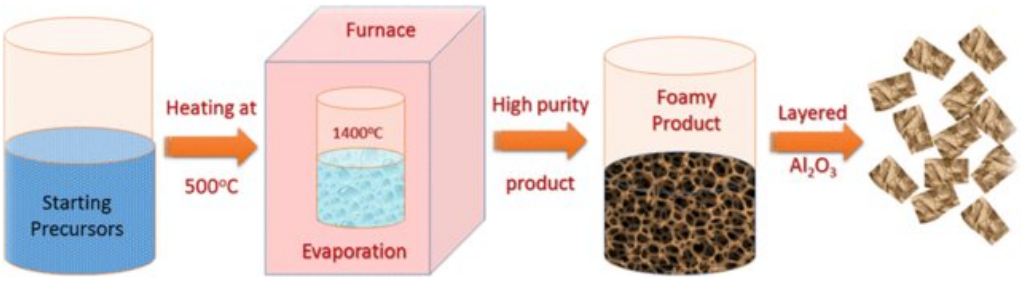

Figure 2.8. Combustion synthesis method

2.2 Characterization

Characterizing the synthesized phosphor material is the final step in the process. Various analytical techniques, such as X-ray diffraction (XRD), photoluminescence (PL) spectroscopy, and scanning electron microscopy (SEM), are employed to evaluate the phosphor's properties. XRD is used to determine the crystalline structure, phase purity, and lattice parameters. PL spectroscopy is essential for studying the luminescent properties of the phosphor, including its emission wavelength, quantum yield, and color quality. SEM is employed to analyze the microstructure and morphology of phosphor material.

The solid-state reaction method offers precise control over the composition, structure, and properties of phosphor materials, making it a valuable technique for developing phosphors for specific applications. The choice of reactants, stoichiometric ratios, and sintering conditions can be adjusted to achieve the desired luminescent properties and optical characteristics, which are crucial in display technologies where accurate and vibrant colors are essential. The solid-

state reaction method is versatile and widely used in materials science due to its flexibility and ability to produce phosphor materials with diverse applications in displays, lighting, and beyond.

2.2.1 XRD studies of phosphor

X-ray Diffraction (XRD) studies of phosphor systems help characterize their crystal structures and compositions. The schematic diagram of X-ray diffraction is shown in Figure 2.9. This information is vital for designing phosphors that emit specific colors, leading to improved color rendition in displays. The detailed structural insights gained through XRD analysis allow for the optimization of phosphor composition, purity, and crystal structure, resulting in more pure and consistent color reproduction in displays. In therapeutic devices, XRD enables the precise development of phosphor materials to emit light at specific wavelengths, making them more efficient and reliable for applications such as photodynamic therapy and medical imaging. Overall, XRD plays a vital role in pushing the boundaries of phosphor technology to improve color rendition and enhance the performance of phosphor-based systems in both display and therapeutic fields. X-ray diffraction (XRD) studies of phosphor systems play a significant role in advancing color rendition in displays and therapeutic applications. Phosphors are luminescent materials used to emit visible light when excited by external energy sources, such as ultraviolet (UV) or X-rays. In the context of displays and therapeutic applications, color rendition, or the ability to accurately reproduce colors, is of paramount importance. In this section, we will explore the ways how XRD studies enhance phosphor systems, leading to improved color rendition in displays and their applications in therapeutic devices.

In display technology, color rendition is a key factor in determining the quality of visual content. Phosphors are used in a variety of display technologies, such as LED and OLED

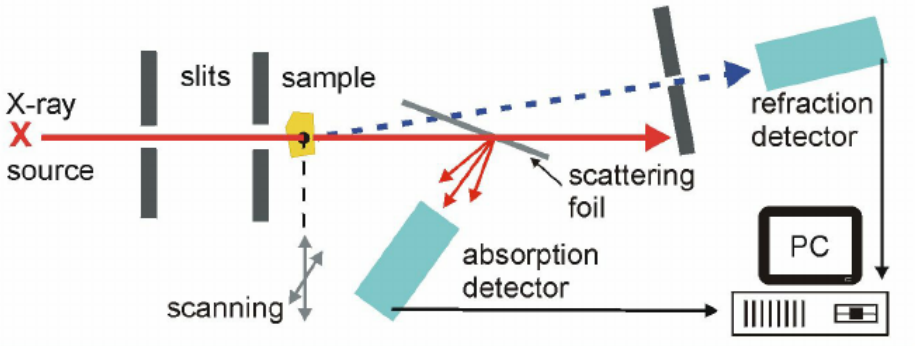

Figure 2.9 : Schematic diagram of X-ray diffraction

screens. XRD analysis of phosphor materials can uncover crucial structural information that

directly impacts their performance. One key aspect is the crystal structure, as different crystal structures can yield varying light emission properties. XRD helps to identify and characterize the crystal phases present in the phosphor material, which can provide insights into the quality and consistency of the material. By understanding the crystal structure, manufacturers can optimize the phosphor composition and structure to enhance color rendition. Furthermore, XRD is valuable in assessing the purity and phase composition of phosphors. In displays, consistent and vibrant color reproduction relies on the purity of the phosphor material. Any impurities or phase changes can lead to shifts in the emitted colors. XRD analysis enables the detection of even trace impurities and offers a quantitative measure of phase composition. Manufacturers can use this data to refine the synthesis process, ensuring that the phosphors used in displays are of high purity, leading to better color rendition and consistent performance over time [21-22].

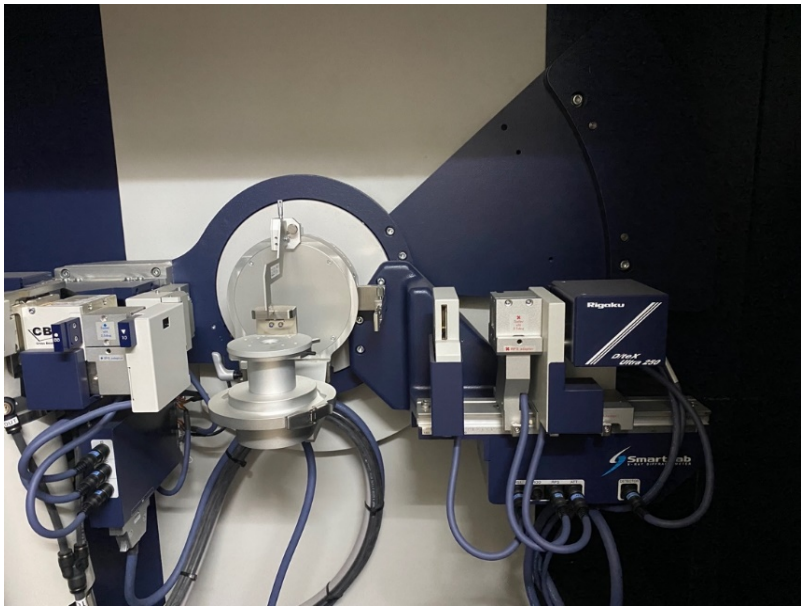

Figure 2.10: X-ray diffraction instrumentation

In therapeutic applications, XRD studies of phosphor systems are instrumental in the development of devices like photodynamic therapy (PDT) and radio luminescent materials for medical imaging. PDT involves the use of photosensitizing phosphors that generate reactive oxygen species when exposed to light, targeting, and destroying cancer cells. Radio luminescent materials, on the other hand, emit visible light when exposed to ionizing radiation, and are used in devices like scintillation detectors for medical imaging. In both cases, the efficiency and reliability of the phosphor are crucial. XRD analysis allows researchers to precisely understand the crystal structure and the phase composition of the phosphors used in these applications,

ensuring they perform as required. The development of phosphor systems for therapeutic applications requires a thorough understanding of the crystal structure and properties of the materials. XRD provides researchers with a wealth of information, including the lattice parameters, crystallite size, and crystal symmetry. This data helps in synthesizing the phosphors to emit light at specific wavelengths, optimizing their efficiency for therapeutic purposes. Moreover, XRD aids in assessing the stability of phosphor materials under exposure to radiation or other external factors, ensuring that they can withstand the demands of the medical applications they are designed for [23-25].

During X-ray diffraction (XRD) investigation, as shown Figure 2.10, a powdered sample is positioned in the trajectory of monochromatic X-rays. In this context, the wavelength (λ) of the X-rays remains constant, while both the angle (θ) and the interplanar spacing (d) undergo changes. Therefore, X-rays are employed to unveil a diverse range of minute crystallites exhibiting various orientations. The reflections occur for values of d, θ, and λ that meet Bragg's law. The powder method, which is widely employed in diffraction analysis for elucidating the structural properties of crystalline solids, represents the subject of discussion in this context. The specimen consisted of a fine powder consisting of a large quantity of randomly oriented little crystallites. The technique of polycrystalline content crushing has been employed to circumvent the repetitious process of single crystal development. In contemporary X-ray diffractometers, a radiation detector, such as an ionization chamber or scintillation detector, is employed to supplant photographic films. This detector is responsible for monitoring the positions and relative intensities of the distinct reflected lines, while also considering the angle 2θ. The detector is affixed to a goniometer and possesses the ability to rotate around the sample at various velocities. The conversion of diffraction peaks to d-spacing enables the identification of minerals, as each mineral possesses a distinct set of d-spacing values.

2.2.2 SEM observations

SEM analysis remains a critical tool for examining the microstructure, particle size, surface morphology, distribution, and impurity levels of phosphor materials. This study helps the researchers make reports from the literature to modify the microstructure, particle size, surface morphology, distribution, and impurity levels of phosphor materials to enhance the color quality of displays. These studies demonstrate that SEM is invaluable for optimizing phosphor synthesis and deposition processes, ultimately leading to displays with more vibrant and consistent colors. Numerous studies have shown that the microstructure of phosphor particles

significantly affects their performance in display applications. The researchers used SEM to analyze the particle size distribution of various phosphor samples. They found that displays incorporating smaller, uniform phosphor particles exhibited enhanced color rendition and reduced color uniformity issues, highlighting the importance of controlling particle size through precise synthesis methods. Surface morphology is another critical factor in color rendition. displays. SEM imaging revealed that phosphors with smoother and more regular surfaces displayed less scattering and higher light extraction efficiency. This led to improved color saturation and brightness, making a strong case for optimizing surface morphology through manufacturing processes [25-26].

Distribution of phosphor particles within the display structure is a key concern for ensuring uniform color rendition. Combined study of SEM and tomography techniques to investigate the three-dimensional distribution of phosphor particles in LED displays. The results of many studies demonstrated that a well-controlled, uniform spatial arrangement of phosphor particles led to more consistent color emission across the entire display, reducing color variation and improving overall color rendition. Furthermore, impurities and inclusions can have a substantial impact on the quality of color produced by phosphor systems. SEM in combination with energy-dispersive X-ray spectroscopy (EDS) to assess impurity levels in phosphor materials. Studies revealed that even trace impurities of certain elements, such as transition metals, could cause unwanted color shifts in LED displays. It emphasized the necessity of rigorous quality control and material purity in the manufacturing of phosphor systems to achieve superior color rendition.

Field-emission scanning electron microscopy (FE-SEM) as shown in Figure 2.11 provides comprehensive topographical and elemental information with an extensive depth of field, with magnifications ranging from 10X to 300,000X. The field emission scanning electron microscope (FE-SEM) is utilized to generate visual representations of a specimen through the process of scanning the surface using a focused electron beam. The interaction between electrons and atoms within the sample facilitates communication, leading to the generation of diverse signals that yield valuable insights about the surface topography and composition of the sample. The FE-SEM (Field Emission Scanning Electron Microscope) generates several signals, including secondary electrons, back-scattered electrons (BSE), distinctive X-rays, light (cathodoluminescence), specimen current, and transmitted electrons. In the field emission scanning electron microscope (FE-SEM), electrons undergo reflection (specifically

backscattering) through elastic scattering interactions with atoms present in the bulk specimen. Backscattered electrons (BSE) refer to electrons with high energy that are emitted from the electron beam and then reflected or scattered in the opposite direction. Backscattered electrons (BSE) are employed in order to identify variations in chemical composition between various regions. This is due to the fact that heavy elements, characterized by a higher atomic number, exhibit a greater intensity of backscattered electrons compared to light elements with lower atomic numbers. Consequently, these heavy atoms appear more prominently in the resulting image, displaying a brighter appearance. The process of inelastic scattering involves the expulsion of low-energy secondary electrons (with an energy of 50 eV) from the k-shell of atoms in the specimen due to interactions with beam electrons.

In the field emission scanning electron microscopy (FE-SEM) technique, an electron beam is generated using thermionic emission. This process involves the emission of electrons from an electron gun that is equipped with a cathode made of tungsten filament in the shape of a pin.

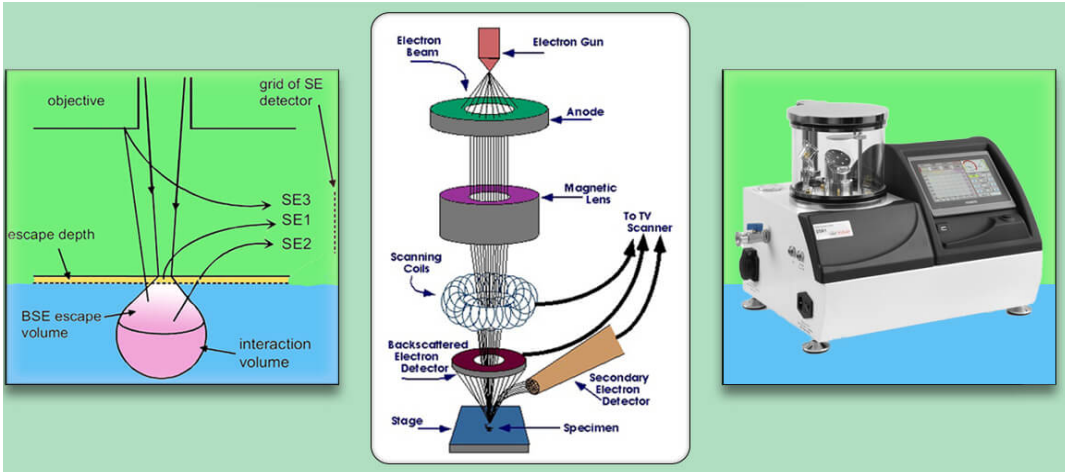

Figure 2.11: Electron interaction with specimen and different parts of SEM

2.2.3 Energy Dispersive X-ray Analysis (EDAX)

Energy Dispersive X-ray Analysis (EDAX) as shown in Figure 2.12 reveals the elemental composition of phosphors, ensuring the right chemical composition for accurate color emission in displays. By identifying and optimizing the elemental content, displays can produce consistent and vibrant colors, leading to improved color rendition. Phosphors are essential components of display technologies, such as LED and OLED screens, and their elemental composition plays a pivotal role in color generation. In this section, we will explore how EDAX analysis provides valuable insights into the elemental makeup of phosphor materials, allowing researchers and manufacturers to fine-tune their properties for superior color rendition.

The elemental composition of phosphor materials directly impacts the colors they emit when excited by an energy source. By using EDAX, researchers can precisely determine the presence and relative quantities of elements within the phosphors. This data is crucial for understanding the color properties of the material, as different elements and their concentrations result in varied color emissions. Europium is commonly used as a dopant in red phosphors, while cerium can influence the emission in green phosphors. By quantifying these elements through EDAX analysis, manufacturers can make phosphor compositions to produce the desired colors with accuracy and consistency. Furthermore, EDAX analysis is instrumental in assessing the purity of phosphor materials. Impurities or foreign elements in phosphors can lead to unwanted color shifts and degradation in color quality. The ability of EDAX to detect and quantify impurities in the material is essential for ensuring that the phosphor is of high purity. This is particularly important in the manufacturing of displays, where consistent and precise color rendition is imperative. By identifying impurities, manufacturers can take corrective measures to minimize their presence and enhance the color consistency of displays.

Figure 2.12 : Energy Dispersive X-ray analysis instrumentation

In addition to determining the elemental composition and identifying impurities, EDAX analysis aids in quality control during the production of phosphor systems. The technique allows for the quantification of elements within the material, enabling manufacturers to set specific quality standards and ensure that the phosphor composition aligns with the desired color properties. For instance, in LED displays, manufacturers can establish tight tolerances for the dopant concentration levels of red and green phosphors to achieve a consistent and accurate color gamut. EDAX assists in verifying that these quality standards are met, contributing to

improved color rendition. Moreover, EDAX analysis is pivotal in troubleshooting color issues in displays. When displays exhibit color shifts or variations, EDAX can be employed to investigate the elemental composition of the phosphor systems. By comparing the elemental data from different parts of the display or from various batches of phosphor materials, researchers can identify the source of color inconsistencies. This diagnostic capability helps pinpoint and resolve manufacturing or material issues that may be affecting color rendition [27-30].

In each element, the atomic structure has a unique electronic configuration, and each electron has a specific orbital/binding energy Eb, so the binding energies of photoelectrons ejected from energy shells/orbitals or radiation emitted from atoms due to electron transitions are characteristic or figure prints of the element from which they are emanated. Fig. 2.9 shows EDX instrumentation schematic. This chemical microanalysis approach complements SEM. When the SEM's electron beam hits the sample's surface, atoms eject electrons. Electrons from a higher state fill the electron vacancies, and an X-ray offsets the energy gap. The element from which X-rays were released can be identified by their energy. This equipment can analyze features or phases as small as 1 μm or less. The FE-SEM electron beam investigates the sample, emitting distinctive X-rays. The EDS's X-ray detector measures X-ray abundance/flux related to energy. Lithium-doped silicon compounds make up the solid-state detector. When an X-ray hits the detector, a charge pulse of the same energy is generated.

A charge-sensitive preamplifier converts the charge pulse to a voltage pulse proportional to X-ray energy. The pulse voltages were sorted using a multichannel analyzer. A device displays and evaluates each incident x-ray based on voltage measurement.

The output is a histogram of the detector's X-ray energy, with discrete peaks that offer a "fingerprint" of the elements present and heights proportional to the sum of each element in the specimen.

2.2.4 Fourier-Transform Infrared (FTIR) spectroscopy

Figure 2.13 shows the FT-IR spectroscopy instrumentation. FTIR analysis aids in understanding phosphor composition, ensuring consistency, and optimizing phosphor materials for display technology. It identifies chemical bonds and impurities, contributing to reliable color rendition. Color rendition improvement is primarily achieved through phosphor design, color filters, and calibration techniques. FTIR helps maintain and fine-tune phosphor quality

for superior display performance. Phosphors are crucial components in various display technologies, including LED, OLED, and plasma screens. The vibrancy and accuracy of colors produced by these displays rely on the composition, structure, and properties of the phosphor materials. FTIR analysis provides insights into the molecular structure, functional groups, and chemical composition of phosphors, offering valuable information to researchers and manufacturers. In this discussion, we will delve into how FTIR analysis contributes to improving color rendition in displays.

Each phosphor compound has a unique molecular arrangement, and different functional groups within the material can influence the absorption and emission of light. FTIR spectroscopy identifies the characteristic vibrational frequencies associated with these molecular bonds and functional groups. By analyzing the FTIR spectra of phosphor materials, researchers can gain a deep understanding of their chemical composition. For instance, compounds containing rare earth elements like europium or terbium can exhibit distinctive FTIR spectra, providing insights into their structural features. This molecular information is invaluable for fine-tuning the chemical composition of phosphors to achieve precise color reproduction in displays.

In addition, FTIR analysis is useful for characterizing the purity of phosphor materials. Impurities or foreign compounds can significantly impact the optical properties of phosphors, resulting in color shifts or variations. FTIR spectroscopy allows researchers to identify the presence of impurities in phosphor samples by detecting unexpected absorption peaks or spectral features. By quantifying the concentration of impurities, manufacturers can take corrective actions to enhance the purity of phosphor materials. In display applications, where consistent color rendition is essential, ensuring high purity is critical for achieving accurate and vibrant colors. Moreover, FTIR analysis is pivotal in monitoring and optimizing the production process of phosphor materials. By regularly analyzing FTIR spectra during synthesis, manufacturers can confirm that the desired chemical composition is being achieved. Any deviations or anomalies in the spectra can highlight issues with the synthesis process, enabling quick adjustments to maintain quality control. FTIR also facilitates the study of intermediate chemical reactions occurring during the synthesis, offering insights into reaction kinetics and the formation of specific phosphor compounds. This real-time process monitoring enhances the reliability and reproducibility of phosphor materials, leading to improved color rendition in displays.

Furthermore, FTIR analysis can assist in addressing color issues in displays by identifying the causes of color inconsistencies. When displays exhibit shifts or variations in color, FTIR can be applied to investigate the chemical composition of phosphor systems. By comparing FTIR spectra from different parts of the display or from various batches of phosphor materials, researchers can pinpoint the source of the color discrepancies. Whether it is an impurity, a compositional variation, or a change in the molecular structure, FTIR can reveal the underlying issue, allowing manufacturers to take targeted corrective actions to improve color rendition [31-34].

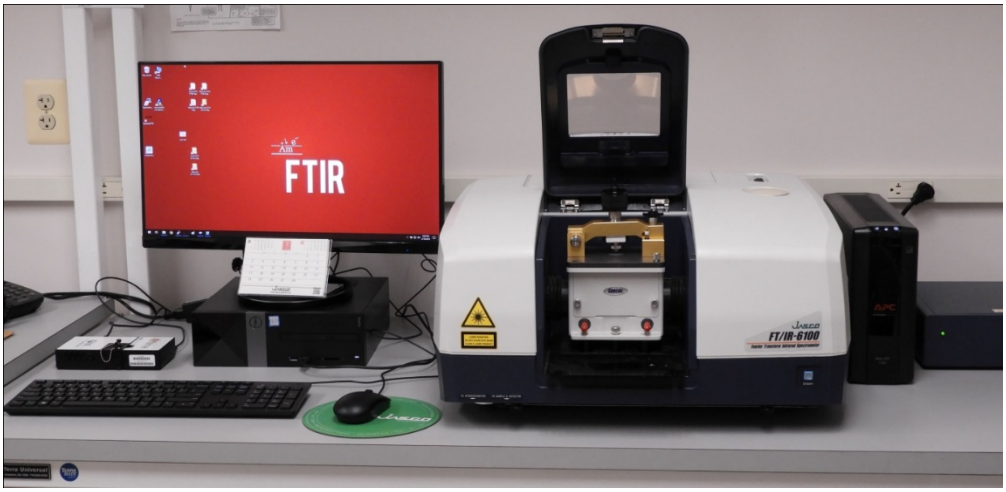

Figure 2.13: FT-IR spectroscopy instrumentation

2.2.5 Photoluminescence Excitation (PLE) and Photoluminescence (PL)

PLE and PL analyses is done using Fluorescence spectrometer as shown in Figure 2.14 and is to optimize phosphor efficiency by determining excitation and emission spectra. This enables precise tuning of phosphor compositions for desired color accuracy in displays. Calibration using PLE and PL data expands the color gamut and minimizes spectral overlaps. This analyses support research and development efforts for improved phosphor materials, contributing to enhanced color rendition in display technology. Phosphors are essential components in various display technologies, such as LED, OLED, and plasma screens, as they are responsible for emitting light of specific colors. PLE and PL analyses offer valuable insights into the excitation and emission spectra of phosphors, allowing researchers and manufacturers to fine-tune their properties for optimal color rendition. Firstly, PLE analysis is employed to study the excitation spectra of phosphor materials. It involves measuring the absorption of photons as a function of their energy, effectively identifying the wavelengths of light that excite the phosphor and cause it to emit light. This technique helps determine the optimal excitation conditions for achieving

true and accurate colors in displays. Research has shown that PLE analysis is essential for characterizing the spectral properties of phosphors. Many study focused on the PLE spectra of various phosphor materials used in LED displays and it revealed the intricate excitation patterns of different phosphors, providing insights into the ideal excitation wavelengths for maximum color saturation and brightness. Secondly, PL analysis complements PLE by examining the emission spectra of phosphors. It measures the light emitted by the phosphor materials when excited by specific wavelengths of light, offering information about the color and intensity of the emitted light. By analyzing PL spectra, researchers can determine the emission characteristics of phosphors, such as the dominant wavelength, full width at half maximum (FWHM), and color coordinates. PL analysis enabled precise characterization of the color gamut and its correlation with specific phosphor compositions, ultimately leading to improved color rendition.

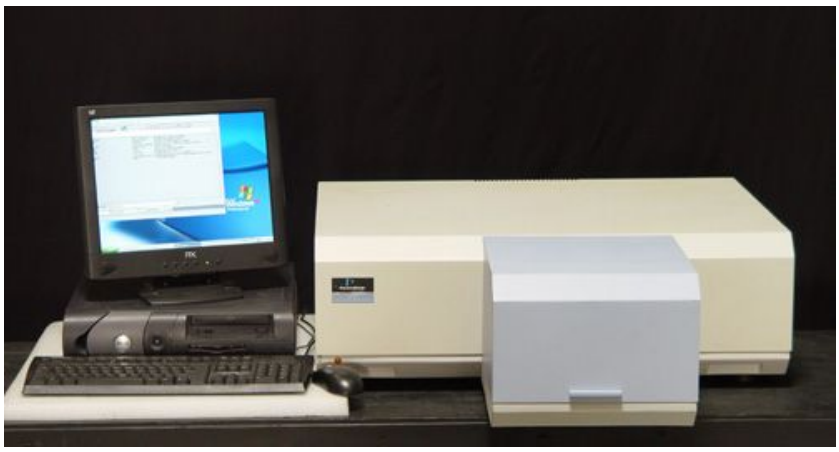

Figure 2.14 : Fluorescence spectrometer

Furthermore, PLE and PL analyses are crucial for optimizing the performance of phosphor systems in displays. These analyses provide a detailed understanding of the excitation and emission properties of phosphor materials, allowing researchers to fine-tune the composition and structure for maximum color rendition. For instance, in LED displays, the choice of phosphor material and its excitation and emission characteristics can significantly impact the overall color quality. By carefully selecting and engineering phosphor materials based on the data obtained from PLE and PL analyses, manufacturers can achieve displays with the highest color accuracy and vibrancy. This not only enhances the visual experience for consumers but also meets industry standards for color quality.

Moreover, PLE and PL analyses are invaluable for assessing the stability and durability of phosphor materials in display applications. Long-term color stability is a critical requirement for display technologies. Research has demonstrated that PLE and PL analyses can be used to

monitor the changes in the excitation and emission spectra of phosphors over time, allowing researchers to predict and address issues related to color stability. The stability of phosphor materials in LED displays using PLE and PL analyses revealed the spectral changes that occur with extended use and provided insights into materials engineering strategies to enhance long-term color stability[35-39].

2.2.6 Temperature-Dependent Photoluminescence (TDPL) analysis

Temperature-Dependent Photoluminescence (TDPL) instrumentation as shown in Figure 2.15 is required for analysis using specialized spectroscopy technique that measures the photoluminescent properties of materials at varying temperatures. It involves exciting the material with light and then detecting and analyzing the subsequent emission as a function of temperature. TDPL is particularly useful for studying phosphor systems used in displays, as it can reveal how the optical properties of these materials change with temperature variations. TDPL analysis provides researchers with valuable data about the temperature-dependent behavior of phosphor systems. This data helps in understanding how temperature affects the emission characteristics, color quality, and stability of the phosphor materials. TDPL analysis of phosphor materials for LED displays. shows how temperature influences the emission spectra, color temperature, and color rendering properties of the phosphors. It revealed that temperature-induced shifts in emission wavelengths can lead to changes in color quality. By using TDPL, researchers were able to precisely quantify these shifts and adjust maintain stable and accurate color rendition across a range of operating temperatures. The data obtained from TDPL analysis is instrumental in optimizing the color quality of displays, particularly in applications where temperature variations are common. In displays, maintaining consistent and accurate colors, regardless of temperature changes, is a crucial requirement.

Figure 2.15 : Temperature-dependent fluorescence spectrometer

TDPL analysis aids in fine-tuning the composition and properties of phosphor materials to confirm they exhibit the desired color performance under varying temperature conditions. By using the insights from TDPL, manufacturers can choose or engineer phosphors that are less susceptible to temperature-induced shifts and provide superior color rendition in a wide temperature range. TDPL analysis is also critical for assessing the stability and reliability of phosphor systems in display applications. Understanding how temperature affects the luminescent properties of phosphors helps in predicting their long-term performance. A study conducted on TDPL to investigate the thermal stability of phosphor materials used in OLED displays. The research revealed how temperature-induced degradation can impact the color properties and overall performance of the materials. With TDPL data in hand, researchers and manufacturers can develop strategies to enhance the stability and reliability of phosphor systems for displays, ensuring that they maintain accurate color rendition over time [40-42].

2.2.7 Particle size distribution analysis

Analysis using Particle size distribution as shown in Figure 2.16 ensures uniformity in phosphor particle sizes, which is crucial for consistent light emission. In displays, this uniformity leads to even color rendition, enhanced brightness, and reduced color variation, contributing to improved display quality. Phosphors play a pivotal role in various display technologies, including LED, OLED, and plasma screens. The particle size of phosphor materials is closely linked to their optical properties and, consequently, color rendition. In this discussion, we will explore the importance of particle size distribution analysis, its impact on color quality, and how it is employed to enhance displays.

Particle size distribution analysis is a method used to determine the range and distribution of particle sizes within a material, such as phosphor systems. In this process, particles are measured for their dimensions, including diameter and shape, and then categorized into different size fractions. The distribution is often represented as a histogram or a cumulative curve, which provides a visual representation of how particles are distributed across the size range. The particle size of phosphor materials is intimately linked to their color rendition capabilities. In displays, color is produced by the interaction of light with the phosphor particles. The size and distribution of these particles can influence the color quality in several ways. For instance, smaller and more uniform particles tend to emit more true and consistent colors. Larger particles or a wide range of particle sizes can scatter and absorb light differently, leading

to variations in color saturation and brightness. Therefore, analyzing and controlling the particle size distribution is vital for achieving accurate and reliable color rendition.

Several studies have explored the relationship between particle size distribution and color rendition in displays. Phosphors with a narrow and well-controlled particle size distribution exhibited enhanced color saturation and uniformity. Furthermore, by changing the particle size distribution, the researchers were able to achieve improved color rendering properties, leading to a more accurate and consistent color performance in LED displays. Particle size distribution analysis is essential for optimizing color rendition in displays. By analyzing and manipulating the distribution of phosphor particle sizes, one can ensure that the emitted light is of the highest quality. This optimization can be especially crucial in applications where maintaining consistent and accurate colors is essential, such as in professional displays or medical imaging equipment. The data obtained from particle size distribution analysis allows to select or engineer phosphor materials with the desired particle characteristics to achieve the best color quality for specific display technologies.

Figure 2.16 : Particle size distribution instrumentation

Particle size distribution analysis is not limited to research settings; it plays a significant role in various real-world applications. For instance, in OLED displays, the particle size distribution of phosphor materials is critical for achieving precise color rendition. By accurately controlling the particle sizes, OLED manufacturers can produce displays with true and uniform colors, ensuring an outstanding viewing experience for consumers. Additionally, in medical imaging devices that use radio luminescent phosphor materials, particle size distribution analysis helps in optimizing the performance of scintillation detectors [43-44].

2.2.8 CIE color coordinates

The International Commission on Illumination (CIE) color coordinates as shown in Figure 2.17 play a fundamental role in the assessment and enhancement of color rendition in displays, especially when it comes to phosphor systems. CIE color coordinates offer a standardized and objective way to quantify and represent colors, which is crucial for achieving accurate and vibrant colors in display technologies. In this section, we will explore the significance of CIE color coordinates in the context of phosphor systems, their impact on color rendition, and their application in display technology with the inclusion of relevant research data.

The CIE established a set of color spaces and coordinates to provide a standardized framework for characterizing colors. The most widely used CIE color space is the CIE 1931 XYZ color space. This color space describes colors using three parameters: X, Y, and Z. X and Y represent the chromaticity coordinates, which describe the hue and saturation of a color, while Z is related to the brightness or luminance of the color. Color rendition in displays depends on the ability of the display's phosphor system to accurately reproduce colors. CIE color coordinates provide a fundamental means to evaluate and optimize color rendition. The CIE 1931 XYZ color space allows for a precise representation of colors in a manner that is perceptually meaningful to the human visual system. By quantifying colors using CIE coordinates, manufacturers can ensure that the displayed colors are not only vivid but also perceptually accurate.

Various studies have leveraged CIE color coordinates to assess and improve the color rendition of phosphor systems in display technologies. The study utilized CIE color coordinates to evaluate the color quality of various LED configurations. By analyzing the data in the CIE color space, the research demonstrated how specific phosphor combinations resulted in improved color rendition, as indicated by the proximity of their CIE coordinates to ideal values that represent true colors. This research underscores the importance of using CIE color coordinates to assess and enhance color quality in LED displays. CIE color coordinates offer a standardized framework for evaluating and optimizing color rendition in displays, particularly in applications where maintaining consistent and true-to-life colors is essential. Manufacturers utilize these coordinates to fine-tune the composition of phosphor materials, ensuring that the emitted light aligns with the intended colors. This optimization is particularly critical in professional displays, medical imaging monitors, and applications where color accuracy plays a pivotal role.

By adhering to CIE standards, manufacturers can guarantee that the light produced by their displays matches the specified colors and is perceived accurately by the human eye.

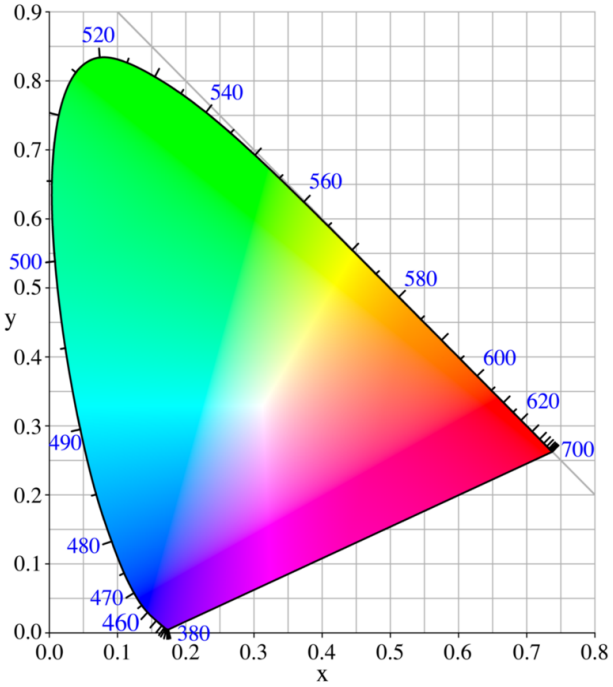

Figure 2.17 : The CIE 1931 colour space chromaticity diagram with wavelengths in nanometers

CIE color coordinates have practical applications in the development and production of various display technologies. In OLED displays, accurate color representation is crucial for creating lifelike and stunning images. Manufacturers use CIE color coordinates to evaluate the performance of OLED materials and ensure that the emitted light closely matches the intended colors. In the field of medical imaging, especially radiology displays, CIE color coordinates are essential for maintaining the precise representation of medical images. Accurate color rendition is critical for the accurate diagnosis of medical conditions, making the faithful representation of colors a matter of utmost importance [45-49].

References

[1] K. N. Shinde, S. J. Dhoble, H. C. Swart, and K. Park, "Phosphate phosphors for solid-state lighting," Springer Science & Business Media, Dec. 2012.

[2] L. Wang, R. J. Xie, T. Suehiro, T. Takeda, and N. HirosakiChemical reviews, vol. 118, no. 4, pp. 1951-2009, Feb. 28, 2018.

[3] W. Pan, G. Ning, X. Zhang, J. Wang, Y. Lin, and J. Ye, Journal of Luminescence, vol. 128, no. 12, pp. 1975-1979, Dec. 1, 2008.

[4] Z. Song, J. Liao, X. Ding, X. Liu, and Q. Liu, Journal of Crystal Growth, vol. 365, pp. 24-28, Feb. 15, 2013.

[5] J. H. Lee and Y. J. Kim, Materials Science and Engineering: B, vol. 146, no. 1-3, pp. 99-102, Jan. 15, 2008.

[6] M. P. Saradhi and U. V. Varadaraju, " Chemistry of Materials, vol. 18, no. 22, pp. 5267-5272, Oct. 31, 2006.

[7] L. T. Vien, N. Tu, M. T. Tran, N. Van Du, D. H. Nguyen, D. X. Viet, N. V. Quang, D. Q. Trung, and P. T. Huy, Optical Materials, vol. 100, p. 109670, Feb. 1, 2020.

[8] A. G. Kirakosyan and D. Y. Jeon, Journal of The Electrochemical Society, vol. 159, no. 2, pp. J29, Dec. 19, 2011.

[9] Y. J. Park and Y. J. Kim, Materials Science and Engineering: B, vol. 146, no. 1-3, pp. 84-88, Jan. 15, 2008.

[10] H. J. Lee, K. P. Kim, G. Y. Hong, and J. S. Yoo, Journal of Luminescence, vol. 130, no. 6, pp. 941-946, Jun. 1, 2010.

[11] X. Li, Z. Yang, L. Guan, C. Liu, and P. Li, Journal of Crystal Growth, vol. 310, no. 12, pp. 3117-3120, Jun. 1, 2008.

[12] Q. Long, C. Wang, Y. Li, J. Ding, X. Wang, and Y. Wang, Materials Research Bulletin, vol. 71, pp. 21-24, Nov. 1, 2015.

[13] Y. Lin, Z. Niu, Y. Han, C. Li, W. Zhou, J. Zhang, L. Yu, and S. Lian, Journal of Alloys and Compounds, vol. 690, pp. 267-273, Jan. 5, 2017.

[14] L. T. Vien, N. Tu, T. T. Phuong, N. T. Tuan, N. V. Quang, H. Van Bui, A. T. Duong, D. Q. Trung, and P. T. Huy, Journal of Luminescence, vol. 215, p. 116612, Nov. 1, 2019.

[15] H. K. Yang and J. H. Jeong, The Journal of Physical Chemistry C, vol. 114, no. 1, pp. 226-230, Jan. 14, 2010.

[16] Y. W. Seo, H. M. Noh, B. K. Moon, J. H. Jeong, H. K. Yang, and J. H. Kim, Ceramics International, vol. 41, no. 1, pp. 1249-1254, Jan. 1, 2015.

[17] D. Choi and P. N. Kumta, Materials Science and Engineering: C, vol. 27, no. 3, pp. 377-381, Apr. 1, 2007.

[18] X. Xu, J. Tang, T. Nishimura, and L. Hao, Acta Mater. vol. 59, no. 4, pp. 1570-1576, Feb. 1, 2011.

[19] Q. Zhang and F. Saito, Advanced Powder Tech, vol. 23, no. 5, pp. 523-531, Sep. 1, 2012.

[20] Zhang P, Li L, Xu M, Liu L. Journal of Alloys and Comp. 2008 May 29;456(1-2):216-9.

[21] Y. Li and X. Liu, Materials Science and Engineering: B, vol. 188, pp. 20-25, Oct. 1, 2014.

[22] F. W. Liu, C. H. Hsu, F. S. Chen, and C. H. Lu, Ceramics International, vol. 38, no. 2, pp. 1577-1584, Mar. 1, 2012.

[23] S. Mondal, S. Park, J. Choi, T. M. Vo, J. H. Shin, Y. H. Kang, and J. Oh, Ceramics International, vol. 46, no. 18, pp. 29249-29260, Dec. 15, 2020.

[24] L. Sutrisno, H. Chen, Y. Chen, T. Yoshitomi, N. Kawazoe, Y. Yang, and G. Chen, Biomaterials, vol. 275, p. 120923, Aug. 1, 2021.

[25] G. Zhao, L. Xu, Y. Guo, J. Hou, Y. Liu, Y. Zhou, J. G. Li, and Y. Fang, Journal of the European Ceramic Society, vol. 41, no. 1, pp. 752-758, Jan. 1, 2021.

[26] Z. Wu, J. Nitsch, and T. B. Marder, Advanced Optical Materials, vol. 9, no. 20, pp. 2100411, Oct. 2021.

[27] K. R. Ashwini, H. B. Premkumar, G. P. Darshan, R. B. Basavaraj, H. Nagabhushana, and B. D. Prasad, J. of Science: Adv Mater and Devices, vol. 5, no. 1, pp. 111-118, Mar. 1, 2020.

[28] S. Sheoran, K. Singh, V. Tanwar, S. Singh, A. Samantilleke, and D. Singh, Rare Metals, vol. 40, pp. 2610-2617, Sep. 2021.

[29] S. Singh, and D. Singh, Journal of Materials Science: Materials in Electronics, vol. 31, pp. 5165-5175, Apr. 2020.

[30] S. Singh, A. P. Samantilleke, and D. Singh, Chemical Physics Letters, vol. 765, p. 138300, Feb. 16, 2021.

[31] W. T. Huang, V. Rajendran, M. H. Chan, M. Hsiao, H. Chang, and R. S. Liu, Advanced Optical Materials, vol. 11, no. 11, p. 2202061, Jun. 2023.

[32]G. N. De Guzman, M. H. Fang, C. H. Liang, Z. Bao, S. F. Hu, and R. S. Liu, Journal of Luminescence, vol. 219, p. 116944, Mar. 1, 2020.

[33] J. Qiao, G. Zhou, Y. Zhou, Q. Zhang, and Z. Xia, Nature Communications, vol. 10, no. 1, p. 5267, Nov. 20, 2019.

[34] M. Zhao, Q. Zhang, and Z. Xia, Accounts of Materials Research, vol. 1, no. 2, pp. 137-145, Oct. 22, 2020.

[35] D. P. Liu, G. Li, A. A. Al Kheraif, and J. Lin, Adv. Optical Mater., vol. 8, no. 16, p. 1901993, Aug. 2020.

[36] A. Balakrishna, L. Reddy, O. M. Ntwaeaborwa, and H. C. Swart, J. Mol. Struct., vol. 1203, p. 127375, Mar. 5, 2020.

[37] M. K. Raju, R. P. Rao, N. Vijayan, and P. A. Azeem, Ceram. Int., vol. 47, no. 19, pp. 26704-11, Oct. 1, 2021.

[38] S. Kaur, A. S. Rao, M. Jayasimhadri, B. Sivaiah, and D. Haranath, J. Alloys Compd., vol. 802, pp. 129-138, Sep. 25, 2019.

[39] S. P. Hargunani, R. P. Sonekar, A. Singh, A. Khosla, and S. Arya, Mater. Technol., vol. 37, no. 7, pp. 450-461, Jun. 7, 2022.

[40] M. K. Sahu, M. Jayasimhadri, and D. Haranath, Solid State Sci., vol. 131, p. 106956, Sep. 1, 2022.

[41] M. H. Fang, P. Y. Huang, Z. Bao, N. Majewska, T. Lesniewski, S. Mahlik, M. Grinberg, G. Leniec, S. M. Kaczmarek, C. W. Yang, and K. M. Lu, Chem. Mater., vol. 32, no. 5, pp. 2166-2171, Feb. 5, 2020.

[42] S. Pradhan, H. Kaur, and M. Jayasimhadri, Ceram. Int., vol. 47, no. 19, pp. 27694-27701, Oct. 1, 2021.

[43] Y. Liu, Z. Qin, and B. Chen, Construction and Building Materials, vol. 231, p. 117131, Jan. 20, 2020.

[44] I. Gupta, S. Singh, S. Bhagwan, and D. Singh, Ceramics Int., vol. 47, no. 14, pp. 19282-19303, Jul. 15, 2021.

[45] M. H. Fang, P. Y. Huang, Z. Bao, N. Majewska, T. Lesniewski, S. Mahlik, M. Grinberg, G. Leniec, S. M. Kaczmarek, C. W. Yang, and K. M. Lu, Chem. Mater., vol. 32, no. 5, pp. 2166-2171, Feb. 5, 2020.

[46] J. Qiao, S. Zhang, X. Zhou, W. Chen, R. Gautier, and Z. Xia, Adv. Mater., vol. 34, no. 26, p. 2201887, Jul. 2022.

[47] A. Wang, Y. Guo, Z. Zhou, X. Niu, Y. Wang, F. Muhammad, H. Li, T. Zhang, J. Wang, S. Nie, and Z. Deng, Chem. Sci., vol. 10, no. 17, pp. 4573-4579, 2019.

[48] Z. Yang, G. Liu, Y. Zhao, Y. Zhou, J. Qiao, M. S. Molokeev, H. C. Swart, and Z. Xia, Adv. Optical Mater., vol. 10, no. 6, p. 2102373, Mar. 2022.

[49] W. P. Lustig, Z. Shen, S. J. Teat, N. Javed, E. Velasco, D. M. O'Carroll, and J. Li, Chem. Sci., vol. 11, no. 7, pp. 1814-1824, 2020.

Chapter - 3

Synthesis and Photoluminescence Characterization of $Ca_2La_2O_5:Eu^{3+}$- A Novel Red-Emitting Phosphor

Features of the Chapter:

The synthesis of a $Ca_2La_2O_5$ lattice doped with Eu^{3+} ions in the range of 0.5-2.5 mol-% was by exploiting a chemical flux having a low melting point during the synthesis. The phosphors were analysed using a range of characterisation techniques including powder X-ray diffraction (PXRD), scanning electron microscopy (SEM), energy dispersive X-ray spectroscopy, particle size distribution, photoluminescence (PL), and Fourier transform infrared spectroscopy. The X-ray diffraction pattern shows that the crystal has a hexagonal crystal structure belonging to the P63/m space group. The experimental results showed that the microstrain (ϵ) had no variation at different dopant concentrations, suggesting the presence of compressive forces within the lattice structure. The scanning electron microscopy (SEM) image showed particles of different sizes and irregular shapes. The EDAX mapping analysis provided confirmation that all components were present in the correct proportions. $Ca_2La_2O_5:xEu^{3+}$ (x = 0.5-2.5 mol-%) phosphor samples showed red photoluminescence with remarkable intensities at 615 and 627 nm when excited at 590 nm, which can be attributed to the Stokes-shifted effects. The emission of light by Eu^{3+} ions, which occurs due to transitions from the $^5D_0 \rightarrow {}^7F_J$ states (J = 0, 1, 2, 3, 4), can be detected in a non-traditional method despite excitation by a wavelength of 590 nm. Another insight was the observation of a significantly higher intensity of photoluminescence (PL) at 627 nm corresponding to the $^5D_0 \rightarrow {}^7F_2$ transition of Eu^{3+} ions, compared to the emission at 615 nm for the same transition category. This discrepancy suggests a high color purity of red-emitting phosphors.

This work has been published in:

Kishore Kumar Aitha, D. Dinakar, Payal P. Pradhan, K. Yadagiri, K. Suresh, Naresh Degda, K.V.R. Murthy & D. Haranath (2023), Journal: **Canadian Metallurgical Quarterly, (2023)**. DOI: https://doi.org/10.1080/00084433.2023.2254128 **(Impact Factor, IF: 0.9)**

3.1 Outline

The electronics industry is experiencing a consistent rise in the need for innovative and highly efficient luminous materials, commonly referred to as phosphors. At present, there exists a diverse range of phosphors that are commercially accessible, and capable of attaining luminous efficacy above 150 lumens per watt. Luminous gadgets have become an indispensable component of our daily urban existence [1], exerting influence across a range of domains including LED televisions, medical applications, and advertising display boards [2]. The devices can be categorized into two main types: incandescence, which exhibits a brilliant glow similar to that of the sun and stars, and luminescence, which is characterized by the emission of cold light from materials [3]. Inorganic compounds that have been doped with rare-earth ions constitute a significant category of phosphors, owing to their notable characteristics including high efficiency in luminescence, the ability to modify emission colors by employing various activators, and exceptional chemical stability [4]. Scholars have been diligently engaged in endeavours to enhance red phosphor owing to its significant market demand in diverse applications such as display and illuminating electronics [5]. The advent of novel light sources such as white-light-emitting diodes (w-LEDs) holds significant promise for general illumination applications owing to their low energy consumption, prolonged lifespan, high color fidelity, and environmentally friendly characteristics [6-10]. The attainment of white-light emission from a phosphor that exists in a single phase is considered to be highly advantageous due to its ability to offer exceptional luminous efficiency [11.12] while avoiding the re-absorption of emitted colours that might potentially arise when several phosphors are used. Phosphors exhibiting white light emission in a single-phase configuration are highly sought after for ultraviolet (UV) pumped white light-emitting diodes (LEDs) due to their ability to improve efficiency and maintain a uniform luminescent output [11,13]. The manipulation of the host crystal's band gap and energy levels via the introduction of rare-earth ion doping is a widely employed technique for attaining desirable luminescence durations. Nevertheless, the establishment of a suitable trap depth in host materials presents a significant obstacle [14-16]. The utilization of the solid-state reaction approach presents several benefits, including simplicity and the ability to produce enormous volumes [17-19].

In the present investigation, we have made alterations to the procedure by integrating a chemical flux characterized by a comparatively low melting point, specifically below 300°C. The investigation of luminous materials based on rare earth elements is significantly enhanced through the utilization of structural and spectral characterization techniques. These approaches facilitate the comprehension of light emission properties and the examination of the

macroscopic and microscopic structure of materials, while also enabling the evaluation of their appropriateness for practical applications.

The europium ion with a trivalent state (Eu^{3+}) displays distinct emission transitions in its spectrum, despite experiencing a minor influence from the surrounding ligand crystal field. This can be attributed to the shielding effect exerted by its outermost electrons. The transitory emission characteristics of Eu^{3+} are greatly influenced by the symmetry of the lattice in which it occurs. The electron transitions occurring in energy levels organized by the 4fn configuration demonstrate parity when there is inversion symmetry, enabling the occurrence of weakly polar magnetic dipole transitions. These transitions follow a selection rule where the total angular momentum quantum number (J) can take values of 0 or 1, except for the forbidden transition from J = 0 to J = 0. Alternatively, in the absence of inversion symmetry in the lattice, electronic-vibrational dipole transitions can take place. The emission lines discussed in the statement are associated with the energy level $^5D_0$ in the excited state. These emission lines originate from the ^7F_J configuration, where J can take on values ranging from 0 to 6. The crystal field's influence on the $^5D_0$ (J = 0) state is negligible, resulting in the splitting of emission transitions at this energy level. The emission lines of Eu^{3+} ions are commonly detected in the red-light spectrum and are widely utilized in luminescent display technologies, including LED-based televisions and fluorescent lights, to improve color accuracy and vibrancy in visual displays. Luminous centres for red-emitting phosphors are frequently utilized [20–27].

3.2 Synthesis

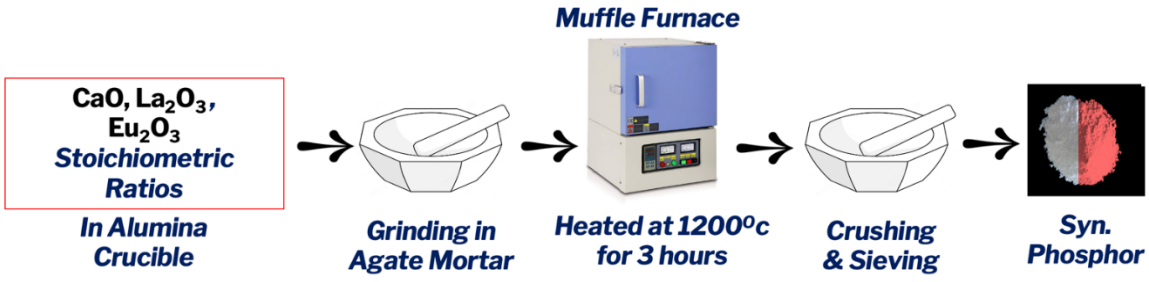

Figure 3.1 : Flow chart depicting the synthesis of phosphor.

The experimental section describes the solid-state reaction (SSR), a widely employed technique for the synthesis of polycrystalline materials using solid chemicals. The solid-state reaction (SSR) entails the utilization of elevated temperatures to initiate the chemical transformation. The process of solid-state reaction (SSR) is influenced by several elements, including the reactivity, surface area, and free energy of the reactants. Additionally, external conditions such as temperature, pressure, and the reaction environment all play a significant role in shaping the SSR process.

The present investigation involves the synthesis of phosphor materials utilizing chemicals of a purity grade of 99.9%. The synthesis process occurs within a muffle furnace with dimensions of 50 cm x 50 cm x 30 cm3. This furnace is equipped with a power rating of 7.5 kilowatts and is capable of reaching a maximum temperature of 1250 degrees Celsius. To enhance the development of the necessary crystalline phase for the lanthanum borate complex during synthesis, an adjustment is made to the solid-state reaction (SSR) method. Specifically, ammonium tetrafluoroborate (ATFB), a chemical flux with a low melting point (<300°C), is intentionally introduced. This addition is made at a concentration exceeding 5 mol%. The compound known as ATFB fulfils two important functions: firstly, it facilitates the promotion of crystalline phase formation when introduced in quantities less than 5 mol-%; secondly, it acts as a precursor for the creation of lanthanum borate complexes when added in quantities exceeding 5 mol-%. The establishment of a $Ca_2La_2O_5$ lattice is ensured by the presence of a specific threshold amount.

Subsequently, a detailed account is provided regarding the preparation of raw materials by precise measurement based on determined proportions, followed by a comprehensive process of blending, and pulverizing within an acetone solution utilizing an agate mortar for 30 minutes, to attain a homogeneous amalgamation. The resulting mixture is subsequently transferred to a recrystallized alumina crucible, together with its cover, and then subjected to sintering at a temperature of 1200°C for three hours within the confines of the muffle furnace. Following the sintering process, the phosphors undergo a natural cooling process until they reach the ambient temperature of approximately 25°C. The resultant sintered mass is further subjected to crushing and milling processes, resulting in the formation of a fine powder that exhibits a white coloration when observed under normal lighting conditions. The completed phosphor material, as shown in Figure 3.1, is subsequently utilized for additional characterization and analysis. Totally five samples were prepared as shown in table 3.1.

The phosphors that have been prepared are subjected to characterization at a temperature of approximately 25°C, utilizing a range of different procedures. The investigation of photoluminescence properties, including excitation and emission investigations, was conducted using an RF-5301PC fluorescence spectrometer that was equipped with a xenon lamp. The $Ca_2La_2O_5:Eu^{3+}$ doped phosphor undergoes phase analysis utilizing the X-ray powder diffraction (P-XRD) technique. The study is conducted using an X'Pert Pro P Analytical Powder Diffractometer equipped with a Cu-Kα radiation source (λ = 1.54 Å). The acquisition of SEM pictures is accomplished through the utilization of a JEOL JSM 5810 LV microscope, while the evaluation of quantitative elemental composition is carried out using an energy-dispersive X-

ray spectroscopy (EDAX) system that is integrated with the SEM instrument. The Fourier transform infrared spectroscopy (FTIR) analysis was conducted employing Perkin Elmer-100 equipment. In addition, the Malvern Mastersizer 3000, a laser diffraction particle size analyzer, is utilized to quantify particle sizes within the range of 0.1 µm to 3 mm. The utilization of emission spectra is also employed in the calculation of chromaticity coordinates, by the standards set by the Commission Internationale de I'Eclairage (CIE). A total of five phosphors were produced by altering the doping concentration of Eu^{3+}.

Table 3.1: Synthesized phosphor with varying dopant concentrations

Sample Number	Host	Dopant	Dopant Concentration
CAL-S1	$Ca_2La_2O_5$	Eu^{3+}	0.5 mol %
CAL-S2	$Ca_2La_2O_5$	Eu^{3+}	1.0 mol %
CAL-S3	$Ca_2La_2O_5$	Eu^{3+}	1.5 mol %
CAL-S4	$Ca_2La_2O_5$	Eu^{3+}	2.0 mol %
CAL-S5	$Ca_2La_2O_5$	Eu^{3+}	2.5 mol %

3.3 Photoluminescence study

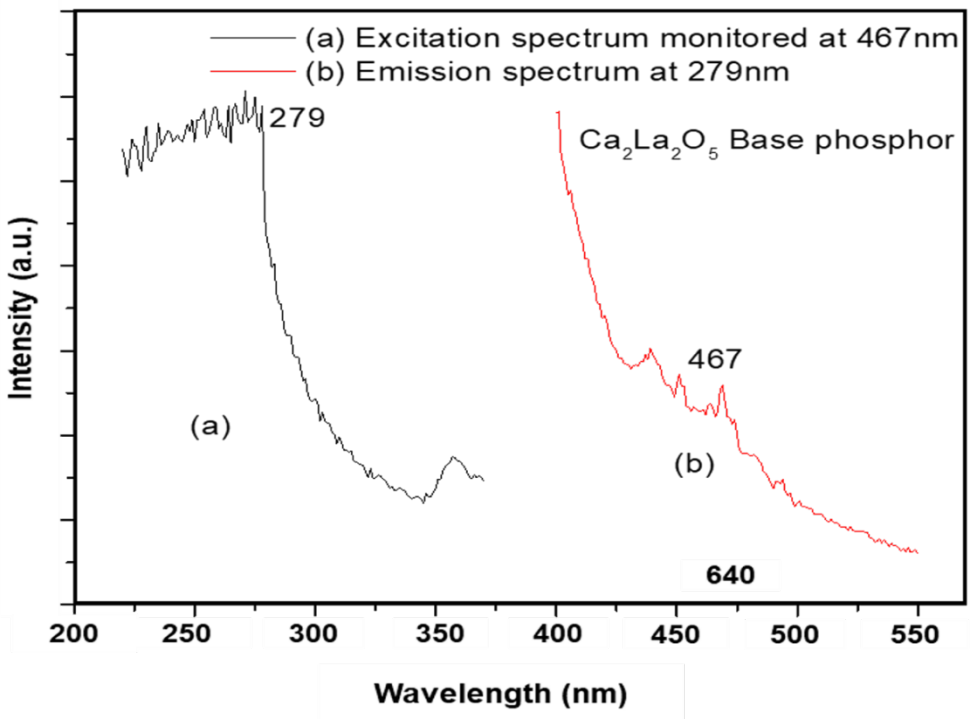

Figure 3.2 : (a) Excitation, and (b) emission spectra of $Ca_2La_2O_5$ host lattice

Figure 3.2 (a-b) depicts the excitation and emission spectra of the intrinsic host lattice (base phosphor) of $Ca_2La_2O_5$ in the absence of any dopant. The absence of discernible peaks for excitation is indicated by the excitation spectra recorded at a wavelength of 467 nm. In contrast, the emission spectra acquired using an excitation wavelength of 279 nm exhibit limited photoluminescence in the visible range. Figure 3.3 displays the spectra of excitation and emission for a $Ca_2La_2O_5$ lattice that has been doped with 2 mol-% Eu^{3+} ions. The excitation spectra were examined at a wavelength of 627 nm, and it was observed that there was a distinct and wide peak at 590 nm. In contrast, the emission spectra acquired at an excitation wavelength of 590 nm exhibit notable photoluminescent peaks at 615 and 627 nm. The emission peak with the greatest intensity is located at a wavelength of 627 nm. In Figure 3.3 (b), it is observed that the phosphor displays discernible fluorescence when excited at a wavelength of 590 nm. This

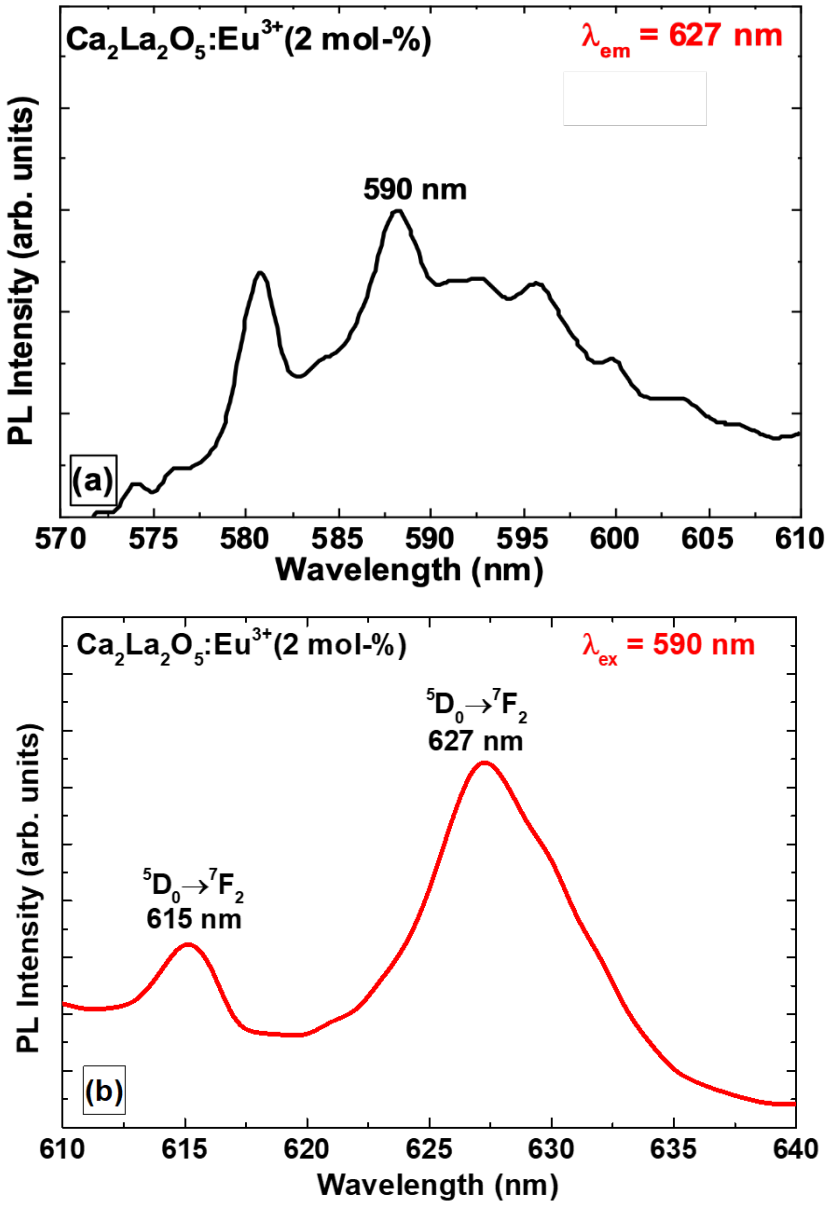

Figure 3.3 : (a) Excitation and (b) emission spectra of $Ca_2La_2O_5$:xEu^{3+} (x= 2 mol%) phosphor

fluorescence can be attributed to the transitions (J=0, J=1, J=2, J=3, J=4) occurring from the $^5D_0 \rightarrow {}^7F_J$ states of Eu^{3+} ions.

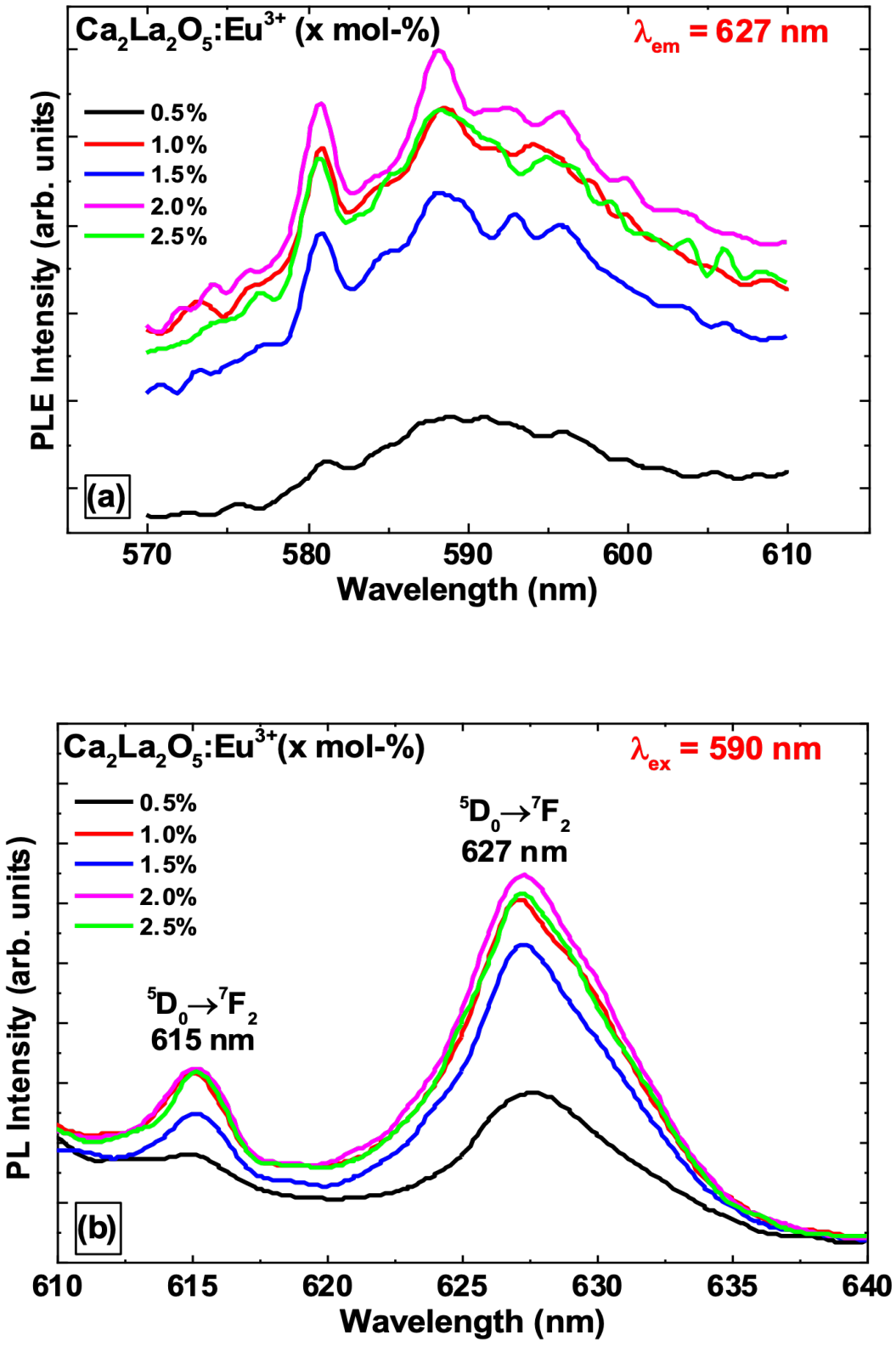

Figure 3.4: (a) Excitation spectra monitored at 627 nm, (b) emission spectra of $Ca_2La_2O_5:xEu^{3+}$ (x=0.5, 1, 1.5, 2 and 2.5%) phosphor excited with 590 nm

The aforementioned findings were derived from investigations on photoluminescence emission, which were carried out using an excitation wavelength of 590 nm. The Eu^{3+} ions demonstrate electronic transition at a wavelength of 615 nm ($^5D_0 \rightarrow {}^7F_2$), and the emission at 627 nm ($^5D_0 \rightarrow {}^7F_2$) which is more prominent compared to the emission at 615 nm. The aforementioned discovery possesses distinct characteristics and lends credence to our assertion that the $Ca_2La_2O_5:Eu^{3+}$ phosphor, when manufactured, exhibits superior color purity compared to other red-emitting phosphor systems. Furthermore, the $Ca_2La_2O_5:Eu^{3+}$ phosphor has a notable level of sensitivity and displays strong electric dipole emissions at wavelengths of 615 and 627 nm. These emissions correspond to the magnetic dipole transition of Eu^{3+} ions at 590 nm and the shift from the $^5D_0 \rightarrow {}^7F_1$ energy levels [28,29]. The emission process of the $Ca_2La_2O_5:Eu^{3+}$ phosphor encompasses multiple channels, which encompass the crystal field environment and coordination number of the surrounding Eu^{3+} ions. The excitation and emission spectra of the phosphor at different concentrations ranging from 0.5 to 2.5 mol % of Eu^{3+} when stimulated at 590 nm are presented in Figure 3.4 (a-b). The quenching effects resulting in a decrease in the photoluminescence (PL) intensity, as depicted in Figure 3.5, occur notably when the concentration of Eu^{3+} approaches 2 mol-% due to quadruple repulsions. To obtain a deeper understanding of concentration quenching, the emission intensity values are presented in Table 3.2.

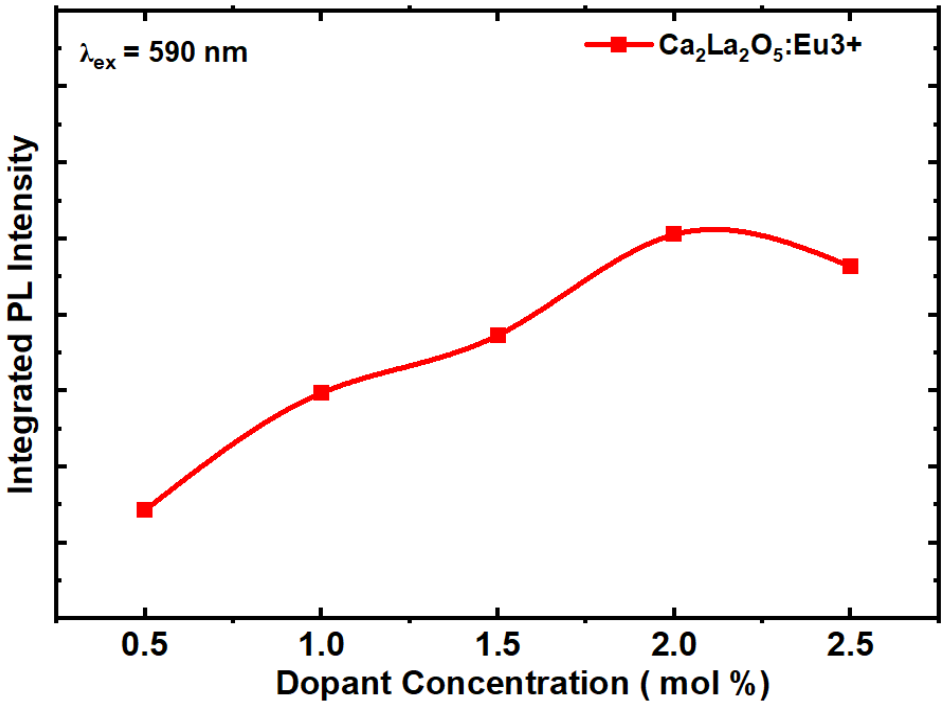

Figure 3.5: Integrated PL intensity of Phosphor with different dopant concentrations from 0.5 to 2.5 mol% when excited with 590 nm

Table 3.2: PL peak intensities of varied doping concentration of Eu^{3+} in $Ca_2La_2O_5$ phosphor when excited by 590 nm

S. No.	Europium Concentration %	PL Emission Intensity	
		Peak Wavelengths	
		615 nm	627 nm
1	0.5	20	41
2	1.0	125	263
3	1.5	161	302
4	**2.0**	**163**	**320**
5	2.5	156	304

3.4 XRD analysis

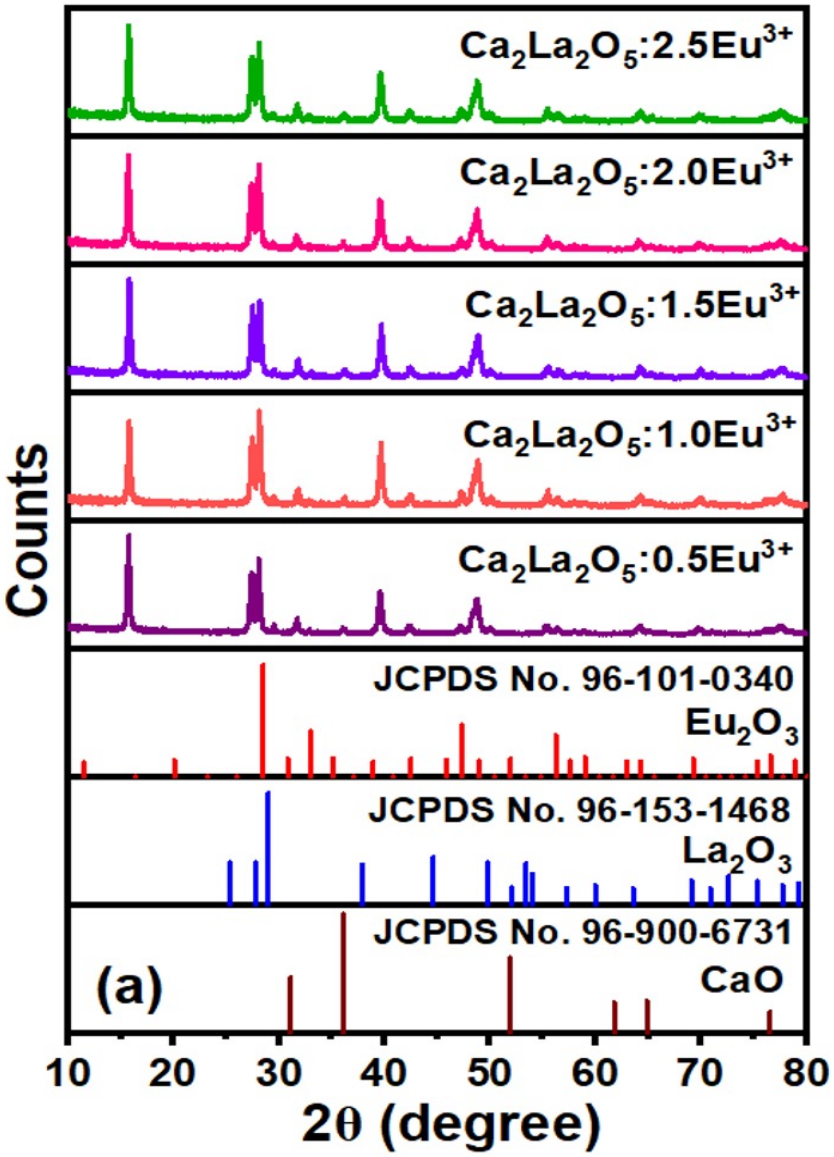

Figure 3.6 : XRD pattern of CaO, La_2O_3, Eu_2O_3, and $Ca_2La_2O_5$:xEu^{3+} (x=0.5, 1, 1.5, 2, 2.5 mol %) phosphor

X-ray diffraction (XRD) study was conducted in order to examine a range of characteristics of the phosphors, encompassing phase, microstrain, stress, dislocation density, crystallite size, and crystal structure. The X-ray diffraction (XRD) patterns of the $Ca_2La_2O_5$:x Eu^{3+} (0.5–2.5 mol-%) phosphor, as depicted in Figure 3.6, exhibit clear and well-defined diffraction peaks. This observation suggests that the phosphor possesses a high degree of crystallinity, surpassing that of established phases such as CaO, La_2O_3, and Eu_2O_3. The detected diffraction peaks exhibited a strong agreement with the anticipated data structure, thereby validating the existence of a hexagonal crystal structure. This validation was achieved by comparing the obtained results with the established JCPDS cards for CaO, La_2O_3, and Eu_2O_3.

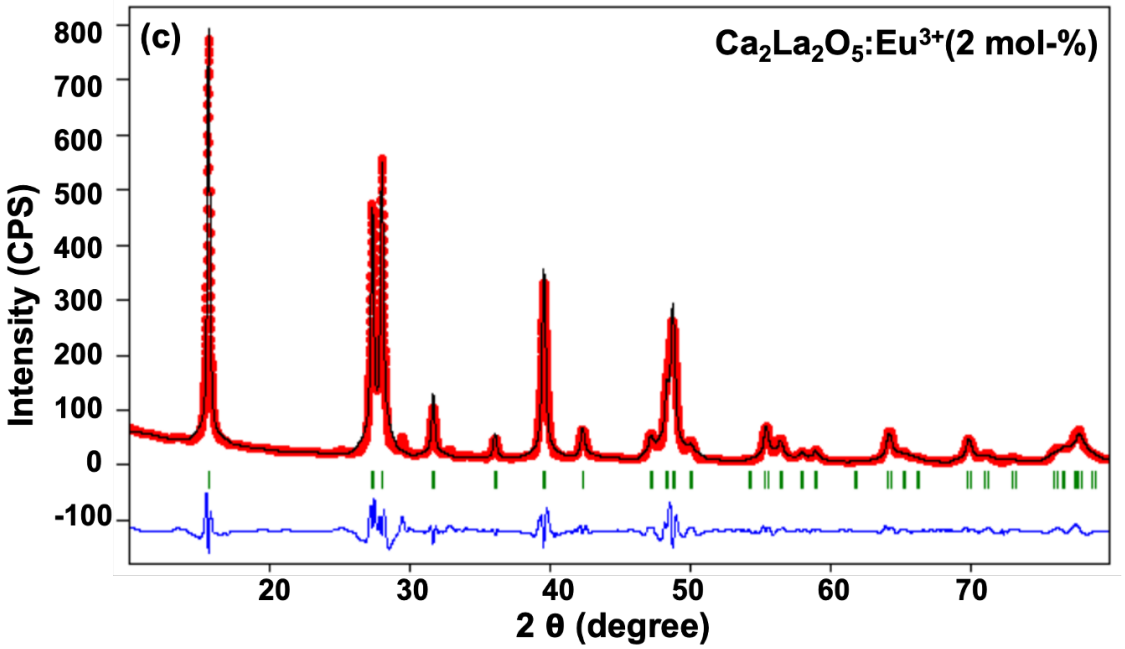

Figure 3.7 : Rietveld refined pattern of $Ca_2La_2O_5$:xEu^{3+} (x= 2 mol %)

The X-ray diffraction (XRD) analysis demonstrated that all of the phosphors that were generated exhibited indistinguishable diffraction patterns. The Rietveld refined pattern for the $Ca_2La_2O_5$ phosphor with a 2 mol-% doping of Eu^{3+} is depicted in Figure 3.7. The Rietveld investigation provided definitive evidence that all phosphors exhibited crystallization only in a pristine hexagonal crystal form, characterized by the space group P63/m. Furthermore, the microstrain (ε) was determined through the utilization of the Williamson-Hall plot, as depicted in Figure 3.8. It was observed that the microstrain remained consistent irrespective of the concentration of the dopant. Moreover, the negative value of the microstrain indicated lattice compression. Table 3.3 presents a comprehensive overview of the lattice parameters obtained by Rietveld refinement for all phosphors.

Debye-Scherer formula is used to analyze X-ray diffraction (XRD) patterns, specifically focusing on the most conspicuous diffraction peak.

$$D_{hkl} = \frac{K\lambda}{\beta Cos\theta}$$

According to the findings presented in Table 3.3, the average size of the crystallites was estimated to be 27.5 nm. This determination was made utilizing a formula that incorporates various parameters, including β (representing the whole width at half maximum), K (a constant), θ (the angle of diffraction), and λ (the wavelength of X-ray). The determined volume of the phosphors' cells was recorded as 142.57 Å3. Finally, the phosphor under investigation had a dislocation density (δ) of 1.32 × 1015 m−2, ascertained by the utilization of the following formula: $\delta = \frac{1}{D^2}$ Here, D = Crystallite size

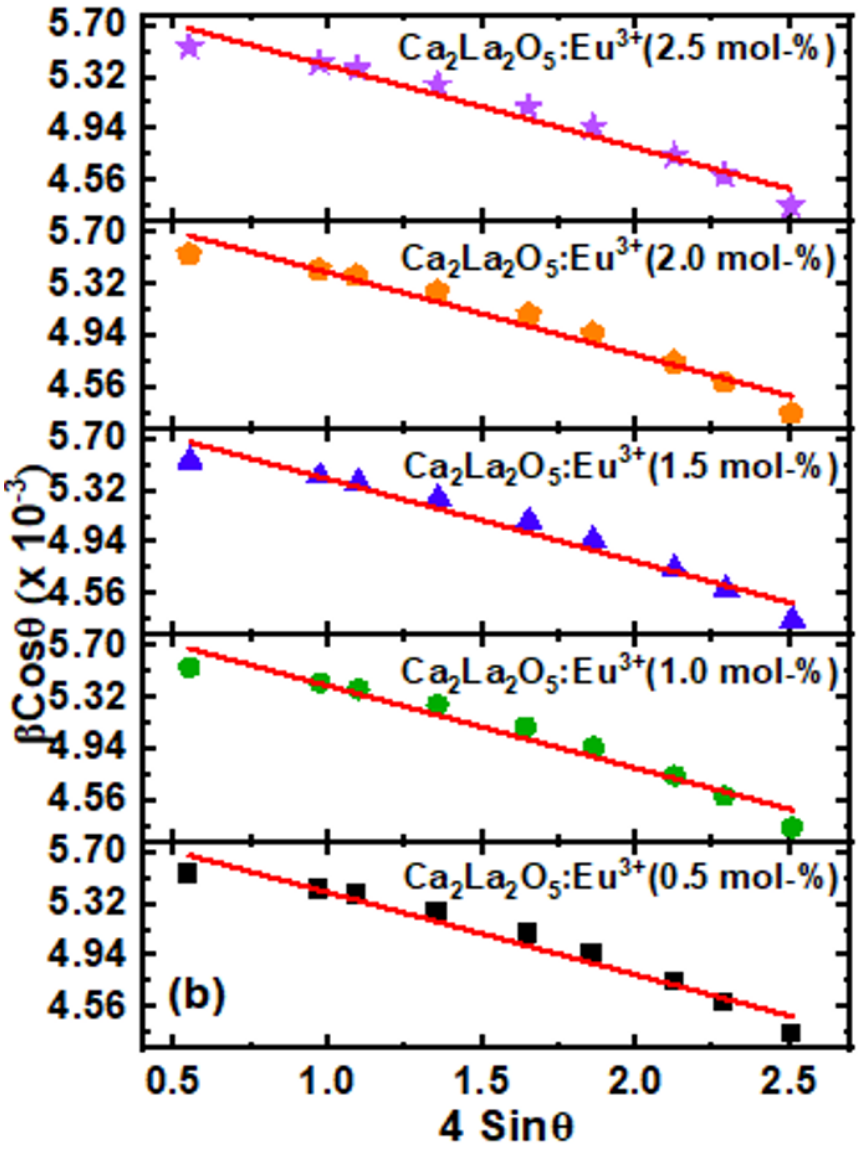

Figure 3.8 : W – H plot of $Ca_2La_2O_5:xEu^{3+}$ (x=0.5, 1, 1.5, 2, 2.5 mol %) phosphor where the slope is considered as ε

Table 3.3 : Lattice parameters of $Ca_2La_2O_5$: xEu^{3+} phosphor

Sample	Structure	a, b, c (Å)			Volume	Crystallite size (nm)
$Ca_2La_2O_5$:0.005Eu^{3+}	Hexagonal	6.566	6.566	3.902	145.68Å^3	28.7
$Ca_2La_2O_5$:0.01Eu^{3+}	Hexagonal	6.558	6.558	3.885	144.69Å^3	28.1
$Ca_2La_2O_5$:0.015Eu^{3+}	Hexagonal	6.546	6.546	3.872	143.68Å^3	27.2
$Ca_2La_2O_5$:0.02Eu^{3+}	Hexagonal	6.535	6.535	3.854	142.57Å^3	27.4
$Ca_2La_2O_5$:0.025Eu^{3+}	Hexagonal	6.528	6.528	3.848	142.00Å^3	27.1

3.5 SEM observations and EDAX analysis

The technology of scanning electron microscopy (SEM) is extensively utilized and frequently deployed in the field of surface science to investigate surface morphology and analysing surfaces. The technique employs a concentrated electron beam to generate high-resolution photographs of surface topography, thereby offering comprehensive insights into the morphology, dimensions, and chemical makeup of particles. Figure 3.9 illustrates a series of photos displaying particles of varying sizes and shapes, each captured at different magnifications. Furthermore, Figure 3.9 illustrates the manifestation of cathodoluminescence (CL), a phenomenon characterized by the emission of light that arises from the interactions

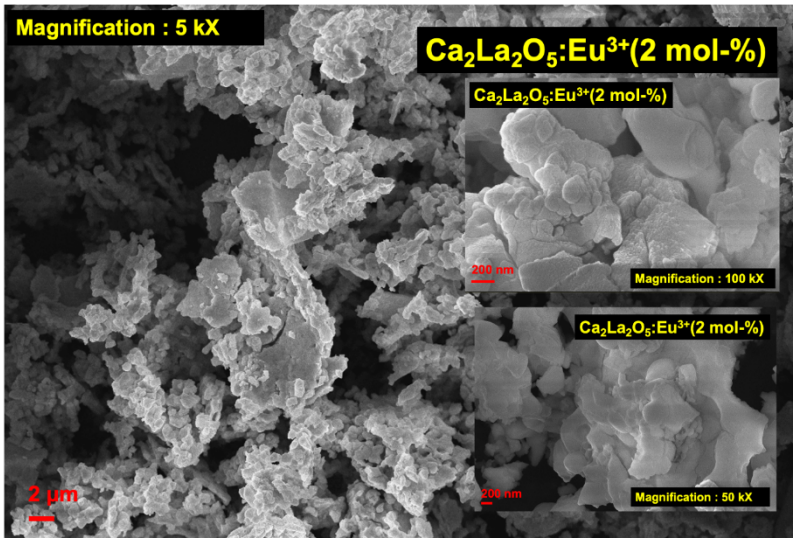

Figure 3.9: SEM image of $Ca_2La_2O_5$:xEu^{3+} (x= 2 mol %) phosphor under different magnifications

between the electron beam and the phosphors under investigation. The utilization of EDAX mapping techniques has facilitated the identification of the presence of all supplementary elements in suitable ratios within the $Ca_2La_2O_5$:0.02 Eu^{3+} phosphor. Figure 3.10 also includes the weight percentage and color-mapped graphics depicting the elements Calcium (Ca), Lanthanum (La), Oxygen (O), and Europium (Eu).

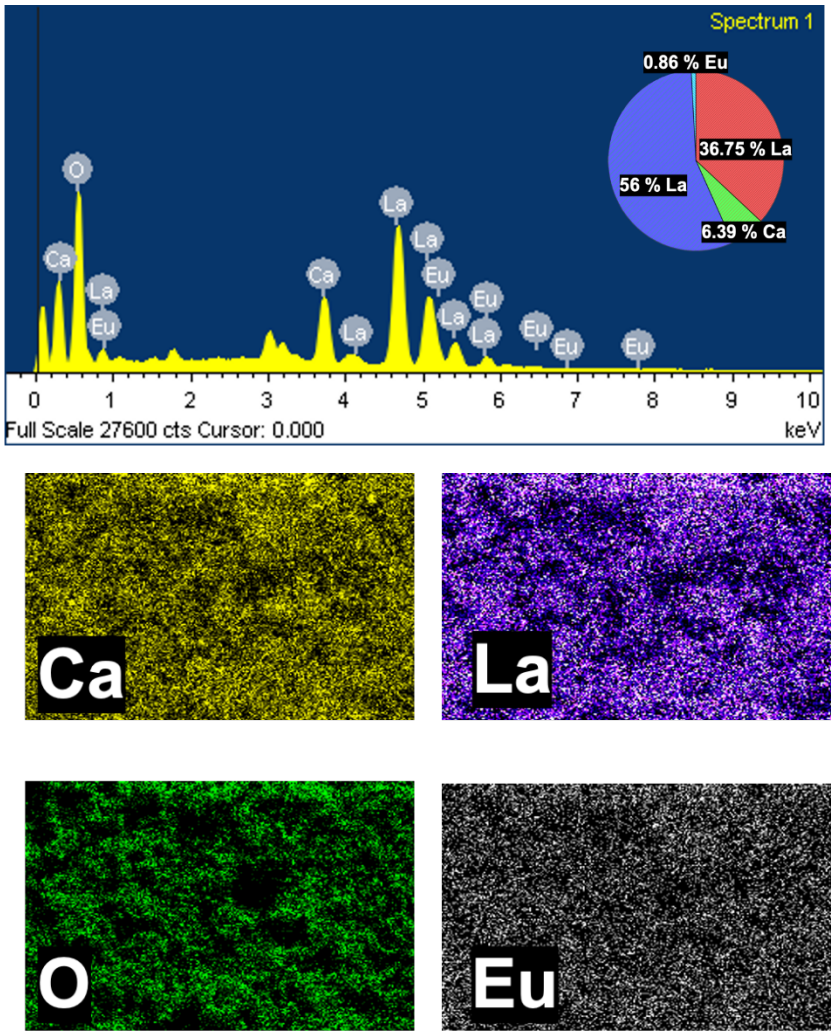

Figure 3.10: EDAX and color mapping results of $Ca_2La_2O_5$:xEu^{3+} (x= 2 mol %) phosphor

3.6 FTIR study

A Fourier Transform Infrared (FTIR) study was performed in order to examine the different vibrational modes of atomic bonds present in the phosphor material, with a particular focus on the bonds between neighboring molecules. The FTIR spectra of the Ca2La2O5 phosphors doped with Eu3+ are presented in Figure 3.11, encompassing a wave-number range from 400 to 4000 cm^{-1}. The Fourier Transform Infrared (FTIR) spectra were acquired utilizing the KBr pellet methodology. It is worth mentioning that the FTIR spectra of all the phosphors doped with Eu^{3+} in $Ca_2La_2O_5$ showed remarkable similarity.

The occurrence of infrared (IR) bands at 620 and 1068 cm^{-1} can be ascribed to the vibrational mode of La-O within the phosphor system. The findings of the study revealed that the identified absorption bands were consistent with the stretching vibrations of base metal oxides and the H-O-H stretching. Significantly, all absorptions seen in the phosphor Fourier Transform Infrared (FTIR) spectra were found to be within an acceptable range and were deemed admissible. The presence of a peak at 3612 cm^{-1} can be attributed to the stretching vibration of H-O-H molecules, which occurs due to the absorption of water molecules from the surrounding atmosphere.

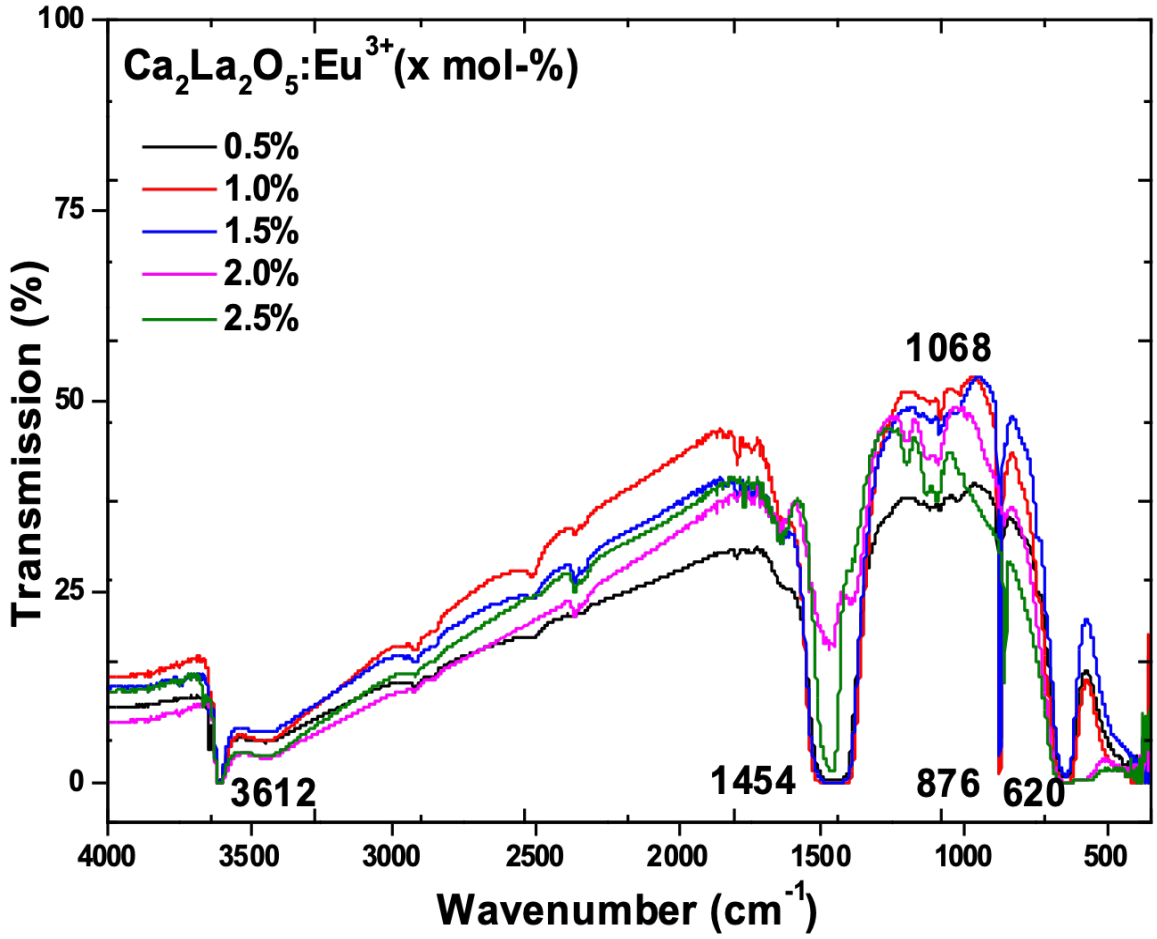

Figure 3.11 : FTIR of $Ca_2La_2O_5:xEu^{3+}$ (x= 0.5 – 2.5mol-%) phosphor

3.7 Particle size analysis

A particle size investigation was performed on the $Ca_2La_2O_5$ phosphor, which was doped with a concentration of 2 mol-% of Eu^{3+}. The distribution of particle sizes is depicted in Figure 3.12. The investigation revealed the presence of two separate distributions. The initial distribution spanned from 0.12–0.6 µm, exhibiting an average size of 0.26 µm. The second distribution had a range spanning from 0.12 to 10.0 µm, with a mean size of 3.0 µm. The investigation of photoluminescence (PL) involved the examination of bulk samples spanning a wide variety of sizes, specifically ranging from 0.12 to 10.0 µm.

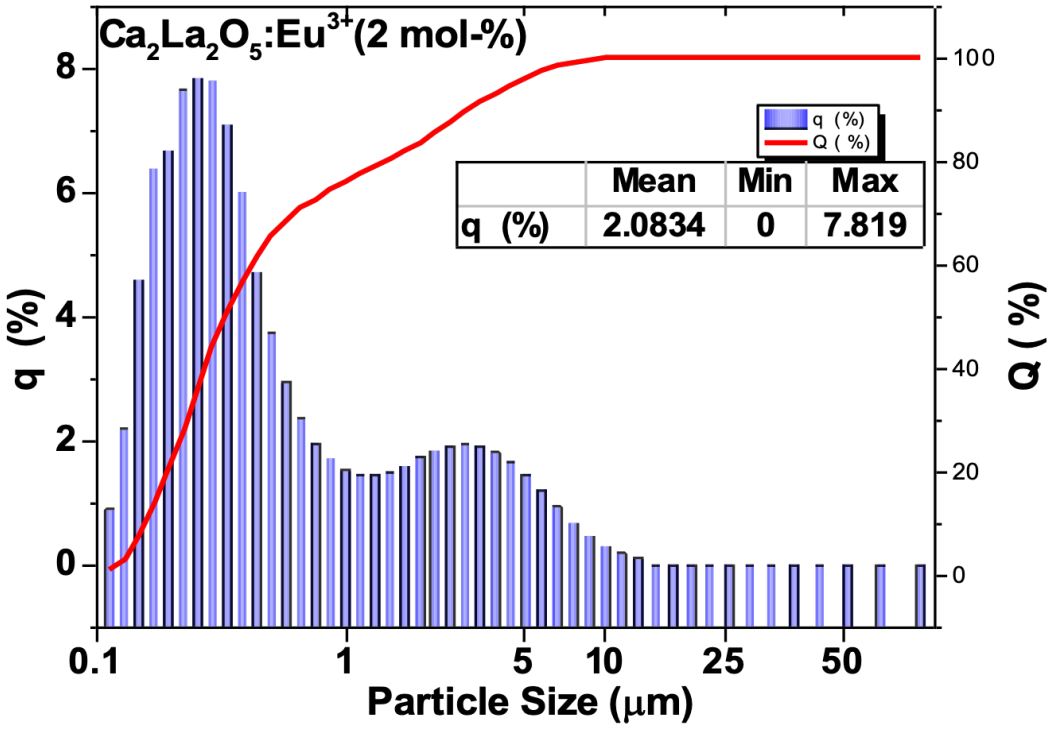

Figure 3.12: Particle size distribution of 2 mol-% of Eu^{3+} in $Ca_2La_2O_5$ phosphor

3.8 Temperature dependent PL

A crucial criterion for phosphor-converted white LEDs is the maintenance of a consistent and unchanging emission of photoluminescence (PL) intensity as the temperature increases, often reaching around 130°C or more for applications involving high-power energy [30]. In the context of illumination applications, phosphors that exhibit less thermal quenching at lower temperatures, specifically within the range of 100-150°C, are considered more desirable. The study involved examining the temperature-dependent photoluminescence (PL) parameters within a temperature range of 30 to 150°C. The objective was to assess the influence of temperature on the response of color emission. Conversely, it was noticed that the intensity of

the emission spectra decreased to a certain degree as the temperature increased. However, the position and form of the photoluminescence (PL) spectra remained unaltered, as depicted in Figure 3.13. At elevated temperatures, the excitation energy of $Ca_2La_2O_5$ phosphors has a

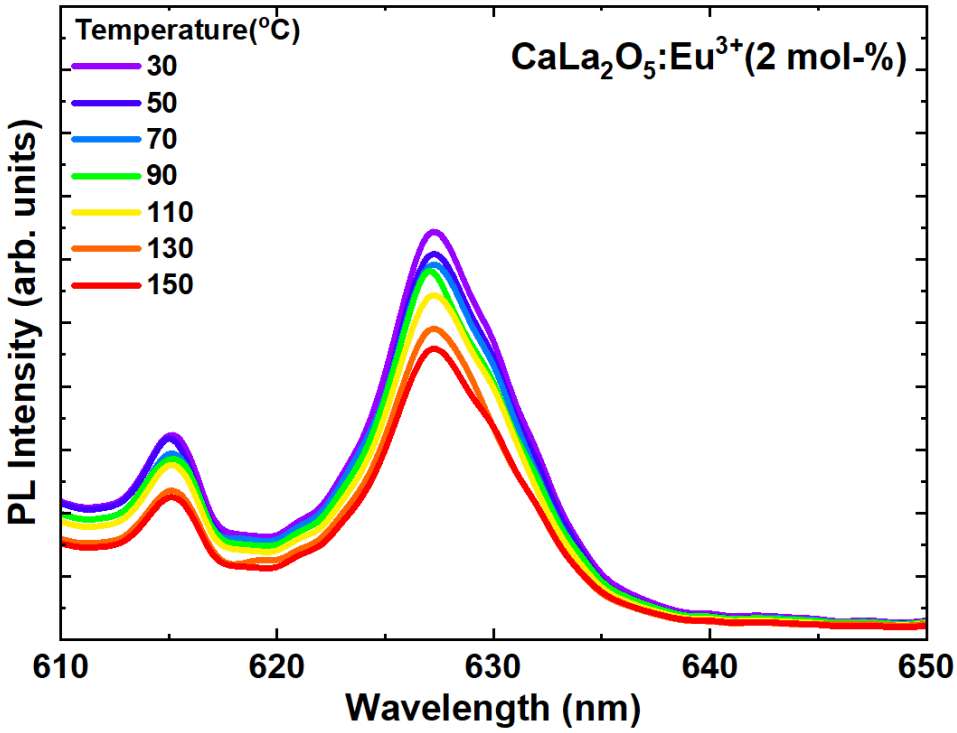

Figure 3.13: PL Spectra of $Ca_2La_2O_5xEu^{3+}$ (x = 2.0 mol-%) from 30°C to 150°C under 590 nm excitation.

greater tendency to be dissipated as non-radiative thermal energy through lattice relaxation, rather than being emitted as visible light from the luminous center. The non-radiative transitions seen in this context are by the Stokes shift phenomenon, resulting in a reduction of photoluminescence (PL) emission due to thermal hindrance. Further, it is plausible that thermal-induced charge transfer and thermally-assisted photoionization may also occur as alternate pathways. Further investigation was conducted to ascertain the practical applicability of $Ca_2La_2O_5:Eu^{3+}$ phosphors in the high-power white light-emitting diode (w-LED) business. Figure 3.13 presents the temperature-dependent photoluminescence (PL) spectra of the $Ca_2La_2O_5:Eu^{3+}$ phosphor. These spectra were acquired using an excitation wavelength of 590 nm and covered a temperature range of 30 to 150°C. At an elevated temperature of 150°C, there is a notable decrease of 29% in the intensity of photoluminescence. This observation suggests that the phosphors under investigation exhibit considerable thermal stability in comparison to phosphors currently utilized in high-power white-light-emitting diodes (w-LEDs). The graphical representation of the correlation between temperature and luminous relative emission intensity may be observed in Figure 3.14. The thermal stability behavior of the $Ca_2La_2O_5:Eu^{3+}$ phosphor was investigated using the Arrhenius fitting of the photoluminescence (PL) intensity

and determination of the activation energy (ΔE). The thermal quenching outcomes are depicted in Figure 3.14.

Equation (4), which is provided below under [31], is used to represent the activation energy (ΔE) $I_T = I_o /1+c \exp(\Delta E/kT)$

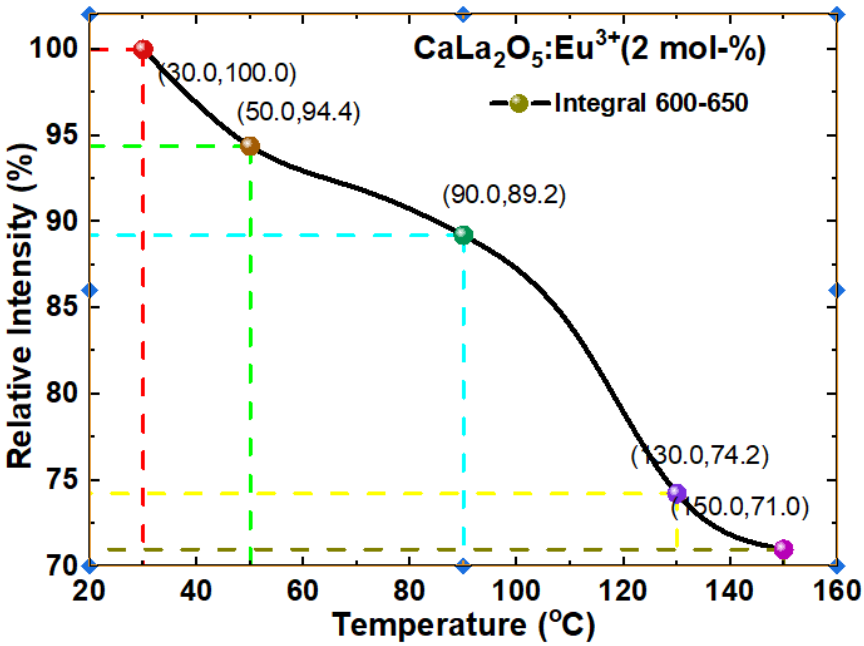

Figure 3.14: Plot showing the relation between relative intensity (%) and temperature for $Ca_2La_2O_5$:xEu^{3+} (x = 2.0 mol-%)

where, I_0 is the $Ca_2La_2O_5$: Eu^{3+} initial PL intensity at room temperature (~25 C), I_T represents the PL intensity at various temperatures; ΔE is the activation energy for thermal quenching, T is final temperature; c is a constant; and k is the Boltzmann constant (1.38×10-23 J/K). Plotting

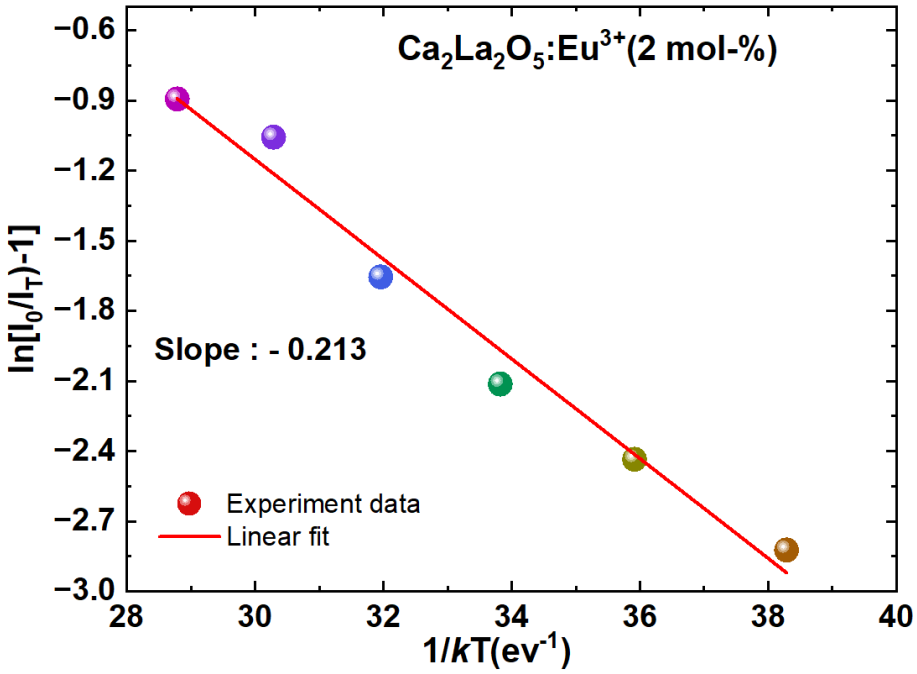

Figure 3.15: Plot showing the relation between ln[(I0/I) - 1] and 1/T for $Ca_2La_2O_5$:xEu^{3+} (x = 2.0 mol-%)

$\ln[(I_0/I_T)-1]$ vs. 1/kT yielded a straight-line graph, as seen in Figure 3.15. Therefore, based on mathematical calculations, the associated activation energy (ΔE) is 0.213 eV which is obtained from the slope of the graph.

3.9 Chromaticity coordinates

The quantitative evaluation of the overall radiated colours was conducted using the chromaticity coordinates provided by the Commission Internationale de I'Eclairage (CIE). The given coordinates represent colours using the (x, y) coordinate system, which is derived from the spectral power distribution. A chromaticity diagram was constructed by correlating the spectra with color-matching functions. Figure 3.16 displays the chromaticity coordinates of a phosphor with a doping level of 2%. The phosphor exhibits deep red emission when stimulated with a

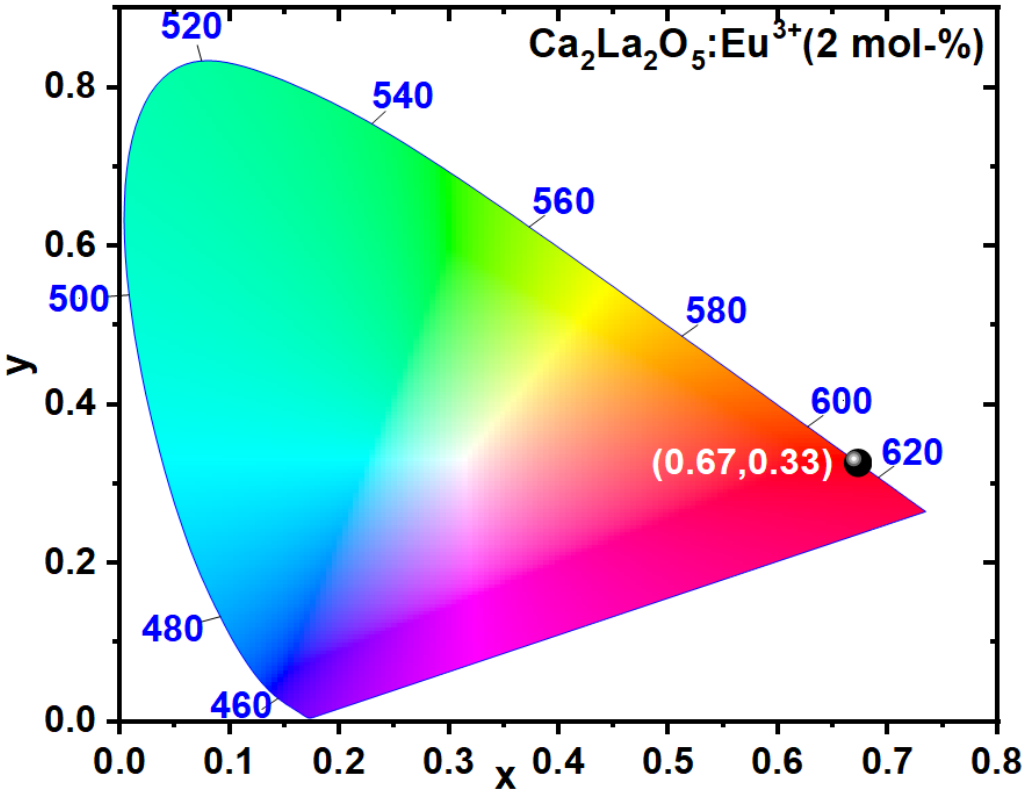

Figure 3.16: CIE coordinates of $Ca_2La_2O_5:xEu^{3+}$ (x= 2 mol-%) phosphors depicted on CIE 1931 chart

wavelength of 590 nm. The chromaticity coordinates are situated within the red zone, which signifies the hue of the light being emitted. The equation provided below serves to reinforce the empirical evidence about the color purity of $Ca_2La_2O_5:Eu^{3+}$, as demonstrated through its computational analysis.

The color purity of the phosphors synthesized can be determined using the formula:

$$\text{Color purity} = \frac{\sqrt{(X-Xs)^2+(Y-Ys)^2}}{\sqrt{(Xd-Xs)^2+(Yd-Ys)^2}} \times 100\%$$

The color coordinates of the synthesized phosphors are represented by (X, Y), with (Xs, Ys) denoting the energy point located at (0.333, 0.333). The boundary coordinates, generated by combining the first two coordinates, are represented by (Xd, Yd) and are located at (0.67, 0.33). When comparing the synthesized phosphor with available red-emitting phosphors such as Y_2O_3:Eu^{3+} and $Ca_2La_2O_5$:Eu^{3+}, it is observed that the latter demonstrates superior CIE color

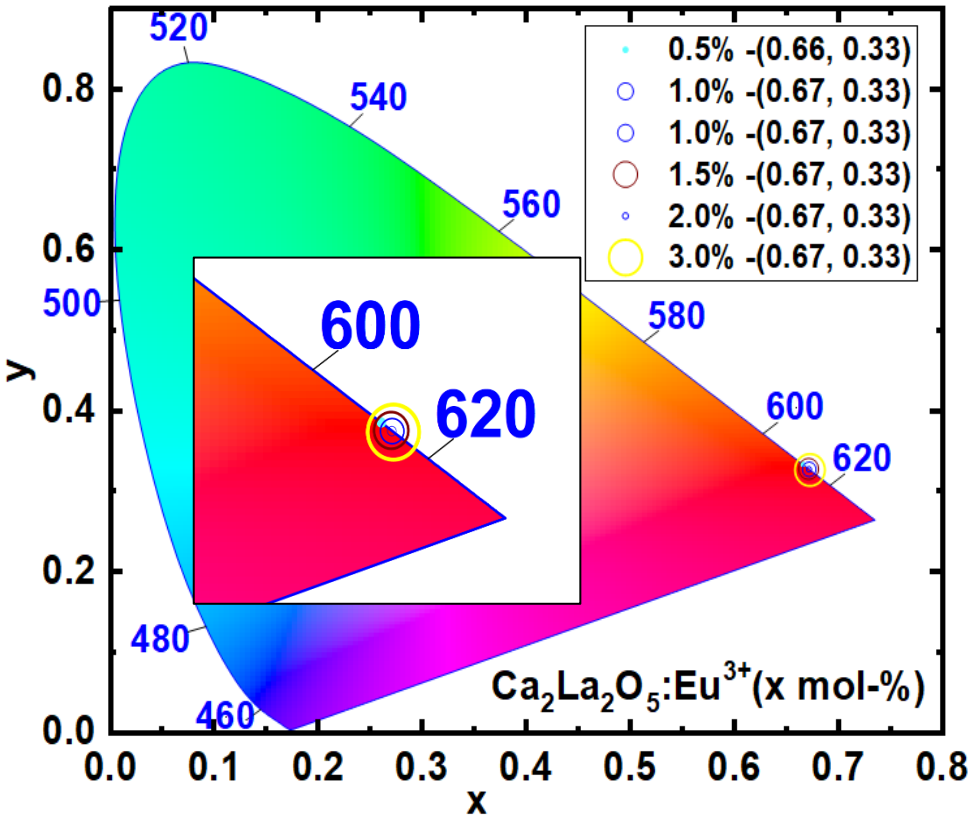

Figure 3.17 : CIE coordinates of $Ca_2La_2O_5$:xEu^{3+} (x=0.5 – 2.5 mol-%) phosphors depicted on CIE 1931 chart

coordinates and color purity. Y_2O_3:Eu^{3+} has color coordinates of (0.62, 0.37; 97.1%) and $Ca_2La_2O_5$:Eu^{3+} has an excitation wavelength in the UV range, unlike the synthesized phosphor which has an excitation wavelength in the visible region at 590 nm [32]. The $Ca_2La_2O_5$: Eu^{3+} phosphor, with its higher CIE color coordinates and color purity of (0.67, 0.33; 99%), outperforms the available phosphors in terms of color quality. The chromaticity color coordinates are calculated in $Ca_2La_2O_5$ at various doping doses of Eu^{3+} (x = 0.5 - 2.5 mol%) as depicted in Figure 3.17. Irrespective of the Eu^{3+} ion concentration, it is apparent from the CIE diagram that the coordinates consistently fall inside the region associated with bright red coloration, specifically at (0.67, 0.33). The chromaticity coordinate values remain constant across different dopant concentrations, suggesting that there is minimal impact on color purity.

3.10 Summary

The present investigation employed a modified solid-state reaction technique, which incorporated a chemical flux with a low-melting temperature, to effectively produce samples of $Ca_2La_2O_5$: Eu^{3+} phosphor exhibiting red emission. The sample $Ca_2La_2O_5$: Eu^{3+} (2 mol-%) is subjected to X-ray diffraction (XRD) analysis, which indicates a significant degree of crystallinity. The analysis further revealed that the sample exhibited a hexagonal phase and belonged to the P63/m space group. The $Ca_2La_2O_5$: Eu^{3+} phosphor samples were observed using scanning electron microscopy (SEM), revealing the presence of irregularly shaped particles. Additionally, the SEM pictures provided evidence of cathodoluminescence. The existence of the activator (Eu^{3+}), as well as all constituent elements (Ca, La, and O) within the host lattice, was established using energy-dispersive X-ray spectroscopy (EDAX) research. Therefore, the aforementioned phosphor material exhibits encouraging outcomes for utilization in both cathodoluminescence and deep red-emission LED technologies.

References

[1] Yokota H, Yoshida M, Ishibashi H, et al. J Alloys Compd. 2010;495:162–166. doi:10.1016/j.jallcom.2010.01.112

[2] Murthy KVR, Virk HS. Defect Diffus Forum. 2013;347:1–34. doi:10.4028/www.scientific.net/DDF.347.1

[3] Yen WM, Weber MJ. Inorganic phosphors: compositions, preparation and optical properties CRC Press; June 22, 2004.

[4] Rao RP, Devine DJ. J Lumin. 2000;87– 89:1260–1263. doi:10.1016/S0022-2313(99)00551-7

[5] Nazarov M, Noh DY, J Rare Earths, 2010;28:1–11. 10.1016/S1002-0721(10)60390-0

[6] Zhang Q, Dandeneau CS, Zhou X, et al. Adv Mater. 2009;21:4087–4108. doi:10.1002/adma.200803827

[7] Tsao JY, Coltrin ME, Crawford MH, et al. Proc IEEE. 2010;98:1162–1179. doi:10.1109/JPROC.2009.2031669

[8] Ye S, Xiao F, Pan YX, et al. Mater Sci Eng R Reports. 2010;71:1–34. doi:10.1016/j.mser.2010.07.001

[9] Höppe HA. Angew Chemie Int Ed. 2009;48:3572–3582. doi:10.1002/anie.200804005

[10] Haitz R, Tsao JY. Phys Status Solidi. 2011;208:17–29. doi:10.1002/pssa.201026349

[11] Jayasimhadri M, Ratnam BV, Jang K, et al. J Am Ceram Soc. 2010;93:3857–3861. doi:10.1111/j.1551-2916.2010. 03963.x

[12] Li XY, Zhou J. The Eighth China National Conference on Functional Materials and Applications; 2014; Trans Tech Publications Ltd, p. 761–769.

[13] Nagpure IM, Pawade VB, Dhoble SJ. Luminescence. 2009;25:9–13.10.1002/bio. 1132

[14] Goktas A.Physica E. 2020;117:113828, doi:10.1016/j.physe.2019. 113828

[15] Aslan F, Arslan F, Tumbul A, et al. Opt Mater (Amst). 2022;127:112270, doi:10.1016/j.optmat.2022.

[16] Zarbali M, Göktaş A, Mutlu IH, et al. J Supercond Nov Magn. 2012;25:2767–2770. doi:10.1007/s10948-011- 1260-z

[17] Goktas A, Aslan E, Arslan F, et al. Opt Mater (Amst). 2022;133:113028, doi:10.1016/j.optmat.2022.113028

[18] Kominami H, Yamashita S, Nakanishi Y, et al. J Illum Eng Inst JAPAN. 2009;93:802–806. doi:10.2150/jieij.93.802
[19] Dang P, Li G, Yun X, et al. Light Sci Appl. 2021;10; doi:10.1038/s41377-021-00469-x
[20] Pekgözlü I, Karabulut H, Mergen A, et al. J Appl Spectrosc. 2016;83:504–511. doi:10.1007/s10812-016-0319-9
[21] Goktas S, Goktas A. J Alloys Compd. 2021;863; doi:10.1016/j.jallcom.2021.158734
[22] Huang Y, Nakai Y, Tsuboi T, et al. Opt Express, 2011;19:6303–6311. doi:10.1364/OE.19.006303
[23] Kishore Babu J, Sridhar M, Sai Prasad AS, et al (2021) Mater Today Proc 44:294–299. doi:10.1016/j.matpr.2020.09. 468
[24] Atchyutha Rao C, Murthy KVR. Int J Adv Res. 2020;8:762–769. doi:10.21474/ijar01/12209
[25] Shinde K N, Dhoble S J. Luminescence. 2012;27:91–94. doi:10.1002/bio.1314
[26] Li Y-C, Chang Y-H, Chang Y-S, et al. J Phys Chem C. 2007;111:10682–10688. doi:10.1021/jp0719107
[27] Wang Y, Liu Y, Guo T, et al. Environ Sci Pollut Res. 2020;27:42868–42880. doi:10.1007/s11356-020-10240-1
[28] Göktaş A, Tumbul A, Aslan F. J Sol-Gel Sci Technol. 2016;78:262–269. doi:10.1007/s10971- 016-3960-0
[29] Bai Y, Jia Z, Gao J, et al. J Mater Chem C. 2022;10:15957–15966.
[30] Y. Tian, J. Solid State Light. **1** (2014) 1–15.
[31] D.L. Geng, H.Z. Lian, M.M. Shang, Y. Zhang, and J. Lin, Inorg. Chem. 53 (2014) 2230–2239.
[32] Sijbom HF, Verstraete R, Joos JJ, et al. Opt Mater Express. 2017;7:3332–3365. doi:10.1364/OME.7.003332.

Chapter - 4

A Novel Narrow-Band Red Emitting Multi-Layer Phosphor for White-Light Emitting Devices

Features of the Chapter:

The standard solid-state reaction technique was used to successfully synthesize $SrZr_2La_2O_7$: Eu^{3+} (0.5-2.5 mol %) phosphors. The photoluminescent and structural properties of the phosphors were investigated using various analytical methods, such as Powder X-ray Diffraction (PXRD), Scanning Electron Microscopy (SEM), Energy Dispersive X-ray Spectroscopy (EDX), Fourier Transform Infrared Spectroscopy (FTIR), and Particle Size Distribution (PSD). Examination of the photoluminescence spectra shows that the phosphor exhibited strong and prominent red emissions at a wavelength of 627 nm. These emissions can be attributed to the electric dipole transition that occurs between $^5D_0 \rightarrow {}^7F_2$ states. The red emissions, particularly at a wavelength of 627 nm, have a narrow bandwidth of 8.0 nm, leading to an increased luminous efficacy. This is indicated by the full width at half maximum (FWHM) measurement. In this study, a newly developed red phosphor specifically designed to improve the red emission of light-emitting diodes is discussed. The phosphor is incorporated into layers of a polymer matrix that have different thicknesses and can be stacked up to a maximum of 400 µm. The enhanced intensity of the red color is due to the phenomenon of self-excitation, in which photon absorption and emission processes play an essential role. Therefore, extensive use of $SrZr_2La_2O_7$ phosphors doped with Eu^{3+} can be observed in the area of red phosphors for UV chip-based white light-emitting diodes (w-LEDs) and displays. The phosphor exhibits a remarkable degree of chromatic purity, with a maximum value of 99%, when measured at a wavelength of 590 nm. The X-ray powder diffraction study confirms the crystalline nature of the phosphor, characterized by a highly ordered structure and a cubic phase.

This work has been published in:

Kishore Kumar Aitha, D. Dinakar, P. Indira, A.S. Sai Prasad, K.V.R. Murthy, D. Haranath, **Results in Chemistry**, Volume 6, 2023, 101100, ISSN 2211-7156, DOI: https://doi.org/10.1016/j.rechem.2023.101100 **(IF: 2.3)**

4.1 Outline

The global population is experiencing growth, while industrialization is advancing rapidly. As a result, there has been a significant increase in the need for energy, which has the potential to exceed the limitations imposed by the depletion of natural resources [1]. The information of concern relates to the projected rise in global energy demand, which is forecast to increase by 48% within the next two decades [2]. This implies that individuals across the globe are subjected to negative outcomes on the global climate and the exhaustion of natural resources and fossil fuels as a consequence of energy production [3]. Energy-efficient technology plays a crucial part in the preservation and conservation of natural resources. The field of energy conservation is rapidly acknowledging and attributing relevance to Solid State Lighting (SSL) [4].

Considerable advancements have been achieved in the research and development of phosphors, which hold great potential for various applications within the realm of LED technology. Considerable investigation has been undertaken into innovative phosphor materials utilized in light-emitting diodes (LEDs), which involve the integration of polymer matrix layers embedded with phosphors. The findings of this study have contributed to the progress of white light-emitting diodes (w-LEDs) and monochrome LEDs, which demonstrate remarkable color purity as shown by Color Rendering Index (CRI) values exceeding 90. Moreover, these light-emitting diodes (LEDs) exhibit a high level of color quality scale (CQS) and possess excellent luminous efficacy in terms of visible light emission rate (LER) [5].

The assessment of luminous efficacy of visible light emission (LER) involves the utilization of the lumens-to-spectral power (watts) ratio [6]. One of the phosphors employed in the production of white light-emitting diodes (w-LEDs) is a phosphor that generates red light. One of the main difficulties associated with red-emitting phosphors is the existence of prominent emission bands and the diminished sensitivity of the human eye towards the near-infrared spectrum (source: [7]). In order to effectively analyze the red spectral spectrum, characterized by an emission peak from 610 to 620 nm, it is crucial to minimize the influence of eye sensitivity towards longer wavelengths. The aforementioned requirement calls for the creation of innovative red phosphors that exhibit very narrow emission bands that are precisely matched with the intended wavelength [8].

The existing literature indicates that a restricted selection of red emitting phosphors satisfies the rigorous requirements for widespread use in commercial LED applications. In particular, it is important for these phosphors to have a notable conversion efficiency while functioning within the parameters of LED operation. Additionally, they should display a limited emission

spectrum characterized by a profound red hue. Currently, the red-emitting phosphors that are now accessible are constrained by their substantial full width half maximum (FWHM), leading to diminished efficacy [9]. Each of the aforementioned choices exhibits a deficiency in terms of accessibility and does not satisfy the requirements for a "high-performance red phosphor." These requirements include a limited emission band spanning from 610 to 630 nm and exceptional stability with regards to luminous qualities. Two notable approaches employed in the production of red phosphors for white-light emitting diodes (w-LEDs) are the utilization of europium-doped compounds and Mn^{4+}-doped fluorides [10]. Quantum dots, often integrating the element cadmium (Cd), demonstrate significant potential as red phosphors. Nevertheless, the notable toxicity and increased costs associated with their manufacture pose considerable limitations. Fluoride materials that have been doped with manganese ions in the Mn^{4+} oxidation state demonstrate a peak emission wavelength range spanning from 630 to 640 nm. On the other hand, these materials exhibit the benefit of possessing inherently limited line emission properties. However, the prolonged durations of decay exhibited by these materials present limitations on their applicability in high-power LEDs. Furthermore, the synthesis processes employed by them often entail the utilization of hydrofluoric acid, a substance that raises substantial issues for human safety and health [11]. Therefore, it is crucial to possess a constrained emission spectrum that demonstrates enhanced effectiveness through the utilization of easily obtainable UV LED sources, specifically at wavelengths of 279 nm or 395 nm [12].

The present study aims to introduce and present the findings on a red-emitting phosphor, namely $SrZr_2La_2O_7$, which has been doped with Eu^{3+} ions. The feasibility of substituting La^{3+} ions with Eu^{3+} ions is presented in this study, based on their comparable valence and ionic radii [13]. The luminescence intensity of the red emission in the $^5D_0 \rightarrow {}^7F_2$ transition of Eu^{3+} is higher when compared to the luminescence intensity of the orange emission in the $^5D_0 \rightarrow {}^7F_1$ transition. This article outlines the process of synthesizing a variety of $SrZr_2La_2O_7$: Eu^{3+} (0.5–2.5 mol%) doped phosphors in order to create a red dominant phosphor that is well-suited for use in white-light emitting diodes (w-LEDs). It has been found that the production of green light in light-emitting diodes (LEDs) generally leads to an augmentation in lumens per watt. Furthermore, it should be noted that a rise in red emission is directly correlated with a corresponding increase in the Color Rendering Index (CRI). Consequently, a decision has been taken on the choice of a red emissive phosphor. The phosphor material exhibits self-excitation by the sequential absorption and emission of photons [14], hence increasing the efficiency of the full width at half maximum (FWHM). This chapter undertakes an examination and

presentation of many conventional characterizations that have been subject to scrutiny and documentation.

4.2 Synthesis

In the synthesis of a series of phosphors, a mixture of two rare earth ions with a +3 charge, one strontium ion with a -2 charge, and one zirconium ion with a +3 charge was utilized. These phosphors were labelled with different concentrations of europium ion with a +3 charge (0.5, 1, 1.5, 2.0, and 2.5 mol%). The employment of an inorganic phosphor for LED applications is a ground breaking advancement in this field. The solid state reactions process (SSR), depicted in Figure 4.1, is widely acknowledged as a sustainable approach within the realm of green chemistry. In this study, the SSR method was utilized to fabricate the phosphor by employing the aforementioned components. Strontium oxide, which is also referred to as strontia (SrO), zirconium oxide (Zr_2O_3), lanthanum oxide (La_2O_3), and europium oxide (Eu_2O_3), all of which were of analytical grade, were chosen in appropriate amounts according to stoichiometric ratios.

$$\mathbf{SrO + Zr_2O_3 + La_2O_3 = SrZr_2La_2O_7\ (Heated\ at\ 1200^oC)}$$

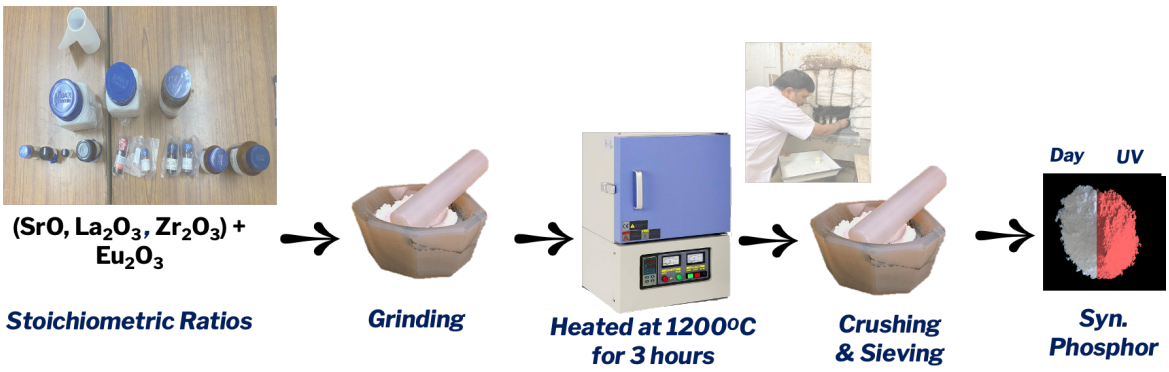

Figure 4.1: Flow chart for the synthesis of phosphor

The quantities of oxides were measured precisely, subsequently blended, and completely mixed in an acetone solution for a duration of 30 minutes utilizing a pestle and Agate mortar.

Table 4.1: Synthesized phosphor with varying dopant concentrations for $SrZr_2La_2O_7$

Sample Number	Host	Dopant	Dopant Concentration
SZL-S1	$SrZr_2La_2O_7$	Eu^{3+}	0.5 mol %
SZL-S2	$SrZr_2La_2O_7$	Eu^{3+}	1.0 mol %
SZL-S3	$SrZr_2La_2O_7$	Eu^{3+}	1.5 mol %
SZL-S4	$SrZr_2La_2O_7$	Eu^{3+}	2.0 mol %
SZL-S5	$SrZr_2La_2O_7$	Eu^{3+}	2.5 mol %

The homogeneous mixture that was made was carefully transferred into alumina crucibles and exposed to a temperature of 1200°C in the presence of air inside a muffle furnace for a period of 3 hours. After undergoing the sintering process, a white powder substance was generated, resulting in the synthesis of a total of five different types as outlined in the accompanying table. Totally five samples were prepared as shown in table 4.1

The excitation and emission spectra were acquired under ambient conditions using a SHIMADZU RF-5301 PC fluorescence spectrometer that was outfitted with a 150 W xenon lamp. The analysis of phosphor phases was performed utilizing the P-XRD (X-ray Powder Diffraction) technique. X'Pert Pro P Analytical Powder Diffractometer was utilized, which was fitted with a Cu-Kα radiation source with a wavelength of 1.54 Å. The instrument was operated using an X-ray generated with voltage of 40 kilovolts (kV) and a current of 40 milliamperes (mA). The scanning range of the device was designed to cover a 2θ range spanning from 20 to 80 degrees. The scanning velocity was consistently upheld at a rate of 0.05 degrees per second. The morphology of the samples was assessed utilizing a scanning electron microscope (SEM) manufactured by JEOL, especially the JSM 5810 LV model. In order to acquire a quantitative analysis of the elemental composition, the integration of an energy dispersive X-ray spectroscopy (EDAX) system with the scanning electron microscope (SEM) was implemented. Fourier-transform infrared (FTIR) spectra were collected using an FTIR Perkin Elmer-100

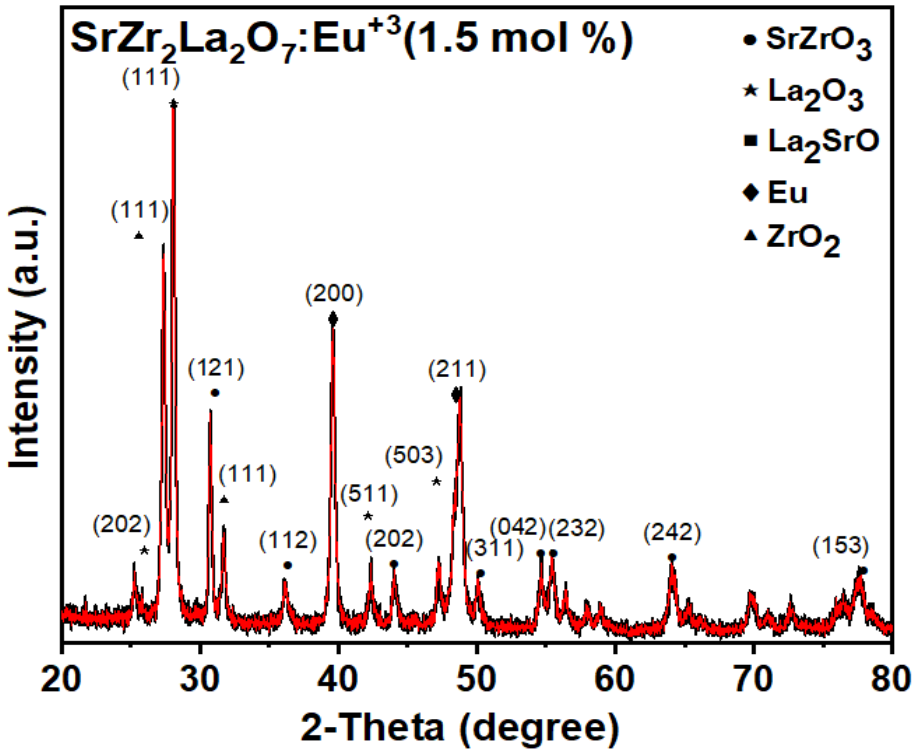

Figure 4.2: XRD pattern of $SrZr_2La_2O_7$: Eu^{3+} 1.5 mol%

equipment. The particle size analyzer utilized in this investigation was Malvern Mastersizer 3000, which had the capacity to measure particle sizes spanning from 0.1 μm to 3 mm.

4.3 X-ray diffraction (XRD) analysis

The X-ray diffraction (XRD) analysis was performed with the X'Pert Pro P Analytical Powder Diffractometer. The radiation source employed in this study was Cu-Kα (λ = 1.54 Å), operating at a voltage of 40 kV and a current of 40 mA. The scanning procedure encompassed a 2θ range spanning from 20 to 80 degrees, with a scan speed of 0.05 degrees per second. The X-ray diffraction (XRD) graph presented in Figure 4.2 showcases the results that were achieved. The X-ray diffraction pattern displayed well-defined peaks at precise angles, specifically 2θ = 15.75◦, 27.41◦, 28.19◦, 30.70◦, 31.65, 39.57◦, and 48.74◦. Furthermore, the experimental data revealed the presence of minor peaks at specific angles, namely 25.23◦, 36.15◦, 42.33◦, 44.00◦, 47.24◦, 50.06◦, 54.65◦, 55.47◦, 64.16◦, and 77.71◦. The peak with the highest intensity at an angle of 15.75◦ was identified as the La_2SrO phase, based on the JCPDS Card No. 00-042-0343 [15]. The peaks detected at angles of 27.41◦, 28.19◦, and 30.70◦ correspond to the monoclinic La_2O_3 (JCPDS Card No. 00-022-0641) [15], monoclinic ZrO_2 (JCPDS Card No. 04-005-5594) [15], and orthorhombic phase of $SrZrO_3$ (JCPDS Card No. 04-002-5371) [15], respectively. In addition, the presence of peaks at 39.57° and 48.74° predominantly indicates the presence of the cubic phase of Europium, as shown by the JCPDS Card No. 04-007-5154 [15]. The occurrence of small intensity peaks at angles of 25.23◦, 42.33◦, and 47.24◦, in conjunction with the observed peaks at angles of 36.15◦, 44.00◦, 50.06◦, 54.65◦, 55.47◦, 64.16◦, and 77.71◦, can be ascribed to the characteristic phases of La_2O_3 and $SrZrO_3$. The quantification of crystallinity

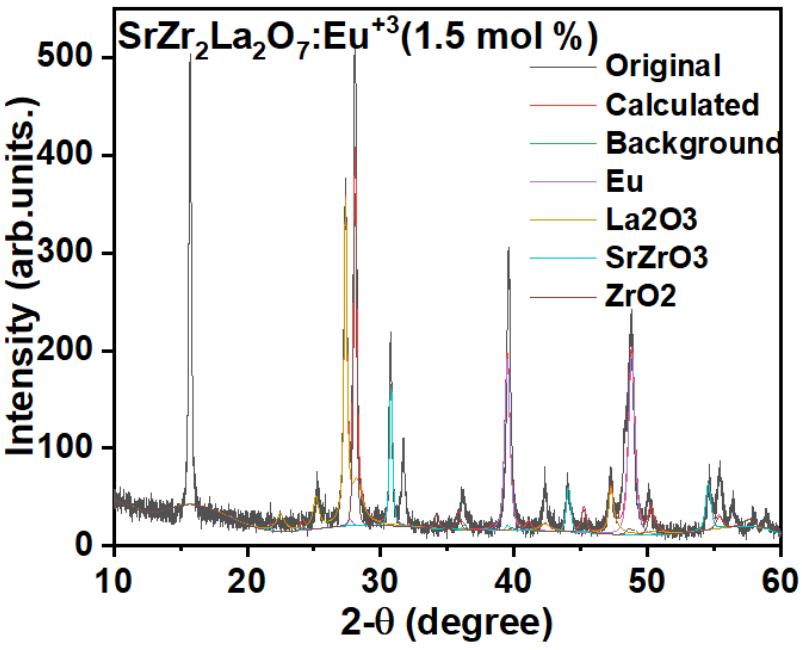

Figure 4.3: Rietveld refinement of the XRD data of $SrZr_2La_2O_7:Eu^{3+}$ 1.5 mol% phosphor

percentage was achieved by computing the integral of the curve corresponding to both the amorphous and crystalline regions of the specimen. The present study resulted in a crystalline component value of 54.2%. In addition, the calculation of the crystallite size of the synthesized sample was performed utilizing Scherrer's equation. The results demonstrate that the average grain size is 32.7 nm, with the smallest and largest grain sizes being 27.1 and 38.4 nm, respectively.

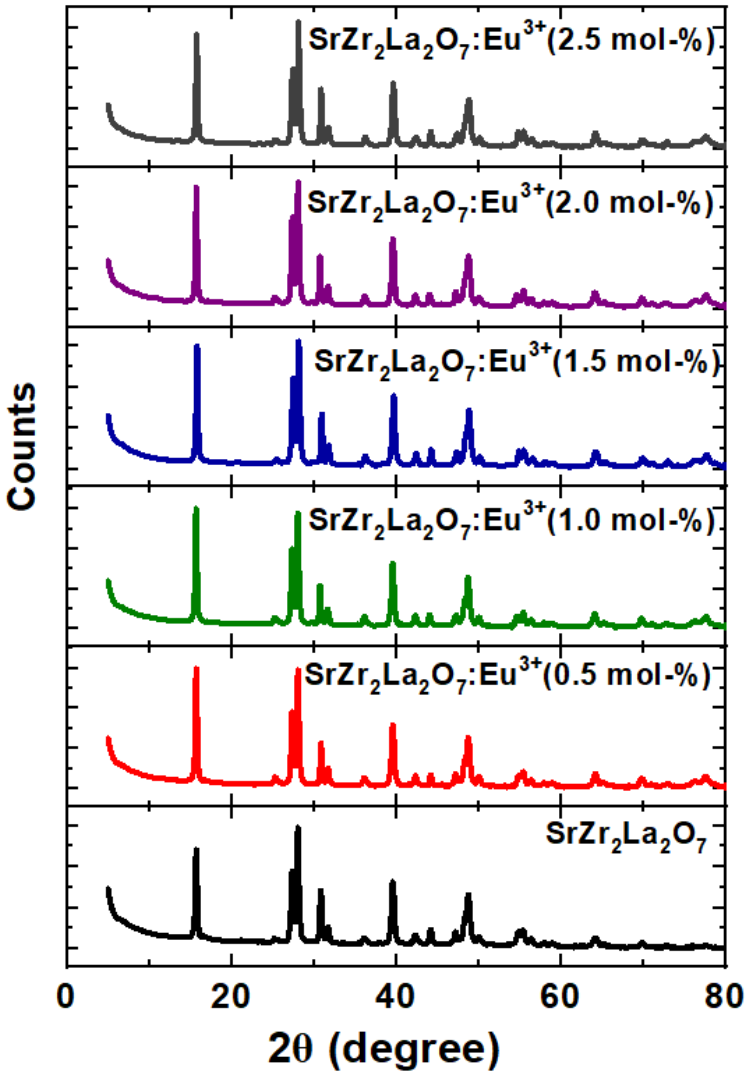

Figure 4.4 : XRD peaks of $SrZr_2La_2O_7$: Eu^{3+} (0.5 to 2.5 mol%) phosphor

Moreover, the samples was taken for Rietveld refinements as depicted in Figure 4.3, which unveiled a significant disparity between the Rwp value (36.06%) and the Rexp value (15.21%). The difference seen in this study can be attributed to the significant noise-to-signal ratio that is apparent in X-ray diffraction (XRD) patterns of nanocrystalline materials (source: https://doi.org/10.1186/2228-5326-3-8). The $\chi 2$ value found was 5.62, indicating a goodness of fit (GoF) score of 2.37. The identification of monoclinic ZrO_2, monoclinic La_2O_3, orthorhombic $SrZrO_3$, and cubic Eu phases was confirmed through thorough investigation of the samples. The

refinement method given estimates for the phase percentages in the sample as follows: Europium (Eu) at 2.23%, Lanthanum oxide (La_2O_3) at 91%, Strontium zirconium oxide ($SrZrO_3$) at 1.46%, and Zirconium oxide (ZrO_2) at 5.30%. As a result, the analysis findings indicate that the identified peaks corresponding to cubic Europium, monoclinic ZrO2 and La_2O_3, and orthorhombic $SrZrO_3$ provide confirmation of the existence of these compounds within the synthesized sample, with the cubic phase being the predominant form. The X-ray diffraction (XRD) peaks corresponding to the different concentrations of Eu^{3+} dopants in $SrZr_2La_2O_7$ are depicted in Figure 4.4. The pattern seen indicates the lack of europium ion impurity peaks inside the host matrix, implying that the dopant ions have been successfully distributed across the designated host matrix.

4.4 Photoluminescence analysis

Figure 4.5 illustrates the excitation spectra of phosphors composed of $SrZr_2La_2O_7$. The phosphor $SrZr_2La_2O_7$: Eu^{3+} showed 5 absorption lines at 279, 395, 467, 540, 590 nm in its excited spectrum [16]. These 5 absorptions are in the range of UV Visible with higher absorption at 279 nm. The highest excitation peak is at 279 nm due to the CTS between Eu^{3+}-

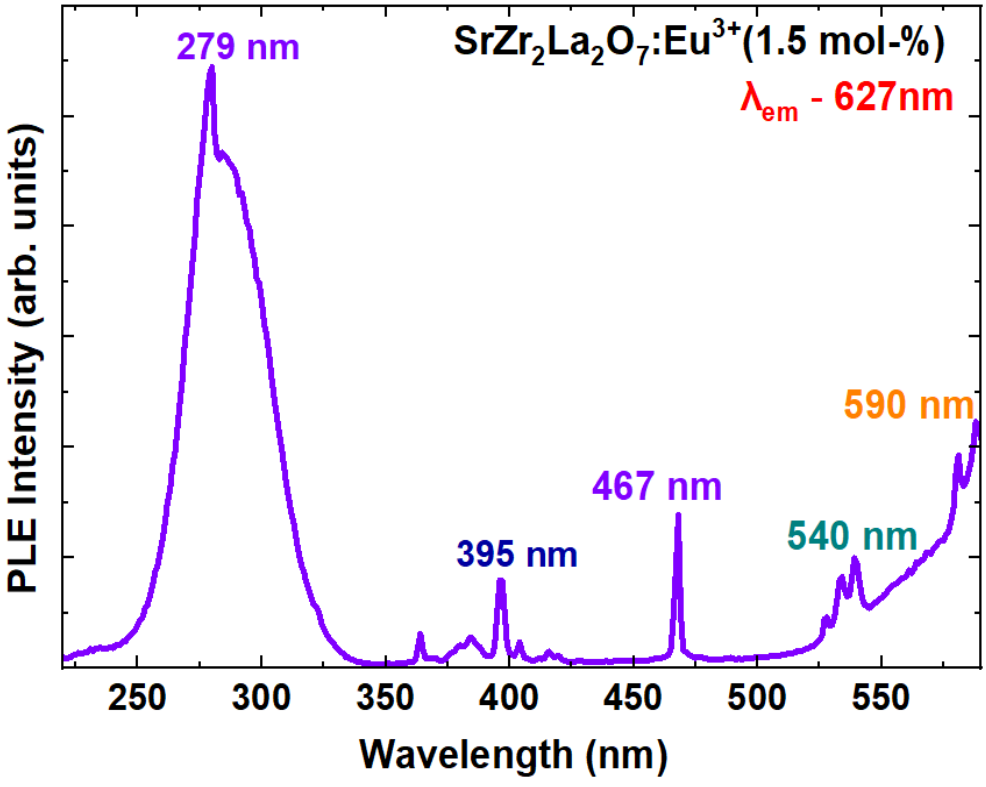

Figure 4.5: PL excitation spectra of $SrZr_2La_2O_7$: Eu^{3+} (λ_{em} = 627nm)

O^{2-} [17]. These absorptions were assigned to the $^7F_0 \rightarrow {}^5H_J + {}^1H_J$ (279 nm), $^7F_0 \rightarrow {}^5L_7$ (395 nm), $^7F_0 \rightarrow {}^5D_2$ (467 nm), $^7F_1 \rightarrow {}^5D_1$ (540 nm) and $^7F_1 \rightarrow {}^5D_0$ (590 nm) transitions of the Eu^{3+}. Because of the near proximity of the $^7F_0$ and $^7F_1$ states, Eu^{3+} containing the absorption transitions not of

the ground state ($^7F_0$), but also of the 1st excited state ($^7F_1$). An analysis of the absorption band positions of the ($^7F_0$, 7F1)- $^5D_1$, $^5D_0$, and $^7F_1$ transitions shows that the energy gap among the ground state ($^7F_0$) and the 1st excited states ($^7F_1$) states is about 350 cm^{-1}. At normal temperature (293 K), the fractional thermal occupation of the $^7F_1$ level cannot be ignored since 65% of Eu^{3+} ions occupy the $^7F_0$ ground state, 30% populate the first excited" state $^7F_1$, and the remaining 5% populate other more excited states [18]. The investigated phosphor could be excited with widely used various UV-LED chips available in the market. Based on the observed absorptions, the examined phosphor was stimulated to record the emissions at 279, 395, 467, 540, and 590 nm. 5 concentrations of material were synthesized by varying the dopant level from 0.5 to 2.5

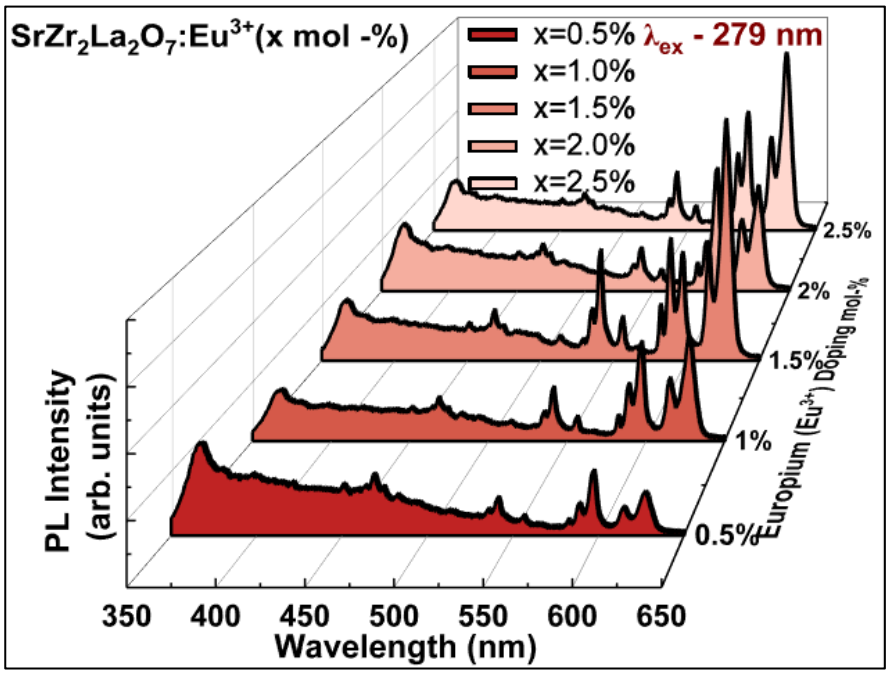

Figure 4.6: PL spectra of $SrZr_2La_2O_7:Eu^{3+}$ (λ_{ex} = 279 nm) at various doping concentrations

mol% and an analysis was performed. The undoped base phosphor doesn't show any emission when excited with the above ab- sorption lines. Figure 4.6 depicts the Phosphor emission spectra with 5 concentration levels when excited with 279 nm. The observed emitted peaks are at 467, 540, 590, and 627 nm with the highest intensity at 627 nm and a narrow FWHM width. This study presents an evaluation of the photoluminescence (PL) properties of $SrZr_2La_2O_7$, with a specific dopant concentration of 1.5 mol%. The emission spectra of the phosphor $SrZr_2La_2O_7$: Eu^{3+}(1.5 mol%) at different stimulated wavelengths are depicted in Figure 4.7.

The photoluminescence emission spectra of the $SrZr_2La_2O_7$ host material, doped with Eu^{3+} ions at ambient temperature are depicted in Figure 4.8. The spectrum acquired exhibits discernible emissions at wavelengths of 467, 540, 555, 590, 615, and 627 nm. The emissions observed at

specific wavelengths of 395, 467, 540, 590, 615, and 627 nm, resulting from excitation at 279 nm, can be ascribed to the electron configuration changes of Eu^{3+} as illustrated in Figure 4.9. The emissions depicted in Figure 4.9, along with other emissions, can be ascribed to the luminescent properties arising from inherent imperfections within the host lattice. The energy levels of Eu^{3+} and their corresponding emissions and associated energy states are depicted in Figure 4.10. The transition from the $^5D_0 \rightarrow {}^7F_2$ energy level, which is associated with the emission of light with a wavelength of 590 nm, is indicative of a magnetic dipole transition. The comprehensive integrated intensity of this transition is impacted by the intensity, which is frequently unaltered by the surrounding environment of the Eu^{3+} ion [19]. The emission observed at a wavelength of 627 nm can be attributed to the transition occurring between the $^5D_0 \rightarrow {}^7F_2$ states. The transition under consideration is regarded as hypersensitive due to its dependence on electric dipole alterations, which are affected by both the Eu^{3+} ion's symmetry and the properties of the ligand [19]. The magnitudes of intensities seen in hypersensitive transitions far exceed the anticipated values for quadrupole transitions by multiple orders of amplitude. As a result, pseudo-quadrupole transitions were also known as hypersensitive transitions [20]. The red emission observed in phosphor materials containing Eu^{3+} can be attributed to the transition from the $^5D_0 \rightarrow {}^7F_2$ state. The phosphor $SrZr_2La_2O_7$: Eu^{3+} shown advantageous properties as a phosphor for white-light emitting diodes (w-LEDs) and as a red-

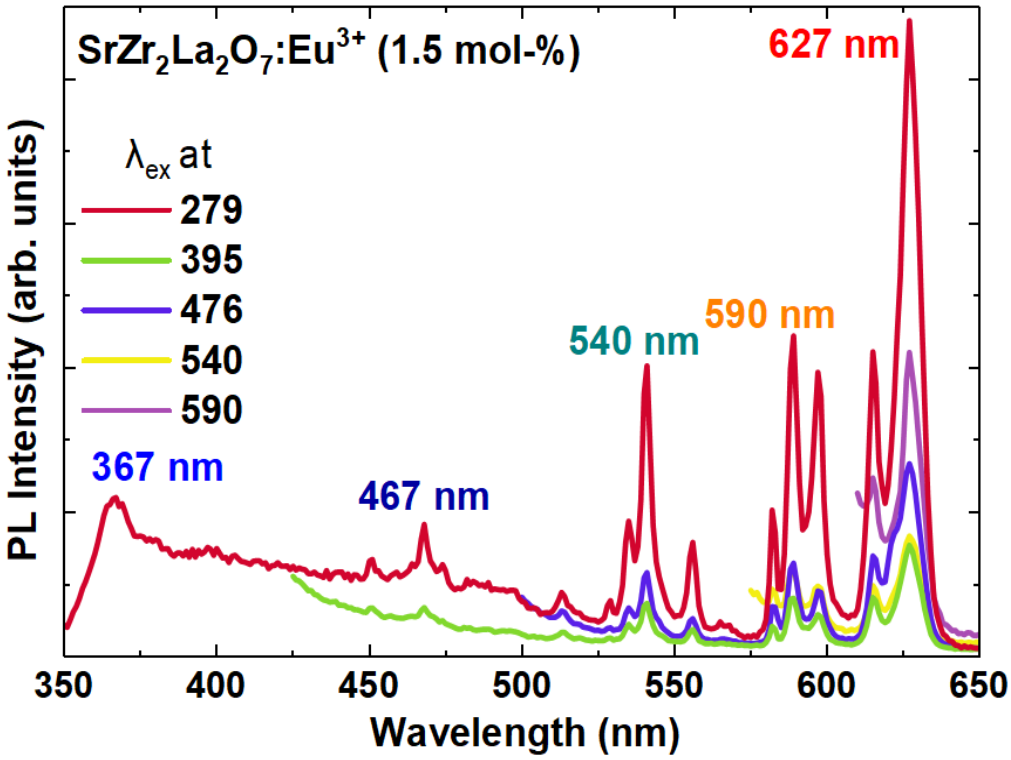

Figure 4.7: PL spectrum of $SrZr_2La_2O_7$: Eu^{3+} at various excitations (1.5 % mol concentration)

emitting phosphor when excited by commonly used ultraviolet (UV) light-emitting diodes (LEDs).

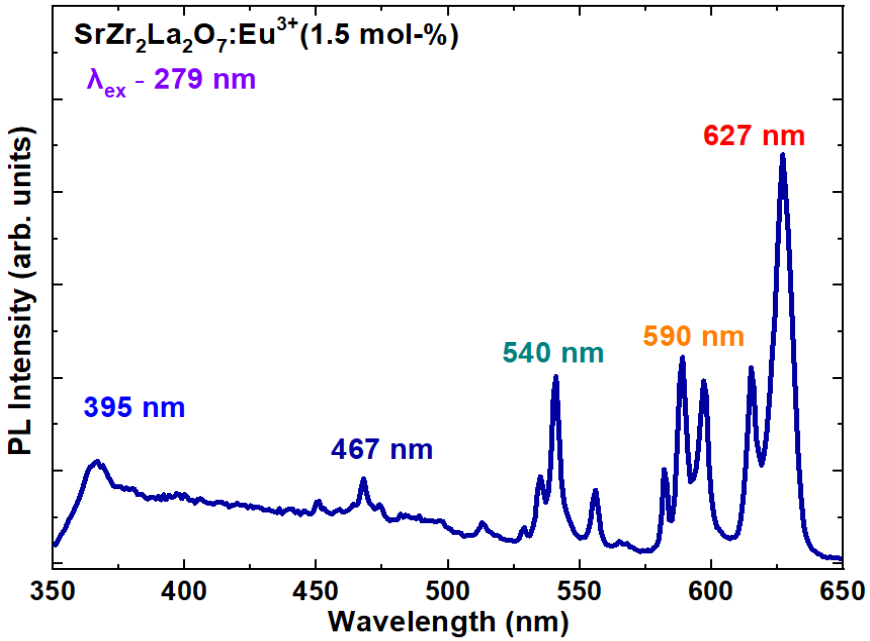

Figure 4.8: PL emission spectrum $SrZr_2La_2O_7:Eu^{3+}$ (λ_{ex} = 279 nm)

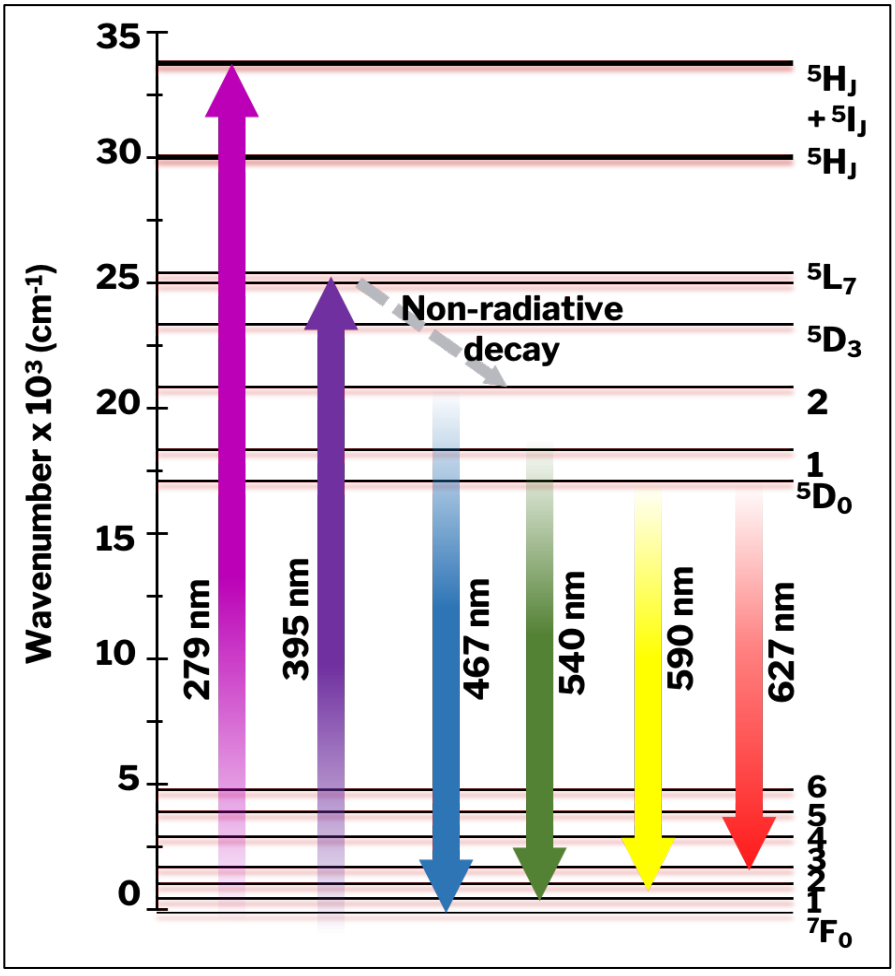

Figure 4.9: Schematic diagram - Energy level of Eu^{3+}

The emission spectrum of the phosphor $SrZr_2La_2O_7$: Eu^{3+} exhibits distinct peaks at wavelengths of 467 nm, 540 nm, 555 nm, 590 nm, 615 nm, and 627 nm when excited at 395 nm. These peaks are illustrated in Figure 4.11. In contrast to the process of excitation, it was noticed that the emission intensities at 279 nm were only one-third of the comparable values.

The emission spectra of the $SrZr_2La_2O_7$ phosphor, doped with Eu^{3+} ions and stimulated at a wavelength of 467 nm, are depicted in Figure 4.12. Emissions were seen at specific wavelengths of 540, 555, 590, 615, and 627 nm. A reduction in intensity was seen in the emission at a wavelength of 555 nm, in comparison to the excitation at 279 nm. Furthermore, it was noted that the intensity of 627 exhibited a substantial increase, in addition to the various emissions. However, when stimulated with light at a wavelength of 279 nm, only a quarter (25%) of the emissions were detected.

The compound $SrZr_2La_2O_7$: Eu^{3+} demonstrated luminescent characteristics upon excitation at a wavelength of 540 nm, resulting in emissions seen at 590 nm, 615 nm, and 627 nm. Figure 4.13 illustrates the emission spectrum. The peak intensities experienced additional reduction when measured at a wavelength of 279 nm. The observed reduction in intensities may be ascribed to the occurrence of partial internal reflection within the crystal lattice.

The emission spectra of $SrZr_2La_2O_7$: Eu^{3+} were examined, with a particular focus on the

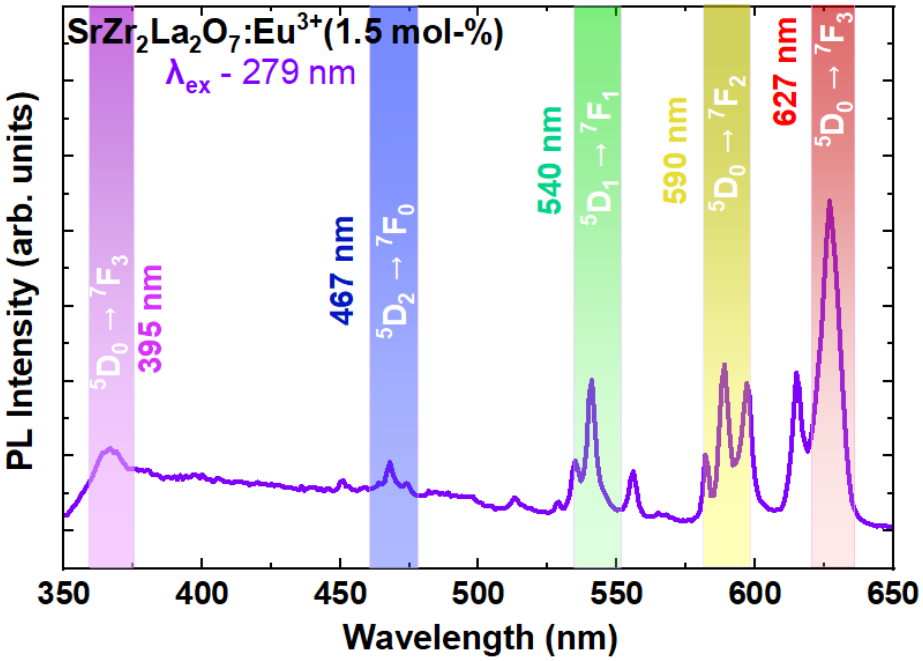

Figure 4.10: PL emission spectrum $SrZr_2La_2O_7$:Eu^{3+} (λ_{ex} = 279 nm) and respective transitions

presence of Eu^{3+} phosphor. Upon excitation at a wavelength of 590 nm, a distinct peak at 627 nm was observed, displaying a significantly elevated intensity. Figure 4.14 illustrates the emission spectrum when stimulated with light at a wavelength of 279 nm, corresponding to an

energy of 2.59 eV, a range of emissions with different intensities was seen. These emissions exhibited colours such as blue, cyan, green, yellow, orange, and red. This particular device demonstrates potential usefulness for applications demanding white light. The phosphor was excited at a wavelength of 467 nm, resulting in the observation of emissions from Eu^{3+} ions in

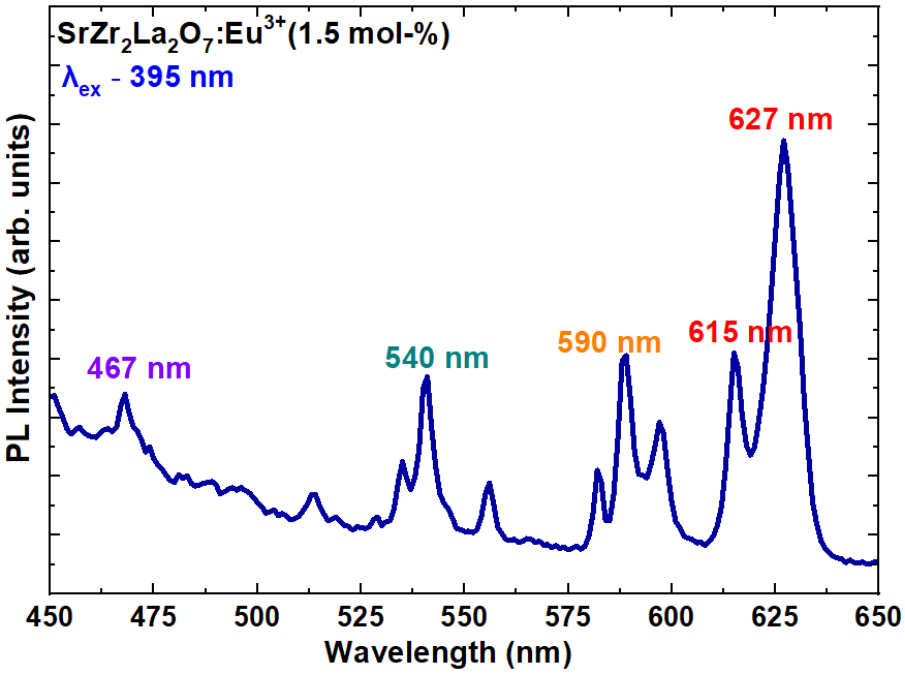

Figure 4.11: PL emission spectrum $SrZr_2La_2O_7:Eu^{3+}$ (λ_{ex} = 395 nm)

several regions of the electromagnetic spectrum, including cyan, green, yellow, orange-red, and red. The above mentioned phenomenon is a crucial requirement for the advancement of Phosphor-based Light Emitting Diodes (p-LEDs) employed in the fabrication of white light. In addition, the phosphor demonstrated emissions of sufficient intensities upon stimulation by wavelengths measuring 590 nm, 615 nm, and 627 nm. Therefore, the above mentioned material can be categorized as a distinct substance based on its absorption peak observed at a wavelength of 590 nm. This absorption subsequently leads to the emission of an electric dipole component that displays very sensitive properties at 615 nm, as well as a quite powerful emission at 627 nm. This material possesses the characteristic of being a red-emitting phosphor and exhibits the capability of self-excitation through the sequential absorption and emission of photons [21]. Consequently, it is considered an appropriate for utilization in LED devices. The dominant feature of the emissions originating from the $SrZr_2La_2O_7$: Eu^{3+} phosphor material is the RED phosphor suitable for RED emitting LEDs. The phosphor is included into polymer matrix layers [22] of different thicknesses, allowing for stacking up to 400 µm. The phosphor material demonstrates a diverse variety of particle sizes, ranging from 0.12 to 10 µm, accompanied by varied size distributions. By integrating the phosphor in close proximity to the active layer of a

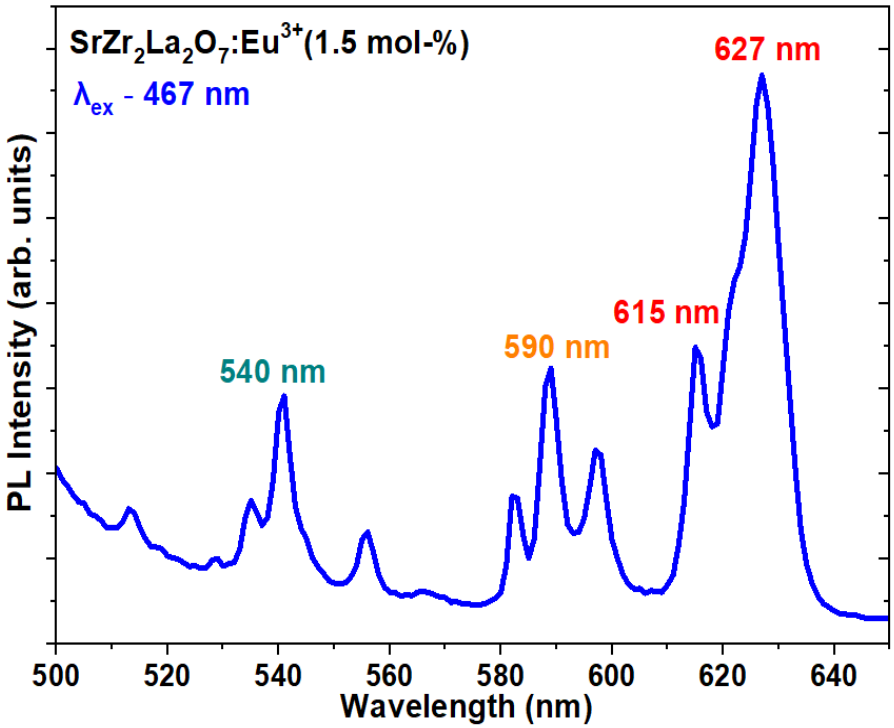

Figure 4.12: PL emission spectrum $SrZr_2La_2O_7:Eu^{3+}$ (λ = 467 nm)

abundance of red emissions, which exhibit a wavelength of 627 nm. This study presents a novel semiconductor LED, with a near conformal distribution, it enables the efficient transmission of emitted visible light across a range of wavelengths (UV-279 nm, NUV-395 nm, Blue LED-467 nm, Green LED-540 nm, and Yellow LED-590 nm) through the phosphor matrix. The thickness

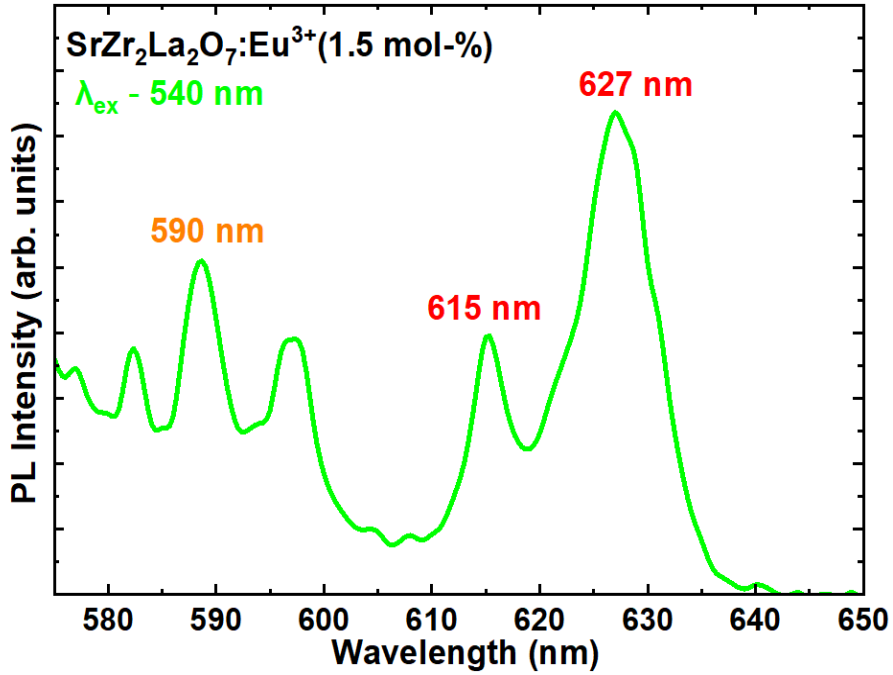

Figure 4.13: PL emission spectrum $SrZr_2La_2O_7:Eu^{3+}$ (λ = 540 nm)

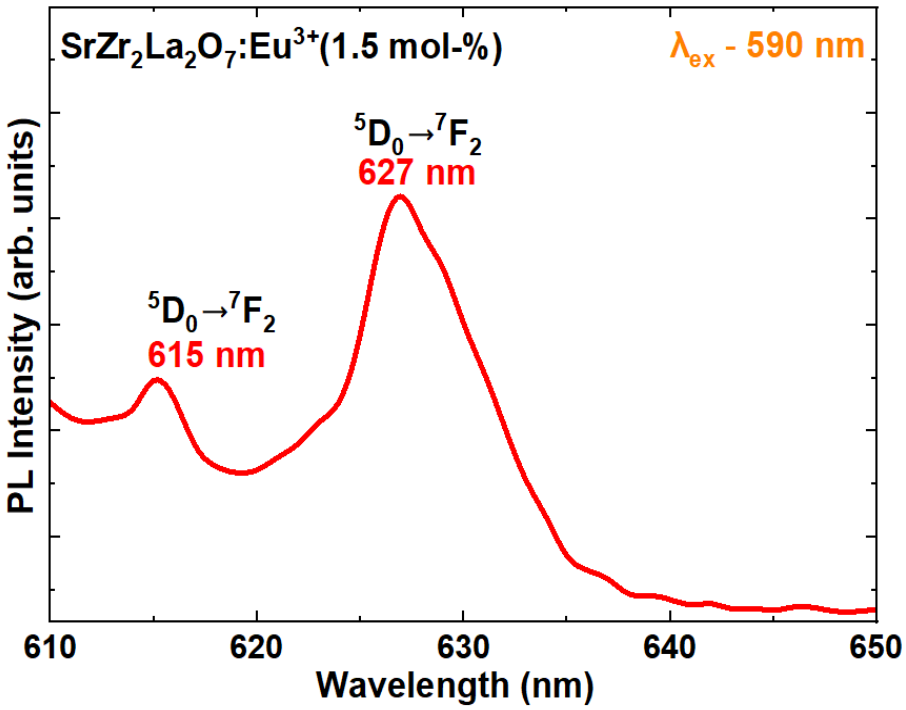

Figure 4.14 PL emission spectrum $SrZr_2La_2O_7:Eu^{3+}$ (λ = 590 nm)

of the phosphor matrix varies from 400 to 500 µm. This transmission occurs within an exceptionally brief time frame of 1 to 2 picoseconds.

The investigation focuses on the analysis of emission spectra produced by different excitation wavelengths. Based on the information supplied, we propose a model that is depicted in Figure 4.15. Based on the above results obtained from a study using 279 excitations and the cumulative emissions resulting from cascade photon absorption and subsequent emissions, we introduce a phosphor that prominently displays a red hue, but with a somewhat lower intensity of blue light emission. Based on the analysis, it can be inferred that the $SrZr_2La_2O_7$: Eu^{3+} phosphor demonstrates favourable attributes for application in light-emitting diodes (LEDs), specifically in the context of a stacked multi-layer arrangement where it functions as a remote phosphor emitting primarily red light. The remote phosphor has a thickness ranging from 100 µm to 400 µm, with a separation of 50–100 µm between each phosphor layers. In this study, we present an innovative methodology. This study emphasizes the utilization of $SrZr_2La_2O_7$: Eu^{3+} phosphor, which has been included into a structure consisting of five distinct layers with differing thicknesses. The objective of this technology is to improve the luminous efficacy and color temperature of light-emitting diodes (LEDs). The emission of 395, 467, 540, and 590 nm emission can be absorbed by the second stack/layer of $SrZr_2La_2O_7$: Eu^{3+} phosphor of the 279 nm LED chip, as it falls within the phosphor absorption (excitation) spectral region, the

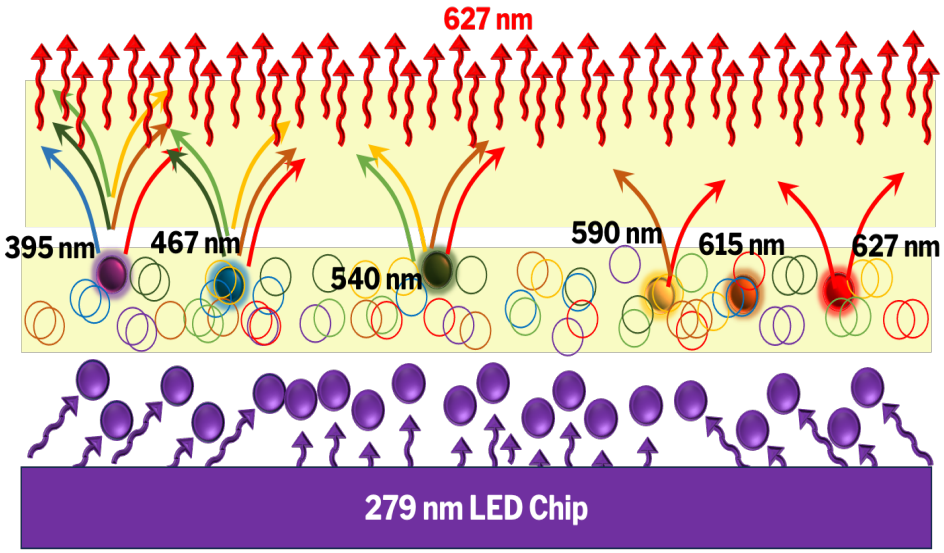

Figure 4.15: Schematic of the Photon Cascade excitation, emission LED made from Phosphor $SrZr_2La_2O_7:Eu^{3+}$ (1.5 mol%)

emission of 615 and 627 nm cannot be absorbed as it falls outside this range. This results in a slight reduction in the red emissions in the phosphor may be due to the reflections. This strategy can increase the amount of red components to achieve a high CRI value (Colour Rendering

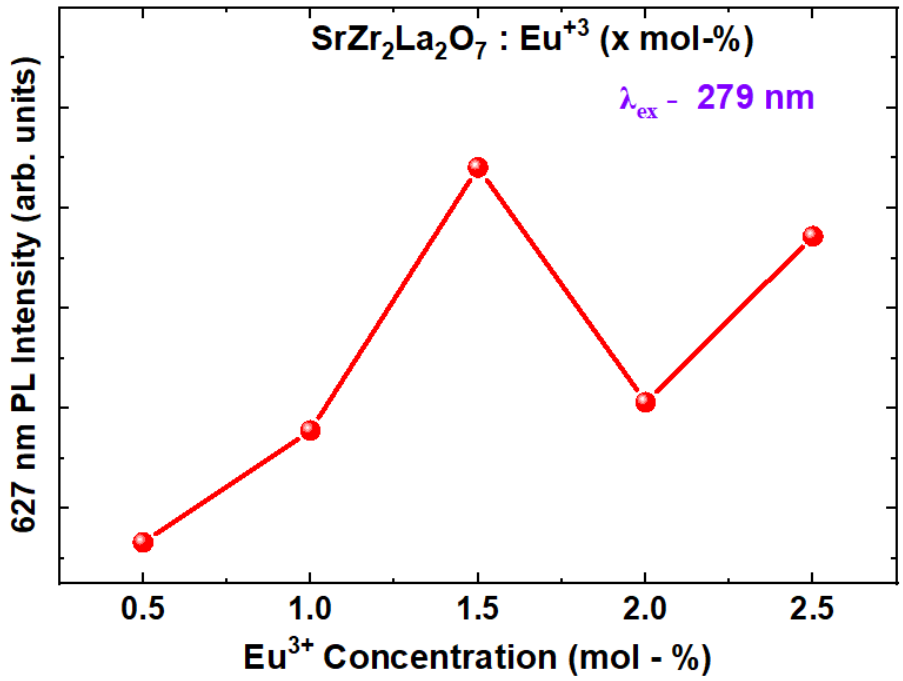

Figure 4.16 PL Intensities of 627 nm emission of $SrZr_2La_2O_7:Eu^{3+}$ (0.5 to 2.5 mol%)

Index) and CQS (Colour Quality Scale). Figure 4.16 shows the intensities at 627 nm when excited at 279 nm for different concentrations. It could be clearly visible in Figure 4.16 that the intensity is higher at a concentration of 1.5 mol% compared to other concentrations. The 627 nm emissions also show a very narrow emission with an FWHM of 8.6 nm which explains the

efficiency and color purity of the emissions with the phosphor studied. The FWHM of the 627 nm emission is shown in Figure 4.17.

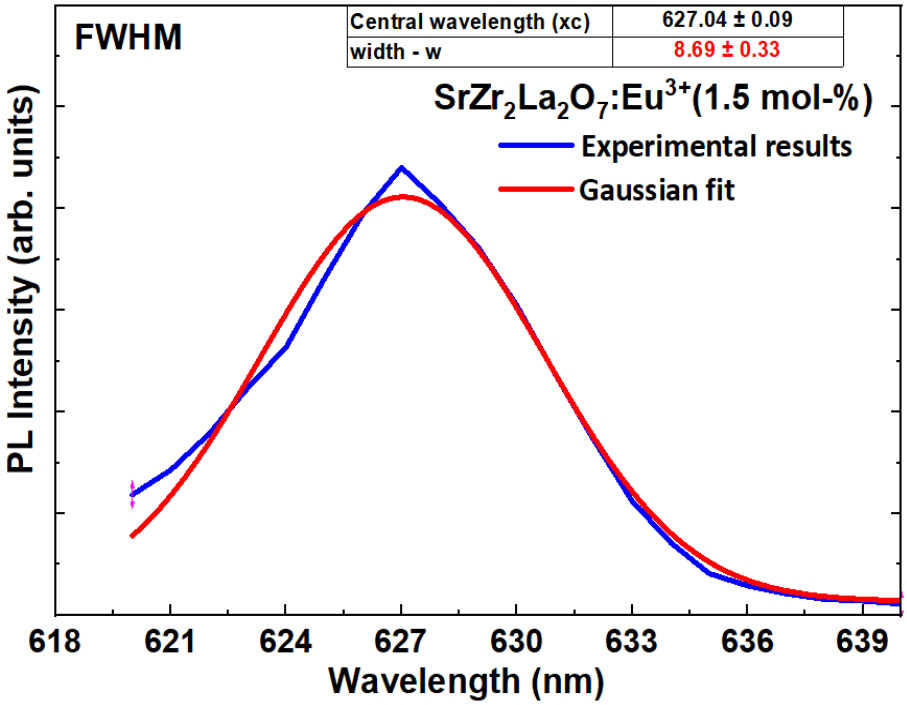

Figure 4.17: 627 nm emission width (FWHM) of $SrZr_2La_2O_7:Eu^3$ (λ_{ex} = 279 nm)

4.5 FSEM analysis

A field emission scanning electron microscopy (FESEM) analysis was performed to investigate the physical characteristics of $SrZr_2La_2O_7$: Eu^{3+}phosphor powders. The FESEM micrographs

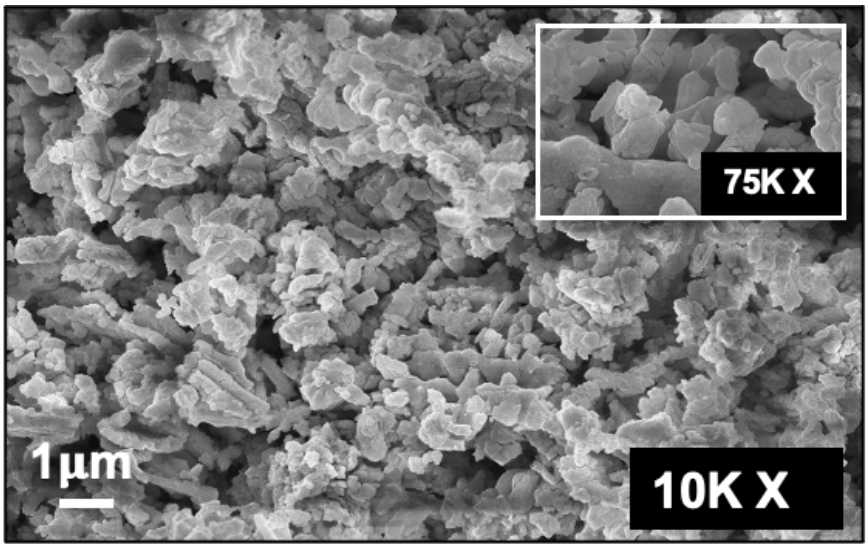

Figure 4.18: SEM Image of $SrZr_2La_2O_7:Eu^{3+}$ (1.5 mol% doping)

of a 1.5 mol% $SrZr_2La_2O_7$: Eu^{3+} sample are shown in Figure 4.18. The inset of the FESEM

image in Figure 4.18 provides higher magnification images of these samples. The FESEM analysis revealed that the particles of the $SrZr_2La_2O_7$: Eu^{3+} sample have an irregular polyhedral shape, with sizes ranging from approximately 100 nm to 10.0 µm. Notably, cathodo-luminescence (CL) was observed when the electron beam light emissions interacted with the investigated phosphors, as illustrated in Figure 4.18.

4.6 Energy Dispersive X-ray Analysis (EDAX)

Table 4.2. Element analysis of $SrZr_2La_2O_7$: Eu^{3+} 1.5 mol%

Element	Weight%	Atomic %
O K	26.84	73.59
Sr L	12.35	6.18
Zr L	6.29	3.03
La L	53.85	17.00
Eu L	0.67	0.19
Totals	100.00	

The chemical composition of the $SrZr_2La_2O_7$:Eu^{3+} phosphor, specifically containing Eu^{3+} ions, was determined through the utilization of Energy Dispersive X-ray Analysis (EDAX). Figure

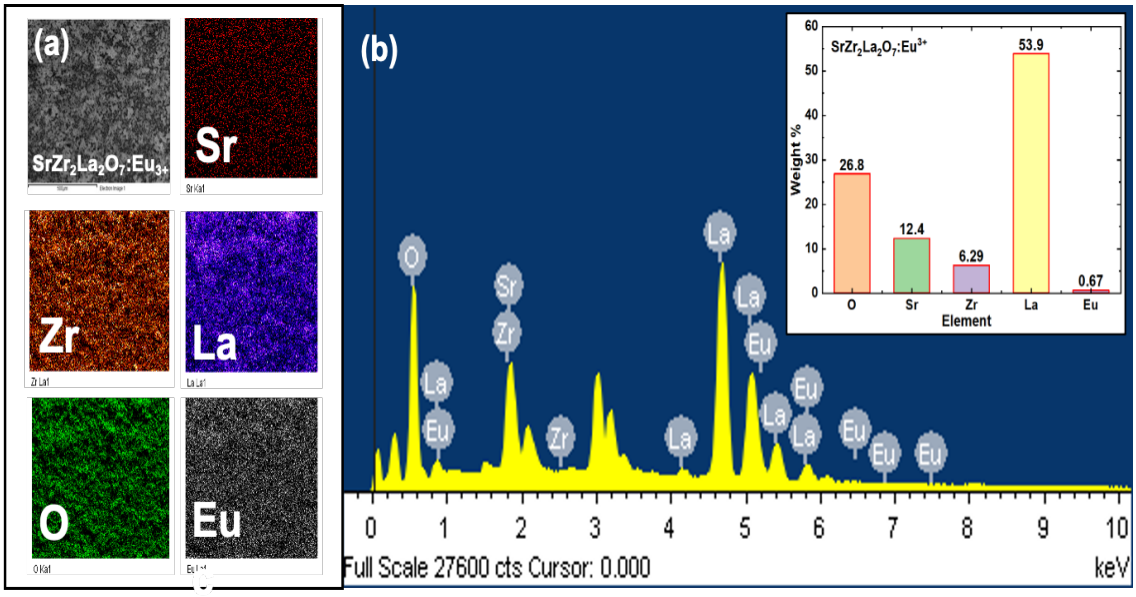

Figure 4.19 (a) Element mapping $SrZr_2La_2O_7$:Eu^{3+} 1.5 mol %), and (b) EDAX spectrum of $SrZr_2La_2O_7$ showing all the elements of synthesized material

4.19a illustrates the Elemental map of the $SrZr_2La_2O_7$:Eu^{3+} phosphor, while Figure 4.19b showcases the EDAX spectrum of the phosphor subsequent to annealing at 1200°C. The

presence of discernible peaks corresponding to La, Zr, O, Sr, and Eu in the EDAX spectra serves to confirm the successful synthesis of the $SrZr_2La_2O_7:Eu^{3+}$phosphor material. Table 4.2 provides elemental analyses, which effectively demonstrate the efficient diffusion of Eu^{3+} ions into the host lattice of $SrZr_2La_2O_7$ and their uniform distribution.

4.7 Fourier Transform Infrared (FTIR) analysis

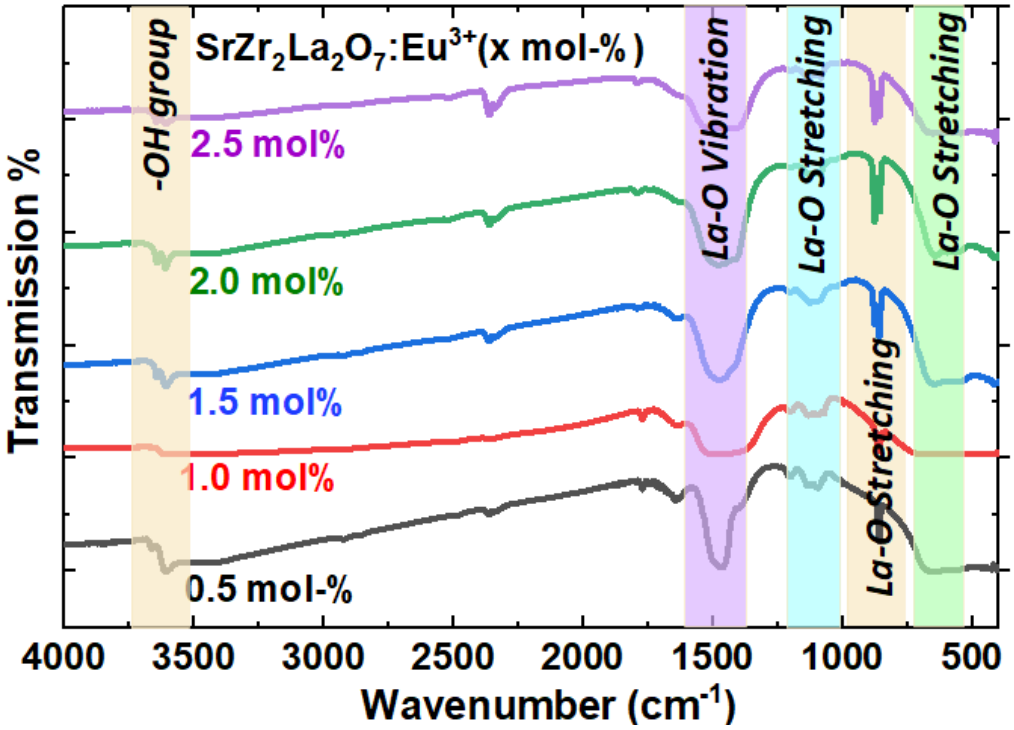

Figure 4.20: FTIR spectra of the $SrZr_2La_2O_7:Eu^{3+}$ phosphors doped with different concentration of Eu3+.

To investigate the vibrational properties of the phosphors under examination, an evaluation using Fourier Transform Infrared (FTIR) spectroscopy was conducted. The FTIR analysis provides information regarding the vibrational modes of the functional groups present in the materials. The KBr pellet method, utilizing Potassium Bromide, was employed to obtain FTIR spectra within the wavenumber range of 400-4000 cm^{-1}. Figure 4.20 illustrates the FTIR spectra of the $SrZr_2La_2O_7$ phosphors doped with varying concentrations of Eu^{3+}. It was observed that all samples examined displayed nearly identical spectra. A minor absorption band, located near 1097 cm^{-1}, was attributed to the La-O vibration mode present in phosphorous systems [23]. The sharp and broad bands observed at 670 cm^{-1}, 858 cm^{-1}, and 1459 cm^{-1} are associated with the La-O stretching vibrations [24]. Furthermore, the sharp absorption peak observed at a higher energy position, centred at 3612 cm^{-1}, is attributed to the presence of the hydroxyl (-OH) group.

4.8 Particle size analysis

The particle size analysis was performed using the Malvern Mastersizer 3000 instrument, as depicted in Figure 4.21. The results indicated that the measured particle size ranged from 0.12 to 9.15 um. This suggests that the phosphor material exhibits a hybrid nature. Subsequent photoluminescence (PL) studies were carried out on these samples. The average particle size, as illustrated in Figure 4.21, was determined to be 2.0 um, with a maximum size of 9.15 µm. Consequently, the synthesized phosphor material demonstrates potential for application in the production of industrial w-LED within the desired size range of 5–10 µm.

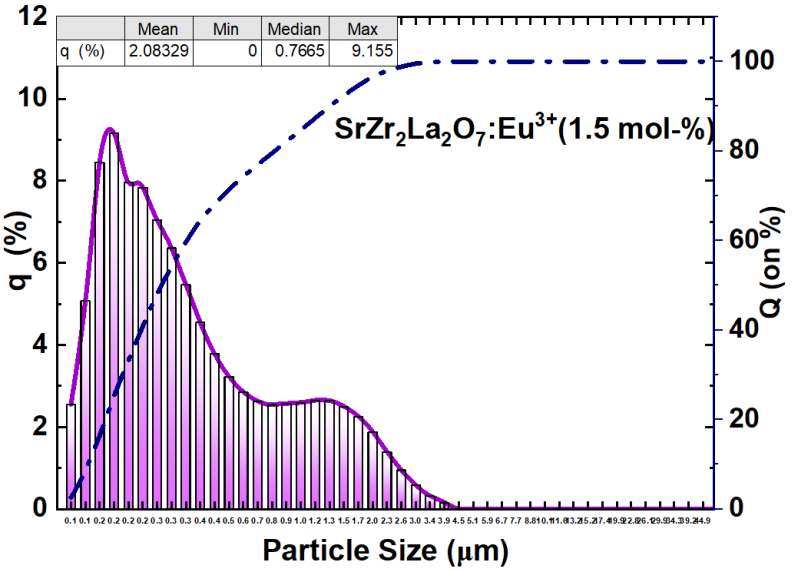

Figure 4.21 : Particle Size Distribution of $SrZr_2La_2O_7:Eu^{3+}$ (1.5 mol %).

4.9 Temperature dependent PL analysis

The thermal challenges associated with the use of UV LEDs in combination with phosphors to produce white light by converting a fraction of the UV light into various colours arise due to the high-energy nature of the UV light. Phosphors capable of directly producing white light can be modified to emit light throughout a broader spectrum of wavelengths, hence leading to a decrease in the concentration of energy within specific wavelength ranges. This particular attribute facilitates the control of heat production. Ensuring the reliability and longevity of LED devices necessitates the utmost attention to maintaining the stability of phosphor under varying temperature conditions. The crystal structure and shape of the phosphor have an impact on its thermal stability and resistance to temperature fluctuations. To investigate the potential relationship between temperature and the intensity of photoluminescence (PL) emission, measurements were carried out on a phosphor of interest. The PL emission was recorded at various temperatures ranging from 323 K to 423 K. This work aims to enhance the

comprehension of the thermal stability, emission intensities, and chromatic aberration features that are found under high temperature conditions.

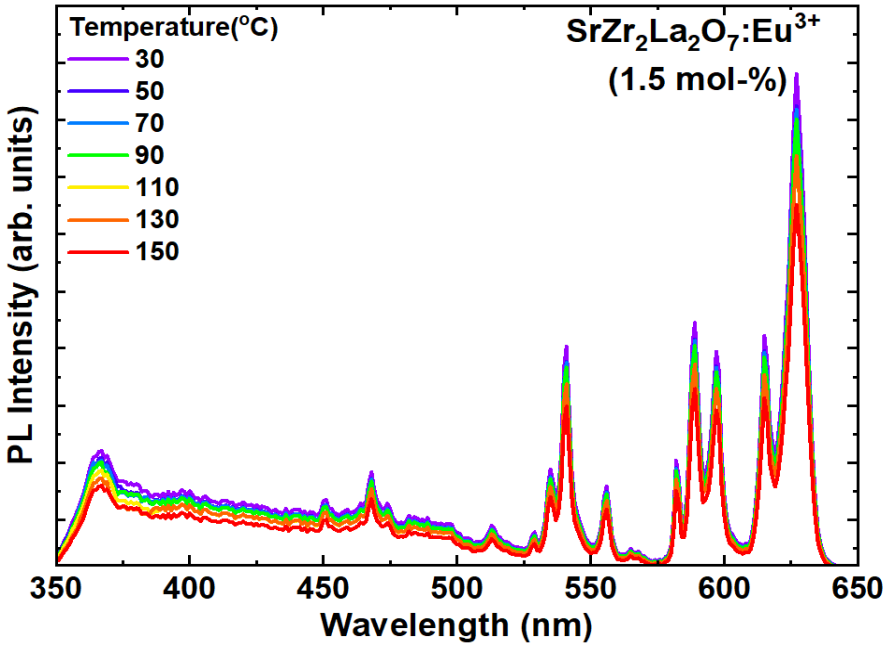

Figure 4.22 PL Spectra of $SrZr_2La_2O_7:Eu^{3+}$ (x = 2.0 mol-%) from 30°C to 150°C under 590 nm excitation.

Figure 4.22 depicts the photoluminescence (PL) spectra of the phosphor at various temperatures. This illustrates that there is a negligible alteration in both the configuration and location of the peak, yet a discernible decline in intensity can be observed. The observed

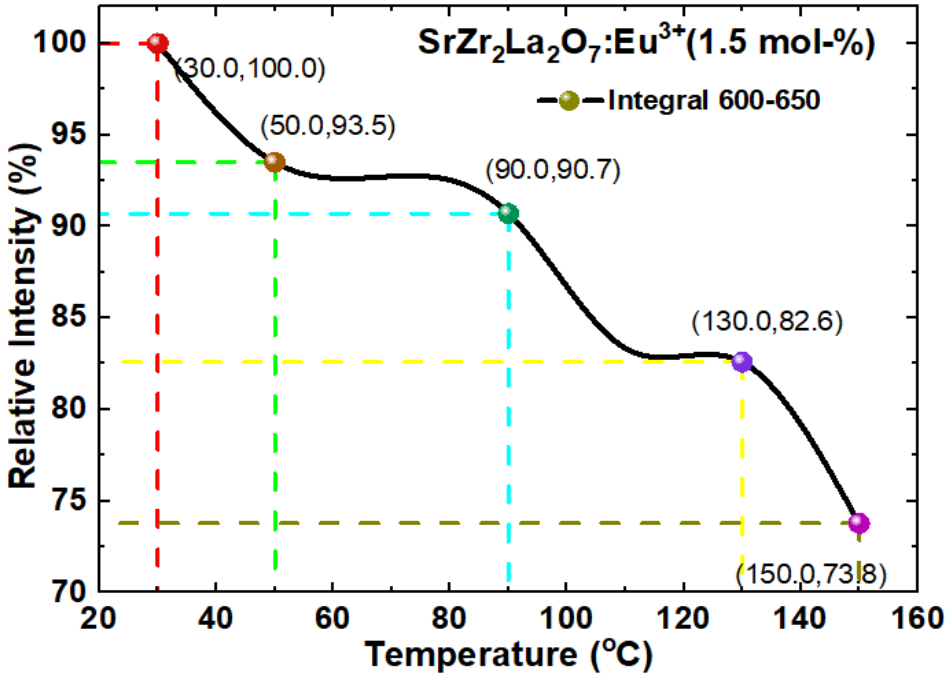

Figure 4.23 Plot showing the relation between relative intensity(%) and temperature for $SrZr_2La_2O_7:Eu^{3+}$ (x = 2.0 mol-%)

phenomena can be explained by the correlation between elevated temperatures and the heightened occurrence of non-radiative transitions, which subsequently leads to a reduction in intensities. The phosphor $SrZr_2La_2O_7:Eu^{3+}$ has a notable reduction in relative photoluminescence (PL) intensity as temperature increases from 323 K to 423 K, as illustrated in Figure 4.23. The magnitude of this reduction is about 27%, a much lesser value compared to the reductions witnessed in phosphors that are now available in the market. Therefore, the $SrZr_2La_2O_7:Eu^{3+}$ phosphor under investigation exhibits remarkable thermal stability. The observed reduction in intensity during the transition from room temperature to 423K can be ascribed to thermal quenching (25). The correlation between temperature and intensity can be elucidated through the utilization of the Arrhenius formula (26).

$$I(T) = \frac{I_o}{1 + c\exp\left(-\frac{Ea}{kT}\right)}$$

Where, the term I(T) is to represent the intensity that is seen at different discrete temperatures. In the provided context, the sign T is used to represent the initial intensity, I_O denotes the original intensity, the symbol k is used to denote the Boltzmann constant (8.629 x 10^{-5} eV/K), the symbol c is used to indicate a constant, and the symbol Ea represents the activation energy and exp(-Ea/kT) denotes the exponential term.

The activation energy for the developed phosphor is determined to be $E_a = 0.18$ eV. This finding provides empirical evidence supporting the favourable thermal stability of the material, as depicted in Figure 4.24, which illustrates the correlation between the natural logarithm of [(I_0/I)

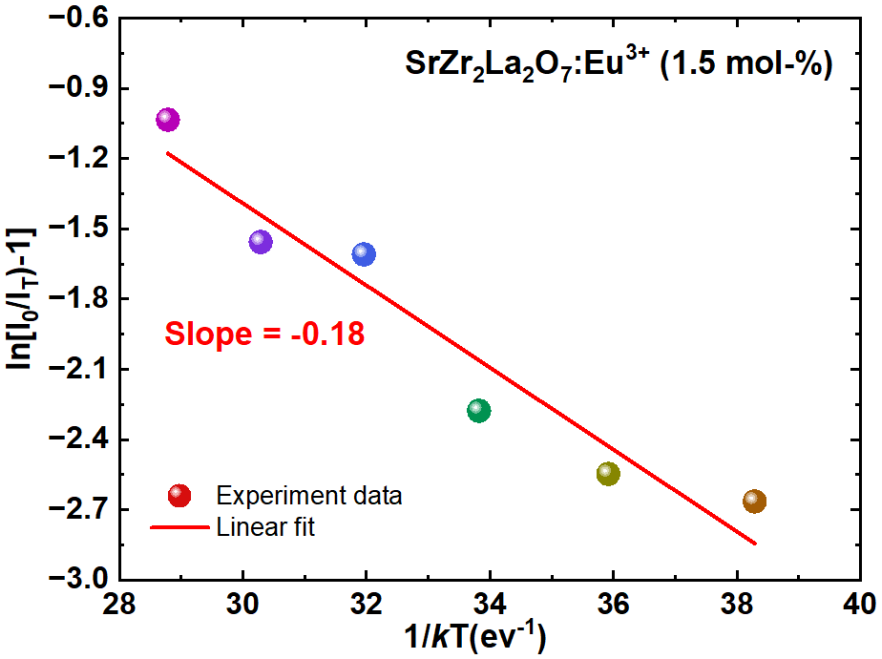

Figure 4.24 Plot showing the relation between ln[(I0/I) - 1] and 1/T for $SrZr_2La_2O_7:Eu^{3+}$ (x = 2.0 mol-%)

- 1] and the reciprocal of temperature (1/T). Phosphors with the potential to generate white light directly can be designed to exhibit enhanced stability and durability, resulting in LED lights and displays characterized by an extended lifespan and increased reliability. The significance of this characteristic is particularly noteworthy in situations where maintenance or replacement challenges arise, such as in the case of streetlights, architectural lighting installations, and display devices.

4.10 Determination of color coordinates

The CIE chromaticity coordinates, provided by the Commission International De I'Eclairage, enable the characterization of colours based on their spectral power distribution using (x, y) coordinates. In the case of $SrZr_2La_2O_7:xEu^{3+}$ (x = 0.5–2.5 mol%) under 590 nm excitation, the CIE chromaticity diagram depicted in Figure 4.25 reveals that the coordinates align with the red color boundary of the CIE map. This indicates that any deviation in the CIE coordinates is minimal and practically insignificant, as illustrated in Figure 4.26. Consequently, alterations in concentration do not result in a substantial modification of the chromaticity. Color purity is determined through the utilization of the following equation [27].

$$Colour\ purity = \frac{\sqrt{(x_s - x_i)^2 + (y_s - y_i)^2}}{\sqrt{(x_d - x_i)^2 + (y_d - y_i)^2}} \times 100\ \%$$

(x_i, y_i) is the chromaticity coordinates of the standard white illuminant (0.333, 0.333)

(x_d, y_d) are and of dominant emission wavelength

(x_s, y_s) are the coordinates for the phosphor

The color purity of $SrZr_2La_2O_7:Eu^{3+}$ (x = 0.5–2.5 mol%) phosphors was calculated in the range of 94.82–99.10%. These findings suggest that the synthesized phosphors exhibit a significantly high red color purity, making them highly suitable for application as phosphors in light-emitting diodes (LEDs). The observed excellent color purity can potentially be attributed to the hypothesized cascading effect resulting from several absorptions and emissions. This observation indicates that the Eu^{3+} ion occupies a non-symmetrical position, as evidenced by its predominant emission occurring at around 627 nm, exhibiting high color purity. Figure 4.26 illustrates the alteration in color coordinates in response to varying concentrations. The graph illustrates that the coordinates exhibit minimal variation, indicating that alterations in dopant concentrations have negligible impact on color purity. This finding is significant for the practical implementation of white light-emitting diodes (w-LEDs).

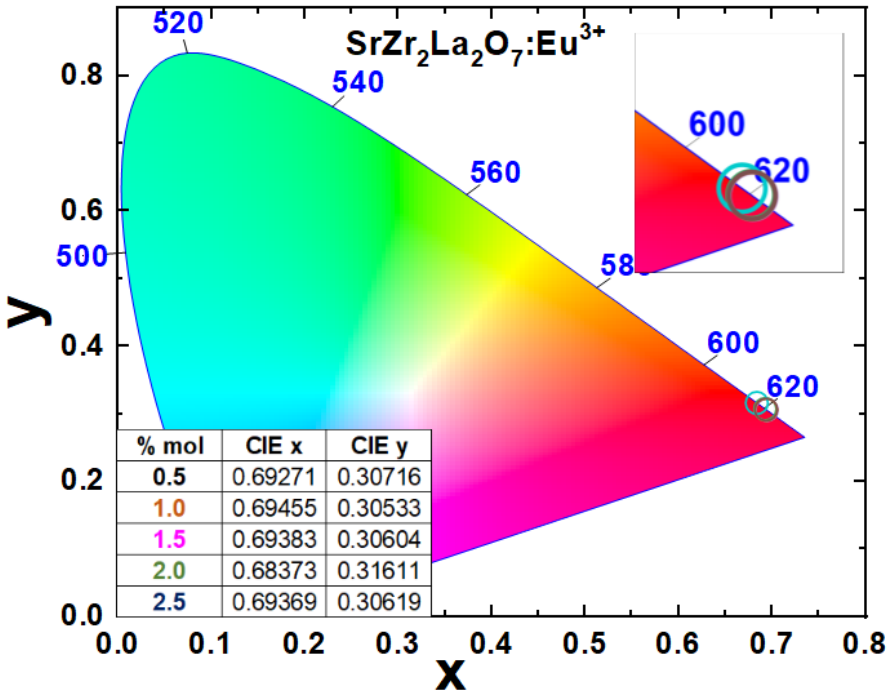

Figure 4.25: CIE chromaticity coordinates for phosphor $SrZr_2La_2O_7:Eu^{3+}$ (x = 0.5–2.5 mol %)

Figure 4.27 displays the chromaticity CIE color coordinates of $SrZr_2La_2O_7:Eu^{3+}$ (1.5 mol%) when stimulated by various absorption wavelengths, namely 279, 395, 476, 540, and 590 nm.

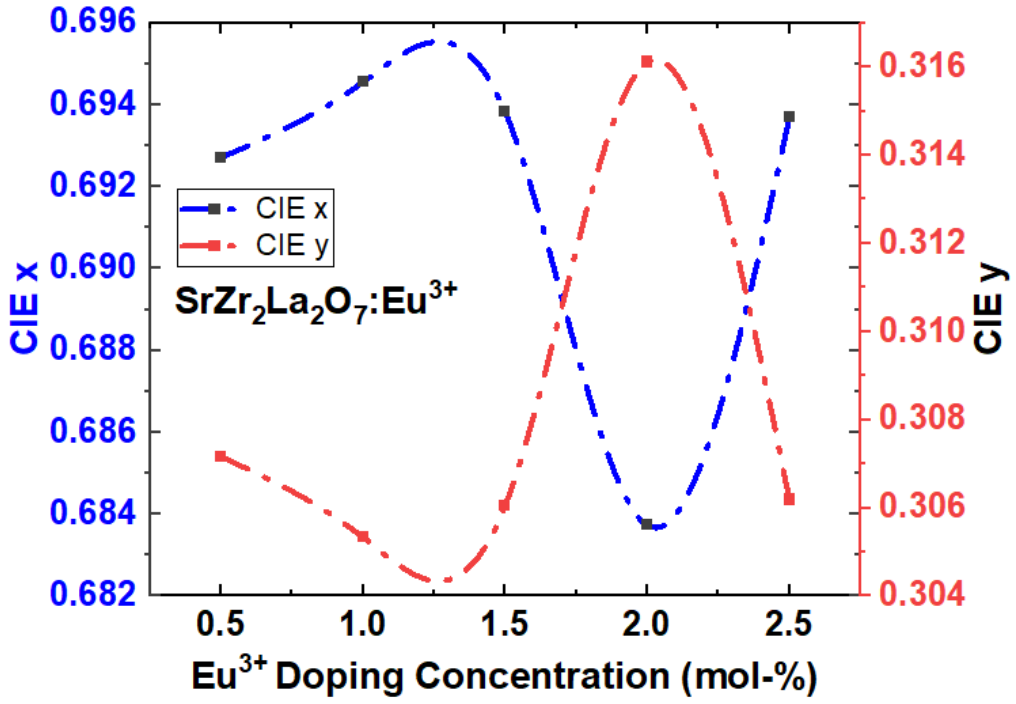

Figure 4.26: Shift in the color coordinates x and y of $SrZr_2La_2O_7:Eu^{3+}$ (x = 0.5–2.5 mol%)

This indicates that the $SrZr_2La_2O_7$ phosphors containing Eu^{3+} ions exhibit a prominent crimson hue. The incorporation of Eu^{3+} doping ions into the $SrZr_2La_2O_7$ phosphor leads to an emission

that exhibits color coordinates (0.690,0.306) closely resembling red light, hence indicating a vivid red emission color. The $SrZr_2La_2O_7:Eu^{3+}$ (1.5%) phosphors demonstrated promise as viable red-emitting candidates for the development of novel light-emitting diodes (LEDs).

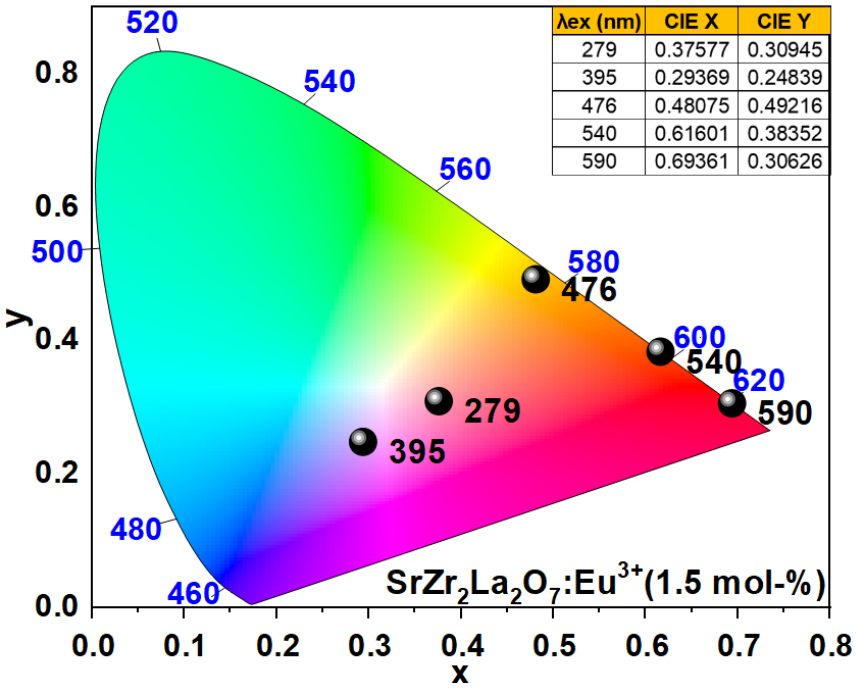

Figure 4.27 : CIE chromaticity coordinates of prepared $SrZr_2La_2O_7:Eu^{3+}$ (1.5 mol %) excited at different absorptions.

4.11 Summary

The solid-state reaction approach was successfully employed to prepare a new phosphor, $SrZr_2La_2O_7:Eu^{3+}$, which exhibits red emission. The photoluminescent and structural characteristics of the phosphors were examined and recorded. Based on the photoluminescence (PL) examination conducted for excitation at a wavelength of 279 nm, it is observed that the phosphor material predominantly emits red light, accompanied by a somewhat lesser intensity of blue emissions. These emissions are attributed to cascade photon emissions, as well as processes of absorption and subsequent emission. Hence, the $SrZr_2La_2O_7:Eu^{3+}$ phosphor, with a concentration of 1.5 mol%, is deemed appropriate for Light-Emitting Diodes (LEDs) that employ stacked multi-layer remote phosphor technology to emit light in the red area. The emissions observed at a wavelength of 627 nm can be attributed to the hyper-sensitive electric dipole transition from the $^5D_0 \rightarrow {}^7F_2$ state. The emission seen at a wavelength of 627 nm exhibited a narrow spectral bandwidth, characterized by a full width at half maximum (FWHM) of 8.6 nm. This emission displayed an improved luminous efficacy, which might potentially be attributed to a series of photon emissions, absorption processes, and subsequent emissions. The phosphor material has a range of particle sizes, spanning from 0.12 to 9.15 µm. These particles

possess a mostly cubic phase and demonstrate a highly crystalline structure. The existence of Eu^{3+} in conjunction with the host matrix $SrZr_2La_2O_7$ has been confirmed using EDAX tests. The presently investigated phosphor material exhibits red-dominating narrow emissions and is well-suited for applications in white-light-emitting diodes (w-LEDs) and other electronic devices.

References

[1] Y. Xu, F. Zhao, Resour. Policy 83 (2023), 103531, https://doi.org/10.1016/j.resourpol.2023.103531.
[2] US Department of Energy. International Energy Outlook 2017. (2017); https:// www.eia.gov/outlooks/ieo/pdf/0484(2017).pdf. (2017).
[3] H.A. Ho¨ppe, Angew. Chem. Int. Ed. Engl. 48 (2009) 3572–3582.
[4] Z. Xia, Z. Xu, M. Chen, Q. Liu, Dalton Trans. 45 (2016) 11214–11232.
[5] P. Pust, P.J. Schmidt, W. Schnick, A revolution in lighting, Nat. Mater. 14 (2015) 454–458.
[6] J.M. Phillips, et al., Laser Photonics Rev. 1 (2007) 307–333.
[7] C.C. Lin, A. Meijerink, R.S. Liu, J. Phys. Chem. Lett. 7 (2016) 495–503.
[8] US Department of Energy. Solid state lighting research and development plan. (2016); https://energy.gov/sites/prod/files/2016/06/f32/ssl_rd-plan_% 20jun2016_2.pdf.
[9] H.A. Ho¨ppe, H. Lutz, P. Morys, W. Schnick, A. Seilmeier, J. Phys. Chem. Solid 61 (2000) 2001–2006.
[10] M. Nasilowski, P. Spinicelli, G. Patriarche, B. Dubertret, Nano Lett. 15 (2015) 3953–3958.
[11] H.-D. Nguyen, R.-S. Liu, J. Mater. Chem. C 4 (2016) 10759–10775.
[12] J.L. Lean˜o, M.-H. Fang, R.-S. Liu, ECS J. Solid State Sci. Technol. 7 (2018) R3111–R3133.
[13] Natalia Miniajluk-Gaweł, Bartosz Bondzior, Vasyl Kinzhybalo, Maciej Ptak, Thi Hong Quan Vu, and Przemysław Jacek Der´en, J. Phys. Chem. C 2023 127 (18), 8680-868610.1021/acs.jpcc.3c01521.
[14] Z. Nie, J. Zhang, X. Zhang, S.Z. Lue, X.G. Ren, G.B. Zhang, X. Wang, J. Solid State Chem. 180 (2007), https://doi. org/10.1016/j.jssc.2007.08.024.
[15] https://instanano.com/product/xrd-reference-file-online/.
[16] M. Babu, Asanapuram, C.J. Bungala, T. Suhasini, T. Rao, L. Moorthy, Solid State Sci. 13 (2011) 574–578, https://doi.org/10.1016/j.solidstatesciences.2010.12.028.
[17] Weijie Zhou, Yiyi Ou, Xiaohui Li, Mikhail G. Brik, Alok M. Srivastava, Ye Tao, and Hongbin Liang, Inorganic Chem. 2018 57 (23), 14872-14881 10.1021/acs.inorgchem.8b02639.
[18] M. Kumar, C.J. Bungala, K. Gopal, R. Ramakrishna Reddy, J. Solid State Chem. 184 (2011) 2145–2149, https://doi.org/10.1016/j.jssc.2011.06.007.
[19] Koen Binnemans, Coordination Chemistry Reviews, Volume 295, 2015, Pages 1-45, ISSN 0010-8545, 10.1016/j. ccr.2015.02.015.
[20] C. Klixbüll Jørgensen, B.R. Judd, Mol. Phys. 8 (3) (1964) 281–290, https://doi.org/10.1080/ 00268976400100321.
[21] A P Vink1, P Dorenbos, J T M de Haas, H Donker, P A Rodnyi, A G Avanesov and C W E van Eijk, J. Phys.: Condensed Matter, 14 (38).
[22] Thi, My Hanh Nguyen, That, Phung Ton, Anh, Nguyen Doan Quoc and Trang, Tran Thanh. Mater. Sci.-Poland, 38 (4), 2020654–660. 10.2478/msp-2020-0076.
[23] Y. Wang, Y. Liu, T. Guo, et al., Environ. Sci Pollut. Res. 27 (2020) 42868–42880, https://doi.org/10.1007/s11356-020-10240-1.

[24] P. Kumar, T.M. Ram, M. Maharajan, A. Chinnasamy, J.P. Pitchiah, K. Santhana Kumar, Innovation 8 (2019) 759–763.
[25] Wanggui Ye, Chong Zhao, Xiaofei Shen, Chaoyang Ma, Zhonghua Deng, Yanbin Li, Yuzhen Wang, Chuandong Zuo, Zicheng Wen, Yingkui Li, Xuanyi Yuan, Chong Wang, and Yongge Cao, ACS Applied Electronic Materials 2021 3 (3), 1403-1412.
[26] A.K. Galwey, M.E. Brown, Themochim. Acta 386(1), (2002), 91–98.
[27] G. Lu, B. Deng, Y. Zhang, Y. Wang, Y. Lin, K. Jiang, Y. Shao, D. Zhang, R. Yu, Sci. Mater. Electron. 33 (2022) 1–13, i.org/10.1007/s10854-022-08649-0.

Chapter - 5

Studies on a Novel $SrZr_2CaLa_2O_8:Eu^{3+}$ Phosphor for Lighting Applications Emitting Direct White Light

Features of the Chapter:

The utilisation of direct white light emitting phosphors holds great importance in the display sector as they possess the capability to enhance the quality, efficiency, and versatility of lighting sources employed in a majority of display technologies. The phosphor $SrZr_2CaLa_2O_8:Eu^{3+}$ under investigation was synthesised using the standard solid-state reaction technique. The significance of the stoichiometric ratio of precursors in influencing the properties of the resulting phosphor has been noted. The X-ray diffraction (XRD) investigation revealed that the phosphor exhibited a hexagonal phase and has a crystal size of approximately 28 nm. Scanning electron microscopy (SEM) examinations unveiled the presence of a conglomerate of elongated objects characterised by an approximate dimension of 0.2 µm. The observed excitation peak maximum at a wavelength of 280 nm can be attributed to the charge transfer phenomenon occurring between Eu^{3+} and O^{2-} ions. The occurrence of additional excitation peaks at ultraviolet (395 nm), blue (about 467 nm), green (around 540 nm), orange (around 590 nm), and red (approximately 627 nm) wavelengths can be attributed to the energy transitions from $^7F_0 \rightarrow {}^5L_6$ and from $^7F_0 \rightarrow {}^5D_2$. These transitions are responsible for the $^5D_0 \rightarrow$ 7FJ (where J ranges from 0 to 4) transitions of Eu^{3+} ions. The estimated CIE chromaticity coordinates for the emissions at wavelengths of 395 nm and 590 nm were (0.37, 0.33) and (0.67, 0.33), respectively. The distinctive emissions shown by Eu^{3+} ions make this innovative phosphor suitable for generating direct white light in LEDs, a feat that is typically challenging to accomplish in systems consisting of a single component. Crystalline nature and cubic phase of the phosphor are confirmed using X-ray powder diffraction analysis.

This work has been published in:

K. K. Aitha, D. Dinakar, K. V. R. Murthy, A. S. S. Prasad, D. Haranath, **Luminescence**, 2023, 1. DOI: https://doi.org/10.1002/bio.4623 **(IF: 2.9)**

5.1 Outline

Solid-state lighting technology has established a prominent presence in the display and lighting sector because of its notable characteristics, including durability, energy efficiency, extended lifespan, and superior light output [1-2]. The utilisation of Yellow (YAG: Ce^{3+}) phosphor and Blue LED chips [3-5] is prevalent in the production of white light light-emitting diodes (W-LEDs). The development and enhancement of LEDs rely heavily on the presence of direct white light-emitting phosphors due to their numerous advantages. These advantages include energy efficiency, high colour quality and rendering, cost-effectiveness, reduced heat generation, increased dependability, longer lifetimes, and enhanced spectral energy distribution [1-6]. In contrast, phosphors containing Ce^{3+} ions exhibit a relatively low conversion efficiency. Additionally, the colour of these phosphors, as determined by the input power [7, 8], is characterised by a deficiency in the red component within the emission spectrum. There is a notable degree of colour rendering index (CRI) deficiency and a relatively low correlated colour temperature (CCT) [9-10]. The accurate replication of natural sunshine using white light is crucial for a wide range of applications, such as indoor lighting, displays, automotive lighting, and other related fields. The capacity to generate white light of superior quality, accompanied by a high colour rendering index (CRI), is crucial in ensuring the accurate and vibrant representation of colours. This attribute holds significant value in activities that necessitate precise colour discrimination, such as art, photography, and medical treatments. The present demanding technology in the market is being dominated by the incorporation of multiphase and multi-layered phosphors, which emit blue, green, and red light from UV InGaN chips [11]. Hence, the development of diverse tricolour phosphors for application in advanced technology poses a significant imperative.

Consequently, numerous red phosphors, including the trivalent Eu^{3+} doped phosphor, have been the subject of intensive investigation in order to address this problem [12]. The Eu^{3+} ion, which is a notable rare earth ion, has the ability to emit light of a pure red colour through transitions from the $^5D_0 \rightarrow {}^7F_J$ states, where J ranges from 0 to 6. Eu^{3+} doped luminescent materials, such as $Y_2O_4S:Eu^{3+}$ and $Y_2O_3:Eu^{3+}$, are widely employed as commercial red phosphors in displays and lights due to their exceptional luminous performance [13]. Most of the phosphors doped with Eu^{3+} exhibit vibrant red or orange emissions, which correspond to the $^5D_0 \rightarrow {}^7F_1$ (590-600 nm) or $^5D_0 \rightarrow {}^7F_2$ (600-620 nm) transitions. The $CaO:Eu^{3+}$ sample demonstrates a variety of orange to red emissions when stimulated by ultraviolet light. It has been observed that the Eu^{3+} ions effectively incorporate themselves into the crystal structure of the CaO host material [14].

Nevertheless, calcium oxide (CaO) exhibits a drawback in terms of its efficacy in producing deep red emission within the wavelength range of 620-630 nm. In contrast, when $SrLa_2O_4$ is doped with Eu^{3+} ions and stimulated with near UV wavelengths, it exhibits broad deep red emissions [15]. In order to address these gaps, the prevailing approach involved the utilisation of UV-LEDs in conjunction with RGB phosphors capable of generating triple wavelengths [16]. In recent years, there has been a significant emphasis on the utilisation of single-phased phosphors for the generation of white light [17–18]. These phosphors have demonstrated greater promise in applications linked to white light-emitting diodes (W-LEDs). The phosphor system SrZr2CaLa2O8:Eu^{3+} being developed is capable of producing the three primary colours, red, green, and blue, which together constitute white light. This phenomenon occurs at different concentrations of Eu^{3+} inside the system.

The need for phosphors that emit direct white light is driven by the requirement for white light sources that are of high quality, energy-efficient, adaptable, and dependable, catering to a wide range of applications. The current research and development efforts in this domain are mostly directed towards the creation of innovative phosphors, with the aim of augmenting the functionalities of light-emitting diodes (LEDs) and rendering them more adaptable for a diverse array of lighting purposes.

5.2 Synthesis

The synthesis of $SrZr_2CaLa_2O_8$ phosphors has been accomplished by the standard solid-state reaction method as shown in Figure 5.1. Phosphors containing Eu^{3+} ions doped into $SrZr_2CaLa_2O_8$ were synthesised using a blend of SrO, Zr_2O_3, La_2O_3, CaO, and Eu_2O_3. Doping concentrations of 0.5, 1.0, 1.5, 2.0, and 2.5 mol% have been systematically doped within the combination as per Table 5.1. Acetone has been employed as a solvent to enhance the process of homogenization.

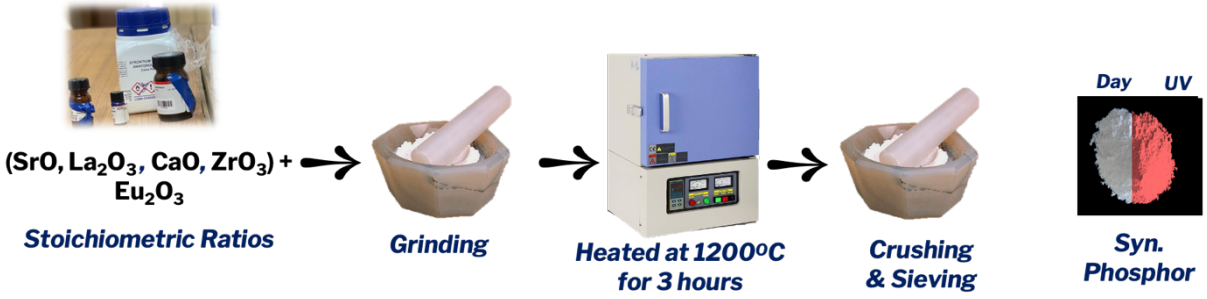

Figure 5.1: Flow chart depicting the synthesis of phosphor $SrZr_2CaLa_2O_8$

The oxides mentioned above were combined in stoichiometric proportions and grinded in an acetone medium for a duration of 30 minutes using an agate mortar and pestle. The dried powder

was placed into recrystallized alumina crucibles and subjected to calcination at a temperature of 1200°C in a muffle furnace, in an air atmosphere. This process led to the formation of a white phosphor substance, as indicated by the chemical reaction provided below.

$$CaO + SrO + Zr_2O_3 + La_2O_3 + Eu_2O_3 \rightarrow SrZr_2Eu_2La_2CaO_{11}$$

Table 5.1: Synthesized phosphor with varying dopant concentrations for $SrZr_2CaLa_2O_8$

Sample	Host	Dopant	Dopant Concentration
SZCL-S1	$SrZr_2La_2O_7$	Eu^{3+}	0.5 mol %
SZCL-S2	$SrZr_2La_2O_7$	Eu^{3+}	1.0 mol %
SZCL-S3	$SrZr_2La_2O_7$	Eu^{3+}	1.5 mol %
SZCL-S4	$SrZr_2La_2O_7$	Eu^{3+}	2.0 mol %
SZCL-S5	$SrZr_2La_2O_7$	Eu^{3+}	2.5 mol %

The PL excitation and emission spectra at room temperature was investigated using a SHIMADZU RF-5301 PC fluorescence spectrometer equipped with a 150 W xenon lamp and appropriate filters. The phase analysis of phosphor was conducted using an X'Pert Pro P Analytical Powder Diffractometer equipped with a Cu-K radiation source (wavelength = 1.54 Å). The instrument was operated at a current of 40 mA and a voltage of 40 kV. The diffraction scan was performed in the 2θ range of 20 to 80 degrees, with a scan speed of 0.05 degree per second. The sample's quantitative elemental composition as well as its shape were analysed using an Energy Dispersive X-ray (EDAX) spectroscopy instrument linked to the Scanning Electron Microscope (SEM) of JEOL make, model: JSM 5810 LV. The Perkin Elmer-100

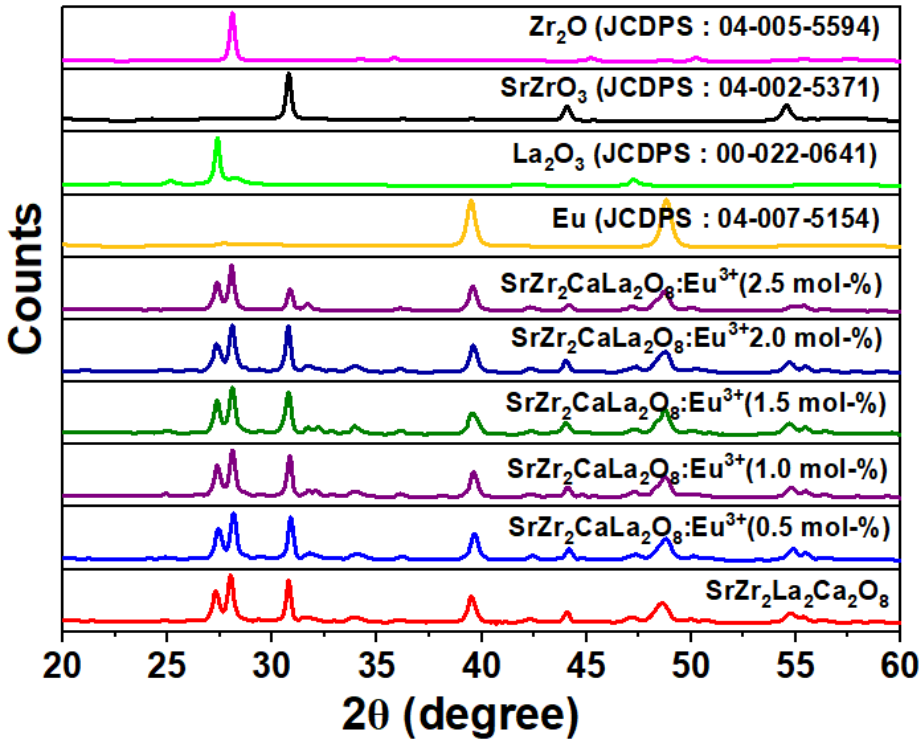

Figure 5.2 : XRD pattern of $SrZr_2CaLa_2O_8:Eu^{3+}$ for different Eu^{3+} concentrations.

instrument was employed for the acquisition of Fourier Transform Infrared (FTIR) spectra in order to ascertain the existence of different chemical bonds and their corresponding vibrational modes. The Malvern Mastersizer 3000 particle size analyzer was utilised to evaluate particle sizes within the range of 0.1 μm to 3 mm.

5.3 Powder XRD analysis

The efficiency of light absorption and emission in phosphors can be influenced by their structural characteristics. Adequately designed structures have the potential to augment the absorption of light and optimise the radiative recombination of excited electrons, resulting in increased efficiency of light emission.

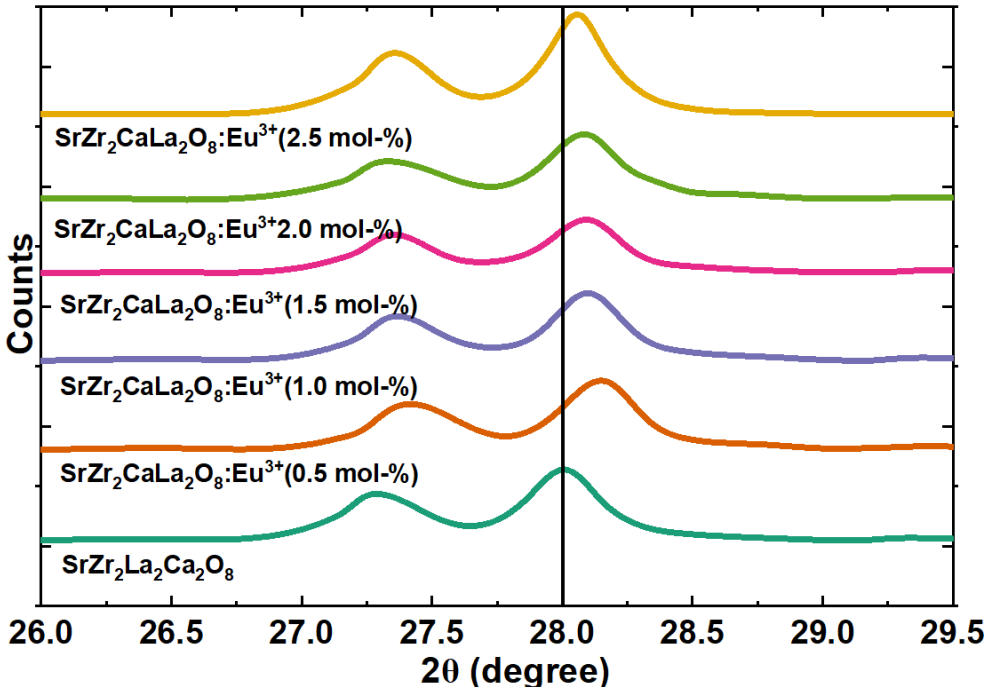

Figure 5.3 A magnified version of the XRD profile's noticeable peak at around 28°

The emission wavelengths of phosphors can be influenced by their crystal structure and shape. The precise adjustment of colour in phosphors enables the fulfilment of diverse LED applications, including a range of white light temperatures from warm to cool, as well as an assortment of colours for displays and ornamental lighting. Therefore, the crystal structure of the phosphors under investigation was determined by the utilisation of X-ray diffraction (XRD). Figure 5.2 displays the X-ray diffraction (XRD) patterns of $SrZr_2CaLa_2O_8$ phosphors, displaying the variations in Eu^{3+} dopant concentrations. The presence of distinct diffraction peaks observed in the X-ray diffraction (XRD) patterns served as an indication of the phosphors' elevated level of crystallinity for all the concentrations of Eu^{3+} ranges from 0.5 to 2.5 mol%. The diffraction patterns of all the phosphor samples exhibited a high degree of similarity, indicating that increase in the dopant concentration of Eu^{3+} ,do not appear to have a discernible

impact on the crystal's structure. Consequently, the phosphors being examined have a hexagonal crystal shape upon crystallisation. The lattice parameters that were observed have been shown in Table 5.2.

Table 5.2 : Summary of lattice parameters determined by XRD analysis

Sample	Crystal Structure	Cell parameters			Cell Volume
		a(Å)	b(Å)	c(Å)	
$SrZr_2CaLa_2O_8:0.005Eu^{3+}$	Hexagonal	6.64	6.64	6.64	151.2 (Å)
$SrZr_2CaLa_2O_8:0.010Eu^{3+}$	Hexagonal	6.60	6.60	6.60	147.1 (Å)
$SrZr_2CaLa_2O_8:0.015Eu^{3+}$	Hexagonal	6.66	6.66	6.66	149.0 (Å)
$SrZr_2CaLa_2O_8:0.020Eu^{3+}$	Hexagonal	6.53	6.53	6.53	141.8 (Å)
$SrZr_2CaLa_2O_8:0.025Eu^{3+}$	Hexagonal	6.51	6.51	6.51	139.5 (Å)

Figure 5.3 displays a magnified representation of the prominent peak observed at around 28 degrees in the X-ray diffraction (XRD) profile. The doping concentration of the Eu^{3+} ion was observed to increase, resulting in a noticeable shift towards higher diffraction angles in the magnified picture of Eu^{3+} doped phosphors.

The observed change in the location of the host lattice's diffraction peak can be explained by "Vegard's law". This law states that the presence of a dopant does not always result in the appearance of a distinct diffraction peak separate from the host peak. Instead, it can lead to a notable shift in the location of the host lattice's diffraction peak due to the substitution of host ions with dopant ions. In the current scenario, it is anticipated that the Eu^{3+} cation, which possesses a smaller radius and a similar valence state, will likely substitute the La^{3+} cation with a larger radius. Consequently, this substitution would result in a shift towards greater diffraction angles for the diffraction peak of the undoped sample. Additional verification was conducted by computing the permissible percentage difference [19], using the following formula:

$$D_r = \frac{R_s(CN) - R_d(CN)}{R_s(CN)} \times 100\%$$

where, R_s and R_d represent the ionic radii of the substituted and doping ions, respectively, whereas CN denotes the coordination number. The calculated value for the relative quantum efficiency (D_r) of the $SrZr_2CaLa_2O_8:Eu^{3+}$ phosphor was determined to be 8.90% which is very much less than 30% [20] further supported Eu^{3+} occupancy at the La^{3+} site. This finding provides more evidence for the presence of Eu^{3+} ions occupying the La^{3+} site. In addition, the

Debye-Scherer formula was utilised to calculate the crystallite size of all the compositions under investigation, as presented below.

$$D_{hkl} = \frac{K\lambda}{\beta \cos\theta}$$

In this context, the symbol K represents a constant, the symbol λ specifies the X-ray wavelength, β represents the full-width at half maximum, and θ marks the angle of diffraction. Based on the use of the Debye-Scherer formula, it has been determined that the average size of crystallites for each phosphor falls within the range of 24 to 30 nm, as presented in Table 5.3.

Table 5.3 : Average crystallite size of phosphor with different dopant concentrations

Sample	Crystallite size (nm)
$SrZr_2CaLa_2O_8$	28.21
$SrZr_2CaLa_2O_8:Eu^{3+}$ (0.5 mol%)	29.64
$SrZr_2CaLa_2O_8:Eu^{3+}$ (1.0 mol%)	27.57
$SrZr_2CaLa_2O_8:Eu^{3+}$ (1.5 mol%)	24.76
$SrZr_2CaLa_2O_8:Eu^{3+}$ (2.0 mol%)	26.96
$SrZr_2CaLa_2O_8:Eu^{3+}$ (2.5 mol%)	26.24

5.4 Photoluminescence studies

Figure 5.4 shows the photoluminescence excitation (PLE) spectrum of $SrZr_2CaLa_2O_8:xEu^{3+}$ (x=2.0 mol%) phosphor, when monitored at 627 nm. The spectra exhibited several distinct peaks of photoinduced light excitations (PLE) at wavelengths of 279/280, 395, 467, and 590 nm. The presence of distinct peaks at 279/280 nm and 395 nm implies that the sample exhibits excitation properties in the Ultraviolet (UV) range. Additionally, the peaks observed at 467 nm and 590 nm show that the sample holds potential for utilisation in white-light emitting diode (w-LED) applications. The dominant excitation peak observed at a wavelength of 280 nm can be attributed to the charge transfer process occurring between the Eu^{3+} and O^{2-} ions. Upon exposure to ultraviolet (UV) radiation, the 2p orbital of the O^{2-} undergoes electron transfer to the 4f orbital of Eu^{3+} ions. The reaction ($O^{2-}+ Eu^{3+}+hv \rightarrow Eu^{2+}+O^{-}$) serves as a representation of the process. When the electrons transition back from Eu^{2+} ions to O- ions, the resultant energy is subsequently transferred via resonance to adjacent Eu^{3+} ions.

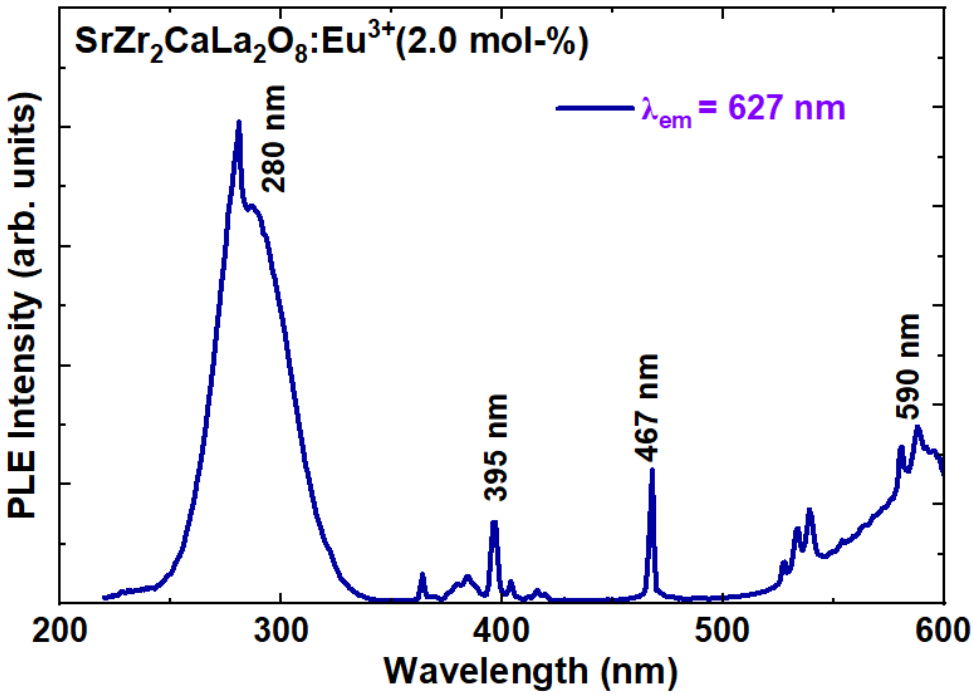

Figure 5.4 : PL excitation spectrum of $SrZr_2CaLa_2O_8:Eu^{3+}$ (λ_{em} = 627 nm) for 2.0 mol% of doping concentration.

Consequently, the electrons have the ability to undergo a transition from their lowest energy level, known as the ground state, to a higher energy state, referred to as the excited state. In the process of transition, an electron undergoes a downward transition from its lowest excited state to its ground state, resulting in the emission of a photon. The phenomenon of charge transfer

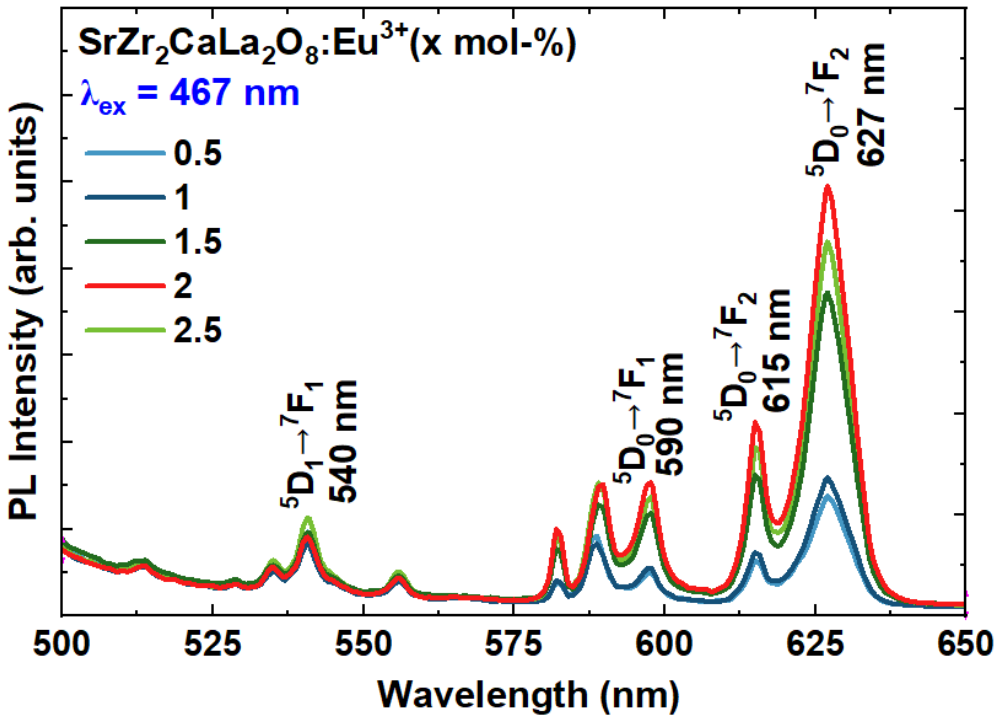

Figure 5.5 : PL emission spectrum of $SrZr_2CaLa_2O_8:Eu^{3+}$ (λ_{ex} = 467 nm)

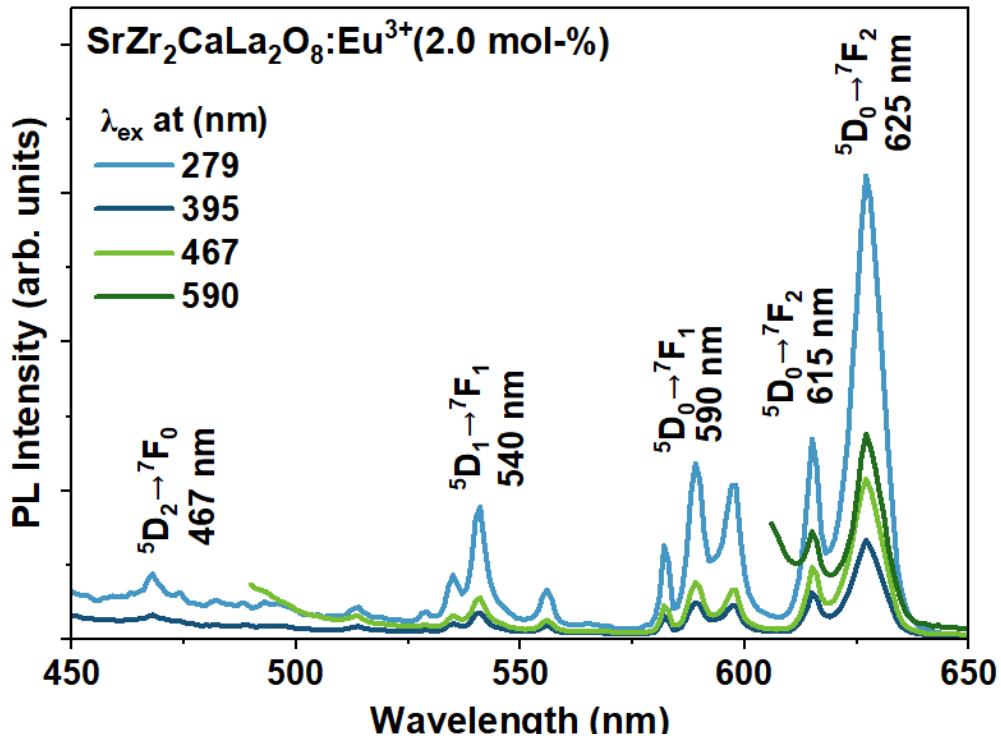

Figure 5.6: PL emission spectrum of $SrZr_2CaLa_2O_8:Eu^{3+}$ (2.0 mol-%) for various absorption lines.

absorption offers a novel mechanism for the excitation of Eu^{3+} ions, demonstrating notable efficacy in instances where $O^{2-}\rightarrow Eu^{3+}$ charge transfer absorption takes place, resulting in the subsequent transfer of energy to neighbouring Eu^{3+} ions. As a result, the photoluminescence excitation (PLE) spectra of samples containing Eu^{3+} ions exhibit prominent absorption bands associated with significant charge transfer[21]. The $SrZr_2CaLa_2O_8$ phosphor being investigated exhibits distinct excitation peaks at UV (395 nm), blue (467 nm), and orange (590 nm) wavelengths. These peaks are attributed to the $^7F_0\rightarrow{}^5L_7$, $^7F_0\rightarrow{}^5D_2$, and $^7F_1\rightarrow{}^5D_0$ transitions of Eu^{3+} levels, respectively. Certain emissions can also be observed in commercially available phosphors, such as Eu^{3+}-doped Y_2O_3 and Y_2O_2S, which are commonly used as red-emitting phosphors in white light-emitting diodes (w-LEDs). However, it should be noted that these phosphors exhibit a notable absorption of approximately 1% for blue radiations (450-480 nm) generated by the GaInN LED device. The current study investigates the unique phosphor system $SrZr_2CaLa_2O_8:Eu^{3+}$, which exhibits notable absorption properties in the ultraviolet (279 nm) and blue (467 nm) regions, making it suitable for usage in light-emitting diodes (LEDs). Additionally, there are absorptions of moderate intensity observed at wavelengths of 395 and 590 nm. Based on the above findings, it can be contended that the $SrZr_2CaLa_2O_8:xEu^{3+}$ phosphor system presents itself as a preferable substitute for widely used red-emitting phosphors, hence boosting the colour rendition of white light-emitting diodes (w-LEDs). In

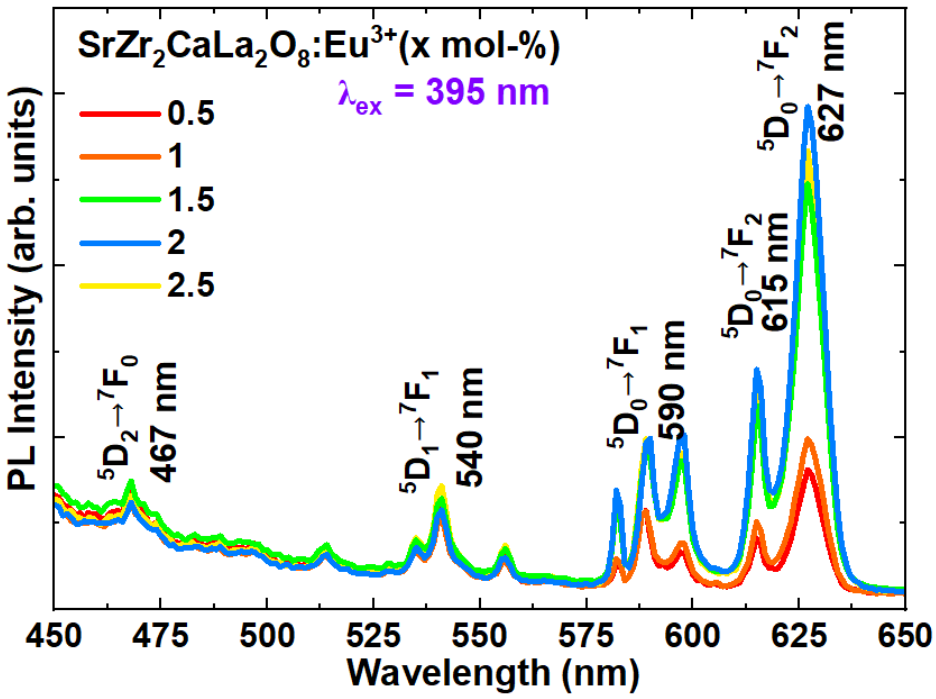

Figure 5.7: PL emission spectrum of $SrZr_2CaLa_2O_8:Eu^{3+}$ (λ_{ex} = 395 nm) for different doping concentrations.

addition, the phosphor under study may be classified as a 'Universal phosphor' due to its ability to be stimulated by a broad range of commercially accessible LEDs, spanning from ultraviolet

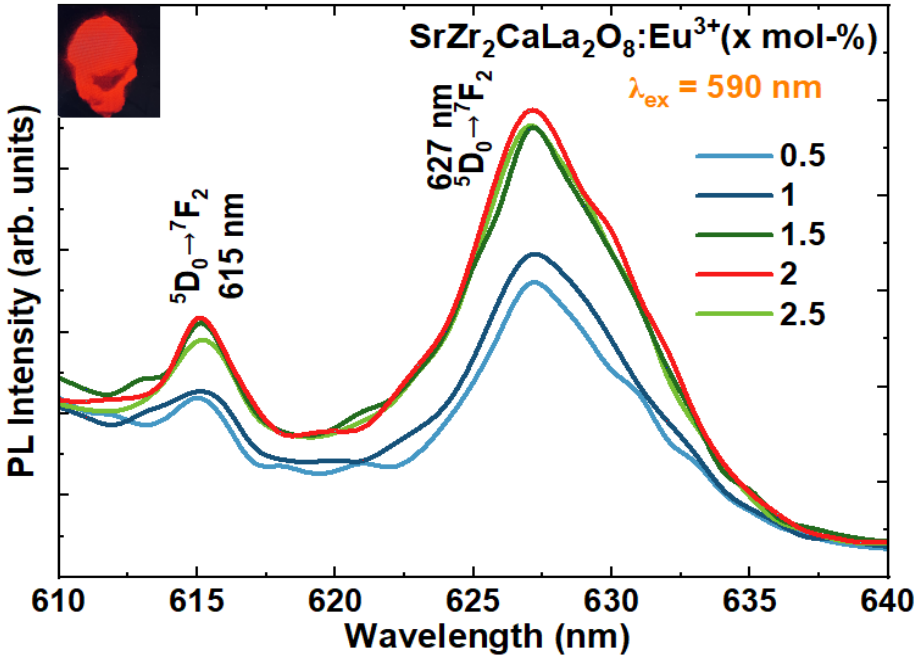

Figure 5.8: PL emission spectrum of $SrZr_2CaLa_2O_8:Eu^{3+}$ (λ_{ex} = 590 nm) for different doping concentrations.

to yellow wavelengths. As depicted in Figure 5.5, the emission spectrum of photoluminescence (PL) when subjected to excitation at a wavelength of 467 nm exhibits discernible spectral lines that correspond to specific transitions, namely $^5D_1 \rightarrow {}^7F_1$ (at a wavelength of 540 nm), $^5D_0 \rightarrow {}^7F_1$

(at 590 nm), $^5D_0 \rightarrow {}^7F_2$ (at 615 nm), and $^5D_0 \rightarrow {}^7F_2$ (at 627 nm). The spectral peak associated with the transition from $^5D_0 \rightarrow {}^7F_2$ (at a wavelength of 627 nm) is the most prominent, whereas the remaining peaks are comparatively less pronounced [22]. Figure 5.6 displays the emission spectra of the phosphor's photoluminescence (PL) at the previously mentioned alternative excitation wavelengths.

The photoluminescence spectrum consists of four distinct sets of lines with wavelengths of 467, 540, 590, and 627 nm. These lines arise from optical transitions of Eu^{3+} ions, specifically the transitions $^5D_2 \rightarrow {}^7F_0$, $^5D_1 \rightarrow {}^7F_1$, and $^5D_0 \rightarrow {}^7F_2$. The sharp line spectrum is indicative of the electronic transition from the $^5D_0 \rightarrow {}^7F_2$ state. The allowable electronic transition, which is reliant on the base symmetry surrounding the Eu^{3+} ions [23], can be attributed to the electrical-dipole interaction. The transition from energy level $^5D_0 \rightarrow {}^7F_2$ in Eu^{3+} ions is induced by the magnetic-dipole interaction and is independent of the surrounding ions base symmetry [24]. The photoluminescence spectra of $SrZr_2CaLa_2O_8:xEu^{3+}$ phosphor exhibit prominent emission peak intensities at wavelengths of 395 nm and 467 nm, which are not often observed in available

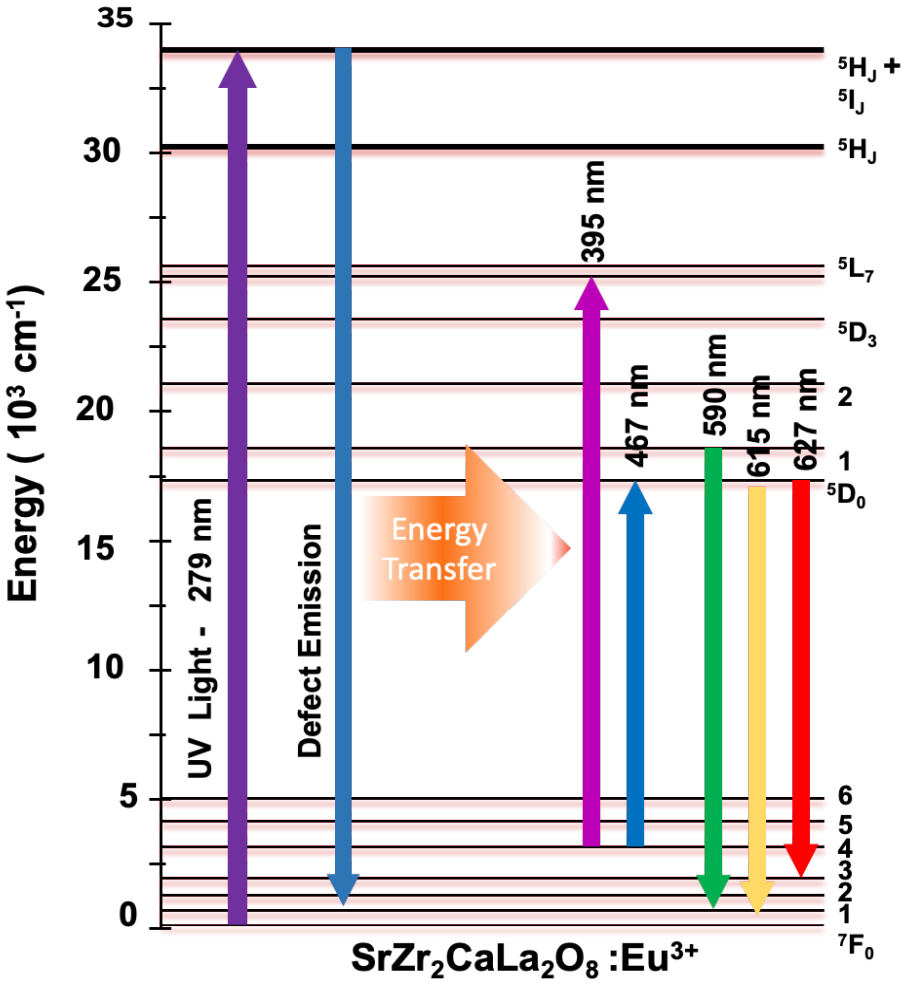

Figure 5.9: Energy transitions of Eu^{3+} ions in the host matrix.

Eu^{3+}-doped Y_2O_3 and Y_2O_2S phosphors routinely employed in white-light emitting diodes (w-LEDs). A comprehensive analysis was conducted to characterise the photoluminescence emissions of $SrZr_2CaLa_2O_8$ phosphors with varying concentrations of Eu^{3+} ranging from 0.5 to 2.5 mol%. This investigation was motivated by the significance of ultraviolet (395 nm) and blue (467 nm) absorptions in the ongoing development of light-emitting diodes (LEDs). The photoluminescence (PL) spectrum of $SrZr_2CaLa_2O_8$:xEu^{3+} phosphor exhibits notable emission peak intensities at 395 nm and 467 nm excitations, as depicted in Figure 5.7. These particular emission peaks are distinct and not usually observed in widely accessible Eu^{3+}-doped Y_2O_3 and Y_2O_2S phosphors that are extensively employed in white light-emitting diodes (w-LEDs). The photoluminescence (PL) spectrum of a range of $SrZr_2CaLa_2O_8$:xEu^{3+} (x=0.5-2.5 mol%) samples, acquired at a wavelength of 467 nm, is depicted in Figure 5.5. The feasibility of directly stimulating the $^5D_0$ level of Eu^{3+} can be attributed to the lower energy of blue light (467 nm) compared to UV light (279 and 395 nm), as depicted in Figure 5.5.

As mentioned earlier, the "red-emitting phosphor" that is widely accessible exhibits a low absorption rate (1 percent) for blue radiation in the range of 450-480 nm. Manufacturers of LEDs employ Y_2O_3: Eu3+ and Y_2O_2S: Eu^{3+} phosphors to enhance the colour rendering of white LEDs. This is due to the absence of alternative phosphors that effectively absorb blue light. The optimisation of doping Eu^{3+} ions concentrations in the lattice was carried out because to the substantial absorption seen at 467 nm by the $SrZr_2CaLa_2O_8$:xEu^{3+} (x=2.0 mol percent) phosphor. Figure 5.8 displays the photoluminescence (PL) spectrum of a range of

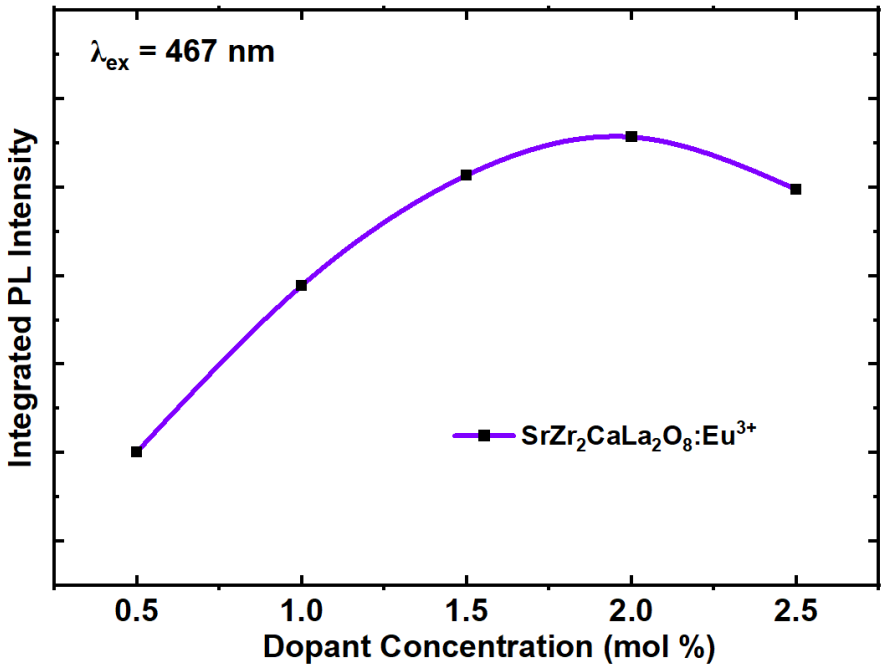

Figure 5.10 : PL integrated intensity of $SrZr_2CaLa_2O_8$:Eu^{3+} at different dopant concertation exhibiting concentration quenching.

$SrZr_2CaLa_2O_8:xEu^{3+}$ (x=0.5-2.5 mol%) samples, obtained under 590 nm excitation. The energy transitions of Eu^{3+} ions in the host matrix are illustrated in Figure 5.9.

The photoluminescence (PL) peak observed at a wavelength of 627 nm exhibited a relatively lower sensitivity to variations in the concentration of Eu^{3+} ions. When the concentration of Eu^{3+} increases, there is a notable increase in the intensity of photoluminescence (PL) observed at 627 nm emission when excited at 467 nm, reaching its peak at a concentration of 2.0 mol%. The decrease in intensity at a wavelength of 627nm occurred prior to this particular concentration due to the phenomenon of concentration quenching, as depicted in Figure 5.10.

As the doping concentration of Eu^{3+} ions increase, there is an observed steady decrease in the average interionic distance between neighbouring Eu^{3+} ions. Additionally, the probability of energy transfer between the neighbouring Eu^{3+} ions is enhanced. When the distance between two neighbouring Eu^{3+} ions exceed the critical distance, the likelihood of energy migration between them surpasses the likelihood of emission [25]. Consequently, the utilisation of $SrZr_2CaLa_2O_8:xEu^{3+}$ (where x represents a concentration of 2.0 mol%) is deemed suitable for the production of red component phosphors characterised by a narrow band emission. The luminescence of Eu^{3+} is subject to the influence of its environment's symmetry in the host lattices, as posited by the Judd-Ofelt theory. The electric dipole transition from the $^5D_0 \rightarrow {}^7F_2$ state, characterised by emission wavelengths of 615 and 627 nm, is particularly susceptible to any perturbations in the inversion symmetry, within the range of 605 to 642 nm. However, the magnetic dipole transition from the $^5D_0 \rightarrow {}^7F_1$ state at a wavelength of 590 nm is not substantially affected by this phenomenon. Hence, an estimation of the symmetry of the local Eu^{3+} environments inside the lattice may be obtained through the analysis of the intensity ratio (R21) between the transitions from the $^5D_0 \rightarrow {}^7F_2$ state and from the $^5D_0 \rightarrow {}^7F_1$. A greater R21 number signifies a diminished degree of symmetry (R21 >1), while a lesser R21 value signifies an elevated degree of symmetry (0 < R21 < 1) [26]. The equation used for the computation of R21 values is as follows:

$$R_{21}=\frac{\int_{605}^{642} I_2 \, d\lambda}{\int_{581}^{605} I_1 \, d\lambda}$$

The R21 ratio of the samples doped with Eu^{3+} has been determined to fall within the range of 1.86 and 2.85. This finding provides significant evidence suggesting that Eu^{3+} primarily occupies the lattice site without inversion symmetry.

The phenomenon of resonance facilitates the transmission of energy from excited electrons in CTB to higher energy levels such as $^5D_3$ of Eu^{3+}. Subsequently, the energy is dissipated to $^5D_1$

or $^5D_0$ states by a non-radiative mechanism [27]. The unique emission of the Eu^{3+} ion is a result of the radiative process. Luminescent materials that are doped with Eu^{3+} ions exhibit numerous advantages in comparison to materials doped with other lanthanide ions, as indicated by several studies [28, 29, 30, 31, 32].

(a) The Eu^{3+} ion exhibits a strong emission in the red region of the electromagnetic spectrum.

(b) The Eu^{3+} ion has the potential to be used as a versatile photoluminescent probe.

(c) The emission level $^5D_0$ and the ground state $^7F_0$ of the Eu^{3+} ion is not degenerate.

(d) The transition from the magnetic dipole $^5D_0$ state to the $^7F_1$ state is allowed for the Eu^{3+} ion.

(e) The covalent nature of the bond between the rare-earth ligand and the Eu^{3+} ion, as well as the symmetry of the Eu^{3+} ion in the host matrix, can both be inferred from the hypersensitive transition $^5D_0 \rightarrow {}^7F_2$.

The quality of the white light generated is determined by the spectrum properties of the photoluminescence emission. Ideally, the emission spectrum should exhibit a high degree of spectral continuity and encompass a wide variety of wavelengths in order to generate a well-balanced and pure white light. The attainment of a high colour rendering index (CRI) holds significance in guaranteeing that the light emitted perfectly portrays the colours of objects when subjected to illumination.

5.5 Field emission- SEM and EDX

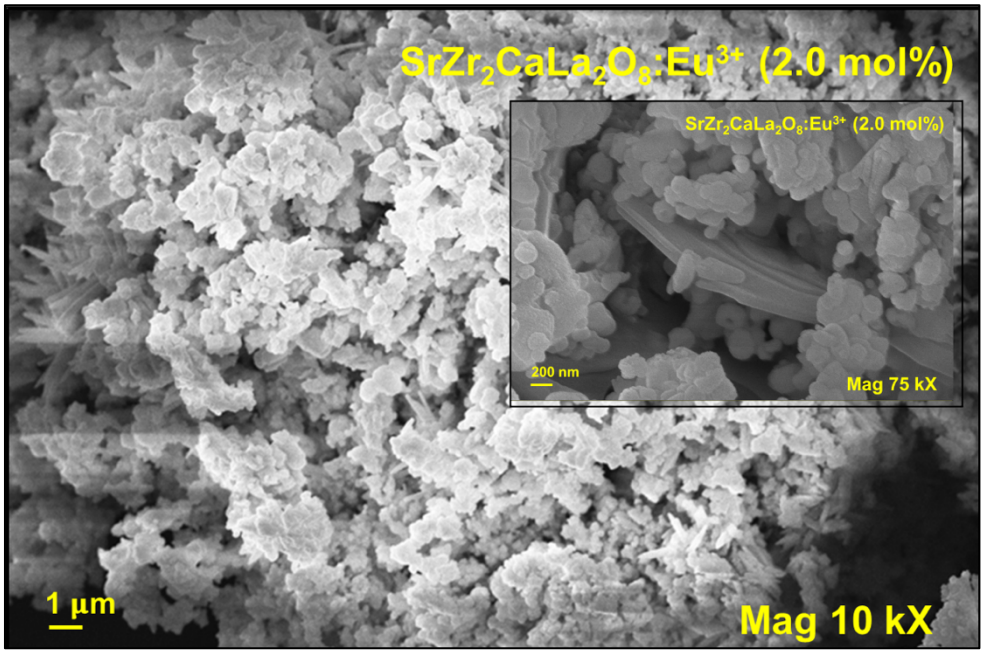

Figure 5.11: SEM Image $SrZr_2CaLa_2O_8:Eu^{3+}$ (2.0 mol-%)

The characteristics of phosphors that emit direct white light can be adjusted precisely by manipulating factors such as material composition, crystal structure, and doping levels. This tuning enables the optimization of phosphors for many specific applications, including lighting, displays, and specialized lighting requirements such as horticulture or medical illumination. Field Emission Scanning Electron Microscopy (FE-SEM) was conducted and observations in conjunction with Energy Dispersive X-ray analysis (EDAX) on the phosphor system that was constructed.

Scanning electron microscopy (SEM) was employed to investigate the morphology and size of $SrZr_2CaLa_2O_8$ formations. Figure 5.11 presents scanning electron microscopy (SEM) images of $SrZr_2CaLa_2O_8:Eu^{3+}$ at both high and lower magnifications. The particle size exhibits a range between 0.2 um and 2.0 um, and its measurement is conducted utilizing the ImageJ software. The presence of rod agglomeration was detected in some regions of the phosphor material, with an average size of 1.2 µm. From figure 5.11, it is evident that the phosphor demonstrates cathodoluminescence (CL) in response to the illumination resulting from the interaction

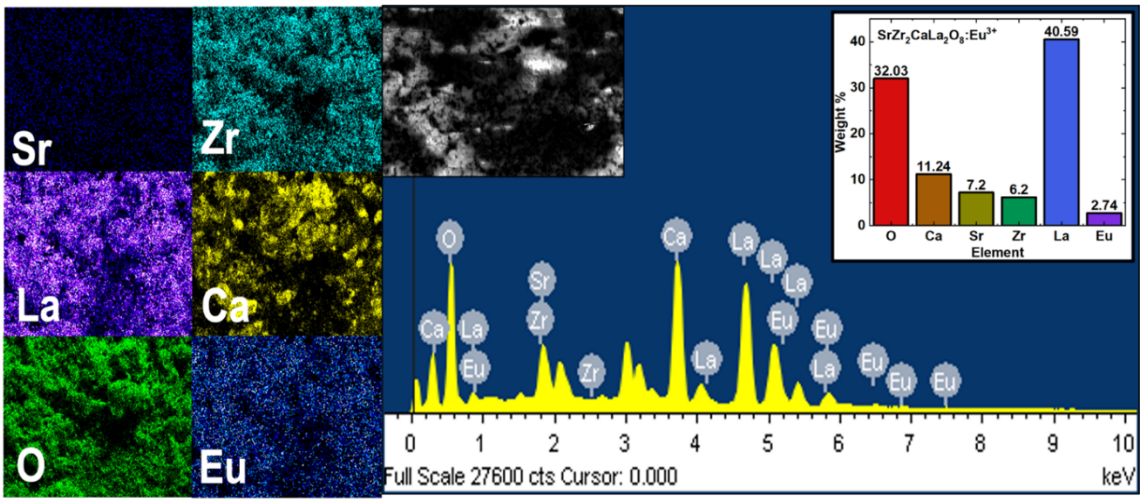

Figure 5.12: EDAX, color overlay images of $SrZr_2CaLa_2O_8:Eu^{3+}$ (2.0 mol%)

between the electron beam and the phosphors.

Figure 5.12 illustrates the EDAX spectra of the $SrZr_2CaLa_2O_8:Eu^{3+}$ particles doped with 2.0% Eu^{3+}. The spectra exhibit the presence of Eu L-fluorescence (specifically Lα, Lβ, and Lγ emissions) within the energy range of 6 to 8 keV. Additionally, Ca K-fluorescence (specifically Kα emission) is observed within the energy range of 0.2-1 keV, La L-fluorescence (specifically Lα emission) within the energy range of 0.5-1 keV, Zr L-fluorescence (specifically Lα emission) at approximately 1.8 keV, and Sr L-fluorescence (specifically Lα emission) within the energy range of approximately 1.8 keV. The constituents comprising the fluorescence

spectrum include strontium (Sr), zirconium (Zr), lanthanum (La), calcium (Ca), zinc (Zn), oxygen (O), and europium (Eu). The atomic ratios of the elements O, Ca, Sr, Zr, La, and Eu are 72.99: 10.22: 3.00: 2.48: 10.66: 0.66. This observation suggests that the components are present in a stoichiometric ratio.

5.6 Particle size analysis

Figure 5.13 illustrates the investigation of particle size analysis carried out using the Malvern Mastersizer 3000 instrument. It elucidates the correlation between the surface area of phosphor particles and their dispersion. The measured particle size ranged from 0.1 to 9.0 um, indicating the particle's hybrid nature. A considerable portion of these particles exhibit diminutive dimensions and are closely arranged, whilst the irregular particles can be attributed to a process characterized by elevated temperatures.

The measurement of particle size was conducted on phosphors containing a dopant concentration of 2.0%. The average size is 2.0 um maximum 9.15 um. Thus, the synthesized phosphor can be used to manufacture industrial w-led, the size of which is 5–10 µm.

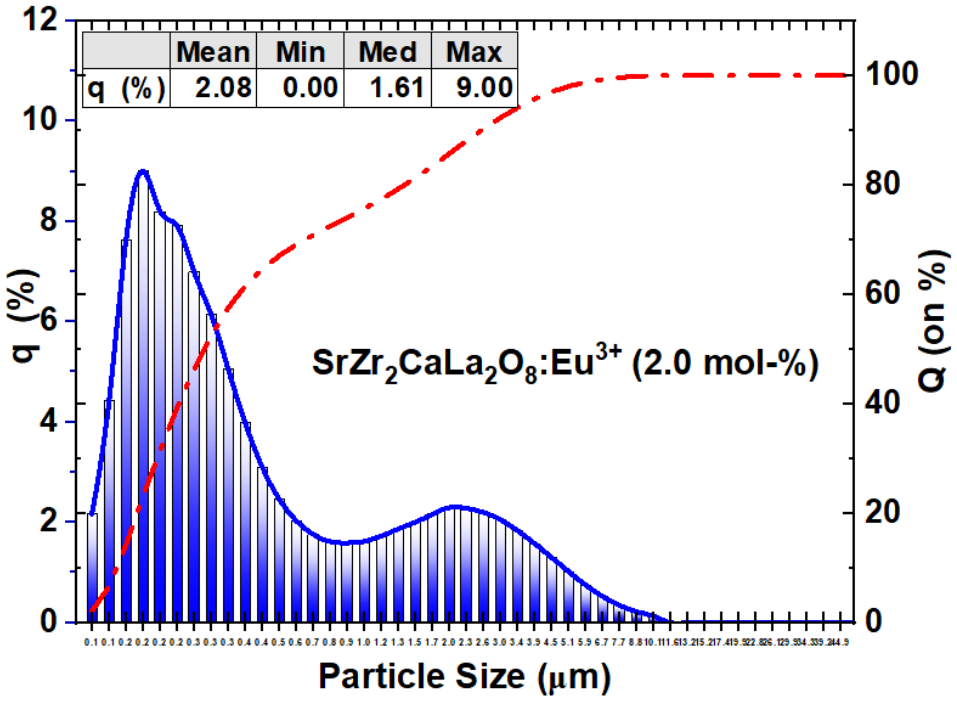

Figure 5.13: Particle size distribution (volume) of $SrZr_2CaLa_2O_8:Eu^{3+}$ (2.0 mol%).

5.7 Temperature-dependent PL Study

The utilization of blue LEDs in conjunction with phosphors to generate white light through the conversion of a portion of the blue light into different colors presents thermal difficulties owing to the presence of high-energy blue light. The optimization of direct white light producing phosphors can result in the emission of light throughout a wider range of wavelengths, hence minimizing the concentration of energy in certain wavelengths. This characteristic can contribute to the effective management of heat generation. The maintenance of phosphor stability across different temperature conditions is of utmost importance in ensuring the dependability and durability of LED devices. The thermal stability and resistance to temperature variations of the phosphor are significantly influenced by its crystal structure and shape. Thermal quenching can be mitigated by the implementation of well-designed structures, which effectively reduce the decline in phosphor efficiency observed at higher temperatures. In order to examine the correlation between temperature and photoluminescence (PL) emission intensity, the PL emission of the phosphor being investigated was measured at different

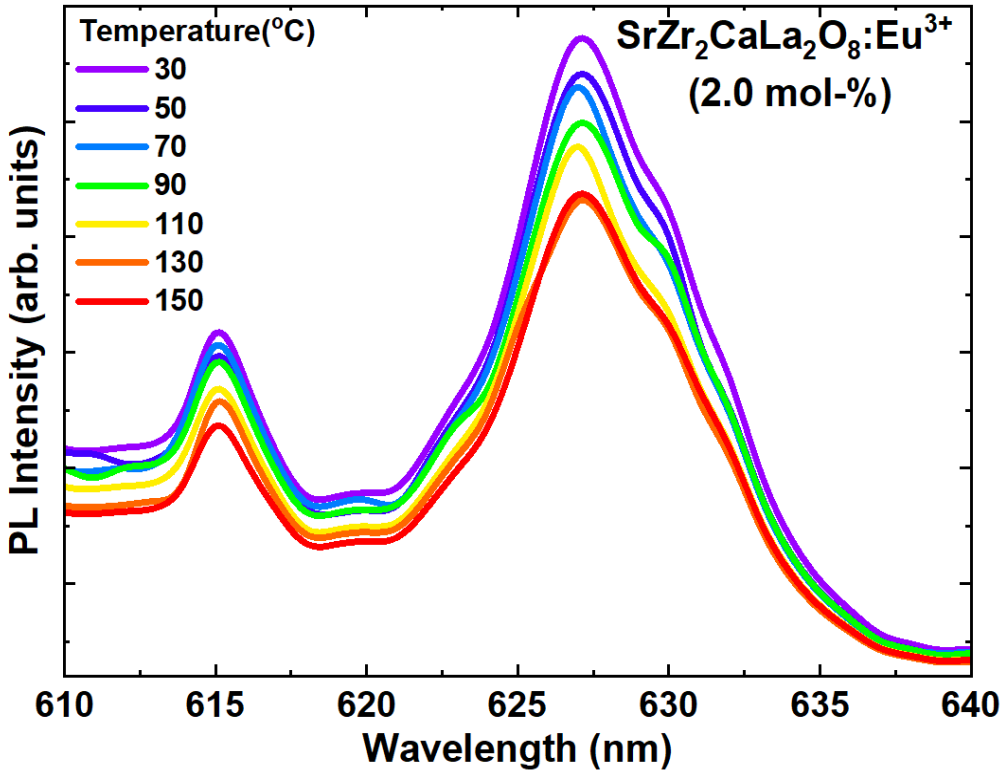

Figure 5.14: PL Spectra of $SrZr_2CaLa_2O_8:Eu^{3+}$ (2.0 mol%) from 30°C to 150°C under 590 nm excitation.

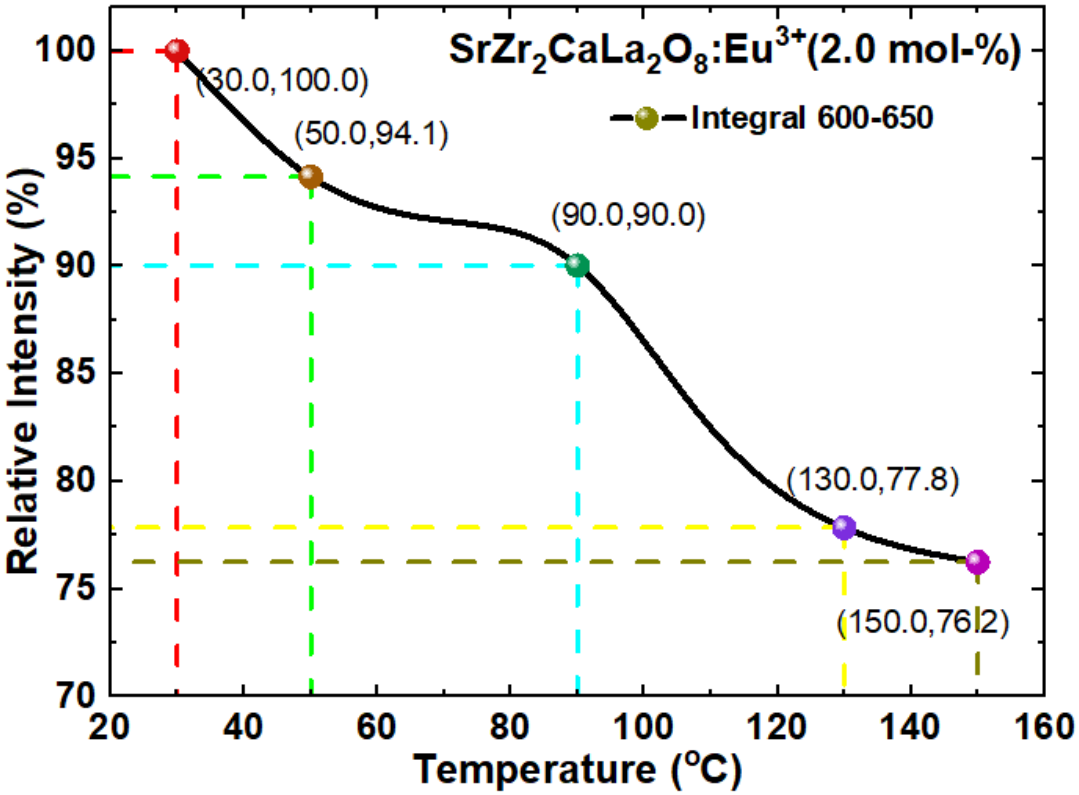

Figure 5.15: Plot showing the relation between relative intensity (%) and temperature $SrZr_2CaLa_2O_8:Eu^{3+}$ (2.0 mol%)

temperatures within the range of 323 K to 423 K. This study facilitates the understanding of the thermal stability, emission intensities, and chromatic aberration characteristics at elevated temperatures. Figure 5.14 illustrates the photoluminescence (PL) spectra of the phosphor at different temperatures. The Figure 5.14 reveals, that there is minimal change in the peak form and position, while a downward trend in intensity is evident. This phenomenon may be attributed to the increase in non-radiative transitions with rising temperatures, resulting in a decrease in intensities. The phosphor $SrZr_2CaLa_2O_8:Eu^{3+}$ exhibits a significant decrease in relative photoluminescence (PL) intensity from its initial value at 323 K to 423 K, as depicted in Figure 5.15. This reduction amounts to only 24%, which is considerably lower than that observed in commercially available phosphors. Consequently, the investigated $SrZr_2CaLa_2O_8:Eu^{3+}$ phosphor has exceptional thermal stability. The decrease in intensity observed when transitioning from room temperature to 423K might be attributed to thermal quenching [33]. The relationship between temperature and intensity can be described by the Arrhenius formula [34].

$$I(T) = \frac{I_0}{1 + c\exp\left(-\frac{Ea}{kT}\right)}$$

Here, I(T) represents intensity at distinct temperatures T, I_0 represents the initial intensity, k denotes the "Boltzmann's constant" (8.629 10^{-5} eV/K), c indicates the constant, and Ea signifies the activation energy. The activation energy (Ea) of $SrZr_2CaLa_2O_8:Eu^{3+}$ has been measured to be 0.20 eV, which exceeds the values reported for other phosphors such as Ca_2YTaO_6: Eu^{3+} (Ea = 0.13 eV) [35], $Gd_2GeO_5:Bi^{3+}$/ Eu^{3+} (Ea = 0.189 eV) [36], and $NaGdF_4$: Eu^{3+} (Ea = 0.18 eV) [37]. This finding illustrates the favourable thermal stability of the material, as depicted in Figure 5.16, plot of the relationship between the natural logarithm of [(I_0/I) - 1] and the reciprocal of temperature (1/T).

Phosphors that emit white light directly can be engineered to exhibit improved stability and durability, resulting in LED products that have extended lifetimes and greater reliability. This holds particular significance in scenarios where the task of maintenance or replacement poses challenges, as observed in applications like streetlights or architectural lighting installations.

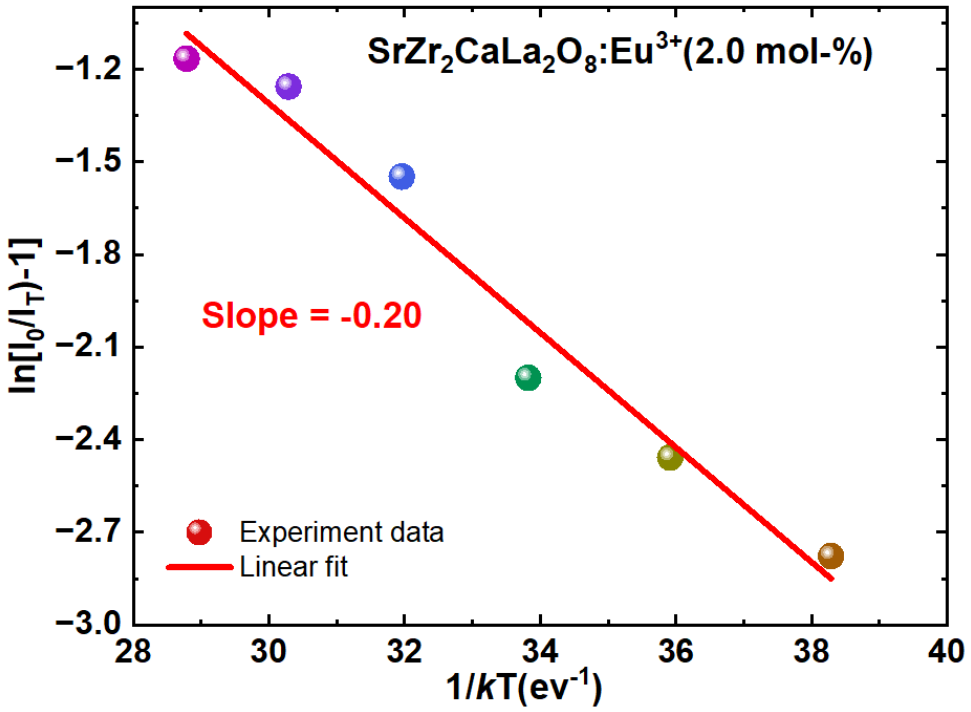

Figure 5.16: Plot showing the relation between ln[(I_0/I) - 1] and 1/T for $SrZr_2CaLa_2O_8:Eu^{3+}$ (2.0 mol%)

5.8 Determination of color coordinates

To provide an optimal visual experience, displays must possess the capability to reproduce colors accurately and vividly. Phosphors capable of emitting direct white light possess the ability to produce a comprehensive and well-balanced spectrum of light. This characteristic allows displays to faithfully replicate a diverse array of colors and attain a notable colour rendering index (CRI). This phenomenon leads to the production of more authentic and dynamic visual representations on display screens. The emission wavelengths of phosphors can be influenced by their crystal structure and shape. Various applications necessitate the utilization of particular colors and colour temperatures of light. Manufacturers can obtain accurate colour tuning for a range of LED applications, including warm to cool white light, as well as varied colors for displays and decorative lighting, by exerting control over the structure and composition of phosphors.

The color coordinates provided by the Commercial International de I'Eclairage (CIE) are highly helpful for the investigation of phosphors, as they enable precise measurement of their emission colour. The CIE chromaticity coordinates of $SrZr_2CaLa_2O_8:Eu^{3+}$ phosphor were determined

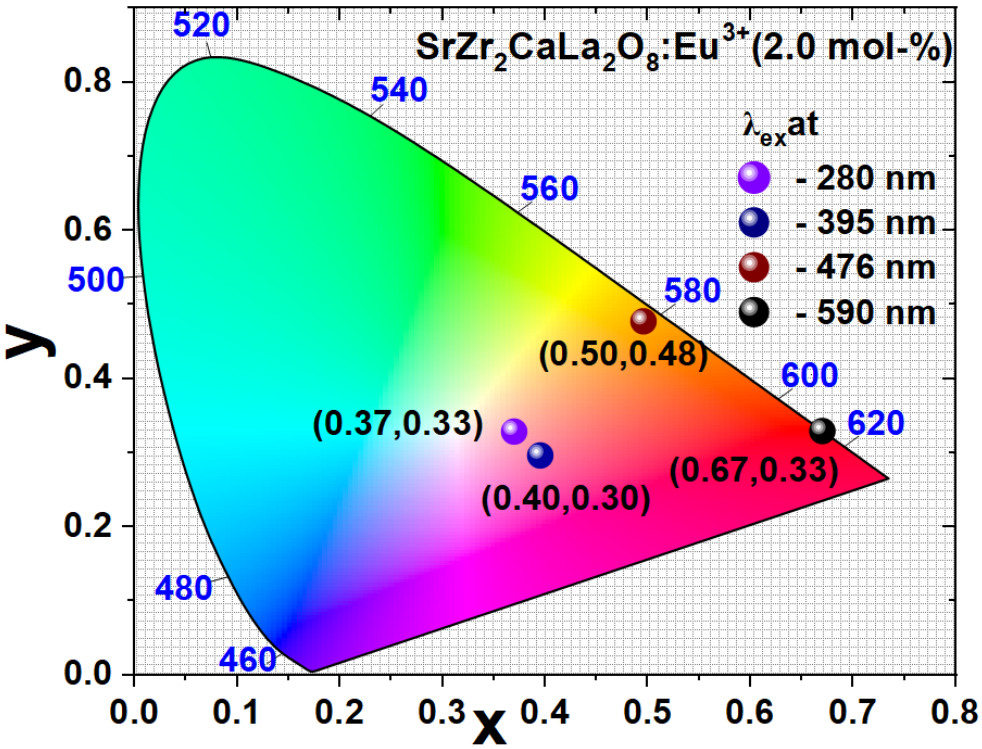

Figure 5.17: CIE Chromaticity coordinates of the prepared $SrZr_2CaLa_2O_8:Eu^{3+}$ (2.0 %) excited at different absorptions.

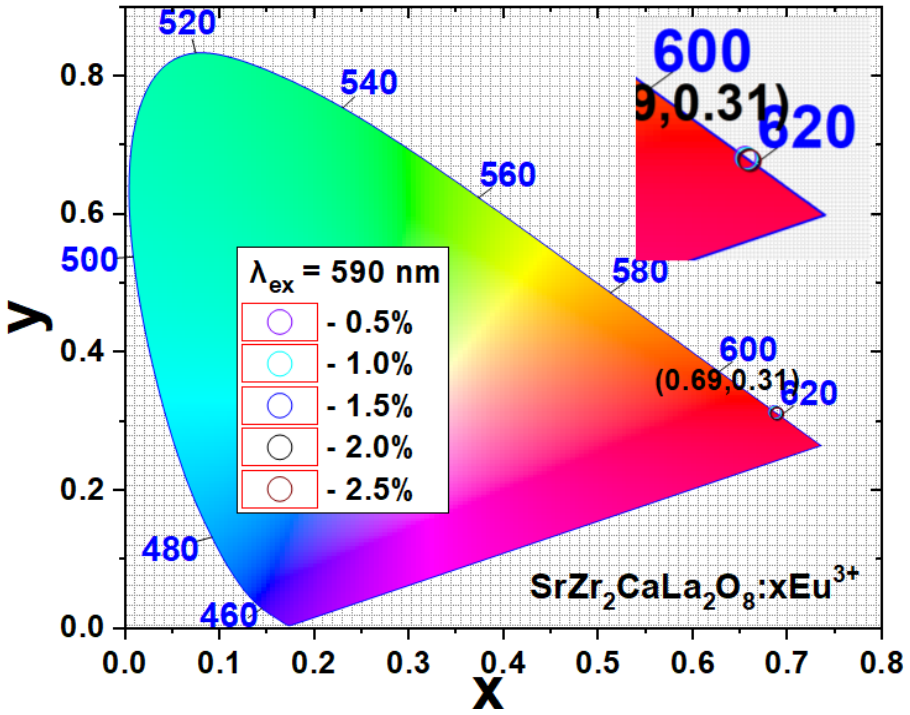

Figure 5.18: CIE Chromaticity coordinates for the as-prepared $SrZr_2CaLa_2O_8:Eu^{3+}$ (x = 0.5–2.5 mol-%) samples.

using an equidistant set wavelength method. The phosphor samples were subjected to different excitation conditions, as illustrated in Figure 5.17. The resulting emissions at various excitation wavelengths (280, 395, 467, and 590 nm) exhibited a colour range from warm-white to red. It is noteworthy to mention that the CIE coordinate (x, y) for 395 nm excitation has a value of (0.37, 0.33), indicating a near proximity to the ideal-white colour coordinates of (0.33, 0.33) as defined by the National Television Standards Committee (NTSC). This suggests that the $SrZr_2CaLa_2O_8:xEu^{3+}$sample, which emits "warm-white light," could be a suitable option for applications involving white light-emitting diodes (w-LEDs). The colour coordinates of phosphor when stimulated with a wavelength of 590 nm for different dopant values, specifically $SrZr_2CaLa_2O_8:xEu^{3+}$ (where x ranges from 0.5 to 2.5 mol%), are illustrated in Figure 5.18. The impact of doping concentration on colour purity is negligible. Therefore, $SrZr_2CaLa_2O_8:xEu^{3+}$phosphors exhibit exceptional colour purity values, making them potential candidates for replacing conventional red phosphors in w-LED applications. The utilization of direct white light generating phosphors has the potential to enhance the visual experience through the provision of a well-balanced and authentic white point. This characteristic compliments the distinctive attributes of the existing phosphor.

5.9 Summary

The present investigation focuses on the development of single-phased phosphors with excellent colour purity, specifically the $SrZr_2CaLa_2O_8:xEu^{3+}$ (x=0.5-2.5 mol-%) phosphors that exhibit unique color-tunable properties. The aforementioned phosphors have the ability to emit light ranging from red to white and can be stimulated by light within the ultraviolet to red spectrum. In the pursuit of energy efficiency within the lighting sector, the integration of direct white light-emitting phosphors presents a promising avenue for decreasing energy usage in contemporary display systems. By enhancing the efficiency of white light generation, displays can attain same levels of brightness while consuming less power. In order to fulfil the aforementioned conditions, a thorough investigation was conducted on Eu^{3+}-doped $SrZr_2CaLa_2O_8$ samples. The unique structural attributes of the subject were identified through meticulous analysis of its structural and morphological properties. The red emission (627 nm) observed from the phosphor that was synthesized can be attributed to the transitions of Eu^{3+} ions from the $^5D_0 \rightarrow {}^7F_2$ energy levels when exposed to blue illumination (467 nm). This finding suggests that these Eu^{3+} ions are highly effective in enhancing the Colour Rendering Index (CRI) of white Light Emitting Diodes (w-LEDs). The utilization of direct white light emitting phosphors in this study offers the advantage of generating a consistent and homogeneous illumination, hence minimizing the occurrence of localized areas of intense brightness, obscured regions, or discrepancies in coloration across the display substrate. This is an additional merit of the present research endeavor.

References

1. X. Luo, R. Hu, S. Liu, and K. Wang, Prog. Energy Combust. Sci. 56, (2016) 1–32.
2. E. F. Schubert and J. K. Kim, Science 308, (2005), 1274–1278.
3. S. Ye, F. Xiao, Y. X. Pan, Y. Y. Ma, and Q. Y. Zhang, Mater. Sci. Eng. 71, (2010), 1–34.
4. Wang XC, Zhao ZY, Wu QS, Li YY, Wang YH. Inorg. Chem. 2016; 55: 11072–7.
5. R. Oh, S.-H. Cho, Y.-H. Lee, Y.R. Do, Electrochem. Solid-State Lett. 13, (2010), J5–J7.
6. Ye S, Xiao F, Pan YX, Ma YY, Zhang QY. Mater Sci Eng, 71, R 2010, 1–34.
7. T. Hussain, L. Zhong, M. Danesh, H. Ye, Z. Liang, D. Xiao, C.-W. Qiu, C. Lou, L. Chi, L. Jiang, Nanoscale 00, (2015), 1–3.
8. C. J. S. Kim, P.E. Jeon, J.C. Choi, H.L. Park, Appl. Phys. Lett. 84, (2004), 2931.
9. Li K, Fan J, Shang MM, Lian HZ, Lin J. J Mater Chem C 2015; 3: 9989–98.
10. H. Zhu, C. C. Lin, W. Luo, S. Shu, Z. Liu, Y. Liu, J. Kong, E. Ma, Y. Cao, R.-S. Liu, and X. Chen, Nat. Commun. 5, (2014), 4312.
11. P.J. Yadav, N.D. Meshram, C.P. Joshi, S.V. Moharil, AIP Conf. Proc. 1728, (2016), 020199.
12. Li JH, Yan J, Wen DW, Khan WU, Shi JX, Wu MM, Su Q, Tanner PA. J Mater Chem C 2016; 4: 8611–23.

13. Behrh GK, Gautier R, Latouche C, Jobic S, Serier-Brault H. Inorg Chem 2016; 55: 9144–6.
14. Kang, M., Liao, X., Kang, Y. et al. J Mater Sci 44, (2009), 2388–2392.
15. R.N, P., S. G, V. E, S. S & V. G (2018). Journal of Materials Science: Materials in Electronics 29(4), 2638–2644.
16. T. Nishida, T. Ban, N. Kobayashi, Appl. Phys. Lett. 82 (2003) 3817–3819.
17. Beczkowski, S.M. Nielsen and Stig LED spectral and power characteristics under hybrid PWM/AM dimming strategy, IEEE, 2010.
18. C.K. Chang, T.M. Chen, Appl. Phys. Lett. 91 (2007) 2010–2013.
19. Peng, Mingying and Pei, Zhiwu & Hong, Guangyan and Su, Qiang. (2003). Journal of Materials Chemistry - J MATER CHEM. 13. 1202-1205.
20. P. Balakrishnan, S. Masilla Moses Kennedy, Solid State Sciences, Volume 118, 2021,106665.
21. Xingyi Cai, Zhongfei Mu, Shaoan Zhang, Daoyun Zhu, Qiang Wang, Yibin Yang, Dongxiang Luo, Fugen Wu, Journal of Luminescence, 200, [2018], 169-174.
22. E. Pavitra, G. Seeta Rama Raju, Jin Young Park, Yeong Hwan Ko, Jae Su Yu, Journal of Alloys and Compounds, 553, 2013, 291-298.
23. A. K. Parchura and R. S. Ningthoujam, RSC Advances, 2 (2012) 10859–10868.
24. Binnemans, Koen, (2015), Coordination Chemistry Reviews. 295. 10.1016/j.ccr.2015.02.015.
25. Jinfeng Lu, Zhongfei Mu, Daoyun Zhu, Qiang Wang, Fugen Wu, Journal of Luminescence, 96, (2018), 50-56.
26. Liang, Z., Mu, Z., Wang, Q. et al. Appl. Phys. A 123, (2017), 612.
27. Chen, F.; Akram, M.N.; Chen, X. Molecules 2023, 28, 1014.
28. Li, Y.; Liu, X., Mater. Res. Bull. 2015, 64, 88–92.
29. Sivakumar, V.; Varadaraju, U.V. J. Solid State Chem. 2008, 181, 3344–3351.
30. Sivakumar, V.; Varadaraju, U.V. J. Electrochem. Soc. 2007, 154, J28–J31.
31. Ye, S.; Wang, C.H.; Liu, Z.S.; Lu, J.; Jing, X.P. Appl. Phys. B 2008, 91, 551–557.
32. Chen, K.N.; Hsu, C.M.; Liu, J.; Chiu, Y.T.; Yang, C.F. Appl. Sci. 2016, 6, 22.
33. Wanggui Ye, Chong Zhao, Xiaofei Shen, Chaoyang Ma, Zhonghua Deng, Yanbin Li, Yuzhen Wang, Chuandong Zuo, Zicheng Wen, Yingkui Li, Xuanyi Yuan, Chong Wang, and Yongge Cao ACS Applied Electronic Materials 2021 3 (3), 1403-1412.
34. A.K. Galwey, M.E. Brown, Acta 386(1), (2002), 91–98.
35. K. Ding, A. Siru, S. Pang, L. Shan, Y. Zhang, P. Sun, B. Deng, R. Yu, J. Rare Earths 39(7), 749–756 (2021).
36. Q. Sun, T. Sakthivel, B. Devakumar, S. Wang, L. Sun, J. Liang, S.J. Dhoble, X. Huang, J. Lumin. 222, (2020), 117127.
37. P. Du, W. Ran, Y. Hou, L. Luo, W. Li, ACS Appl. Nano Mater. 2(7), (2019), 4275–4285.

Chapter - 6

Dual Wavelength Excitable Novel Phosphor for use in Display Devices and Cognitive Therapy

Features of the Chapter:

The synthesis of $Ca_2La_2O_5:Eu^{3+}$ (x=0.5 to 2.5 mol%) was achieved by a solid-state reaction procedure with the incorporation of a chemical flux. This phosphor demonstrates a unique ability to tune its hue. The phosphor $Ca_2La_2O_5:Eu^{3+}$ has unique characteristics as a dual-wavelength excitable material, mostly attributed to its exceptional absorption spectra that covers a wide range from 250 to 600 nm. The material demonstrates a wide range of photoluminescence (PL) in the white (400–650 nm) and red (627 nm) regions, which can be attributed to the $^5D_0$–^7F_J (J =1–4) transitions of the Eu^{3+} ion. An observable energy transfer between La3+ and Eu^{3+} ions was detected after a progressive increase in the concentration of Eu^{3+} ions. The utilization of scanning electron microscopy revealed the presence of elongated rod-shaped structures, with an average diameter of 2.0 µm. The positional coordinates (x, y) of the white (0.41, 0.35) and red (0.62, 0.38) zones were determined in relation to the respective excitation wavelengths of 395 nm and 467 nm. Further, a study was conducted on the luminescence spectra of $Ca_2La_2O_5:Eu^{3+}$ at different temperatures, with excitation occurring at a wavelength of 467 nm. The material exhibited favourable thermal stability at a temperature of 150°C, while the photoluminescence (PL) intensity at ambient temperature was approximately 72.8%. The activation energy was determined through mathematical estimation to be 0.19 electron volts (eV). The findings indicate that the phosphor exhibits favourable characteristics for cognitive treatment as a result of its emissions at a wavelength of 627 nm. Additionally, its predominant red content in white-LEDs renders it appropriate for display device applications that are typically challenging to attain in systems consisting of a single component.

This work is under review :

Dual excitable novel phosphor for use in display devices and cognitive therapy. **Kishore Kumar Aitha,** D. Dinakar, D. Y. Kolbe, K. V. R. Murthy, and D. Haranath. **Ceramics International**, (Under Review, MS No. CERI-D-23-14900, 01 Dec 2023) **(IF: 5.2)**

6.1 Outline

Rare-earth (RE) ions serve as activators in minute quantities and demonstrate photoluminescence (PL) when incorporated into an appropriate host matrix. Phosphors, which are materials capable of emitting light, are of significant importance in display applications [1]. The phenomenon of the Stokes shift is observed in these materials, wherein they exhibit the absorption of radiation with higher frequencies and subsequent emission of radiation with lower frequencies. Materials with luminous qualities have significantly propelled the progress of solid-state technology, particularly in the domains of lighting and display applications [2-3]. The aforementioned technology has not only facilitated the development of sophisticated items within the respective industry, but has also incited a paradigm shift by virtue of its compact design and utilization of low-voltage power. These materials have the capability to emit radiation with a high level of efficiency, a regulated profile, and an extremely narrow emission bandwidth[4-5], as indicated by the host matrix. Even the most little impact of temperature variations provides supplementary benefits in the expansion of a diverse array of items. The gadgets' environmentally friendly nature provides supplementary benefits for applications in the fields of biomedicine, biochemistry, and related disciplines[6-9].

Hence, phosphors doped with rare earth elements have established a distinct position in cutting-edge research, paving the way for advancements in field emission (FE) displays, paints, 3D displays, tri-color lights, white light-emitting diodes (w-LEDs), and medical applications. An example of an application within the medical field is photo-biomodulation, which involves the utilization of a 627 nm red LED light as a form of cognitive therapy [10]. Photo-biomodulation refers to a therapeutic approach that utilizes light sources, such as LEDs, to heal soft tissue injuries, lesions, as well as alleviate symptoms of inflammation and discomfort. Transcranial photo-biomodulation (t-PBM) is a non-invasive technique that utilizes 627 nm LED light to enhance cognitive functions in individuals, regardless of their health status [11]. Consequently, w-LEDs and narrow-band single-color LEDs are increasingly significant in their respective applications, ranging from replacement devices to the medical industry. The utilization of RE-doped oxide compounds for the purpose of generating a white light spectrum in the manufacturing of light-emitting diodes (LEDs) is highly recommended and has demonstrated its commercial feasibility[12-13]. This is primarily attributed to the compounds' exceptional stability across a broad temperature range, as well as their cost-effectiveness and low energy consumption. Commercial white light-emitting diodes (w-LEDs) are commonly fabricated using $Y_3Al_5O_{12}:Ce^{3+}$ materials[14]. These LEDs employ blue InGaN chips and exhibit a lack

of red emission components. Nevertheless, this particular category of light-emitting diodes (LEDs) has a diminished color rendering index (CRI) and a deficient representation of red hues. Consequently, the prevailing approach involves the generation of white light through the utilization of ultraviolet (UV) or blue light-emitting diodes (LEDs) in conjunction with tri-color phosphors[15]. The inclusion of a red component with a narrow width at half-maximum (FWHM) is crucial in the development of light-emitting diodes (LEDs) that possess both high color rendering index (CRI) and an appropriate wavelength for medical applications as described above. In recent times, there have been advancements in the development of various materials that exhibit a broader spectrum of properties. A phosphor composition exhibiting full width at half maximum (FWHM) emissions of approximately 5 nm at a wavelength of 616 nm has been created by Sharma et al. in 2023[16]. The attainment of a limited bandwidth was accomplished, but, it is deemed unsuitable for implementation in medical contexts. The objective of our research is to create a phosphor material capable of creating the desired red emission at a wavelength of 627 nm. This phosphor should possess the ability to produce ideal white light by modulating the excitation wavelengths. The aforementioned circumstance gives rise to a disparity in existing technological capabilities, necessitating the development of a novel phosphor possessing the ability to emit numerous wavelengths, with a particular emphasis on surpassing the red component and achieving red emission at a wavelength of 627 nm.

6.2 Synthesis

The synthesis of the phosphor was effectively achieved through the utilization of a modified solid-state reaction (SSR) technique, wherein the addition of a chemical flux facilitated the development of the crystalline phase. The constituent raw ingredients were combined in stoichiometric proportions and mechanically mixed in an acetone solvent using an agate pestle-mortar for approximately 30 minutes. Subsequently, the composite substance was introduced into a crucible and subjected to a sintering process at a temperature of 1200°C for a duration of 3 hours. Following the sintering process, the phosphor underwent natural cooling within the oven. Subsequently, the resulting sintered mass was subjected to grinding, resulting in the production of a fine powder. This powder was subsequently utilized for several characterisation purposes.

The phosphors developed underwent characterization at a temperature of around 25°C, which is considered to be room temperature. The photoluminescence properties, including excitation and emission spectra, were evaluated using an RF-5301PC fluorescence spectrometer that was

equipped with a xenon lamp. The phase analysis of the $Ca_2La_2O_5:Eu^{3+}$ doped phosphor was conducted using X-ray powder diffraction (P-XRD) technique. The produced materials underwent characterization using the X'Pert Pro P analytical powder diffractometer equipped with a Cu-Kα radiation source (wavelength of 1.54 Å). The instrument was operated at 40 kV and 40 mA, and the scan speed was set at 0.05 degrees per second. The SEM images were obtained using a JEOL JSM 5810 LV microscope, while the quantitative study of elemental composition was conducted using an energy-dispersive X-ray spectroscopy (EDAX) device integrated within the SEM instrument. The Perkin Elmer-100 device was utilized to do Fourier transform infrared spectroscopy (FTIR) analyses. The particle size analysis was conducted using the Malvern Mastersizer 3000, a laser diffraction instrument capable of measuring particles within the size range of 0.1 µm to 3 mm. In addition, the chromaticity coordinates were derived from the emission spectra in accordance with the norms set by the Commission Internationale de I'Eclairage (CIE).

6.3 Photoluminescence properties of $Ca_2La_2O_5:Eu^{3+}$ phosphor

Figure 6.1 illustrates the excitation spectra of the $Ca_2La_2O_5:Eu^{3+}$ phosphors under observation at a wavelength of 627 nm. The excitation spectrum is evaluated within the wavelength range

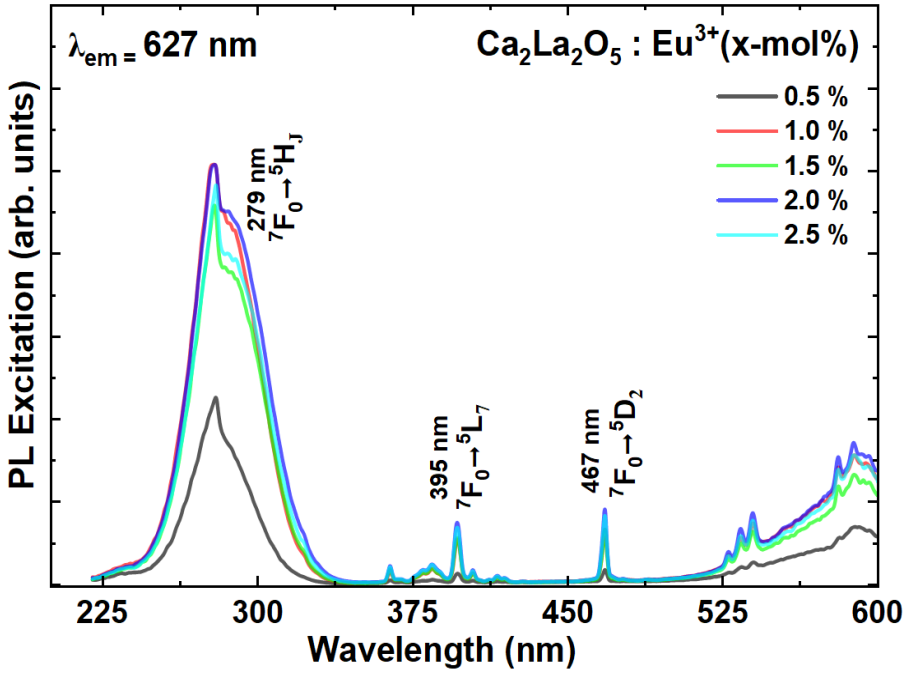

Figure 6.1 : PL excitation spectrum in the range 225 – 600 nm of $Ca_2La_2O_5:Eu^{3+}$ (λ_{em} = 627 nm) for 2.0 mol-% of doping concentration.

spanning from 250 to 600 nm. The excitation spectra consist of a succession of peaks that are predominantly located at wavelengths of 279 nm, 395 nm, 467 nm, and 590 nm. The excitation

spectra exhibit distinct peaks that can be attributed to certain transitions. These transitions include $^7F_0 \rightarrow {}^5H_J + {}^1H_J$ (279 nm), $^7F_0 \rightarrow {}^5L_7$ (395 nm), $^7F_0 \rightarrow {}^5D_2$ (467 nm), and $^7F_1 \rightarrow {}^5D_0$ (590 nm) [17]. The selection of excitation wavelengths of 395 nm, 467 nm, and 590 nm was based on the presence of prominent excitation peaks, which are comparable to the 279 nm wavelength. The

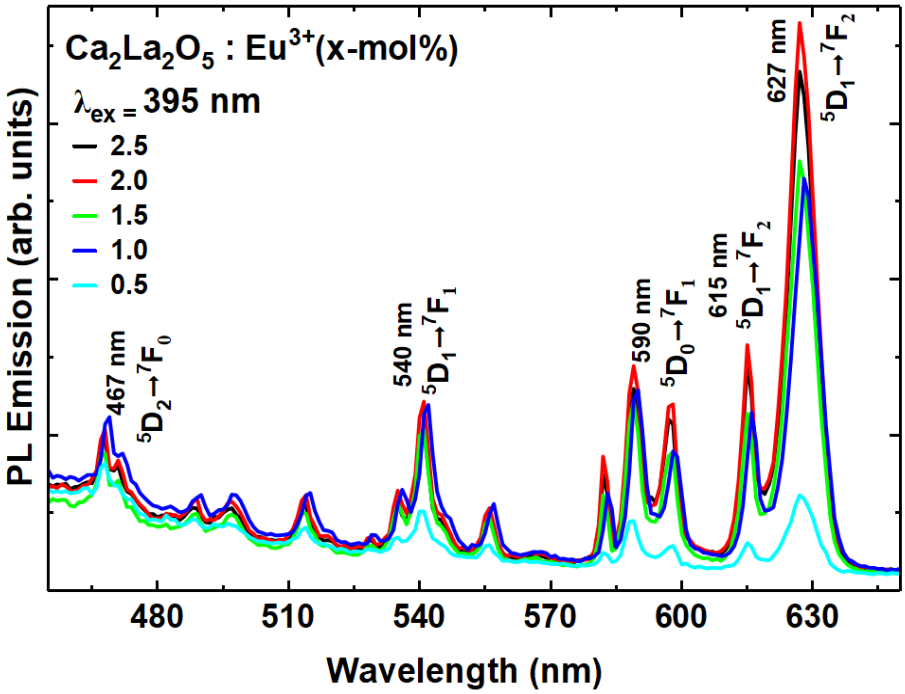

Figure 6.2 : PL emission spectrum of $Ca_2La_2O_5:Eu^{3+}$ (λ_{ex} = 395 nm) for 2.0 mol-% of doping concentration.

selection of 279 nm for excitation was not made due to its placement in the ultraviolet (UV) region, which is associated with elevated energy levels and limited capacity to yield substantial quantum efficiency. Figure 6.2 illustrates the emission spectra of the $Ca_2La_2O_5:Eu^{3+}$ phosphor when subjected to excitation at a wavelength of 395 nm.

The presence of narrow band emissions at specific wavelengths, namely 467, 540, 590, 615, and 627 nm, is frequently observed in emission spectra, providing evidence that the europium ion exists in the Eu^{3+} state. The emission peaks observed in the 4f-4f transitions of Eu^{3+} ions were identified as resulting from the specific transitions of $^5D_1 \rightarrow {}^7F_1$ (540 nm), $^5D_0 \rightarrow {}^7F_1$ (590 nm), $^5D_0 \rightarrow {}^7F_2$ (615 nm), and $^5D_0 \rightarrow 7{}^7F_2$ (627 nm).

The phenomenon of crystal field splitting results in the division of emission lines into distinct groups, such as (540 nm, 590 nm) and (615 nm, 627 nm) [18]. The observed peaks at wavelengths of 614 nm and 627 nm can be due to magnetic dipole transitions, as supported by

previous studies [20–22]. On the other hand, the peaks observed at 588 nm and 597 nm are believed to be a result of forced electric dipole mechanisms.

The energy level diagram of the $Ca_2La_2O_5:Eu^{3+}$ phosphor, illustrating its optical transitions, is depicted in Figure 6.3. This illustrates the excitation of Eu^{3+} ions to the $^5L_6$ excited state, followed by their subsequent transition to the $^5D_0$ state via a non-radiative mechanism. The transition from the excited states $^5D_1$ and $^5D_0$ to the $^7F_1$ and $^7F_2$ states is accompanied by the

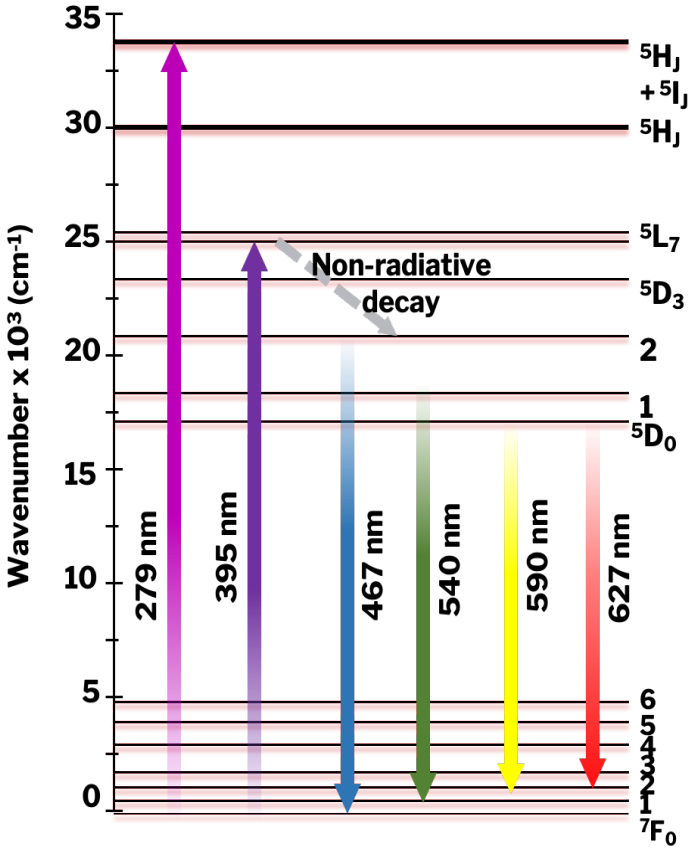

Figure 6.3 : Schematic diagram - Energy level of

emission of light in the green, orange, and red regions of the electromagnetic spectrum, namely at wavelengths of 540 nm, 590 nm, 615 nm, and 627 nm[23]. Additionally, it exhibits a blue emission at a wavelength of 467 nm as a result of charge transfer. The figure 6.4 illustrates the emission spectra of the $Ca_2La_2O_5:Eu^{3+}$ phosphor when subjected to excitation at a wavelength of 467 nm. The phosphor exhibits analogous behaviour to the emission observed at a wavelength of 395 nm when subjected to excitation at 467 nm, so suggesting its emission range to be between 540 nm and 627 nm. This implies that the identical phosphor can be employed in conjunction with ultraviolet (UV) and blue chip light-emitting diodes (LEDs) to provide a white light spectrum including a prominent red constituent. Conversely, upon excitation at a wavelength of 467 nm, the phosphor exhibits an emission with a red hue at a wavelength of 627

nm. This particular emission has potential applications in the field of cognitive therapy, namely for photo-biomodulation purposes.

Additionally, an investigation was conducted to analyze the impact of varying quantities of Eu^{3+} ions on the emission of $Ca_2La_2O_5:Eu^{3+}$ phosphor. Figure 6.5 illustrates the correlation between emission intensity and the concentration of Eu^{3+} ions. The research findings indicate a

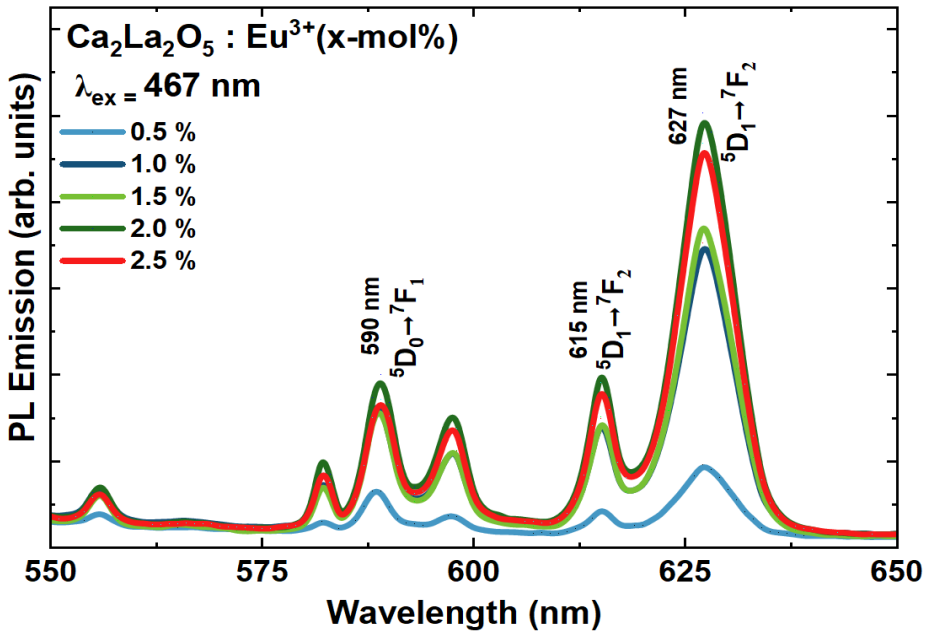

Figure 6.4 : PL emission spectrum of $Ca_2La_2O_5:Eu^{3+}$ (λex = 467 nm) for 2.0 mol-% of doping concentration.

positive correlation between emission intensity and concentration, namely within the range of 0.5 to 2 mol%. The emission intensity exhibits a sudden decrease following the concentration of 2.5 mol%. The observed phenomenon could potentially be due to the concentration-

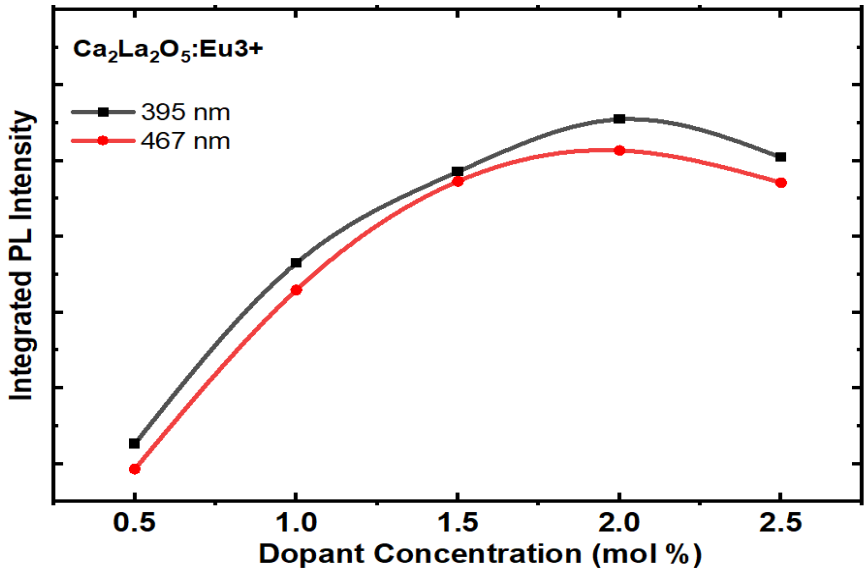

Figure 6.5 : Integrated PL intensity of $Ca_2La_2O_5:Eu^{3+}$, excited with 395 and 467 nm for different dopant concentrations.

quenching effect [24] which is inherent in energy transfer mechanisms. The phosphor $Ca_2La_2O_5:Eu^{3+}$ demonstrates its maximum emission intensity when doped with 2 mol% of Eu^{3+} ions. In addition to alterations in emission intensity, the emission spectra retain their original form as concentrations increase.

6.4 Powder X-ray diffraction (PXRD) analysis

Powder X-ray diffraction (PXRD) is employed for the purpose of verifying the purity of the Eu^{3+}-activated Ca2La2O5 phosphors that have been synthesized. The data obtained from the experiment is presented in Figure 6.6. The observation is that the X-ray diffraction patterns (PXRD) of the produced phosphors exhibit a strong resemblance to the standard Inorganic Crystal Structure Database (ICSD) pattern (ICSD No. 96-153-1468), and the absence of any discernible impurity peaks, indicates that the Eu^{3+} ions possess comparable ionic radii and valences to La^{3+}. Consequently, they can successfully substitute La^{3+} inside the crystal lattice. The confirmation of a hexagonal crystal structure was achieved through the comparison of recorded diffraction peaks with the typical JCPDS maps of CaO, La_2O_3, and Eu_2O_3, as depicted in Figure 6.6.

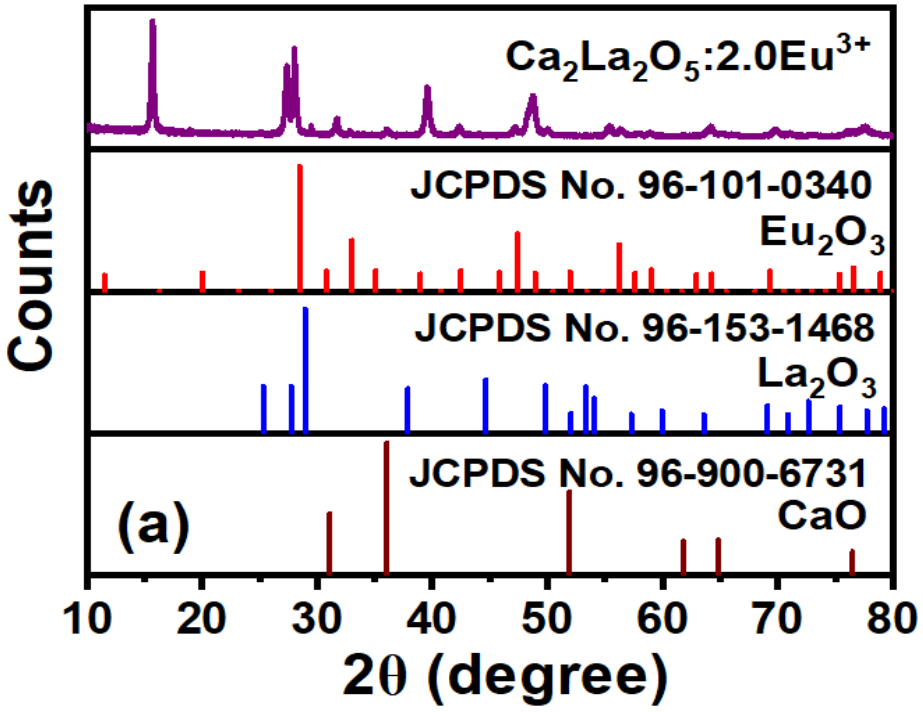

Figure 6.6 : XRD pattern of $Ca_2La_2O_5:Eu^{3+}$ for 2.0 mol-% of doping concentration along with standard JCDPS patterns

6.5 Surface Morphology and EDAX analysis

The assessment of optical qualities in synthetic phosphors is heavily influenced by the surface shape. The examination of the morphology, form, and size distribution of the produced phosphors can be efficiently conducted by the utilization of scanning electron microscopy (SEM). SEM analysis was employed to investigate the microstructure and morphology of the

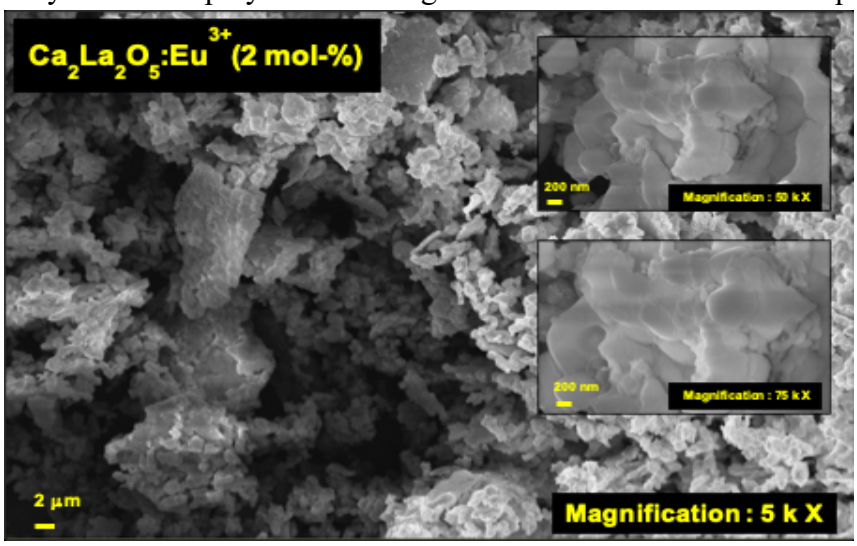

Figure 6.7 : Surface morphology of $Ca_2La_2O_5:Eu^{3+}$ from SEM analysis at various magnifications.

phosphors synthesized by this method. The scanning electron microscope (SEM) pictures depicting the phosphors are presented in Figure 6.7. The presence of particle sizes ranging from 0.2 to 10 µm indicates the occurrence of agglomeration and the non-uniform shape of the synthesized phosphors. The uniform distribution of elements within the particles was confirmed

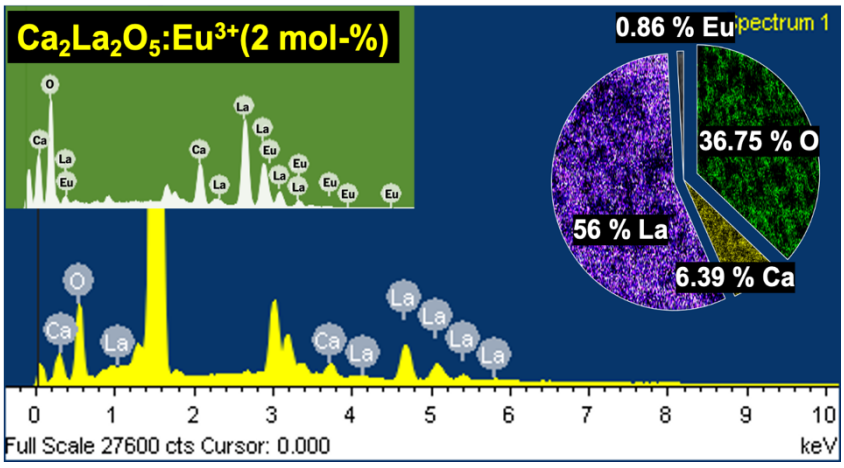

Figure 6.8 EDAX, color overlay images of $Ca_2La_2O_5:Eu^{3+}$ (2.0 mol-%)

using elemental mapping as shown in Figure 6.8. The EDAX spectrum provided insights into the fundamental characteristics of the $Ca_2La_2O_5:Eu^{3+}$ phosphors. The EDAX spectrum depicted in Figure 6.8 provides unequivocal evidence of the presence of all elements (Calcium, Oxygen,

Lanthanum, and Europium), thus confirming the successful inclusion of all essential ingredients.

6.6 Fourier-transform infrared (FT-IR) Study

The provided diagram depicts the Fourier-transform infrared (FT-IR) spectrum of a phosphor material known as $Ca_2La_2O_5:Eu^{3+}$, which has been activated by the inclusion of Eu^{3+} ions. The Fourier Transform Infrared (FT-IR) study was conducted to determine the stretching frequency of various groupings, as depicted in Figure 6.9. The production of the infrared bands at 620 cm^{-1} and 1068 cm^{-1} in the phosphorus system can be attributed to the vibration mode of La-O. The findings of the experiment indicate that the observed absorption bands align with the H-O-H stretching characteristic of base metal oxides. Significantly, all observed absorption in the Fourier Transform Infrared (FTIR) spectra of the phosphor were within the permissible limit. The band observed at 3612 cm^{-1} is attributed to the stretching vibration of H-O-H molecules, which arises from the absorption of water molecules from the ambient atmosphere.

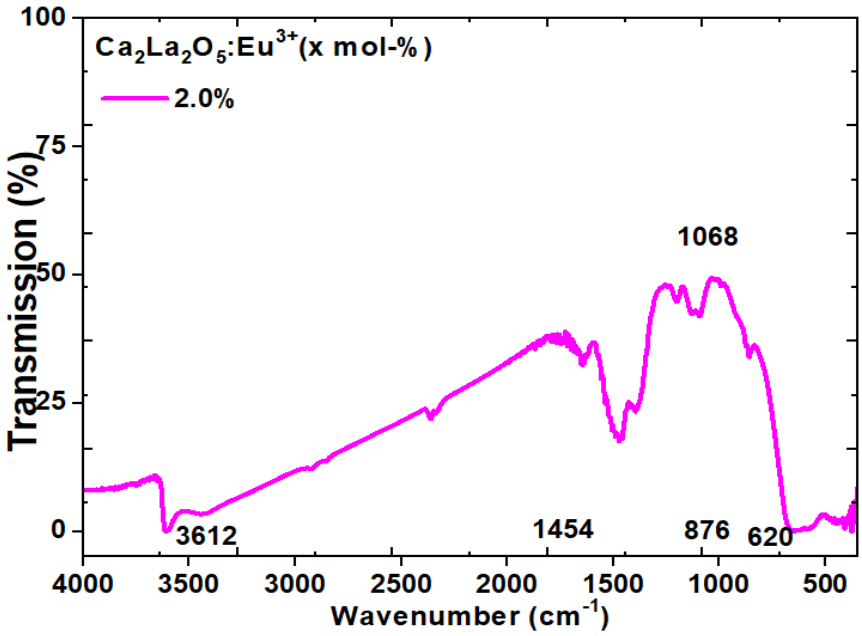

Figure 6.9: FTIR spectra of the $Ca_2La_2O_5:Eu^{3+}$ phosphors doped with 2 mol -% concentration of Eu^{3+}

6.7 Temperature dependence of PL

Extended operation of light-emitting diodes (LEDs) results in the production of thermal energy, which in turn diminishes the luminous output and color rendering index (CRI) efficacy of the

LEDs. Thermal quenching is identified as a primary factor contributing to the observed decline in performance. The parameter under consideration holds significant importance in the context

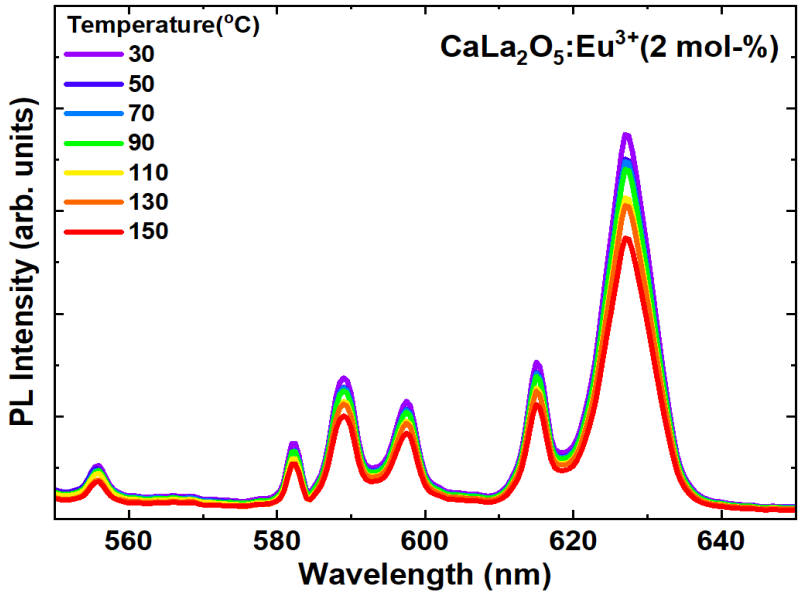

Figure 6.10 : PL Spectra of $Ca_2La_2O_5:Eu^{3+}$ (x = 2.0 mol-%) from 30°C to 150°C under 467 nm excitation

of LEDs incorporating phosphors, since it exerts a substantial influence on the aforementioned parameters. Hence, it is imperative for the phosphors to exhibit stability in order to maintain consistent performance during the operation of light-emitting diodes (LEDs). The temperature at the junction of light-emitting diodes (LEDs) can exceed 120°C within the temperature range of 120 - 150°C. The manifestation of thermal quenching becomes readily apparent when the temperature exceeds 120°C, resulting in a discernible reduction in the intensity of luminescence

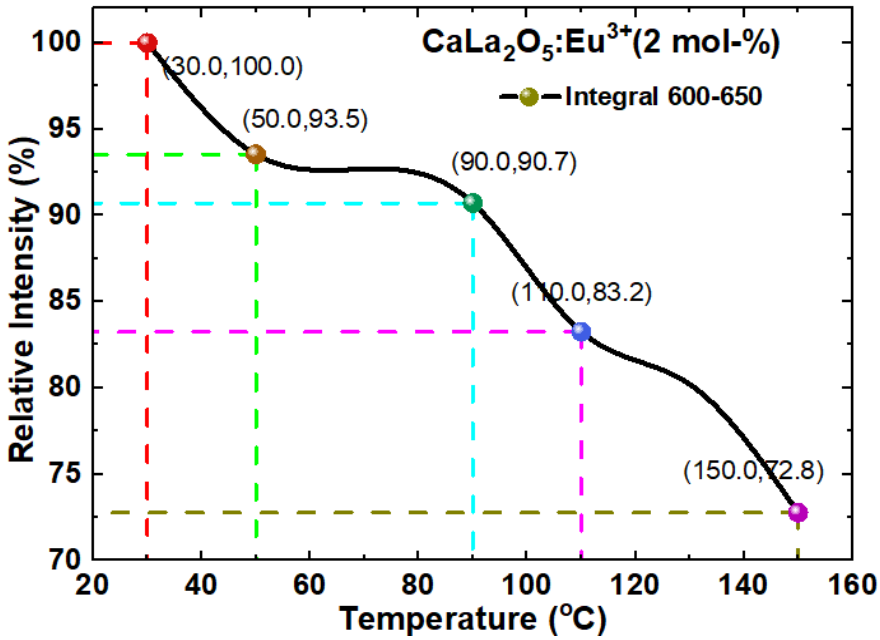

Figure 6.11 Plot showing the relation between relative intensity (%) and temperature for $Ca_2La_2O_5:Eu^{3+}$ (x = 2.0 mol-%)

and a shift in color, so rendering light-emitting diodes (LEDs) susceptible to thermal instability. In order to ascertain the stability of the phosphor that was generated, temperature-dependent

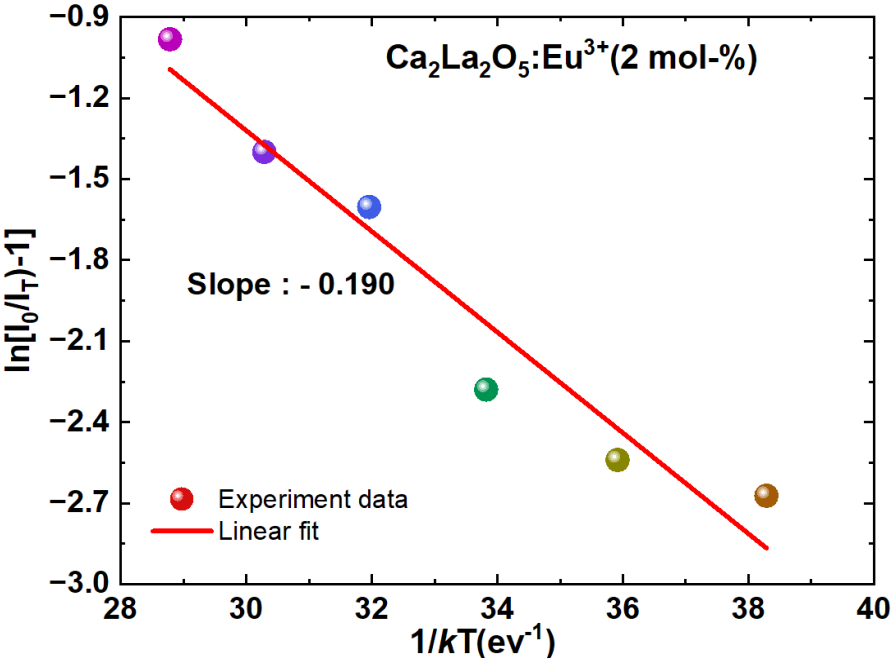

Figure 6.12 : Plot showing the relation between ln[(I_0/I_T) - 1] and 1/T for $Ca_2La_2O_5:Eu^{3+}$ (x = 2.0 mol-%)

photoluminescence (PL) tests were conducted using an excitation wavelength of 467 nm as shown in Figure 6.10. The provided figure 6.10 illustrates the photoluminescence (PL) emissions of $Ca_2La_2O_5:Eu^{3+}$ (2 mol%) at various temperatures, ranging from 30 to 150°C, with equal intervals between measurements. The photoluminescence (PL) emission exhibited a non-linear decline in response to changes in temperature, which can be attributed to the phenomenon of thermal quenching. The observed drop in intensity at a temperature of 150°C was found to be just 27.2% as shown Figure 6.11 compared to the intensity at room temperature. This finding suggests a reduced thermal quenching effect and the absence of any shift in emission peaks. The Arrhenius equation was used to calculate the activation energy[25].

$$I_t = I_o / 1+c \exp(\Delta E/kT$$

I_0 - PL intensity at room temperature,

I_t - PL intensity at various temperatures,

c is a constant,

Energy of activation in the process of thermal quenching is shown as ΔEa, and k denotes the Boltzmann constant (8.629×10^{-5} eV K^{-1}).

The figure 6.12 illustrating the relationship between the natural logarithm of $[(I_0/I_t) - 1]$ and the reciprocal of the product of Boltzmann's constant and temperature (1/kT) was presented in Figure 6.12. The diagram exhibits a linear regression with a negative slope of -0.190, indicating a relationship between the variables. This slope value can be interpreted as the activation energy, measured in electron volts (eV), which is found to be 0.190. The values mentioned in Table 6.1 exhibit similarity to those published in prior studies on red-emitting Eu^{3+} phosphors, such as $Na_2La_4(WO_4)_7$: Eu^{3+} (0.236 eV), $BaZrGe_3O_9$: Eu^{3+} (0.175 eV), and $K_2Gd(PO_4)(WO_4)$:Eu^{3+} (0.19 eV). The table 6.1 presents a comparison of the activation energy and thermal stability between the aforementioned phosphors and the materials that have been produced. This statement elucidates that the phosphor that has been produced exhibits exceptional thermal stability.

Table 6.1: Activation energy and thermal stability of Synthesized Phosphor along with other phosphors.

S.No	Phosphor composition	Activation energy Δ_{Ea} (eV)	Thermal stability at 423 K	Ref.
1	$Na_2La_4(WO_4)_7$: Eu^{3+}	0.236	69.75%	[26]
3	$K_2Gd(PO_4)(WO_4)$:Eu^{3+}	0.19	72%	[27]
3	$BaZrGe_3O_9$:Eu^{3+}	0.175	72.8%	[28]
4	$Ca_2La_2O_5$:Eu^{3+}	0.190	72.8%	Present Work

6.8 Photometric characterization

In order to assess the appropriateness of the synthesized phosphors for display applications and photo modulation therapy, the CIE 1931 color coordinates were measured for the generated phosphors. The diagram depicted in Figure 6.13 illustrates the CIE coordinates of the phosphor, which were obtained by the analysis of its emission spectra triggered at a wavelength of 395 nm. The experiment revealed that when the concentration of Eu^{3+} powder ranged from 0.5 to 2.5 mol%, the CIE coordinates (x, y) for the 395 nm excitation were measured to be (0.42, 0.35). These coordinates closely resemble the ideal white color coordinates (0.33, 0.33) established by the NTSC ("National Television Standards Committee"). This statement elucidates that synthesized phosphor has optimal characteristics for white light-emitting diode (w-LED) applications. The optimal concentration for achieving maximum PL integral intensity

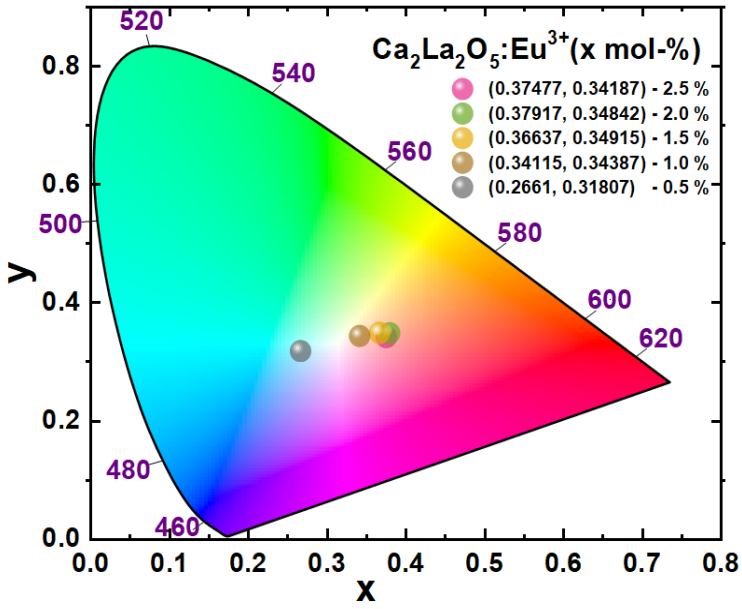

Figure 6.13 : CIE chromaticity coordinates for phosphor $Ca_2La_2O_5:Eu^{3+}$ (x = 0.5–2.5 mol %) on excitation with 395 nm

and CIE in $Ca_2La_2O_5$ is determined to be 2 mol% Eu^{3+}. Figure 6.14 displays the CIE color coordinates of $Ca_2La_2O_5:Eu^{3+}$ (2 mol%) and reveals that they reside within the deep red region. The wavelength at which the highest intensity occurs is measured at 627 nm, while the

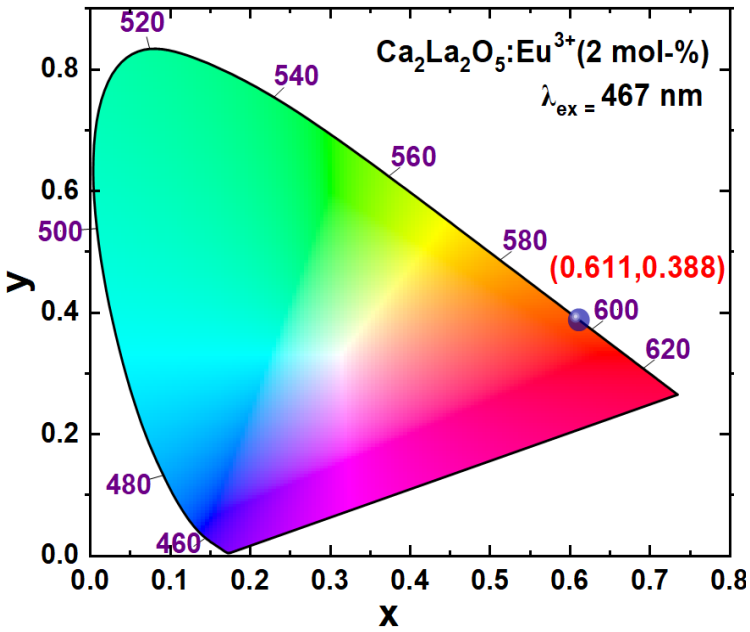

Figure 6.14 : CIE chromaticity coordinates of prepared $Ca_2La_2O_5:Eu^{3+}$ (2.0 mol %) excited at 467 nm

corresponding coordinates are determined to be (0.62, 0.38). Therefore, the utilization of a 2% concentration powder has been found to be applicable in a range of scenarios, including its use in w-LED devices and cognitive photo-biomodulation therapy, where it serves as a red phosphor when subjected to 467 nm excitation.

6.9 Summary

To summarize, the $Ca_2La_2O_5$: Eu^{3+} phosphors were prepared through the utilization of the modified high-temperature solid-state reaction technique with the inclusion of a chemical flux. Subsequently, a comprehensive investigation was conducted to analyze their optical characteristics. The emission of narrow-band red light in all phosphor compositions is a result of the electric dipole transition occurring at a wavelength of 627 nm. The excitation and emission spectra of $Ca_2La_2O_5$:Eu^{3+} phosphors were found to be consistent across all concentrations. However, concentration quenching was detected specifically at a concentration of x = 2.5 mol%. Based on the findings of a temperature-dependent photoluminescence (PL) investigation, it has been shown that the phosphors exhibit a thermal stability of around 73%. Additionally, the activation energy (Ea) associated with the observed phenomenon is measured to be 0.19. The phosphor composition $Ca_2La_2O_5$:Eu^{3+} (2 mol%) was selected as the most suitable choice for LED manufacturing due to its ability to effectively cover both the white and red spectra. The findings of this study indicate that the red phosphor now under investigation holds significant potential as a viable alternative for white light-emitting diodes (w-LEDs), display technologies, and as red light-emitting diodes (LEDs) for cognitive therapy employing photo-biomodulation.

References

1. H. Hu, W. Zhang, Opt. Mater. (2006), https://doi.org/10.1016/j. optmat. 2005.03.015.
2. K.N. Shinde, S.J. Dhoble, H.C. Swart, K. Park, Phosphate Phosphors for Solid- State Lighting, 2012.
3. S. Sheoran, V. Singh, S. Singh, S. Kadyan, J. Singh, D. Singh, Sci. Mater. Int. (2019), https://doi.org/ 10.1016/j.pnsc.2019.07.003.
4. F. Zhang, B. Liu, J. Alloys Comp. 542 (2012) 276–279.
5. A.K. Parchur, R.S. Ningthoujam, RSC Adv. 2 (2012) 10859–10868.
6. V.B. Pawade, N.S. Dhoble, S.J. Dhoble, Optoelectronic. Adv. Mater. Rapid Commun. (2011).
7. D.J. Naczynski, M.C. Tan, M. Zevon, B. Wall, J. Kohl, A. Kulesa, S. Chen, C. M. Roth, R.E. Riman, P.V. Moghe, Nat. Commun. (2013), https://doi.org/ 10.1038/n comms3199.
8. V.B. Pawade, S.J. Dhoble, Opt Commun. (2011), https://doi.org/ 10.1016/j. optcom.2011.05.015.
9. D.P. Dutta, V. Sudarsan, P. Srinivasu, A. Vinu, A.K. Tyagi, J. Phys. Chem. C (2008), https://doi.org/10.1021/jp800576y.
10. Salehpour F, Majdi A, Pazhuhi M, Ghasemi F, Khademi M, Pashazadeh F, Hamblin MR, Cassano P. Photobiomodul Photomed Laser Surg. 2019 Oct;37(10):635-643.
11. Salehpour, F., Mahmoudi, J., Kamari, *Mol Neurobiol* **55**, 6601–6636 (2018).

12. W. Feng, T. Wee Beng, Z. Yong, F. Xianping, W. Minquan, Nanotechnology 17 (2006) R1.
13. H. Wang, M. Uehara, H. Nakamura, M. Miyazaki, H. Maeda, Adv. Mater. 17 (2005) 2506–2509.
14. V.R. Bandi, B.K. Grandhe, H.-J. Woo, K. Jang, D.-S. Shin, S.-S. Yi, J.-H. Jeong, J. Alloys Comp. 538 (2012) 85–90.
15. Kang X, Lu S, Wang H, Ling D, Lü W. 2018 Dec 5;3(12):16714-16720. doi: 10.1021/acsomega.8b01952. PMID: 31458301;
16. Divi, Haranath & Pradhan, Payal Priyadarshini & Muddamalla, Rakshita & Sharma, Aachal & Prasad, K.A.K & Khanapuram, Uday Kumar & Kumar, Rajaboina. (2023). 10.2139/ssrn.4563009.
17. G. Lakshminarayana, Hucheng Yang, Jianrong Qiu, Journal of Solid State Chemistry,Volume 182, Issue 4, 2009, Pages 669-676.
18. Mei Yang, Haiyan Shi, Liwei Ma, Qingyuan Gui, Jinlei Ma, Mimi Lin, Anwar Sunna, Wenjing Zhang, Liming Dai, Jia Qu, Yong Liu,
19. Yang, Mei, Haiyan Shi, Liwei Ma, Qingyuan Gui, Jinlei Ma, Mimi Lin, Anwar SunnaJournal of Alloys and Compounds, Volume 695, 2017,Pages 202-207.
20. M. Chandrasekhar, H. Nagabhushana, S.C. Sharma, K.H. Sudheer kumar, N.Dhananjaya, D.V. Sunitha, C. Shivakumara, B.M. Nagabhushana, J. Alloys Compd. 584 (2014) 417.
21. M. Venkataravanappa, H. Nagabhushana, B. Daruka Prasad, G.P. Darshan, R.B. Basavaraj, G.R. Vijayakumar, Ultrasonics Sonochemistry 34 (2017) 803.
22. N.Baig, N.S. Dhoble, A.N. Yerpude, V. Singh, S.J. Dhoble, Optik 127 (2016) 6574.
23. Nair, Govind & Dhoble, S J. (2016), 26, 1865–1873. 10.1007/s10895-016-1880-6.
24. Meza O, Villabona-Leal EG, Diaz-Torres LA, Desirena H, Rodríguez-López JL, Pérez E. J Phys Chem A. 2014 Feb 27;118(8):1390-6. doi: 10.1021/jp4119502.
25. A.K. Galwey, M.E. Brown, Ther- mochim. Acta 386(1), (2002), 91–98.
26. Xiaoyong Huang, Bin Li, Heng Guo, , Ceramics International, Volume 43, Issue 13, 2017,Pages 10566-10571.
27. Qiang Zhang, Xicheng Wang, Xin Ding, and Yuhua Wang, *Inorganic Chemistry* 2017 *56* (12), 6990-6998
28. Zhu, G.; Ci, Z.; Shi, Y.; Que, M.; Wang, Q.; Wang, Y. J. Mater. Chem. C2013, 1(37), 5960–5969.

Chapter - 7

Summary, Conclusion and Future Scope of Work

Features of the Chapter:

This chapter offers a comprehensive overview of the main results of the dissertation as well as overarching findings and observations from current research. Potential areas for further research were also suggested.

7.1 Summary

Narrow-band phosphors with a red-spectral distribution are difficult to develop. Phosphor for white light-emitting diodes has been extensively studied for color accuracy and efficiency. The modified white spectrum of the pc-WLEDs brings red into the sensitive zone of the eye. These advances enable warm white pc-WLED lighting. Current research focuses on narrow-bandwidth red-emitting phosphors. The research focuses on their improved color rendering index. These phosphors improve LCD backlighting by expanding the color spectrum. Several methods have been used to find novel red-emitting phosphors with narrow bandwidth and good optical properties. Changes in the crystal structure of the host material, the activator ion, and the local environment affect the peak wavelength. Regulate the crystal structure, increase crystal stiffness, maintain ambient symmetry, and maximize activator sites to maximize red-emitting spectral width at half maximum.

To address the specific requirements of narrow-bandwidth phosphors in display applications, it is imperative to study the relationship between the inherent optical properties of new red-emitting narrow-bandwidth phosphors and their potential to enhance the efficacy of lighting applications. These materials influence light perception, color saturation, and warm white pc-WLED lighting. The focus is on exploring different approaches that manipulate the peak position and bandwidth of the red phosphor, the intensity of which increases the CRI.

Current commercial red-emitting phosphors do not produce narrow-band light between 610 and 630 nm and do not exhibit good photo stability. In addition to europium, quantum dots and Mn^{4+}-doped fluorides are common red phosphors used in white LEDs. Quantum dots with Cd have higher red phosphorescence but higher toxicity and production cost. Therefore, there is great demand for novel red phosphors with narrow emission bandwidths and increased UV LED chip efficiency.

The current investigation focuses on the preparation of Eu^{3+}-doped compounds, particularly $Ca_2La_2O_5$, $SrZr_2La_2O_7$, and $SrZr_2CaLa_2O_8$. A significant amount of phosphors and their corresponding host lattices were prepared and subsequently subjected to various characterization. The prepared phosphors were prepared subjected to several characterization namely, Photoluminescence (PL), Powder X-ray Diffraction (PXRD), Scanning Electron Microscopy (SEM), Fourier Transform Infrared (FTIR) Spectroscopy, Energy Dispersive X-ray Analysis (EDAX), and Particle Size Distribution (PSD), etc. The results of these analyses were recorded and reported accordingly. The CIE chromaticity coordinates were calculated and then recorded subsequently. The current study focused on the development of functional materials as phosphors for white LED technology.

7.2 Highlights

1. Red-emitting phosphors have great potential to improve the color purity and color rendering index (CRI) of LED devices, as currently existing phosphors suffer from a lack of sufficient red components. The synthesis of $Ca_2La_2O_5:xEu^{3+}$ phosphors in a single phase was achieved by using a modified high-temperature solid-state reaction approach. Confirmation of the formation of a single monoclinic phase of synthesized phosphors is supported by the observed XRD patterns. The lattice strain was determined using the W–H method, and the negative sign indicated the presence of compressive strain within the structure. The SEM images showed a surface morphology resembling the accumulation of small particles. Furthermore, the presence of elemental composition in $Ca_2La_2O_5:xEu^{3+}$ phosphors was confirmed by the EDAX spectrum. The phosphors have an average particle size of approximately 2.0 μm.

2. The $Ca_2La_2O_5:xEu^{3+}$ phosphor exhibited a distinct red emission (~627 nm) when excited at ~590 nm, which originates from the $^5D_0 \rightarrow {}^7F_2$ transitions of the Eu^{3+} ions. The phenomenon of PL emission was studied with different amounts of dopants ranging from 0.5 to 2.5 mol%. The phenomenon of quadruple repulsion occurs when the concentration of Eu^{3+} exceeds 2 mol%. This leads to quenching effects, which subsequently lead to a decrease in photoluminescence (PL) intensity. The investigation of thermal stability with respect to photoluminescence (PL) was carried out through a study examining the temperature dependence of PL. The synthesized phosphor is able to withstand air temperatures up to 150°C, resulting in a 29% reduction in integrated intensity. The associated activation energy (ΔE) is 0.213 eV, calculated from the slope of the diagram between $\ln[(I_0/I_T)-1]$ vs. 1/kT.

3. The synthesized phosphor $Ca_2La_2O_5:xEu^{3+}$ was subjected to excitation with commercially available LEDs emitting at wavelengths of 395 nm and 476 nm. When stimulated with a wavelength of 395 nm, the phosphor showed the ability to emit white light with a significant red component. At a wavelength of 476 nm, light was emitted in the yellow-orange spectrum with a distinct red hue. Confirmation of color purity and emitted color was achieved by using the CIE chromaticity calculation, which yielded coordinates that lay within the white and yellow regions, respectively.
4. The chromaticity coordinates of a phosphor with a doping level of 2% were determined using the CIE diagram. The phosphor showed a deep red emission when excited at a wavelength

of 590 nm. The chromaticity coordinates (0.67, 0.33) are in the red zone, indicating that the light produced has 99% color purity.

5. A unique category of $SrZr_2La_2O_7$: Eu^{3+} phosphor powder with red emission properties was synthesized by a solid-state reaction method at a high temperature of 1200°C. During monitoring, several absorption lines were observed at a wavelength of 627 nm. The absorption lines were assigned to the transitions $^7F_0 \rightarrow {}^5H_J + {}^IH_J$ (279 nm), $^7F_0 \rightarrow {}^5L_7$ (395 nm), $^7F_0 \rightarrow {}^5D_2$ (467 nm), $^7F_1 \rightarrow {}^5D_1$ (540 nm) and $^7F_1 \rightarrow {}^5D_0$ (590 nm). The photoluminescence (PL) emission of the material was examined by excitation at a specific wavelength of 467 nm. This excitation leads to the emission of light with distinct spectral lines that can be assigned to specific transitions. These transitions include $^5D_1 \rightarrow {}^7F_1$, which emits light at a wavelength of 540 nm, $^5D_1 \rightarrow {}^7F_1$ at 590 nm, $^5D_0 \rightarrow {}^7F_2$ at 615 nm, and $^5D_0 \rightarrow {}^7F_2$ light at 627 nm. The spectral peak corresponding to the transition of $^5D_0 \rightarrow {}^7F_2$, which occurs at a wavelength of 627 nm, has the highest significance, while the other peaks have relatively lower significance. The synthesized $SrZr_2La_2O_7$:Eu^{3+} phosphor shows the ability to emit yellow light with a significant red component. The above observation was confirmed by the CIE coordinates (0.48, 0.50), which indicate that the color falls in the yellow-orange range when excited with blue light. The results of this study show that the presence of Eu^{3+} ions significantly improves the CRI of white Light Emitting Diodes (w-LEDs). The use of direct white light-emitting phosphors in this research offers the advantage of producing uniform and consistent illumination, thereby reducing the presence of concentrated areas of high brightness, obscured regions, or color variations on the display substrate. This is an additional advantage of the current research undertaking.
6. $SrZr_2La_2O_7$: Eu^{3+} was excited at 395 nm with PL emission in white with maximum intensity component as red color. This synthesized phosphor is a multi-wavelength excitable phosphor suitable for various w-LED applications. The distinctive structural characteristics of the subject were determined by studying its structural and morphological aspects. The measured crystal size is in the range of 27.1 to 38.4 nm.
7. The synthesis of $SrZr_2CaLa_2O_8$:Eu^{3+} phosphors was carried out using a solid-state reaction method at a temperature of 1200°C. The structural phase properties of $SrZr_2CaLa_2O_8$:Eu^{3+} phosphor were investigated by analysing XRD peaks using Scherrer equation. Examination of FE-SEM images showed that the particles have irregular polyhedral shapes with sizes ranging from 0.10 to 10.0 μm.

8. Additionally, for $SrZr_2CaLa_2O_8:Eu^{3+}$ phosphor, photoluminescence (PL) emission was observed at about 467, 590, 615, and 627 nm when excited by light at ~395 nm. The wavelength of 627 nm is observed to be more prominent compared to the other emitted wavelengths, resulting in white emission with a dominant red hue. A comprehensive study was carried out to investigate the temperature dependence of photoluminescence (PL). It was found that at a temperature of 150°C, the integrated intensity of PL decreased to 26%. This intensity reduction exceeds the performance of commercially available phosphors, which typically have an activation energy of 0.18 eV. Confirmation of PL emission was achieved using the CIE chromaticity diagram with the x and y values determined to be 0.68 and 0.31, respectively. These values indicate that the emitted color is in the deep red range and has a high color purity of 99.10%.
9. Three different phosphors $Ca_2La_2O_5:xEu^{3+}$, $SrZr_2La_2O_7: xEu^{3+}$, and $SrZr_2CaLa_2O_8:xEu^{3+}$ were synthesized with Eu^{3+} concentration varying between 0.5 and 2.5 mol%. The achieved optimized performance in terms of PL intensities is given in the following Table 7.1:

Table 7.1: List of phosphors synthesized with optimized dopant concentration.

Phosphor	Optimized mol % (dopant concentration)
$Ca_2La_2O_5:xEu^{3+}$	2.0 %
$SrZr_2La_2O_7: xEu^{3+}$	1.5 %
$SrZr_2CaLa_2O_8:xEu^{3+}$	2.0 %

10. A comparative study was carried out with the above phosphors talking into account their respective concentrations and the following criteria and results listed in Table 7.2.
    a. An integrated PL intensity at excited wavelengths of 395, 467, and 590 nm, as shown in Figures 7.1, 7.2 and 7.3, respectively.
    b. Emission width, Full-Width at Half Maximum (FWHM) of 3 phosphors as shown in Figures 7.4, 7.5 & 7.6.
    c. Wavelength of emissions.
    d. CRI
    e. CIE chromaticity coordinates.

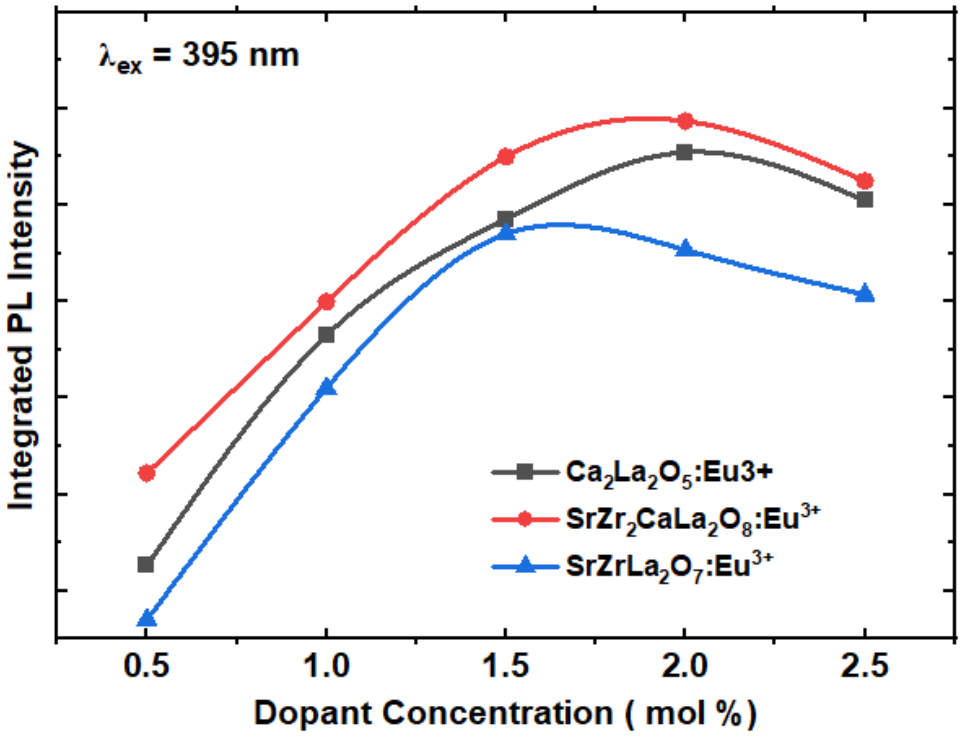

Figure 7.1: Comparison of the integrated PL intensity of three types of phosphors for different dopant concentrations under 395 nm excitation.

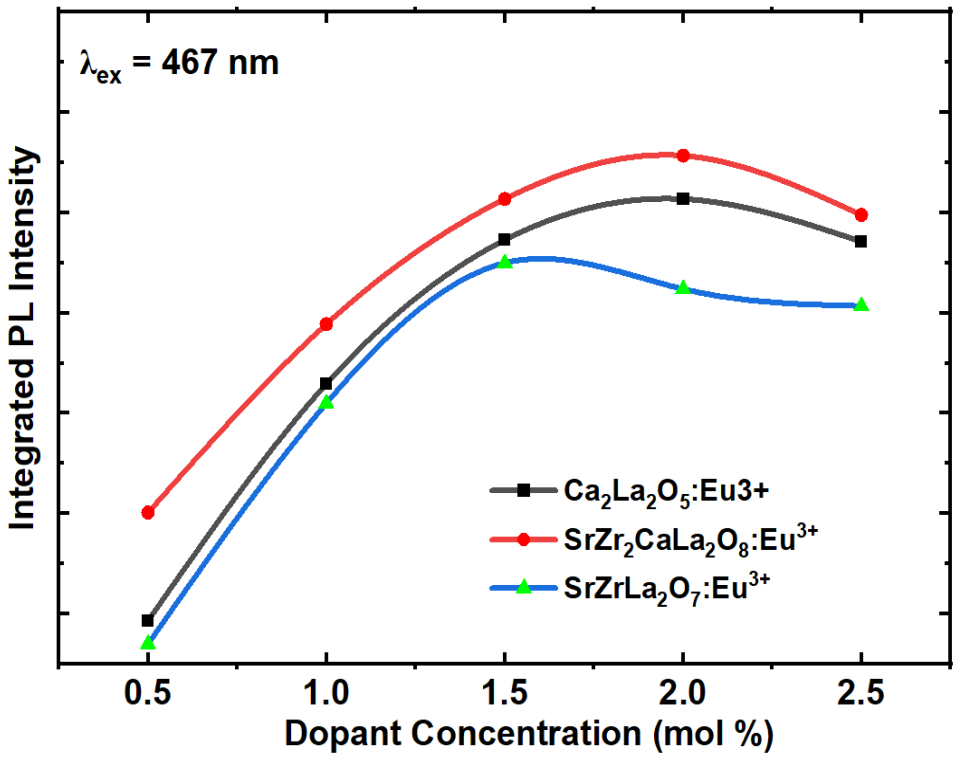

Figure 7.2: Comparison of the integrated PL intensity of three types of phosphors for different dopant concentrations under 467 nm excitation.

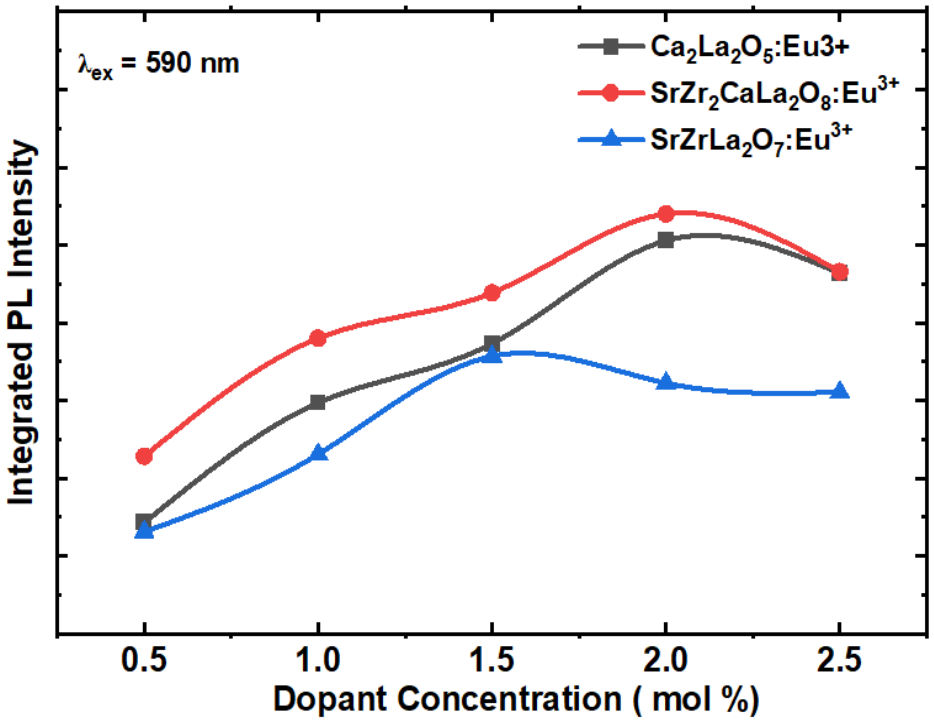

Figure 7.3: Comparison of the integrated PL intensity of three types of phosphors for different dopant concentrations under 590 nm excitation.

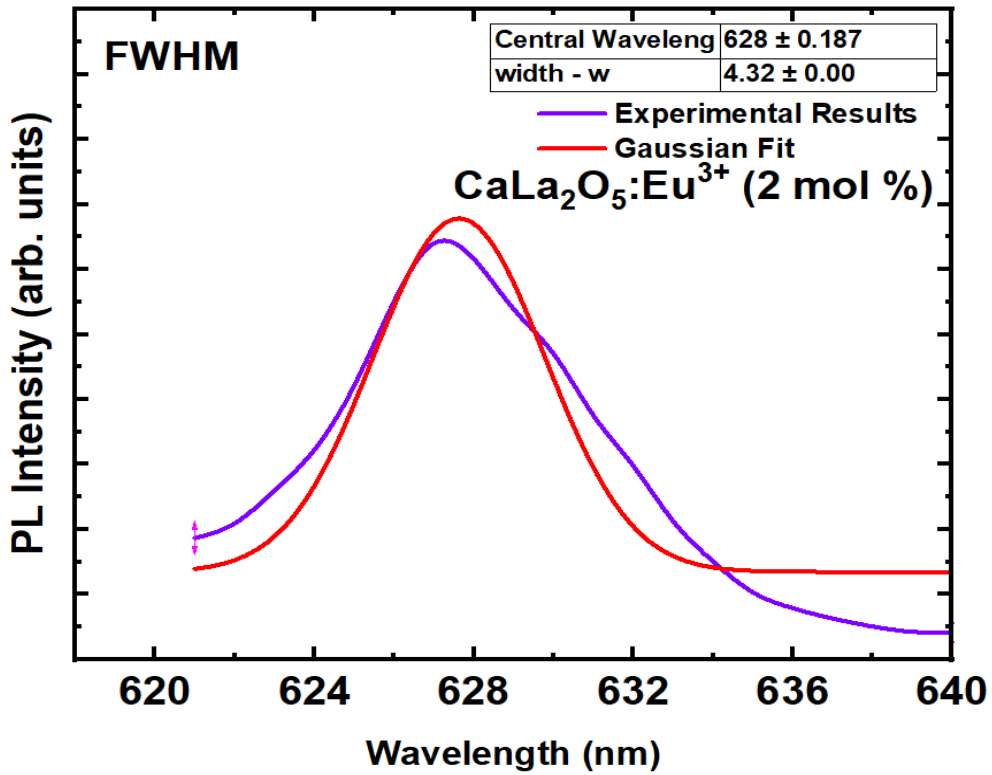

Figure 7.4: FWHM of the 627 nm emission of $CaLa_2O_5:Eu^{3+}$ phosphor

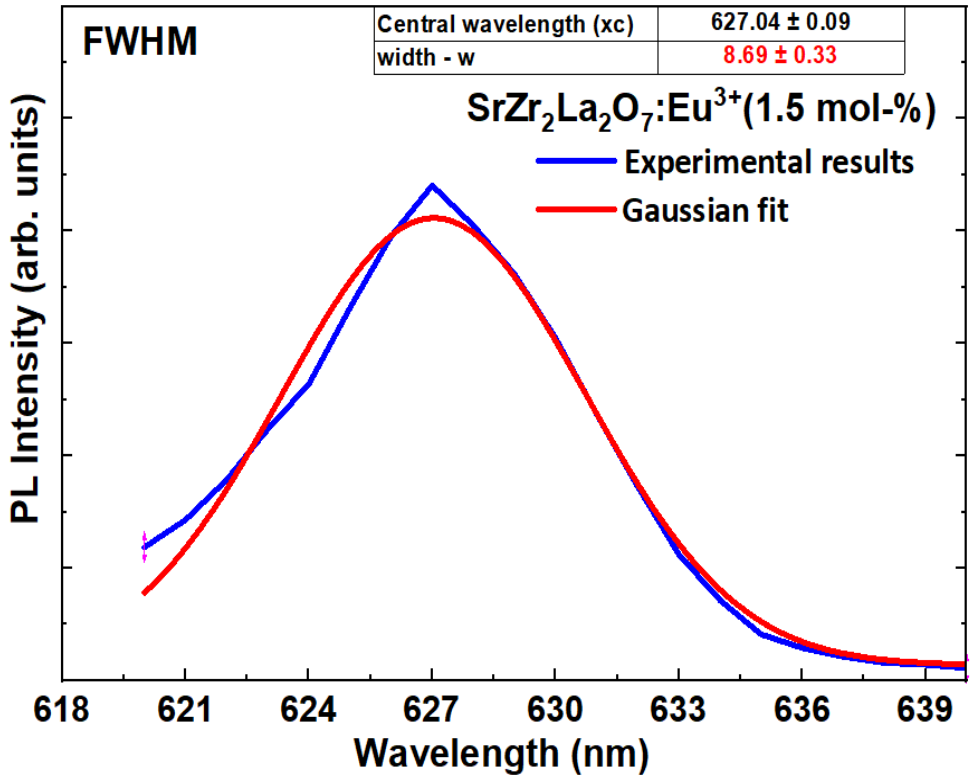

Figure 7.5: FWHM of the 627 nm emission of $SrZr_2La_2O_7$: Eu^{3+} phosphor

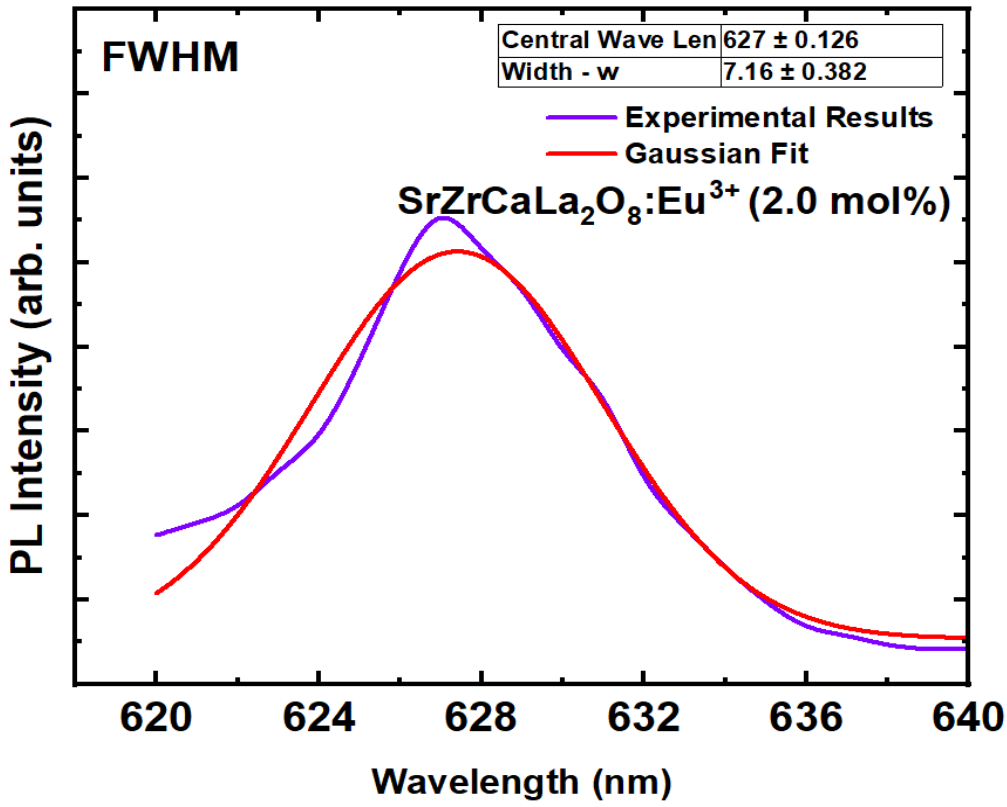

Figure 7.6: FWHM of the 627 nm emission of $SrZrCaLa_2O_8$: Eu^{3+} phosphor

Table 7.2: The results of the comparative study of performance parameters.

Synthesized phosphor	PL Intensity	Color purity	FWHM (nm)	CRI	Emitted Wavelength	CIE (x, y)
$Ca_2La_2O_5:Eu^{3+}$	Minimum	99%	4.32	82	627 nm	0.67, 0.32
$SrZr_2La_2O_7:Eu^{3+}$	Mean	97%	8.7	83	627 nm	0.69, 0.30
$SrZr_2CaLa_2O_8: Eu^{3+}$	Maximum	99.1%	7.16	90	627 nm	0.69,0.31

7.3 Conclusions

1. Three kinds of phosphors with warm white, yellow and red-emission were successfully synthesized.
2. Detailed optical, structural and morphological analysis were carried out for all three phosphors.
3. Multi-excitable phosphors have been prepared, which can be excited by widely used and easily available LEDs in the local market.
4. The luminescence properties of red phosphor such as color purity (99%), FWHM (~7.0 nm) and CRI (90) were significantly improved.
5. Spectral parameters such as CIE coordinates and color purity were calculated.
6. Of the three synthesized phosphors, the optimized $SrZr_2CaLa_2O_8:Eu^{3+}$ phosphor was identified and used for possible use in device fabrication.

7.4 Scope for Future Work

1. The development of novel synthesis methods is expected to improve the shape and morphology of particles, improve their luminescence ability, and reduce their overall size.
2. It is necessary to develop a prototype of a multilayer phosphor using thin film technology and then study its properties.
3. There is a substantial need for red-emitting phosphors that offer suitable properties for a number of important applications. Therefore, it is important to focus on developing red-emitting phosphors that have a dominant red component compared to green and blue-emitting phosphors. In order to improve the luminescence properties of Eu^{3+}-doped phosphor, it is necessary to use a suitable co-dopant. For example, the Bi^{3+} ion can act as a

sensitizer due to its ability to enhance the energy transfer process. This can be attributed to the fact that the excitation peak of the Eu^{3+} ion exactly matches the emission of the Bi^{3+} ion.

4. Commercialization of the optimized phosphor has low raw material prices and facilitates the production of light-emitting diodes (LEDs).
5. The potential applications of this phosphor can be applied to various fields such as solar cells, infrared (IR) detection, ultraviolet (UV) detection, etc.

Research Publications to Scholar's Credit

SCI Journal Publications

1. *Synthesis and photoluminescence characterisation of $Ca_2La_2O_5:Eu^{3+}$, a novel red-emitting phosphor: a comprehensive study*, **Kishore Kumar Aitha,** D. Dinakar, Payal P. Pradhan, K. Yadagiri, K. Suresh, Naresh Degda, K.V.R. Murthy & D. Haranath **Canadian Metallurgical Quarterly, (2023)**. DOI: https://doi.org/10.1080/00084433.2023.2254128 **(Impact Factor, IF: 0.9)**

2. *A novel narrow-band red-emitting multi-layer phosphor for white – Light emitting devices.* **Kishore Kumar Aitha,** D. Dinakar, P. Indira, A.S. Sai Prasad, K.V.R. Murthy, D. Haranath, **Results in Chemistry**, Volume 6, 2023, 101100, ISSN 2211-7156, DOI: https://doi.org/10.1016/j.rechem.2023.101100 **(IF: 2.3)**

3. *Studies on a novel $SrZr_2CaLa_2O_8:Eu^{3+}$ phosphor for lighting applications emitting direct white light.* **Kishore Kumar Aitha,** D. Dinakar, K. V. R. Murthy, A. S. Sai Prasad, and D. Haranath. **Luminescence**, 2023, 1. DOI: https://doi.org/10.1002/bio.4623 **(IF: 2.9)**

4. *Dual excitable novel phosphor for use in display devices and cognitive therapy.* **Kishore Kumar Aitha,** D. Dinakar, D. Y. Kolbe, K. V. R. Murthy, and D. Haranath. **Ceramics International**, (Under Review, MS No. CERI-D-23-14900, 01 Dec 2023) **(IF: 5.2)**

Papers Presented in International/National Conferences and Seminars

1. A new UVA Emitting Eu^{+2} Doped $SrCaZrBi_2La_2O_3$ Phosphor

International Conference on Recent Trends in Renewable Energy & Sustainable Development, held at Bhilai Institute of Technology, Raipur, during 29-30 April 2022

2. Photoluminescence Studies of Sr0.1Ca0.1Zr0.1La1.6907:1%Eu3+: A Multiple Excitation Phosphor

International seminar on Advance Materials and Applications held at MS University, Vadodara, during 18-19 July 2022.

3. Studies on $Sr_{0.1}Zr_{0.1}La_{1.79}O_6$: 1% Eu^{3+}: A Multiple Excitation Phosphor

First International Conference on Functional Materials held at Pt. Ravishankar Shukla University, Raipur, during 24-26 August 2022.

4. Synthesis of $SrCaZrLaO_7$: 1% Eu^{3+} Phosphor and its Photoluminescence Studies

International Seminar on Luminescence Materials held at Trivandrum Kerala, Organized by Luminescence Society of India, Baroda & Department of Nano Science and Nano Technology, Kerala University, Kerala, during 09-10 December 2022.

5. $SrZr_2La_2O_7:Eu^{3+}$- A Narrow Width Red-Emitting Phosphor with Photon Cascading Absorption and Emissions for White Light-Emitting Devices Driven by UV LED

7th International Conference Luminescence and its Applications held at CSIR-IICT Hyderabad, during 02-06 July 2023.

CANADIAN METALLURGICAL QUARTERLY
https://doi.org/10.1080/00084433.2023.2254128

Synthesis and photoluminescence characterisation of $Ca_2La_2O_5:Eu^{3+}$, a novel red-emitting phosphor: a comprehensive study

Kishore Kumar Aitha[a], D. Dinakar[a], Payal P. Pradhan[a], K. Yadagiri[a], K. Suresh[b], Naresh Degda[c], K.V.R. Murthy[d] and D. Haranath[a]

[a]Department of Physics, National Institute of Technology Warangal, Hanumakonda, India; [b]Department of Physics, Government College (Autonomous), Rajahmundry, India; [c]Department of Physics, Faculty of Science, The M.S. University of Baroda, Vadodara, India; [d]Applied Physics Department, Faculty of Engineering & Technology, The M.S. University of Baroda, Vadodara, India

ABSTRACT

A novel low-melting-temperature chemical flux method was used to synthesise a $Ca_2La_2O_5$ lattice doped with Eu^{3+} ions in the range of 0.5-2.5 mol-%. The phosphors were characterised by powder X-ray diffraction (PXRD), scanning electron microscopy (SEM), energy dispersive X-ray spectroscopy, particle size distribution, photoluminescence (PL), and Fourier transform infrared spectroscopy, respectively. The PXRD pattern revealed the hexagonal crystal structure with the space group P63/m. The microstrain (ε) was found to not vary with different concentrations of dopant and the negative means compression in the lattice. Particles of varying sizes and irregular shapes were observed from the SEM micrographs. The EDAX mapping revealed that all the constituent elements were found to be in appropriate ratios. Interestingly, the $Ca_2La_2O_5$: xEu^{3+} (x = 0.5-2.5 mol-%) phosphor samples were excited at 590 nm, showing a Stokes-shifted red-PL with significant intensities at 615 and 627 nm. Unconventionally, when the phosphor is excited at 590 nm, the Eu^{3+} ion-characteristic luminescence owing to $^5D_0 \rightarrow {}^7F_J$ (J = 0, 1, 2, 3, 4) transitions are manifested. Another remarkable observation is that the PL at 627 nm corresponding to $^5D_0 \rightarrow {}^7F_3$ transition was much stronger than the 615 nm emission of Eu^{3+} corresponding to $^5D_0 \rightarrow {}^7F_3$ transition, indicating high colour purity among the available red-emitting phosphors.

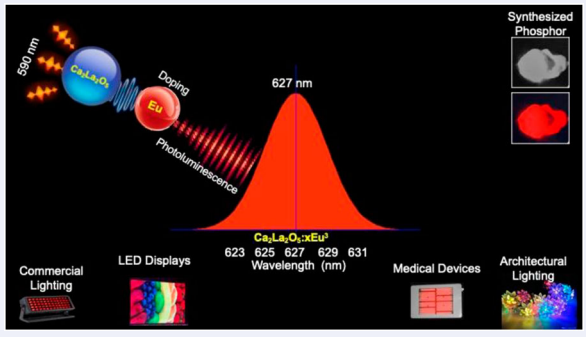

On a utilisé une nouvelle méthode de flux chimique de fusion à basse température pour synthétiser un réseau de $Ca_2La_2O_5$ dopé avec des ions Eu^{3+} dans la gamme de 0.5 à 2.5% mol. On a caractérisé les luminophores par diffraction des rayons X de la poudre (PXRD), microscopie électronique à balayage (MEB), spectroscopie de rayons X à dispersion d'énergie, distribution granulométrique, photoluminescence (PL) et spectroscopie infrarouge à transformée de Fourier, respectivement. Le modèle de PXRD a révélé la structure cristalline hexagonale du cristal avec le groupe spatial P63/m obtenu à 1200°C. On a constaté que la microdéformation (ε) ne variait pas avec les différentes concentrations de dopant et que la valeur négative signifie une compression dans le réseau. On a observé des particules de tailles variables et de formes irrégulières à partir des micrographies du MEB. La cartographie EDAX a révélé que tous les éléments constituants se trouvaient dans les rapports appropriés. Il est intéressant de noter que les échantillons luminophores $Ca_2La_2O_5$:xEu^{3+} (x=0.5-2.5% mol) étaient excités à 590 nm, montrant une PL-rouge décalée de Stokes avec des intensités importantes à 615 et 627 nm. De manière non conventionnelle, lorsque le luminophore est également excité à 590 nm, la luminescence caractéristique de l'ion Eu^{3+}, due aux transitions $^5D_0 \rightarrow {}^7F_J$ (J=0, 1, 2, 3, 4), se

ARTICLE HISTORY
Received 5 June 2023
Accepted 25 August 2023

KEYWORDS
Solid-state reaction; photoluminescence; phosphor; red-emitting; PXRD

CONTACT Kishore Kumar Aitha kishorekaitha@gmail.com Department of Physics, National Institute of Technology Warangal, Hanumakonda, Telangana 506004, India

Results in Chemistry 6 (2023) 101100

Contents lists available at ScienceDirect

Results in Chemistry

journal homepage: www.sciencedirect.com/journal/results-in-chemistry

A novel narrow-band red-emitting multi-layer phosphor for white – Light emitting devices

Kishore Kumar Aitha [a,*], Dinakar D.[a], Indira P.[b], Sai Prasad A.S.[c], Murthy K.V.R.[d], Haranath D.[a]

[a] Department of Physics, National Institute of Technology Warangal, Hanumakonda 506004, Telangana, India
[b] Department of Physics, Government Degree College, Ongole 523001, A.P, India
[c] Department of Physics, Vasavi College of Engineering, Hyderabad, Telangana, India
[d] Applied Physics Department, Faculty of Engineering & Technology, The M.S. University of Baroda, Vadodara 39001, Gujarat, India

ARTICLE INFO

Keywords:
Photoluminescence [PL]
RED Phosphor
Narrow emission
Cascading absorption and emissions
Morphology
Phosphor

ABSTRACT

$SrZr_2La_2O_7$: Eu^{+3} (0.5–2.5 mol %) phosphors have been synthesized through the standard solid-state reaction technique. The photoluminescent and other structural properties such as PXRD (Powder X-ray Diffraction), SEM (Scanning Electron Microscopy) and Energy Dispersive X-ray spectroscopy (EDX), FTIR (Fourier transform infrared spectroscopy), PSD (Particle Size Distribution) of the phosphors were learned. The photoluminescence spectra show that the phosphor exhibited intense and dominant red emissions at 627 nm belonging to the $5D_0 \rightarrow 7F_2$ electric dipole transition. The FWHM of the red emissions at 627 nm is only 8.0 nm increasing in luminous efficacy. Hereby we propose a novel RED phosphor for RED emitting LEDs with phosphor-embedded polymer matrix layers of variable thickness and stacking up to 400 μm. The intensity of the red color was enhanced by self-excitation of photon absorption and emission. As a result, Eu^{3+}doped $SrZr_2La_2O_7$ phosphors can be widely used as red phosphors in UV chip-based WLEDs and displays. The phosphor exhibits high color purity up to 99% when excited at 590 nm. X-ray powder diffraction analysis confirms that the phosphor is highly crystalline and has a cubic phase.

Introduction

Due to the growing population worldwide and rapidly increasing industrialization, the demand for energy is increasing rapidly and can exceed the limits of increasingly scarce natural resources [1]. The alarming news is that demand for global energy is projected to rise by 48% in the next 20 years [2]. This requires that every person on Earth endure negative impacts on global climate and loss of natural reserves/fossils derived from energy production [3]. Energy-saving technologies play a crucial role in protecting natural resources. Solid State Lighting (SSL) is fast becoming a household name and is playing an important role in energy conservation [4]. Phosphors for various LED applications have achieved a breakthrough in achieving the same. However intensive research has been carried out on new phosphor material used for LEDs with phosphor-embedded polymer matrix layers, resulting in the development of w-LED and monochrome LEDs with high color purity (For instance, CRI (Colour Rendering Index) values above 90), color quality scale (CQS) and high luminous efficacy of visible LER (Light Emission Radiation) [5]. Lumens to spectral power (watts) ratio is used to determine the luminous effectiveness of visible light emission (LER) [6]. One of phosphor used for these w-LEDs is red-emitting phosphor. Large "emission bands of red phosphors and a decrease in the human eye's sensitivity to the near-infrared region are the major causes of red-emitting phosphor difficulties [7]. In order to to effectively covering the red spectral spectrum (emission maximum between 610–620 nm) while reducing the effects of effectiveness because of eye sensitivity at longer wavelengths, new red phosphors with extraordinarily thin bands of emission at the appropriate wavelength are" needed [8].

From the literature studies, the high requirements of commercial LED applications are fulfilled by only a few red emitting phosphors; with respect to a high conversion efficiency under LED working circumstances, narrow emission brands with deep red colour. Presently available red-emitting phosphors suffer by the large FWHM and thus low efficacy [9]. None of them are accessible, and none of them match the requirements for a "high-performance red phosphor, which include a narrow band emission between 610 and 620 nm along with exceptional stability of its luminous qualities. Aside from europium-doped compounds, quantum dots and Mn^{4+}-doped fluorides are two key

* Corresponding author.
E-mail address: kishorekaitha@gmail.com (K.K. Aitha).

https://doi.org/10.1016/j.rechem.2023.101100
Received 24 August 2023; Accepted 4 September 2023
Available online 6 September 2023

Received: 25 August 2023 | Revised: 9 October 2023 | Accepted: 19 October 2023

DOI: 10.1002/bio.4623

RESEARCH ARTICLE

LUMINESCENCE The Journal of Biological and Chemical Luminescence WILEY

Studies on a novel $SrZr_2CaLa_2O_8:Eu^{3+}$ phosphor for lighting applications emitting direct white light

Kishore Kumar Aitha[1] | Dantala Dinakar[1] | K. V. R. Murthy[2] | A. S. Sai Prasad[3] | Divi Haranath[1]

[1]Department of Physics, National Institute of Technology Warangal, Hanumakonda, Telangana, India

[2]Department of Physics, Faculty of Science, The M.S. University of Baroda, Vadodara, Gujarat, India

[3]Department of Physics, Vasavi College of Engineering, Hyderabad, Telangana, India

Correspondence
Kishore Kumar Aitha, Department of Physics, National Institute of Technology Warangal, Hanumakonda 506004, Telangana, India.
Email: kishorekaitha@gmail.com

Funding information
No funding.

Abstract

Direct white light emitting phosphors play a significant role in the display industry due to their ability to improve the quality, efficiency, and versatility of lighting sources used in most of the displays. The currently investigated phosphor $SrZr_2CaLa_2O_8:Eu^{3+}$ was prepared by a conventional solid-state reaction method. It has been observed that the stoichiometric ratio of all precursors plays an important role in determining the characteristics of the final phosphor. From X-ray diffraction (XRD) analysis, the phosphor was observed to have a hexagonal phase and a crystal size of ~28 nm. Scanning electron microscopy (SEM) observations revealed a cluster of rod-like structures with an average diameter of ~0.2 μm. The excitation peak maximum observed at 280 nm is due to charge transfer between Eu^{3+}-O^{2-} ions. The energy transitions $^7F_0 \rightarrow {}^5L_6$ and $^7F_0 \rightarrow {}^5D_2$ are responsible for the appearance of other excitation peaks at ultraviolet (UV) (395 nm), blue (~467 nm), green (~540 nm), orange (~590 nm), and red (~627 nm) attributed to $^5D_0 \rightarrow {}^7F_J$ ($J = 0$–4) transitions of europium ion (Eu^{3+}). The Commercial International de l'Eclairage (CIE) chromaticity coordinates were estimated to be (0.37, 0.0.33) and (0.67, 0.33) for the emissions corresponding to 395 and 590 nm, respectively. The characteristic emissions of Eu^{3+} ions allow this novel phosphor to be used to generate direct white light in light-emitting diodes (LEDs), which is otherwise difficult to achieve in single-component systems.

KEYWORDS
multiple-excitation, phosphor, photoluminescence, W-LED

1 | INTRODUCTION

Solid-state lights have made their position in the display and lighting industry owing to their distinct properties like robustness, energy-saving capacity, long lifetime, and high light efficiency [1, 2]. Yellow trivalent cerium-doped yttrium aluminum garnet (YAG:Ce^{3+}) phosphor and blue light-emitting diode (LED) chips [3–5] are prominently used for generating white light in LEDs. Direct white light-emitting phosphors are crucial for the development and improvement of LEDs for several reasons such as energy efficiency, color quality, and rendering; cost-effectiveness, reduced heat generation, reliability, longer lifetimes, and improved spectral energy distribution [1–6]. Cerium ion (Ce^{3+}) phosphors, however, have a low conversion efficacy, and their color based on the input power [7, 8] also has a red component deficiency in this emission spectrum. They suffer from high color rendering index (CRI) and low correlated color temperature (CCT) [9, 10]. The white light that closely mimics natural sunlight is essential for various applications, including indoor lighting, displays, automotive

Digital Receipt

This receipt acknowledges that Turnitin received your paper. Below you will find the receipt information regarding your submission.

The first page of your submissions is displayed below.

Submission author:	Haranath D
Assignment title:	AAS
Submission title:	Development of Functional Materials as White-LED Phosphor...
File name:	Aitha_Kishore_thesis_for_similarty_index.pdf
File size:	17.07M
Page count:	177
Word count:	47,498
Character count:	274,508
Submission date:	07-Dec-2023 12:29PM (UTC+0530)
Submission ID:	2216074309

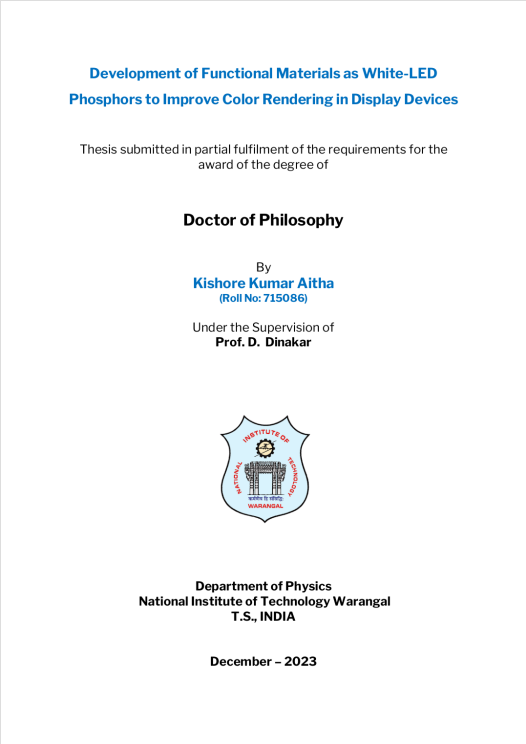

Development of Functional Materials as White-LED Phosphors to Improve Color Rendering in Display Devices

Thesis submitted in partial fulfilment of the requirements for the award of the degree of

Doctor of Philosophy

By

Kishore Kumar Aitha
(Roll No: 715086)

Under the Supervision of
Prof. D. Dinakar

Department of Physics
National Institute of Technology Warangal
T.S., INDIA

December – 2023

Development of Functional Materials as White-LED Phosphors to Improve Color Rendering in Display Devices

ORIGINALITY REPORT

11%	6%	7%	2%
SIMILARITY INDEX	INTERNET SOURCES	PUBLICATIONS	STUDENT PAPERS

PRIMARY SOURCES

1	www.science.gov Internet Source	1%
2	worldwidescience.org Internet Source	1%
3	www.researchgate.net Internet Source	1%
4	Submitted to Queen's University of Belfast Student Paper	1%
5	pubs.rsc.org Internet Source	<1%
6	discovery.researcher.life Internet Source	<1%
7	"Phosphors, Up Conversion Nano Particles, Quantum Dots and Their Applications", Springer Science and Business Media LLC, 2017 Publication	<1%